frontiers | Research Topics

Exploring the impact of genetics on new drugs and potential drug targets: A multi-omics approach to improve personalized therapeutics

Edited by
Shaoqiu Chen and Jian Gao

Published in
Frontiers in Genetics
Frontiers in Pharmacology

ISSN 1664-8714
ISBN 978-2-8325-5147-9
DOI 10.3389/978-2-8325-5147-9

About Frontiers

Frontiers is more than just an open access publisher of scholarly articles: it is a pioneering approach to the world of academia, radically improving the way scholarly research is managed. The grand vision of Frontiers is a world where all people have an equal opportunity to seek, share and generate knowledge. Frontiers provides immediate and permanent online open access to all its publications, but this alone is not enough to realize our grand goals.

Frontiers journal series

The Frontiers journal series is a multi-tier and interdisciplinary set of open-access, online journals, promising a paradigm shift from the current review, selection and dissemination processes in academic publishing. All Frontiers journals are driven by researchers for researchers; therefore, they constitute a service to the scholarly community. At the same time, the *Frontiers journal series* operates on a revolutionary invention, the tiered publishing system, initially addressing specific communities of scholars, and gradually climbing up to broader public understanding, thus serving the interests of the lay society, too.

Dedication to quality

Each Frontiers article is a landmark of the highest quality, thanks to genuinely collaborative interactions between authors and review editors, who include some of the world's best academicians. Research must be certified by peers before entering a stream of knowledge that may eventually reach the public - and shape society; therefore, Frontiers only applies the most rigorous and unbiased reviews. Frontiers revolutionizes research publishing by freely delivering the most outstanding research, evaluated with no bias from both the academic and social point of view. By applying the most advanced information technologies, Frontiers is catapulting scholarly publishing into a new generation.

What are Frontiers Research Topics?

Frontiers Research Topics are very popular trademarks of the *Frontiers journals series*: they are collections of at least ten articles, all centered on a particular subject. With their unique mix of varied contributions from Original Research to Review Articles, Frontiers Research Topics unify the most influential researchers, the latest key findings and historical advances in a hot research area.

Find out more on how to host your own Frontiers Research Topic or contribute to one as an author by contacting the Frontiers editorial office: frontiersin.org/about/contact

Exploring the impact of genetics on new drugs and potential drug targets: A multi-omics approach to improve personalized therapeutics

Topic editors

Shaoqiu Chen — University of Hawaii at Mānoa, United States

Jian Gao — Shanghai Children's Medical Center, China

Citation

Chen, S., Gao, J., eds. (2024). *Exploring the impact of genetics on new drugs and potential drug targets: A multi-omics approach to improve personalized therapeutics*. Lausanne: Frontiers Media SA. doi: 10.3389/978-2-8325-5147-9

Table of contents

frontiers | Frontiers in Genetics

TYPE Case Report
PUBLISHED 20 April 2023
DOI 10.3389/fgene.2023.1167470

OPEN ACCESS

EDITED BY
Shaoqiu Chen,
University of Hawaii at Mānoa,
United States

REVIEWED BY
Fang Qi,
Peking University, China
Bo Zhou,
Beijing Tiantan Puhua International Hospital, China

*CORRESPONDENCE
Zhengrong Wu,
wuzhengrong2023@163.com

RECEIVED 16 February 2023
ACCEPTED 03 April 2023
PUBLISHED 20 April 2023

CITATION
Liu X, Yang F, Jia D, Dong X, Zhang Y and Wu Z (2023), Case report: A case study on the treatment using icaritin soft capsules in combination with lenvatinib achieving impressive PR and stage reduction in unresectable locally progressive pancreatic cancer and a literature review. *Front. Genet.* 14:1167470.
doi: 10.3389/fgene.2023.1167470

Case report: A case study on the treatment using icaritin soft capsules in combination with lenvatinib achieving impressive PR and stage reduction in unresectable locally progressive pancreatic cancer and a literature review

Xiaolong Liu[1], Feimin Yang[2], Dunmao Jia[3], Xinyu Dong[1], Yizhuo Zhang[1] and Zhengrong Wu[1]*

[1]Department of General Surgery, Sir Run Run Shaw Hospital, Zhejiang University School of Medicine, Hangzhou, China, [2]Department of Nursing, Sir Run Run Shaw Hospital, School of Medicine, Zhejiang University, Hangzhou, China, [3]Department of General Surgery, Affiliated Run Run Shaw Hospital, Jiangshan Branch, Harbin Medical University, Quzhou, China

Background: Pancreatic cancer is one of the most deadly malignancies in the world. It is characterized by rapid progression and a very poor prognosis. The five-year survival rate of pancreatic cancer in China is only 7.2%, which is the lowest among all cancers and the use of combined paclitaxel albumin, capecitabine, and digital has been the clinical standard treatment for advanced pancreatic cancer since 1997. Also, the application of multidrug combinations is often limited by the toxicity of chemotherapy. Therefore, there is an urgent need for a more appropriate and less toxic treatment modality for pancreatic cancer.

Case presentation: The patient was a 79-year-old woman, admitted to the hospital with a diagnosis of unresectable locally advanced pancreatic cancer (T3N0M0, stage IIA), with its imaging showing overgrowth of SMV involvement and unresectable reconstruction of the posterior vein after evaluation. As the patient refused chemotherapy, lenvatinib (8 mg/time, qd) and icaritin soft capsules (three tablets/time, bid) were recommended according to our past experience and a few clinical research cases. The tumor lesion was greatly reduced by 57.5% after the treatment, and the extent of vascular involvement also decreased. The aforementioned medication resulted in a significant downstaging of the patient's tumor.

Conclusion: Better results were achieved in the treatment with icaritin soft capsules and lenvatinib in this case. Because of its less toxic effect on the liver and kidney and bone marrow suppression, it was suitable to combine icaritin soft capsules with targeted drugs for treating intermediate and advanced malignancies, which brings hope to patients who cannot or refuse to take chemotherapy.

KEYWORDS

icaritin soft capsules, lenvatinib, advanced pancreatic cancer, combined treatment, tumor downstaging

Preface

Today, pancreatic cancer is one of the deadliest malignancies. The global tumor registry data of 2020 show that pancreatic cancer ranks 12th in incidence but 7th in mortality among malignancies (Hu et al., 2021). It is mostly characterized by rapid progression and a very poor prognosis. The five-year survival rate of pancreatic cancer in China is only 7.2%, the lowest among all tumor types (Zhao et al., 2019). Most patients are diagnosed with locally advanced pancreatic cancer or distant metastases when the tumor is detected, so only 15%–20% of patients have the opportunity to accept surgical treatment with a better prognosis (Van Veldhuisen et al., 2019). A total of 95,000 new cases of pancreatic cancer were diagnosed in China in 2015, while 85,000 deaths occurred, with generally higher morbidity and mortality rates in men and in urban areas (Jia et al., 2018).

Gemcitabine has been the standard chemotherapy for advanced pancreatic cancer since 1997. Several phase III clinical trials have tried chemotherapy with gemcitabine to improve outcomes. However, most of these trials failed to show an improvement in overall survival, except for two studies. A phase III trial of erlotinib and gemcitabine showed very limited improvement compared to gemcitabine alone (Moore et al., 2007). Also, in the ACCORD 11 study, better results were observed with FOLFIRINOX chemotherapy (five-fluorouracil, oxaliplatin, and irinotecan with folinic acid), which showed an improvement in overall survival by more than four months (from 6.8 to 11.1 months) compared to gemcitabine (Conroy et al., 2010). However, the significant toxicity of multidrug chemotherapy often limits its use to the extent that some patients refuse it. Therefore, there is an urgent need for a more efficient and less toxic treatment modality for pancreatic cancer.

Studies have concluded that most pancreatic cancers are blood-deprived tumors with insignificant angiogenesis, and therefore, there is little data about the anti-angiogenic drugs for clinical treatment. However, one study showed that the ORR of lenvatinib for the treatment of pancreatic neuroendocrine tumors was up to 44.2% and the DCR was 96.2%, which proves its effectiveness (Capdevila et al., 2021). Other cases of target-free combination therapy for pancreatic tumors have also been reported, such as a 55-year-old pancreatic cancer patient (cT4N1M1) with liver and lung metastases who carried ERBB2 mutation and had high tumor mutational load (TMB) being treated with lenvatinib in combination with pembrolizumab; it achieved partial remission for up to 5 months after a series of treatments failed (Chen et al., 2019). A 48-year-old patient with metastatic pancreatic alveolar cell carcinoma treated with lenvatinib and sintilimab demonstrated significant tumor remission and long-term progression-free survival (>21 months) (Qin et al., 2021). The data previously discussed suggest that lenvatinib and immunologic agents may be effective in the clinical treatment of pancreatic cancer.

Icaritin soft capsules are an original small-molecule immunomodulator with independent intellectual property rights in China; it is a first-in-class original drug in the world, and it was approved by China's National Medical Products Administration (NMPA) in January 2022. The results of its preclinical studies and *in vivo* pharmacodynamic study showed that epimedium had a significant dose-effect positive correlation in inhibiting tumor growth in the human-derived hepatocellular carcinoma Hep G2 mouse liver, which is an *in situ* transplantation tumor model, and also had different inhibition of tumor growth in the human-derived breast cancer BCAP-37, human-derived prostate cancer PC-3, and other subcutaneous transplantation tumor models, which also showed a certain quantitative-effect relationship (Huang et al., 2007; Tong et al., 2011; Sun et al., 2021), confirming its significant and broad-spectrum antitumor activity. As a novel small-molecule immunomodulator, it can inhibit inflammatory signaling pathways, reduce the release of inflammatory factors, enhance antigen presentation, decrease expression of PD-L1 and MDSC, increase T-cell termination, and improve the immune microenvironment of tumors through dual activation of intrinsic and adaptive immunity. The current indication of the icaritin soft capsule is approved for the first-line treatment of hepatocellular carcinoma (Guo et al., 2011). As far as we know, there are many studies about liver cancer treatment with icaritin soft capsule, and no related research concerning different stages of pancreatic cancer treatment with icaritin soft capsule in practice.

This article reports a case of a patient with locally progressive unresectable pancreatic cancer who refused chemotherapy and achieved PR after treatment with lenvatinib and icaritin soft capsules with satisfactory efficacy and controlled safety.

Case presentation

The patient is a 79-year-old woman admitted to our hospital in mid-August 2022 for "distension and pain in the upper and middle abdomen for 1 week and pancreatic occupancy for 6 days." In fact, the patient could maintain a normal life and take care of herself except for distension and pain in the upper and middle abdomen without any cause, accompanied by nausea and a small amount of vomiting, which were mostly gastric contents. The KPS score of the patient was approximately 80. The aforementioned condition could evidently be aggravated by hunger and was relieved by eating small amounts of food. There was no fever, chills, diarrhea, or black stool. At first, she went to the local hospital to find elevated CA 19-9 levels (details unknown), and abdominal ultrasonography suggested an occupancy in the head of the pancreas. For further diagnosis and treatment, the patient came to our hospital with a diagnosis of pancreatic mass. The patient denied a past history of hypertension, diabetes mellitus, hepatitis, tuberculosis, etc. and denied any history of surgical trauma. The hospital conducted a physical examination as follows: T 36.9°C, R 19°bpm, HR 85°bpm, BP 159/72 mmHg, and pain score 1. The patient was conscious and mentally competent. The skin and sclera were not yellowish and without enlarged superficial lymph nodes, with clear breath sounds in both lungs and uniform heart rhythm without cardiac murmur. The abdomen was flat with normal bowel sounds and negative shifting dullness.

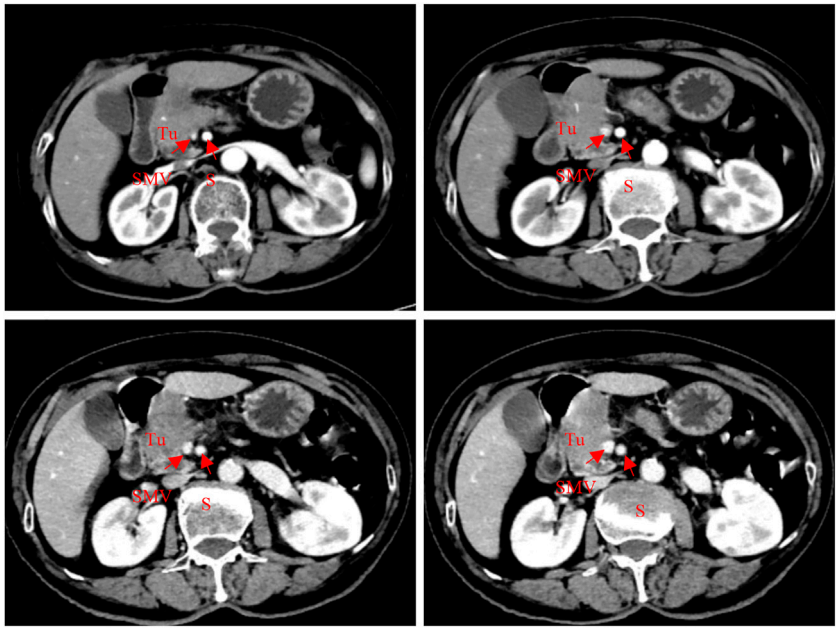

FIGURE 1
Abdominal CT scan (2022-08-05): a soft tissue mass shadow was seen in the pancreas head, approximately 57*32 mm; meanwhile, the gastroduodenal artery and superior mesenteric vein were also involved.

The whole abdomen was soft without abnormal masses and pressure pain or rebound pain. There was no edema in both lower extremities, and the pathological features were negative.

The supplementary examination included the blood count: WBC, 6.0*10^{9}/L; Neo, 3.32*10^{9}/L; HB, 128 g/L; and Plt, 254*10^{9}/L.

Blood biochemistry was reported as follows: K, 3.78 mmol/L; ALT, 19 U/L; AST, 17 U/L; AKP, 123 U/L; γGGT, 45 U/L; ALB, 42.9 g/L; TBIL, 6.3 μmol/L; and DBIL, 1.0 μmol/L. Blood glucose was 11.4 mmol/L. Tumor markers included CA 19-9, 69.8 IU/mL; CEA, 1.39 ng/mL; CA 15-3, 10.60 U/mL; CA 125, 14.30 U/mL; and AFP, 1.77 ng/mL. CT scan images of admission (Figure 1) showed occupancy in the pancreas head, which was considered to be cancer, with an involvement of the gastroduodenal artery and the superior mesenteric vein, and a soft tissue mass shadow was observed in the pancreas head, approximately 57*32 mm.

Ultrasound endoscopy showed a well-defined and irregular hypoechoic mass in the pancreatic head with a vascular invasion of approximately 43*29 mm. The preliminary diagnosis was considered pancreatic malignancy (cT3N0M0, stage IIA), which indicated the clinical diagnosis stage. Due to excessive SMV involvement and evaluation of posterior venous unresectable reconstruction, the disease was diagnosed as locally progressive unresectable pancreatic cancer. The current standard first-line treatment for advanced unresectable pancreatic cancer is based on a gemcitabine regimen. However, the patient insistently refused chemotherapy after repeated communication and explanation, and based on its immune regulation mechanism, combining our previous medication experience with the icaritin soft capsule, we tried to recommend lenvatinib and icaritin soft capsule for treatment. To the best of our knowledge, no case study was found to be reported to treat pancreatic cancer until now.

The patient underwent a CT review after 1 month of medication, and although the huge mass did not shrink and significant cystic necrosis was visible inside, in the meantime, the significant spillage of the contrast agent could be observed, suggesting the possibility of bleeding inside a tumor. It was inferred that the disease has been controlled (Figure 2). Since the tumor envelope was still intact, it was considered that the risk of progressive bleeding could be avoided by self-compression to stop the bleeding. Generally speaking, short-term and small amounts of bleeding have limited harm, but it could lead to death with a large amount of bleeding. The patient was discharged after conservative treatment in the hospital.

The patient came to our hospital for the second time due to sudden abdominal pain. The routine blood tests showed WBC, 12.0*10^{9}/L; Neo, 9.82*10^{9}/L; CRP, 188.5 mg/L; blood amylase, 239 IU/L; and lipase, 231.10 IU/L; all of the aforementioned indicators were elevated. The tumor biomarker of CA 19-9 showed a decrease from 70 IU/mL to 30 IU/mL, and the imaging showed a 52% reduction in tumor size (35*28 mm), a reduction in superior mesenteric vein (SMV) involvement, and significant relief of vascular stenosis. The efficacy of lenvatinib and icaritin soft capsules was evaluated comprehensively and reached PR with significant tumor remission after 2 months (Figure 3). Anti-infective and amylase-lowering symptomatic treatment was given for acute pancreatitis after her admission into the hospital.

On 15 October 2022, the patient was readmitted to the hospital again with sudden onset of abdominal pain for 1 day, and routine blood showed WBC, 14.7*10^{9}/L; Neo, 11.98*10^{9}/L; CRP, 156.3 mg/L; blood amylase, 211.6 IU/L; and lipase, 224.0 IU/L. CT of the abdomen showed a diffuse inflammatory exudate below the pancreas, suggesting secondary acute pancreatitis (Figure 4). Also, the tumor lesion was approximately 20% smaller than last time and 57.5% smaller overall than before treatment. The vascular

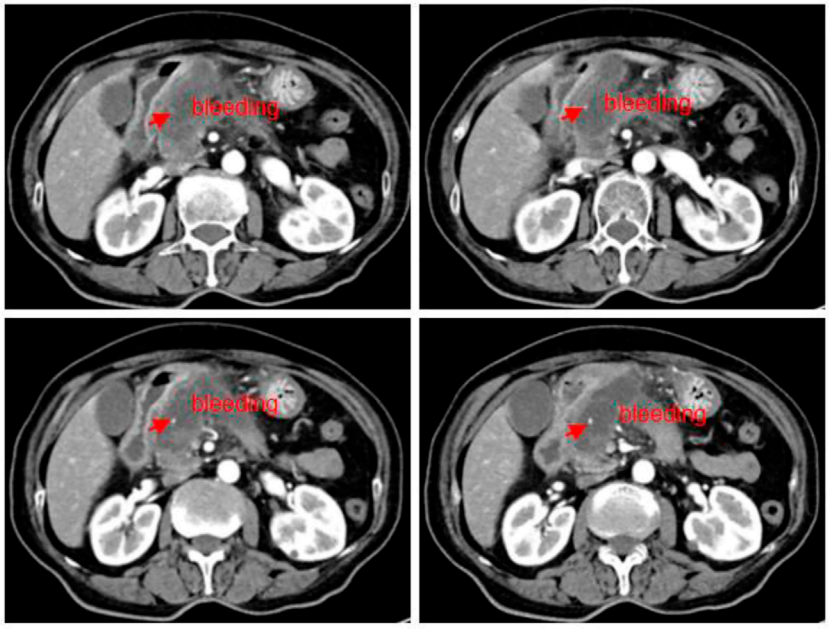

FIGURE 2
Abdominal CT scan (2022.08.27): a mass of shadow in the neck of the pancreatic head, approximately 57*32 mm; tumor with cystic necrosis was considered as a small amount of local bleeding.

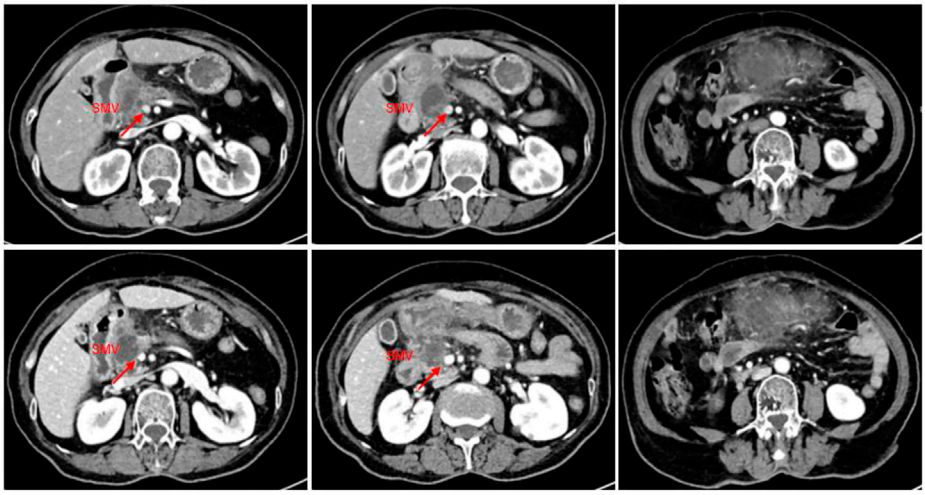

FIGURE 3
CT imaging of the abdomen (2022.9.26): a slightly hypodense mass of approximately 35*28 mm with mild enhancement at the margin was observed in the neck of the pancreatic head, and the right wall of the proximal end of the adjacent superior mesenteric vein was involved with a slightly narrower lumen. The tumor was 52% smaller than before treatment.

involvement was also reduced and the proximal stenosis of SMV was also relieved with a better contour. The patient's condition was regarded to be locally advanced pancreatic cancer as before, and the surgical assessment met the criteria for SMV resection and reconstruction (Figure 4). Therefore, its TNM stage was downgraded from T3N0M0 (stage IIA) before the treatment to T2N0M0 (stage IB) after the treatment, and surgery was recommended as an effective treatment choice. Meanwhile, the patient requested the surgery after another two cycles of medication due to the results being beyond her expectation. The patient was admitted to the hospital only for an anti-infective symptomatic treatment of secondary acute pancreatitis.

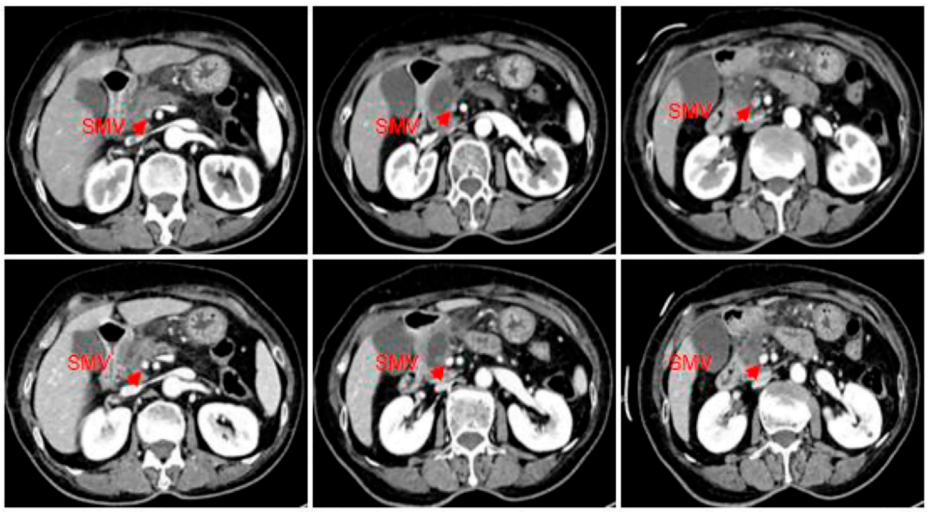

FIGURE 4
CT scan of the abdomen (2022.10.15): a slightly hypodense mass of approximately 35*28 mm with mild edge enhancement was seen in the neck of the pancreatic head, with a slightly reduced lesion compared to the last imaging (2022.09.26), and with a relief of the proximal stenosis in the adjacent SMV. It showed better improvement than before for the vague edema and thickening of the lateral wall of the greater curvature of the gastric antrum and the colorectal wall, and the vague inflammatory exudation of the gastrocolic ligament. The tumor was 20% smaller than in the last review.

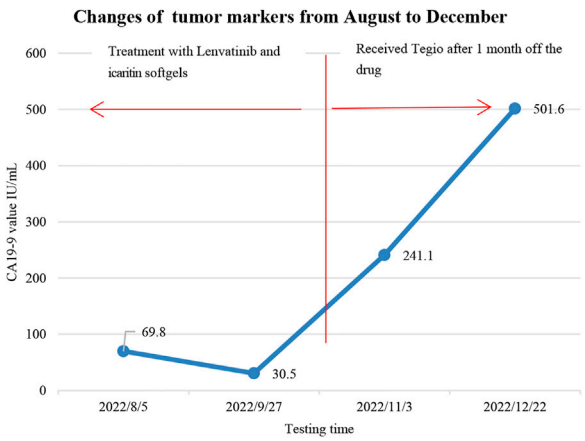

FIGURE 5
Changes in tumor markers: the patient took two drugs for 2 months between August and stopped them in early October for financial reasons, later replaced them with Tegio in early November, and followed up about 3 months after the drug's withdrawal.

Unfortunately, the patient stopped taking these two drugs for financial reasons and was re-examined 1 month later, which showed an increase of 1 cm in the active component of the primary pancreatic lesion (original necrotic part), an increment of 2 cm in the tumor located in the pancreatic hook, and multiple metastases in the hepatoduodenal ligament and the hepatogastric ligament based on the results of abdominal CT imaging. Also, increased tumor biomarkers, such as CA 19-9 (241.1 U/mL) and ferritin (686.0 ng/mL), on November 3 suggested tumor progression. Later, the patient took Tegio as treatment, and CA 19-9 increased to 501.6 U/mL in December without a CT review (Figure 5). Also, the patient is still alive today.

Treatment summary

Icaritin soft capsules are now widely used as an immunomodulatory agent in the treatment of solid tumors. In this case, a 79-year-old woman with nausea and vomiting was found to have elevated CA 19-9 at a local hospital, while an ultrasonic examination showed an occupied lesion in the patient's pancreatic head. In our hospital, it just presented with the symptoms or signs of slightly elevated blood pressure, blood glucose, and mild abdominal pain. The patient was initially diagnosed with pancreatic cancer with T3N0M0 (stage IIA). The evaluation revealed a tumor invading an SMV, which was unfit for removal and reconstruction, and it can be classified as an unresectable, locally advanced pancreatic cancer. Generally, pancreatic cancer at this stage can be treated with gemcitabine combined with albumin paclitaxel (GN) or gemcitabine and cisplatin (GP) according to the new guidelines recommended by CSCO, whose efficiency can reach 20%–30% (Cui et al., 2022). However, the fact lies in the low validity as expected, and some serious side effects with chemotherapy. Therefore, the patient's family insisted on refusing chemotherapy. The choice of icaritin soft capsules and lenvatinib was mainly based on the following reasons:

1) Due to economic reasons, the patient refused gene sequencing, including the BRAC1/2 gene and other tumor-associated genes, and no targeted drugs could be chosen and applied without the definite gene status of the BRAC1/2 gene; meanwhile, the patient refused radiotherapy.
2) Icaritin soft capsules are a broad-spectrum immunomodulator for solid tumors, with enough evidence for a favorable experience of clinical application and good security.
3) There are some data to support the use of lenvatinib in the clinical treatment of pancreatic cancer.

Pancreatic cancer is generally a blood-deprived tumor with insignificant angiogenesis; therefore, the role of anti-angiogenic drugs in the treatment of pancreatic cancer remains to be proven. Studies have shown that all types of tumors require vascularization to provide the oxygen and nutrients, which tumors need to grow (Craven et al., 2016). According to Haltly's research, the vasculature was generally divided into visualized tumor vessels and microscopic microvasculature. Now, the microvessel density is thought to be a better indicator of tumor metabolic load than visual angiogenesis. Therefore, it is believed that tumors lacking blood supply can also benefit from anti-angiogenic therapy (Lynn et al., 2002). Although there are fewer visualized vessels in pancreatic cancer, a higher microvessel density suggests the possible benefits of the anti-VEGF treatment. However, the clinical practice has shown that small-molecule TKIs, including bevacizumab and aparatinib in combination with chemotherapy for pancreatic cancer, did not meet the expectations due to insignificant OS prolongation and even shorter survival than chemotherapy alone in some cases (Kindler et al., 2010; Gonçalves et al., 2012; Bergmann et al., 2015; Kim et al., 2015). This may be related to the fact that targeted drugs increase the side effects and prevent patients from the full course of chemotherapy, which leads to poor treatment effects.

Generally, due to the complex mechanism of tumorigenesis and metastasis, combination therapy can inhibit tumors from multiple mechanisms to achieve better clinical results; therefore, multiple combined medication schemes are recommended by NCCN, ASCO, and CSCO guidelines in the clinical practice at present. There are data about the treatment of pancreatic cancer with lenvatinib. In fact, lenvatinib is a synthetic multi-target inhibitor of tyrosine kinase with oral activity, which is most effective for the VEGFR2 (KDR)/VEGFR3(Flt-4) gene mutation of cancer. Also, we think that it is an anti-tumor drug, not an immune modulator. There is a report that the ORR reached 44.2% with lenvatinib after the treatment of the pancreatic neuroendocrine tumor, and DCR was up to 96.2%, which showed higher efficiency but a poor safety profile. The common adverse events often included fatigue, hypertension, and diarrhea, and approximately 93.7% of patients would have dose reduction requirements or treatment interruption (Capdevila et al., 2021). Another study also exhibited its inhibition focused on the growth of pancreatic cancer graft tumors and also mentioned that microvascular density may be related to the efficacy of anti-angiogenic drugs (Yamamoto et al., 2014). This inferred the therapeutic effects of pancreatic cancer with lenvatinib.

There are few clinical precedents of targeted-drug monotherapy for pancreatic cancer until now. In this case, based on two case reports of lenvatinib and immune-related drugs of pancreatic tumors and our experience (Yi et al., 2019), and the patient's opinion of refusing chemotherapy, icaritin soft capsule, as a new small-molecule immunomodulator, and lenvatinib was used in the treatment for the patient. It is believed that immunomodulation of icaritin soft capsule plays an important role in tumor cells and the microenvironment, including 1) icaritin suppresses IL-6/JAK2/STAT3 signaling pathway by inhibiting JAK2 and STAT3 phosphorylation, leading to downregulation of its downstream-related genes (Zhu et al., 2015); 2) directly binds MyD88/IKKα and inhibits the TLR-MyD88-IKK-NFκB-signaling pathway, which in turn reduces TNF-α, IL-6, and other factors' production and downregulates the IL-6/JAK2/STAT3-signaling pathway (Li et al., 2021). It is shown that the two signaling pathways aforementioned are complementary and can exhibit anti-tumor effects by downregulating inflammatory factors, such as TNF-α, IL-6, and PD-L1 expression. The results demonstrated that the number and proportion of $CD8^+$ T cells in tumor tissues of mice were significantly increased, and the proportion of MDSCs was significantly reduced in the icaritin soft capsule group in the related immune microenvironment studies, indicating that it not only increased the number and activity of $CD8^+$ T cells but also effectively reduced the proportion of immunosuppressive cell MDSCs (Hao et al., 2019). It is concluded that restoring the ability of $CD8^+$ T cells could contribute to producing IFN-γ and improving the tumor microenvironment to prevent tumor growth.

The patient was re-examined after 1 month of medication, and CT showed that the lesion did not shrink but a larger internal cystic necrosis and notable contrast spillage were seen, suggesting the presence of tumor bleeding and the possibility of tumor remission. After the whole treatment, significant tumor remission and a good quality of life improvement were observed in this patient, and it proved the treatment effective. This may be related to the combined potency of the two drugs. Cytokine IL-6 has various pro-tumor activities, such as promoting the release of angiogenic factors leading to neovascularization (Fisher et al., 2014); therefore, downregulation of IL-6 expression may enhance the inhibition of tumor microangiogenesis and thus increase its effects of anti-angiogenic drugs.

The commonly mutated genes in pancreatic cancer include BRCA1/2, CDKN2A, PALB2, ATM, TP53, STK11, and PRSS1. Currently, patients with a family history of pancreatic cancer are mostly recommended to undergo BRCA1/2 and other related genetic tests to clarify the possibility of tumor heritability, and to help targeted-drug screening and clinical treatment on the other hand. Lenvatinib is a receptor tyrosine kinase (RTK) inhibitor that inhibits the VEGF receptor VEGFR1/2/3 kinase activity and also inhibits pathological tumor angiogenesis, thereby inhibiting tumor growth and progression. It is approved for unresectable hepatocellular carcinoma primarily based on the results of the non-inferiority, multicenter randomized REFLECT Phase III clinical study compared with sorafenib. The Phase II clinical trial of GETNE1509 with lenvatinib also demonstrated efficacy against progressive advanced pancreatic and gastrointestinal neuroendocrine cancers (Capdevila et al., 2021). There are details about gene mutations in pancreatic cancer (Table 1). Another phase II clinical study of lenvatinib in combination with a PD1 inhibitor for unresectable cholangiocarcinoma has also shown good efficacy and promise (Zhang et al., 2021). Because of the indications for advanced hepatocellular carcinoma of lenvatinib, it is currently less used in the clinical treatment of pancreatic cancer. Therefore, there is no expert consensus or guidelines for selecting lenvatinib for locally progressive unresectable pancreatic cancer based on its tumor-related driver gene by gene sequencing. Nevertheless, high-throughput sequencing will undoubtedly become a key cornerstone of pharmacogenomics and individualized therapy during the treatment of tumors (Morganti et al., 2019). In this case, the patient had significant efficacy with two cycles of lenvatinib and icaritin soft capsules, considering the possible existence of VEGFR1/2/3 gene variants and their benefits. In the future, the treatment of pancreatic cancer may require more high-throughput

TABLE 1 Common pancreatic cancer-related gene variations and possible effective targeted drugs (some table contents based on the public data of COSMIC).

Common pancreatic cancer-related gene	Point mutation		Copy number variation		Gene expression		Targeted drug
	% mutated	Tested	Variant %	Tested	% regulated	Tested	
BRCA1	2.32	2,891	0.22	898	6.15 (Over expressed) 0.56 (Under expressed)	179	PARP inhibitors: oplaparib, rucaparib, and niraparib
BRCA2	3.83	3,079			5.59 (Over expressed)	179	The same as aforementioned
CDKN2A	7.64	4,582	4.68	898	12.29 (Over expressed)	179	CDk4/6 inhibitors: palbociclib
PALB2	1.27	2,828			4.47 (Over expressed) 1.68 (Under expressed)	179	May benefit from PARP inhibitors treatment
ATM	5.7	3,649			3.35 (Over expressed)	179	May benefit from oplaparib treatment
TP53	38.53	5,076			7.82 (Over expressed) 9.5 (Under expressed)	179	
STK11	1.81	3,932	0.22	898	3.91 (Over expressed) 10.61 (Under expressed)	179	PARP inhibitors: bemcentinib + pembrolizumab
PRSS1	0.65	2,011			3.35 (Over expressed)	179	

sequencing as an important means and tool for treatment selection. With the discovery of more tumor-driver genes and the research and application of related targeted drugs, the treatment of pancreatic cancer and its clinical prognosis can be expected. The tumor is actually a chronic inflammatory process accompanied by changes in various inflammatory factors. Because we paid more attention to clinical symptoms during the treatment course, the related clinical symptoms, imaging findings, and hematological examination could only indicate therapeutic effects, while neglecting the tumor microenvironment change without conducting for the inflammatory factor test. In the future, more observation and research should be conducted on the changes in relevant inflammatory factors in the tumor treatment.

At present, tumor immunotherapy is widely carried out; unfortunately, the effect is not clear with many clinical studies of immunotherapy in combination with chemotherapy, chemoradiotherapy, vaccines, and cytokine antagonism in patients with pancreatic cancer (Sahin et al., 2017). Generally, the microenvironment of pancreatic cancer is thought to create an immunosuppressive environment for its low immunogenicity, and there is currently no immunotherapy approved for these patients with pancreatic cancer. Also, the FDA approved the use of pembrolizumab in the treatment of microsatellite unstable cancers unrelated to the type of cancers, which seems to depend on the synergistic effect with increased response rates when a combinatorial approach of immunotherapy in conjunction with other modalities is being used (Schizas et al., 2020; Zhao and Liu, 2020). Therefore, a comprehensive treatment using different therapeutic strategies with immunotherapy may bring hope to pancreatic cancer patients (Schizas et al., 2020).

The patient stopped the medication in early October 2022 for financial reasons, and she was subsequently transferred to the hospital for the treatment due to tumor progression. From her tumor marker changes and abdominal CT results, it showed (Figures 4, 5) that the effect of Tegio chemotherapy was not satisfactory and the efficacy was much less than that of lenvatinib and icaritin soft capsules. Although the patient had to switch drugs for economic reasons, it provided clinical application evidence and reference for the subsequent combination treatment with targeted and immune-related drugs in advanced pancreatic cancer.

It is noteworthy that there were two sudden onsets of acute pancreatitis during the treatment in this case. Icaritin soft capsules as a new class I drug were launched in May 2022, the total number of users is currently small, and no reports related to triggering pancreatitis have been seen in phase III clinical studies, but cases of lenvatinib leading to pancreatitis have been reported (Kawakami et al., 2018). Therefore, it cannot be excluded that patient's two acute pancreatitis were related to the application of lenvatinib. The safety

of the combined application of the two drugs was positive throughout the treatment, with no serious complications. Moreover, because it was administered orally, the patient complied well and never discontinued the drug except for economic reasons, confirming the safety of the drug.

Summary

Overall, the efficacy of icaritin soft capsules in combination with lenvatinib in this case of advanced pancreatic cancer is very remarkable. Also, because icaritin soft capsules have minimal effects on liver and kidney function and bone marrow suppression, it is well suited for combination with targeted or immune drugs for the treatment of advanced malignancies, bringing new hope to patients with advanced pancreatic cancer who are unable or refuse to receive first-line treatment with chemotherapy, at least, as an alternative treatment.

Data availability statement

The raw data supporting the conclusion of this article will be made available by the authors, without undue reservation.

Ethics statement

Ethical review and approval was not required for the study on human participants in accordance with the local legislation and institutional requirements. The patients/participants provided their written informed consent to participate in this study. Written informed consent was obtained from the individual(s) for the publication of any potentially identifiable images or data included in this article.

Author contributions

In this manuscript, XL and FY conceived and designed the study; ZW and DJ performed the experiments; YZ and XD analyzed the data during the study and participated in the writing of the manuscript; ZW and XL revised the grammar of the manuscript accordingly. We would like to thank all the authors for their contributions to this manuscript.

Conflict of interest

The authors declare that the research was conducted in the absence of any commercial or financial relationships that could be construed as a potential conflict of interest.

Publisher's note

All claims expressed in this article are solely those of the authors and do not necessarily represent those of their affiliated organizations, or those of the publisher, the editors, and the reviewers. Any product that may be evaluated in this article, or claim that may be made by its manufacturer, is not guaranteed or endorsed by the publisher.

References

Bergmann, L., Maute, L., Heil, G., Rüssel, J., Weidmann, E., Köberle, D., et al. (2015). A prospective randomised phase-II trial with gemcitabine versus gemcitabine plus sunitinib in advanced pancreatic cancer: A study of the CESAR central European society for anticancer drug research-EWIV. *Eur. J. Cancer* 51 (1), 27–36. doi:10.1016/j.ejca.2014.10.010

Capdevila, J., Fazio, N., Lopez, C., Teulé, A., Valle, J. W., Tafuto, S., et al. (2021). Lenvatinib in patients with advanced grade 1/2 pancreatic and gastrointestinal neuroendocrine tumors: Results of the phase II TALENT trial (GETNE1509). *J. Clin. Oncol.* 39, 2304–2312. doi:10.1200/JCO.20.03368

Chen, M., Yang, S., Fan, L., Wu, L., Chen, R., Chang, J., et al. (2019). Combined antiangiogenic therapy and immunotherapy is effective for pancreatic cancer with mismatch repair proficiency but high tumor mutation burden: A case report. *Pancreas* 48 (9), 1232–1236. doi:10.1097/MPA.0000000000001398

Conroy, T., Desseigne, F., Ychou, M., Ducreux, M., Bouche, O., Guimbaud, R., et al. (2010). Randomized phase III trial comparing FOLFIRINOX (F: 5FU/leucovorin [LV], irinotecan [I], and oxaliplatin [O]) versus gemcitabine (G) as first-line treatment for metastatic pancreatic adenocarcinoma (MPA): Preplanned interim analysis results of the PRODIGE 4/ACCORD 11 trial. *J. Clin. Oncol.* 28, 4010. doi:10.1200/jco.2010.28.15_suppl.4010

Craven, K. E., Gore, J., and Korc, M. (2016). Overview of pre-clinical and clinical studies targeting angiogenesis in pancreatic ductal adenocarcinoma. *Cancer Lett.* 381 (1), 201–210. doi:10.1016/j.canlet.2015.11.047

Cui, J., Jiao, F., Li, Q., Wang, Z., Fu, D., Liang, J., et al. (2022). Chinese Society of Clinical Oncology (CSCO): Clinical guidelines for the diagnosis and treatment of pancreatic cancer. *J. Natl. Cancer Cent.* 2 (4), 205–215. doi:10.1016/j.jncc.2022.08.006

Fisher, D. T., Appenheimer, M. M., and Evans, S. S. (2014). The two faces of IL-6 in the tumor microenvironment. *Semin. Immunol.* 26 (1), 38–47. doi:10.1016/j.smim.2014.01.008

Gonçalves, A., Gilabert, M., François, E., Dahan, L., Perrier, H., Lamy, R., et al. (2012). BAYPAN study: A double-blind phase III randomized trial comparing gemcitabine plus sorafenib and gemcitabine plus placebo in patients with advanced pancreatic cancer. *Ann. Oncol.* 23 (11), 2799–2805. doi:10.1093/annonc/mds135

Guo, Y. M., Zhang, X. T., Meng, J., and Wang, Z. Y. (2011). An anticancer agent icaritin induces sustained activation of the extracellular signal-regulated kinase (ERK) pathway and inhibits growth of breast cancer cells. *Eur. J. Pharmacol.* 658 (2–3), 114–122. doi:10.1016/j.ejphar.2011.02.005

Hao, H., Zhang, Q., Zhu, H., Wen, Y., Qiu, D., Xiong, J., et al. (2019). Icaritin promotes tumor T-cell infiltration and induces antitumor immunity in mice. *Eur. J. Immunol.* 49, 2235–2244. doi:10.1002/eji.201948225

Hu, J. X., Zhao, C. F., Chen, W. B., Liu, Q. C., Li, Q. W., Lin, Y. Y., et al. (2021). Pancreatic cancer: A review of epidemiology, trend, and risk factors. *World J. Gastroenterol.* 27 (27), 4298–4321. doi:10.3748/wjg.v27.i27.4298

Huang, X., Zhu, D. Y., and Lou, Y. (2007). A novel anticancer agent, icaritin, induced cell growth inhibition, G(1) arrest and mitochondrial transmembrane potential drop in human prostate carcinoma PC-3 cells. *Eur. J. Pharmacol.* 564 (1–3), 26–36. doi:10.1016/j.ejphar.2007.02.039

Jia, X., Du, P., Wu, K., Xu, Z., Fang, J., Xu, X., et al. (2018). Pancreatic cancer mortality in China: Characteristics and prediction. *Pancreas* 47, 233–237. doi:10.1097/MPA.0000000000000976

Kawakami, H., Kubota, Y., and Hosokawa, A. (2018). Lenvatinib-Induced acute pancreatitis associated with a pancreatic pseudocyst and splenic pseudoaneurysms. *Pancreas* 47 (6), e34–e35. doi:10.1097/MPA.0000000000001061

Kim, E. J., Semrad, T. J., and Bold, R. J. (2015). Phase II clinical trials on investigational drugs for the treatment of pancreatic cancers. *Expert Opin. Investig. Drugs* 24 (6), 781–794. doi:10.1517/13543784.2015.1026963

Kindler, H. L., Niedzwiecki, D., Hollis, D., Sutherland, S., Schrag, D., Hurwitz, H., et al. (2010). Gemcitabine plus bevacizumab compared with gemcitabine plus placebo in patients with advanced pancreatic cancer: Phase III trial of the cancer and leukemia group B (CALGB 80303). *J. Clin. Oncol.* 28 (22), 3617–3622. doi:10.1200/JCO.2010.28.1386

Li, H., Liu, Y., Jiang, W., Xue, J., Cheng, Y., Wang, J., et al. (2021). Icaritin promotes apoptosis and inhibits proliferation by down-regulating AFP gene expression in hepatocellular carcinoma. *BMC Cancer* 21, 318. doi:10.1186/s12885-021-08043-9

Lynn, H., Hahnfeldt, P., and Folkman, J. (2002). Clinical application of antiangiogenic therapy: Microvessel density, what it does and doesn't tell us, JNCI. *J. Natl. Cancer Inst.* 94 (12), 883–893.

Moore, M. J., Goldstein, D., Hamm, J., Figer, A., Hecht, J. R., Gallinger, S., et al. (2007). Erlotinib plus gemcitabine compared with gemcitabine alone in patients with advanced pancreatic cancer: A phase III trial of the national cancer institute of Canada clinical trials group. *J. Clin. Oncol.* 25 (15), 1960–1966. doi:10.1200/jco.2006.07.9525

Morganti, S., Tarantino, P., Ferraro, E., D'Amico, P., Duso, B. A., and Curigliano, G. (2019). Next generation sequencing (ngs): A revolutionary technology in pharmacogenomics and personalized medicine in cancer. *Adv. Exp. Med. Biol.* 1168, 9–30. doi:10.1007/978-3-030-24100-1_2

Qin, L., Shen, J., Yang, Y., and Zou, Z. (2021). Rapid response to the combination of lenvatinib and sintilimab in a pancreatic acinar cell carcinoma patient with elevated alpha-fetoprotein: A case report. *Front. Oncol.* 11. doi:10.3389/fonc.2021.692480

Sahin, I. H., Askan, G., Hu, Z. I., and O'Reilly, E. M. (2017). Immunotherapy in pancreatic ductal adenocarcinoma: An emerging entity? *Ann. Oncol.* 28 (12), 2950–2961. doi:10.1093/annonc/mdx503

Schizas, D., Charalampakis, N., Kole, C., Economopoulou, P., Koustas, E., Gkotsis, E., et al. (2020). Immunotherapy for pancreatic cancer: A 2020 update. *Cancer Treat. Rev.* 86, 102016. doi:10.1016/j.ctrv.2020.102016

Sun, Y., Qin, S., Li, W., Guo, Y., Zhang, Y., Meng, L., et al. (2021). A randomized, double-blinded, phase III study of icaritin versus huachashu as the first-line therapy in biomarker-enriched HBV-related advanced hepatocellular carcinoma with poor conditions: Interim analysis result. *J. Clin. Oncol.* 39, 4077. doi:10.1200/jco.2021.39.15_suppl.4077

Tong, J. S., Zhang, Q. H., Huang, X., Fu, X. Q., Qi, S. T., Wang, Y. P., et al. (2011). Icaritin causes sustained ERK1/2 activation and induces apoptosis in human endometrial cancer cells. *PLoS One* 6 (3), e16781. doi:10.1371/journal.pone.0016781

Van Veldhuisen, E., van den Oord, C., Brada, L. J., Walma, M. S., Vogel, J. A., Wilmink, J. W., et al. (2019). Locally advanced pancreatic cancer: Work-up, staging, and local intervention strategies. *Cancers (Basel)* 11 (7), 976. doi:10.3390/cancers11070976

Yamamoto, Y., Matsui, J., Matsushima, T., Obaishi, H., Miyazaki, K., Nakamura, K., et al. (2014). Lenvatinib, an angiogenesis inhibitor targeting VEGFR/FGFR, shows broad antitumor activity in human tumor xenograft models associated with microvessel density and pericyte coverage. *Vasc. Cell* 6, 18. doi:10.1186/2045-824X-6-18

Yi, M., Jiao, D., Qin, S., Chu, Q., Wu, K., and Li, A. (2019). Synergistic effect of immune checkpoint blockade and anti-angiogenesis in cancer treatment. *Mol. Cancer* 18 (1), 60. doi:10.1186/s12943-019-0974-6

Zhang, Q., Liu, X., Wei, S., Zhang, L., Tian, Y., Gao, Z., et al. (2021). Lenvatinib plus PD-1 inhibitors as first-line treatment in patients with unresectable biliary tract cancer: A single-arm, open-label, phase II study. *Front. Oncol.* 11, 751391. doi:10.3389/fonc.2021.751391

Zhao, C., Gao, F., Li, Q., Liu, Q., and Lin, X. (2019). The distributional characteristic and growing trend of pancreatic cancer in China. *Pancreas* 48, 309–314. doi:10.1097/MPA.0000000000001222

Zhao, Z., and Liu, W. (2020). Pancreatic cancer: A review of risk factors, diagnosis, and treatment. *Technol. Cancer Res. Treat.* 19, 1533033820962117. doi:10.1177/1533033820962117

Zhu, S., Wang, Z., Li, Z., Peng, H., Luo, Y., Deng, M., et al. (2015). Icaritin suppresses multiple myeloma, by inhibiting IL-6/JAK2/STAT3. *Oncotarget* 6 (12), 10460–10472. doi:10.18632/oncotarget.3399

frontiers | Frontiers in Genetics

TYPE Review
PUBLISHED 26 May 2023
DOI 10.3389/fgene.2023.1187985

OPEN ACCESS

EDITED BY
Jian Gao,
Shanghai Children's Medical Center, China

REVIEWED BY
Chen Qi,
Guizhou Provincial People's Hospital, China
Zhuo Wang,
Shanghai Changhai Hospital, China

*CORRESPONDENCE
Yong Yang,
yyxpower@163.com

†These authors have contributed equally to this work and share first authorship

RECEIVED 16 March 2023
ACCEPTED 17 May 2023
PUBLISHED 26 May 2023

CITATION
Li Q, Chen Z, Zhou X, Li G, Zhang C and Yang Y (2023), Ferroptosis and multi-organ complications in COVID-19: mechanisms and potential therapies. *Front. Genet.* 14:1187985. doi: 10.3389/fgene.2023.1187985

Ferroptosis and multi-organ complications in COVID-19: mechanisms and potential therapies

Qi Li[1,2†], Zeyuan Chen[3†], Xiaoshi Zhou[1,2], Guolin Li[1,4], Changji Zhang[1,4] and Yong Yang[1,2*]

[1]Department of Pharmacy, Sichuan Academy of Medical Sciences & Sichuan Provincial People's Hospital, School of Medicine, University of Electronic Science and Technology of China, Chengdu, China, [2]Personalized Drug Therapy Key Laboratory of Sichuan Province, School of Medicine, University of Electronic Science and Technology of China, Chengdu, China, [3]Department of Pharmacy, Luxian People's Hospital, Luzhou, China, [4]School of Basic Medicine and Clinical Pharmacy, China Pharmaceutical University, Nanjing, China

COVID-19 is an infectious disease caused by SARS-CoV-2, with respiratory symptoms as primary manifestations. It can progress to severe illness, leading to respiratory failure and multiple organ dysfunction. Recovered patients may experience persistent neurological, respiratory, or cardiovascular symptoms. Mitigating the multi-organ complications of COVID-19 has been highlighted as a crucial part of fighting the epidemic. Ferroptosis is a type of cell death linked to altered iron metabolism, glutathione depletion, glutathione peroxidase 4 (GPX4) inactivation, and increased oxidative stress. Cell death can prevent virus replication, but uncontrolled cell death can also harm the body. COVID-19 patients with multi-organ complications often exhibit factors related to ferroptosis, suggesting a possible connection. Ferroptosis inhibitors can resist SARS-CoV-2 infection from damaging vital organs and potentially reduce COVID-19 complications. In this paper, we outline the molecular mechanisms of ferroptosis and, based on this, discuss multi-organ complications in COVID-19, then explore the potential of ferroptosis inhibitors as a supplementary intervention for COVID-19. This paper will provide a reference for the possible treatment of SARS-CoV-2 infected disease to reduce the severity of COVID-19 and its subsequent impact.

KEYWORDS

COVID-19, ferroptosis, iron, ROS, GPX4, multi-organ complications, inhibitors

1 Introduction

Due to its rapid spread and rising mortality rate, the pandemic brought on by the severe acute respiratory syndrome coronavirus 2 (SARS-CoV-2), also known as Corona Virus Disease 2019 (COVID-19), has had a significant influence on the entire world. Globally, more than 6.8 million fatalities and over 755 million occurrences of COVID-19 have been reported as of February 2023 (Organization, 2023). Some infected individuals exhibit only mild signs and symptoms like fever, tiredness, and a chronic cough, a subset develops severe COVID-19 (Borges do Nascimento et al., 2020). Patients with severe COVID-19, however, may experience immunological and coagulation abnormalities and organ damage to the lungs, heart, kidneys, brain, liver, and other organs (Mehta et al., 2020). In addition, individuals with varying degrees of COVID-19 severity, including those with mild to

moderate symptoms, often experience neurological, respiratory, or cardiovascular symptoms that can persist for weeks or months, commonly called "post-COVID-19 syndrome" or "long COVID" (Yong, 2021). Although vaccines for COVID-19 are widely available, the emergence of mutant strains of the virus still poses a threat. While antiviral small-molecule oral drugs such as Paxlovid and Molnupiravir have proven to help avoid hospital stays and death in high-risk COVID-19 patients and have been approved for treatment, they have strict population and timing restrictions to use. There have also been reports of recurrent infection and symptom rebound after a 5-day course of therapy with Paxlovid (Rubin, 2022).

Cell death is a two-edged sword in viral infections (Imre, 2020). It can remove cells infected with SARS-CoV-2, thereby inhibiting virus replication and spread. Still, dysregulated cell death can lead to uncontrolled cellular damage and immune responses, contributing to the multi-organ manifestations observed in COVID-19 patients during acute infection and potentially leading to long COVID. Ferroptosis, a type of cell death brought on by the small molecule erastin, was initially identified in 2012 (Dixon et al., 2012). As opposed to apoptosis, a type of programmed cell death, ferroptosis is primarily brought on by a buildup of intracellular lipid reactive oxygen species (ROS), leading to fatal lipid peroxidation (Hadian and Stockwell, 2020). This process is called ferroptosis because iron ion overload is an essential factor in lipid peroxidation. 4-Hydroxynonenal (4-HNE), a breakdown product of lipid peroxidation leading to ferroptosis, can be used as a marker for ferroptosis. The pathology report of a COVID-19 patient in 2020 showed a decreased lymphocyte count and positive staining of the proximal renal tubules and myocardial tissue, suggesting an association between ferroptosis and organ damage caused by COVID-19 (Jacobs et al., 2020). A growing number of studies now suggest a strong link between ferroptosis and COVID-19. This paper discusses the main molecular mechanisms of ferroptosis and its association with multi-organ complications in COVID-19, providing directions for the potential treatment modalities to weaken the effects of COVID-19.

2 Molecular mechanisms of ferroptosis

Production of ROS has been reported to occur in the mitochondrial membrane and the mitochondrial and endoplasmic reticulum membranes (Neitemeier et al., 2017). Mitochondria are the metabolic center in most mammalian cells and are an efficient source of ROS. The imbalance between oxidative and antioxidant systems prevents ROS from being removed. The intrinsic/enzyme-regulated pathways mainly involve the inhibition of glutathione peroxidase 4 (GPX4) (Stockwell et al., 2017). Thus, the primary oxidative and antioxidant mechanisms of ferroptosis are analyzed below.

2.1 Oxidation mechanisms

2.1.1 Lipid peroxidation

Long-chain fatty acids, which contain more than two double bonds, are called polyunsaturated fatty acids (PUFA). PUFA is a critical component of cell membranes and is vital in regulating biological functions, including physiological and immune responses (Gill and Valivety, 1997). Due to the large number of double bonds, PUFA has less stability and is highly sensitive to oxygen (Yin et al., 2011). Arachidonic acid (AA) and adrenic acid (AdA) are the lipids most vulnerable to oxidation. Generally, lipid peroxidation can be divided into two types: enzymatic oxidation (with enzymes) and free radical chain reactions (non-enzymatic), through which PUFA can be oxidized and broken down into toxic derivatives such as 4-HNEs and malondialdehyde (MDA) (Feng and Stockwell, 2018).

Several enzyme species are involved in the type of lipid peroxidation caused by enzyme oxidation (Figure 1). The ROS catalyzed by NADPH oxidase (NOX) is the primary source of ROS in the cellular oxidative stress process. Moreover, enzymes such as lipoxygenases (LOXs) are essential in triggering cell ferroptosis (Doll et al., 2019). LOX can directly oxidize phosphatidylethanolamine-adrenic acid/arachidonic acid (AA/AdA-PE) into peroxide products (AA/AdA-PE-OOH), which are ferroptosis signals. However, the conversion of AA and Ada to AA/AdA-PE cannot occur without acyl-coenzyme A synthase long-chain family member 4 (ACSL4) and lysophospholipid acyltransferase 3 (LPCAT3). After ACSL4 ligated coenzyme A (CoA) to AA/AdA, forming AdA-CoA, LPCAT3 facilitates AdA-CoA esterification in the cell membrane to develop AA/AdA-PE (Kagan et al., 2017). The LOX catalytic process contributes to the LOOH cell pool and makes the cells sensitive to ferroptosis. However, some cell lines susceptible to ferroptosis do not express any significant LOX (Shah et al., 2018). Therefore, LOX may not be required in ferroptosis. Non-enzymatic lipid peroxidation is powered by carbon and oxygen-centered free radicals, such as ferroptosis triggered by an iron-dependent free radical mechanism, where it undergoes a free radical chain reaction of lipid peroxidation (Shah et al., 2018).

2.1.2 Iron cycle

Fenton reaction, the oxidation of Fe^{2+} and H_2O_2, catalyzes the production of ROS and is the beginning of the non-enzymatic reaction of lipid peroxidation (Hendren et al., 2020). Iron overload is an indispensable link to turning on lipid peroxidation with a critical position in inducing ferroptosis (Figure 2). Usually, iron is absorbed from the intestine into the body as ferrous ions (Fe^{2+}) and subsequently oxidized to ferric ions (Fe^{3+}). The primary protein for transporting iron is transferrin. Iron ions bind to transferrin outside the cell and then attach to membrane transferrin receptor 1 (TFR1), entering the cell through endocytosis and colonizing the endosome (Andrews and Schmidt, 2007; Frazer and Anderson, 2014). Upon entry into the cell, in acidic endosomes, the six transmembrane epithelial antigens of prostate 3 (STEAP3) decrease Fe^{3+} to Fe^{2+}. Fe^{2+} is transported to the cytoplasm via divalent metal transporter protein 1 (DMT1) and eventually liberated into the cytoplasm and mitochondria to form a labile iron pool (LIP). In contrast, excess iron, which forms redox-inactive heterogeneous polymers, is stored in ferritin to protect tissues and cells from damage (Ryu et al., 2017; Philpott, 2018). Ferroportin (FPN), the only known mammalian protein, can export intracellular iron out of cells when needed (Ganz, 2005). Iron import, storage, and export imbalance lead to iron overload (Stockwell et al., 2017).

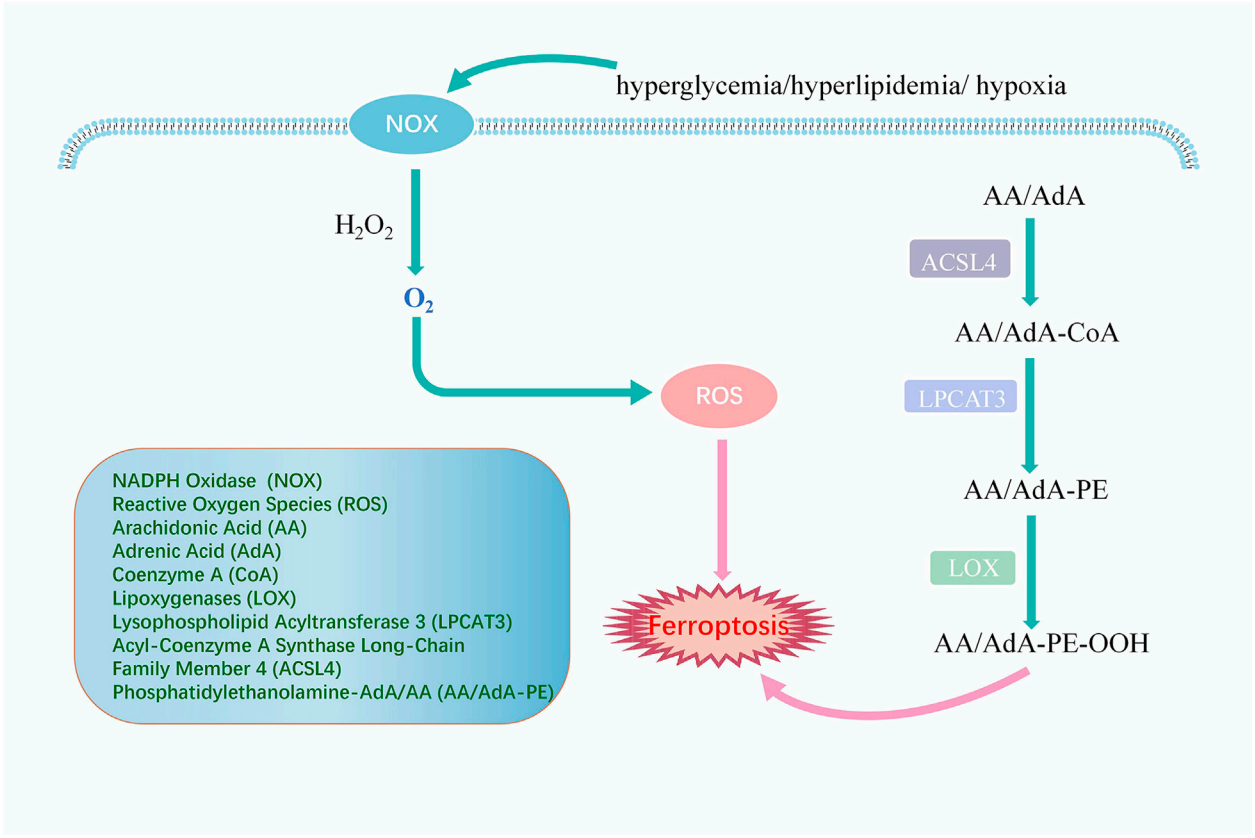

FIGURE 1
The Signaling Pathway of lipid peroxidation. In hyperglycemia, hyperlipidemia, and hypoxia, NOX catalyzes the reaction of H_2O_2 with lipids to produce ROS, leading to ferroptosis. ACSL4 attaches coenzyme A (CoA) to AA/AdA forming AdA-CoA, then LPCAT3 facilitates AdA-CoA esterification in the cell membrane to form AA/AdA-PE which could be directly oxidized to AA/AdA-PE-OOH by LOX, eventually causing ferroptosis.

Worthy of mention is that nuclear receptor coactivator 4 (NCOA4) can promote iron storage or release from ferritin and plays a crucial function in maintaining a dynamic balance of intracellular iron. Indeed, when cellular iron levels are low, ferritinophagy, cell-selective autophagy mediated by NCOA4, can degrade ferritin, leading to the release of ferritin-bound iron as free iron (Santana-Codina and Mancias, 2018). The evidence has shown that NCOA4-mediated degradation of proteins may also be an essential mechanism for the occurrence of ferroptosis. Additionally, Haeggstrom and Funk (2011) introduced the notion of atypical ferroptosis in 2008, demonstrating that an increase in the intracellular LIP caused by iron overload leads to the over-activation of heme oxygenase-1 (HO-1), which ultimately induces atypical ferroptosis.

2.2 Antioxidant system

Lipid peroxidation could induce ferroptosis. If the antioxidant is deactivated in the cell, lipid peroxides cannot be removed and thus accumulate, eventually leading to cellular damage and death (Figure 3). Glutathione (GSH) and oxidized glutathione (GSSG) are widely available in cells for controlling intracellular oxidation levels. GSH is mainly available in the cytoplasm and, to a lesser extent, in organelles such as mitochondria and is involved in many biological processes (Dolma et al., 2003). GSH is equipped with the biological function of scavenging ROS to play a crucial role in preventing ferroptosis. Cysteine is an essential precursor of GSH. The solute carrier family seven-member 11 (SLC7A11) and the solute carrier family three member 2 (SLC3A2) comprise the heterodimer referred to as system Xc-, a cysteine and glutamate reverse system (Chen et al., 2021). The system Xc-allows cysteine to enter the cell in its oxidized form and reduces it again to cysteine within the cell.

Glutathione peroxidase 4 (GPX4) is an oxidation inhibitor protein and belongs to the selenoproteins. GPX4 protects cells from lipid peroxidation by catalyzing the occurrence of reduction reactions, of which GSH is the most prevalent reducing agent (Ursini et al., 1995). GPX4 converts GSH to GSSG and also returns the phospholipid polyunsaturated fatty acid peroxides (PL-PUFA-OOH) to the corresponding phosphatidyl alcohol (PL-PUFA-OH) for reducing the accumulation of peroxidized lipids and inhibiting ferroptosis (Florez and Alborzinia, 2021). As a phospholipid hydroperoxide, Gpx4 is expressed or active under the regulation of selenium and GSH. Inhibition of the GPX4-GSH-cysteine axis is a significant factor contributing to ferroptosis.

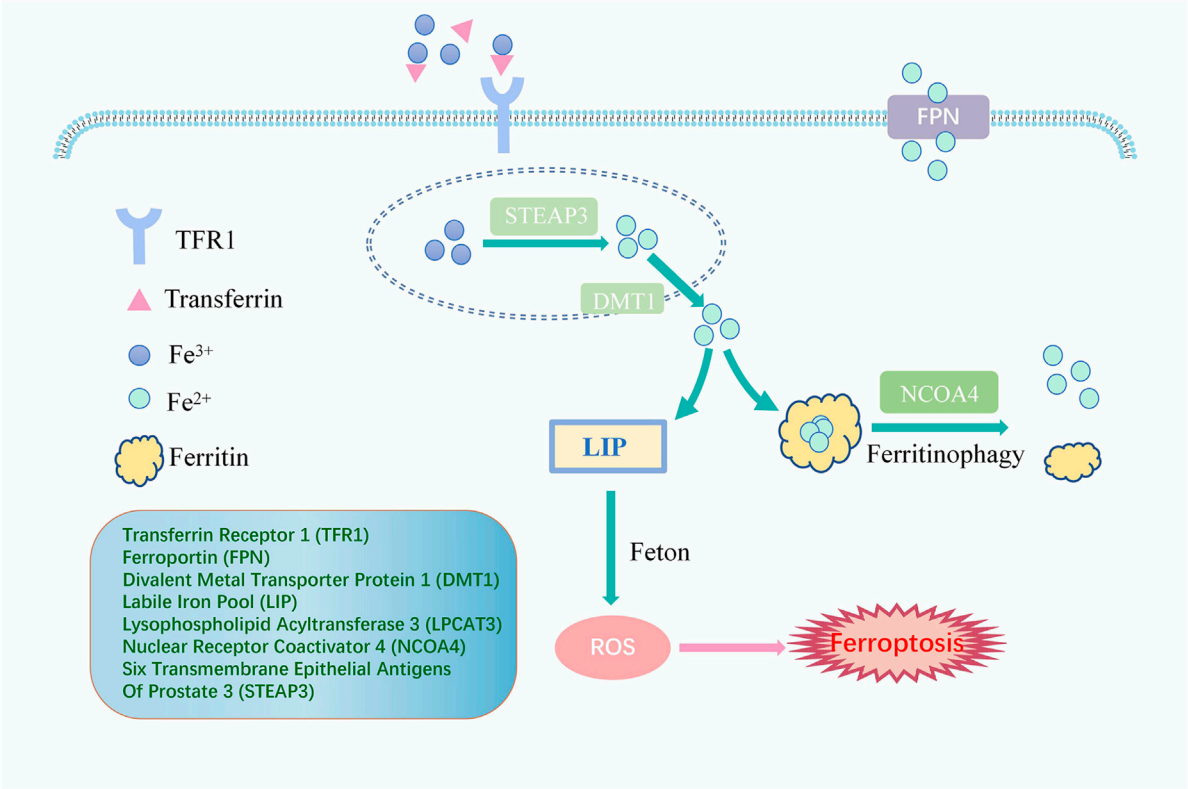

FIGURE 2
The Signaling Pathway of lipid peroxidation iron cycle. Fe^{3+} binds to transferrin outside the cell and then attaches to TFR1, entering the cell. Fe^{3+} is converted to Fe^{2+} by STEAP3. Fe^{2+} is transported to the cytoplasm via DMT1 to form a LIP which happens Fenton reaction, and excess iron is stored in ferritin. Ferritinophagy, mediated by NCOA4, can degrade ferritin, releasing ferritin-bound iron as free iron, and FPN exports intracellular iron out of cells when needed. Free iron generates ROS through the Fenton reaction, eventually leading to ferroptosis.

3 Association between ferroptosis and COVID-19

3.1 Signitures of ferroptosis in COVID-19 multi-organ complications

Although respiratory symptoms are the most common symptom of COVID-19, severe patients may experience pulmonary, cardiac, nephritic, neurological, gastric, and hepatic damage, as well as impaired immune and coagulation function (Gupta et al., 2020) (Figure 4). Moreover, some patients with long COVID may suffer from persistent dyspnea, chest pain, headache, and decreased mental status even after negative SARS-CoV-2 RNA tests or weeks to months following initiation of the disease. These symptoms appear to be common in heavy patients and groups of young people or children who do not require respiratory support, affecting the patient's daily routine and survival after infection.

Angiotensin-converting enzyme 2 (ACE2) has been reported to be a common viral receptor (Perico et al., 2020). During infection, SARS-CoV-2 forms a complex by binding the tegument-expressed stinging protein (protein S) to the viral receptor ACE2, after which the complex is endocytosed, and the virus enters the host cell. The virus binds to ACE2 present in lung cells to infect the organism, resulting in symptoms including mild upper respiratory symptoms or severe dyspnea. The lungs of dead patients due to COVID-19 can be seen: severe endothelial damage, intracellular SARS-CoV-2, and extensive microangiopathy with vascular thrombosis (Ackermann et al., 2020). ACE2, a crucial enzyme of the renin-angiotensin-aldosterone system (RAAS), is expressed in multiple organs all over the system and is vital in sustaining blood pressure and cardiovascular, renal, immune, and nervous system homeostasis. Considering the association of SARS-CoV-2 and ACE2, Patel et al. (2017) have hypothesized that COVID-19 can cause an imbalance in RAAS. The broad distribution of ACE2 throughout the body may explain the extra-pulmonary manifestations of COVID-19, and it supports the idea that SARS-CoV-2 infection is a multi-system disease affecting the lungs. However, the pathogenesis of long COVID is not yet conclusive. The most supported theory is that it occurs through an autoimmune process with exaggerated innate immune responses and cytokine activation (Lechner-Scott et al., 2021). Ferroptosis plays an important role in the immune response and cytokine activation induced by SARS-CoV-2. In the late stages of infection, various cell deaths, including ferroptosis, promote inflammatory cytokine release, exacerbating immune and inflammatory system dysfunction and causing associated damage

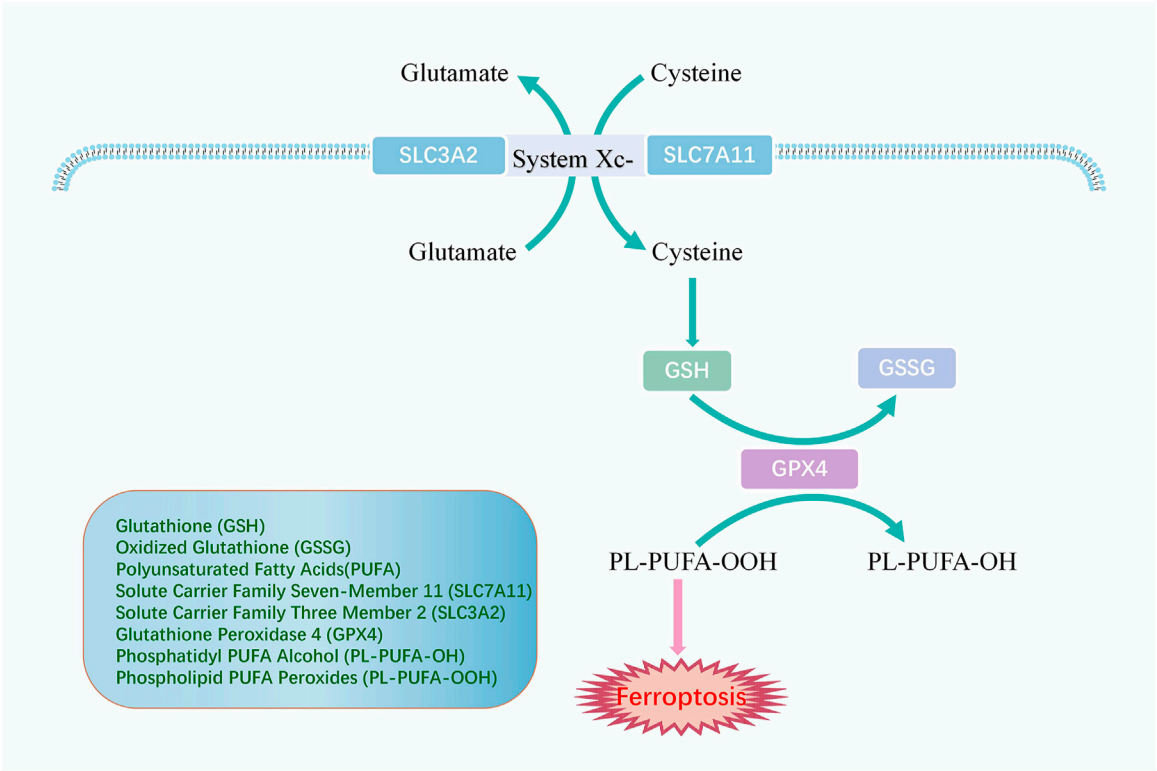

FIGURE 3
The mechanism of antioxidant system. System Xc-comprises SLC3A2 and SLC7A11 and promotes cellular uptake of cysteine, an essential precursor for GSH synthesis. GPX4 converts GSH to GSSG and returns PL-PUFA-OOH to the PL-PUFA-OH, achieving ferroptosis resistance.

that ultimately leads to COVID-19 multi-organ complications (Sun et al., 2022). We describe the frequent organ complications in COVID-19 and ferroptotic signitures below.

3.1.1 Heart

Data indicate that the heart is the second most affected organ with the entry of SARS-CoV-2 into the host through binding to ACE2 (Zou et al., 2020). Commonly reported cardiovascular complications involving COVID-19 include myocardial injury, acute myocardial infarction (AMI), and arrhythmias. Severe patients are usually accompanied by increased cardiovascular complications, including thoracic pain, tachypnea, fainting, tachycardia, and other common symptoms (Zou et al., 2020). Infection with the virus in the coronary region could trigger thrombosis and lead to acute coronary syndrome (Chieffo et al., 2020). Moreover, patients with COVID-19 who have underlying cardiovascular disease have been proven to have a higher chance of poor prognosis (Guo et al., 2020; Ni et al., 2020). However, given the limited evidence of direct cardiac infection by SARS-CoV-2 in animal models and patient autopsy samples, Nishiga et al. (2022) suggested that cardiac injury in COVID-19 could also be an indirect result of the cytokine storm. For example, ferroptosis during acute SARS-CoV-2 infection triggers the death of sinus node pacing cells, causing irreversible sinus node damage and ultimately leading to bradycardia (Han et al., 2022). Activation of the ferroptosis signaling pathway by viral infection may explain part of the mechanism of COVID-19 cardiovascular complications.

3.1.2 Brain

Clinical data reveal that central nervous system symptoms are present in 36% of patients with COVID-19 (Mao et al., 2020). Inflammation and hypoxia in the brain caused by SARS-CoV-2 infection can impact the center nerve system, leading to various neuropsychiatric symptoms such as cognitive impairment, insomnia, and anxiety that can last for months after the respiratory symptoms have subsided (Boldrini et al., 2021). ACE2 is more abundant in the brainstem than in other brain regions. The viral proteins of SARS-CoV-2 and the evidence of pathological immunity were discovered in dead patients' brainstems (Matschke et al., 2020). Furthermore, ferroptosis is connected with the pathology of several neuronal degeneration diseases, such as the Alzheimer as well as the Parkinson. It is hypothesized that the virus can damage the brain either through direct infection of the brain tissue or by inducing a series of pro-inflammatory and immune response pathways. Ferroptosis, associated with neuroinflammatory processes, may promote brain damage and psychiatric symptoms emerging in COVID-19 patients. Brain injury disorders, including cerebrovascular lesions, ischemic stroke, and cerebral hemorrhage, have been observed in COVID-19 patients. Furthermore, critically unwell patients have a high rate of brain injury than those who are not critically ill (Koralnik and Tyler, 2020; Lee et al., 2021).

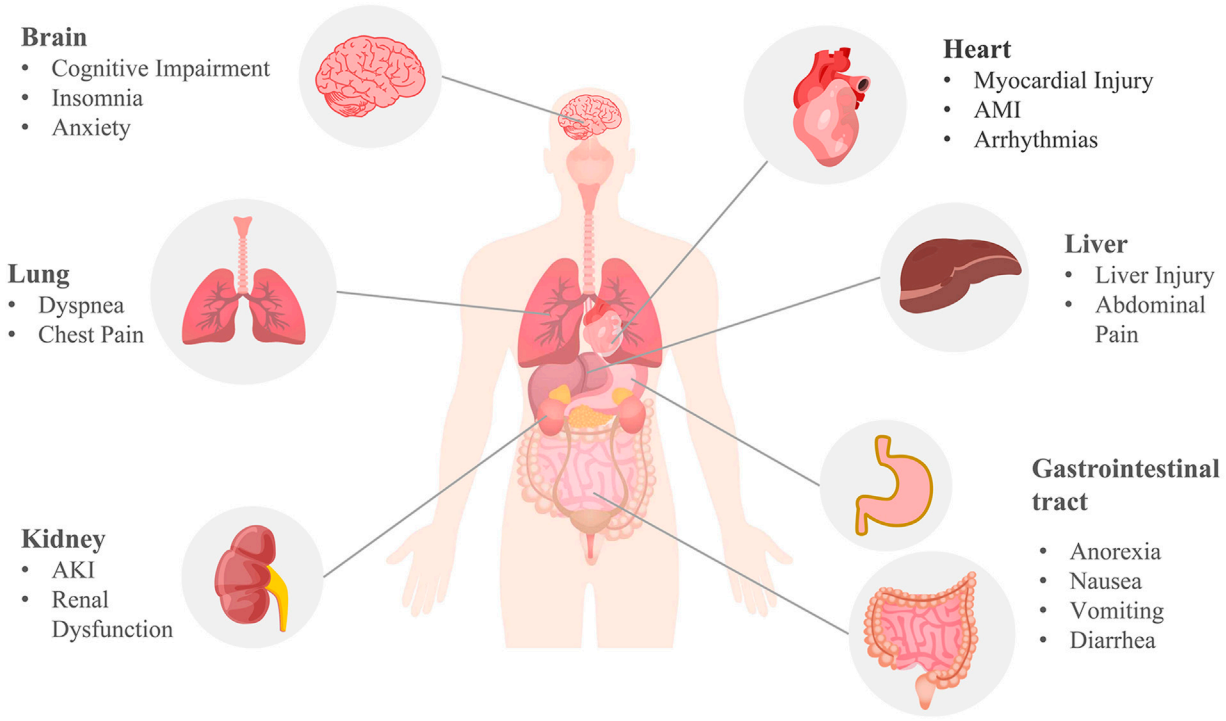

FIGURE 4
Multi-organ complications of COVID-19. COVID-19 involves the lungs, heart, brain, kidneys, liver, and gastrointestinal tract. Pulmonary symptoms include dyspnea and chest pain; common cardiovascular complications include myocardial injury, acute myocardial infarction (AMI), and arrhythmia; brain complications often include cognitive impairment, insomnia, anxiety, and other central nervous symptoms; acute kidney injury (AKI) and renal dysfunction are the main renal manifestations; anorexia, nausea, vomiting, diarrhea, abdominal pain, and liver injury are common digestive symptoms of COVID-19. The mechanism of COVID-19 multi-organ complications may be correlated with ferroptosis.

Therefore, severe SARS-CoV-2 infection has a strong potential to cause an acute stroke.

3.1.3 Kidney

The kidney is one of the most frequently attacked targets of SARS-CoV-2. Acute kidney injury (AKI) is the most commonly observed renal impairment in clinical practice, and its pathogenesis is believed to be multifactorial. AKI could be brought on by the virus itself, hypoxia, or shock (Amann et al., 2021). Clinical studies have revealed that severe COVID-19 patients, even without a history of renal disease, can develop renal dysfunction or impairment (Ronco et al., 2020). Autopsy data from COVID-19 patients have indicated SARS-CoV-2 was present in various renal compartments, particularly in the parenchyma of the kidney, cells of glomerular epithelial, endothelial, and tubular (Puelles et al., 2020). An analysis conducted in the United Kindom has revealed that COVID-19 patients with chronic kidney disease had a higher mortality risk than those with other recognized risk factors, such as chronic cardiopulmonary disease (Williamson et al., 2020). Infecting SARS-CoV-2 could induce renal dysfunction or injury in patients without underlying renal disease and aggravate pre-existing renal damage, thereby increasing mortality risk. The virus can cause kidney injury through direct infection with ACE2, which is widely expressed in different kidney regions. Additionally, SARS-CoV-2 can aggravate kidney injury by inducing coagulation dysfunction or cytokine and complement activation. The kidney is vulnerable to oxidative stress, and excessive accumulation of ROS can cause kidney injury. Therefore, disruption of lipid metabolism is considered a common mechanism for the progression of various types of kidney diseases (Ratliff et al., 2016; Zhou et al., 2022). Inhibition of ferroptosis might have an improving effect on kidney injury induced by SARS-CoV-2 infection.

3.1.4 Gastrointestinal tract

ACE2 is also expressed in the digestive system, including the duodenum, jejunum, and liver (Li et al., 2020). Therefore, the digestive system is susceptible to SARS-CoV-2 infection. Patients infected with SARS-CoV-2 frequently present with digestive symptoms in addition to the commonly reported respiratory symptoms. Anorexia, nausea, vomiting, diarrhea, abdominal pain, and liver injury are common digestive symptoms of COVID-19 and may appear during infection or after negative SARS-CoV-2 RNA tests (Chen et al., 2020; Brussow and Timmis, 2021). Diarrhea is the most frequently observed gastrointestinal symptom among COVID-19 patients. A study found viral RNA in stool samples from almost half of the patients, including those with negative respiratory tests (Cheung et al., 2020). SARS-CoV-2 infection can disrupt the adhesion and tight junctions between the endothelium and intestinal epithelium, leading to dysbiosis of the intestinal flora and immune activation (Guo et al., 2021). The virus causes damage to the gastrointestinal tract by activating innate immune cells and promoting the release of inflammatory factors, leading to a cytokine

10.3389/fgene.2023.1187985

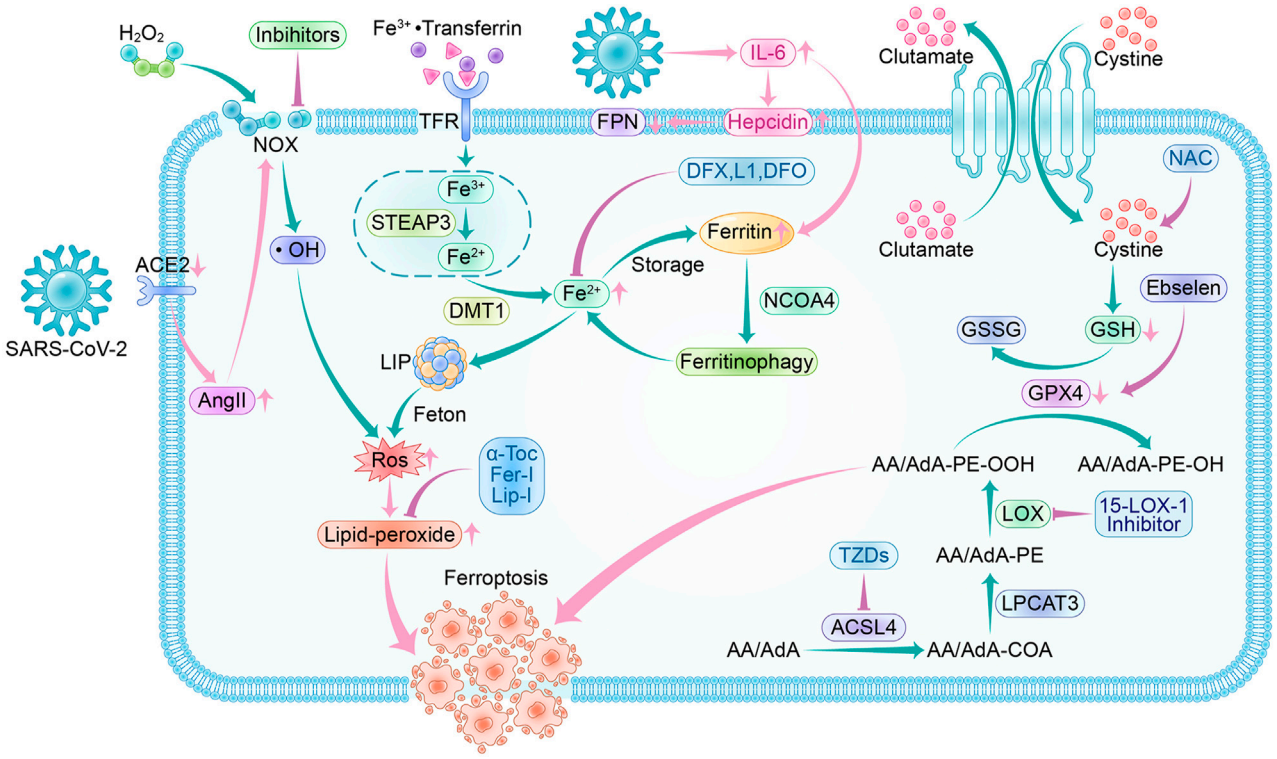

FIGURE 5
Ferroptosis pathway and inhibitors in SARS-CoV-2 infection. Crossover of SARS-CoV-2 infection and ferroptosis pathway:SARS-CoV-2 invades cells by binding to ACE2, and a feedback increase in circulating AngII triggers NOX activation leading to increased ROS production. During the acute phase of SARS-CoV-2 infection, a surge in IL-6 promotes hepcidin and ferritin synthesis. Hepcidin decreases FPN expression levels, resulting in a decrease in intracellular free iron output. The increased ferritin guarantees intracellular iron storage, and in inflammatory conditions, ferritin is degraded to release free iron, leading to a raised LIP, which generates ROS through the Fenton reaction. SARS-CoV-2 infection depletes intracellular GSH and attenuates Gpx4 activity, exacerbating lipid peroxidation. Ferroptosis inhibitors: NOX inhibitor, 15-LOX-1 inhibitor, and ACSL4 inhibitor-thiazolidinediones (TZDs) are the main oxidase inhibitors; α-Tocopherol (α-Toc), ferroportin-1 (Fer-1) and Liproxstatin-1 (Lip-1) can trap peroxyl radicals; they can prevent lipid peroxidation from occurring. Desferrioxamine (DFO), deferiprone (L1), and deferasirox (DFX) can form complexes with iron to reduce LIP, thus interrupting lipid peroxidation caused by iron overload. Ebselen acts as a selenium supplement to maintain GPX activity and N-acetylcysteine (NAC) increases GSH levels *in vivo*; they enhance the XC--GSH-Gpx4 axis to reduce lipid peroxide accumulation to resist ferroptosis.

storm. After SARS-CoV-2 infects gastrointestinal cells via ACE2 may lead to RAAS dysregulation, exacerbating ionic imbalance and inflammation, affecting cellular metabolic status, flora composition, and cell viability, resulting in increasing gastrointestinal dysfunction in COVID-19 patients (Megyeri et al., 2021).

3.1.5 Liver

The liver is an essential part of the digestive system with immune function and contains many cells associated with immune response. After the virus infects the liver, immune cells may become over-activated and secrete a large number of inflammatory factors, leading to cytokine storm and inducing ferroptosis, resulting in lung injury and ischemia, and hypoxia. Ischemia and hypoxia trigger systemic inflammatory response syndrome (SIRS), which can cause damage to vital organs throughout the body, including further liver cell damage and death (Tian and Ye, 2020). Therefore, ferroptosis may be one of the critical mechanisms of COVID-19 liver injury. It is worth noting that the expression of ACE2 in hepatocytes increases under liver fibrosis/cirrhosis conditions (Paizis et al., 2005). Patients with underlying liver disease and COVID-19 are more likely to suffer from viral attacks on their liver and are at a greater risk of developing severe COVID-19.

3.2 Link between SARS-CoV-2 infection and ferroptosis signaling pathway

Most patients who have acute COVID-19 exhibit significantly elevated serum levels of pro-inflammatory cytokines. This can cause a cytokine storm, leading to an abnormal systemic inflammatory response. Once the cytokine storm occurs, the immune system response becomes uncontrollable and can attack multiple tissues and organs of the body, causing multi-organ damage (Xu Z. et al., 2020). COVID-19 patients also experience systemic hyperinflammation, characterized by elevated ROS and cytokine storm (Girelli et al., 2021). As a result, there may be a link between SARS-CoV-2 infection and the ferroptosis signaling pathway. Using ferroptosis inhibitors to block the signaling pathway may reduce the multi-organ damage caused by SARS-CoV-2 (Figure 5).

3.2.1 Lipid peroxidation and coagulation in SARS-CoV-2 infection

It was demonstrated that angiotensin II (Ang II), hyperglycemia, hyperlipidemia, or hypoxia are associated with NOX activation, leading to excessive production of mitochondrial ROS (Dikalov and Nazarewicz, 2013). SARS-CoV-2 invades cells by binding to ACE2, which leads to downregulation of ACE2 and feedback increased Ang II in the circulation, thus triggering NOX activation, resulting in oxidative stress and inflammation (Hikmet et al., 2020). Clinical observations indicate that thrombotic complications have become an essential issue in patients with COVID-19 (Guan et al., 2020). It has been reported that NOX2 was triggered in COVID-19, with higher values in critically ill patients than in non-critically ill patients, strongly linked to thrombotic events (Violi et al., 2020).

Inflammation initiates coagulation through tissue factor TF, which is present in monocytes and vascular endothelial cells (Iba et al., 2019). Oxidative stress products have been shown to promote TF expression and initiate monocyte inflammatory programs. At the same time, activated endothelial cells are fully responsible for initiating coagulation using TF-expressing inflammatory monocytes (Owens et al., 2012; von Bruhl et al., 2012). The accumulation of lipid peroxidation products in the COVID-19 patients' lungs and cardiovascular system may also be involved in the process of coagulation initiation (Merad and Martin, 2020), contributing to a hypercoagulable state of blood in patients. A clinical study supported the association of COVID-19 severity with a hypercoagulable state (Helms et al., 2020). The dislodgement of the formed thrombus caused by the hypercoagulable state leads to fatal complications such as strokes in patients. In addition, iron oxide accelerates serum coagulation by interacting with coagulation cascade proteins. Methemoglobinemia and free iron may also contribute to the COVID-19 hypercoagulable state (Jankun et al., 2014). Lipid peroxidation and iron overload are ferroptosis-related factors, so we speculate that the increased incidence of cardiovascular and cerebrovascular complications in patients with moderate to severe COVID-19 may be related to iron death.

3.2.2 Iron metabolism in SARS-CoV-2 infection

It has been shown in clinical studies that COVID-19 patients have abnormal iron metabolism, with patients having low serum iron levels but elevated serum iron levels after treatment (Bellmann-Weiler et al., 2020; Zhao et al., 2020). Besides, those COVID-19 patients with significantly lower serum iron concentrations and transferrin levels are commonly anemic, indicating a potential inverse relationship between serum iron levels and the severity of COVID-19. Hepcidin, an antimicrobial cysteine-rich peptide synthesized and secreted by the liver, is abundantly expressed during the immune process and plays a role in regulating iron homeostasis in the body. It could regulate the expression levels of iron transport-related proteins, especially FPN, to decrease iron export from cells and increase iron storage. During the emergency phase of SARS-CoV-2 infection, the abrupt increase of IL-6 in a highly inflammatory state promotes the synthesis of hepcidin and ferritin.

Additionally, pathogens' iron may be deprived and coupled with transferrin to enter cells via TFR1, increasing the amount of intracellular iron. Iron can be sequestered in cells by hepcidin, leading to decreased iron efflux from cells, while increased ferritin allows sufficient iron stores. Notably, it has been suggested that ferritin leaks out of cells damaged by inflammation, having lost most of its iron in the process, and that iron remains in the cell unconnected (Kell, 2010). A rise in intracellular free iron caused by the above pathways may explain the decrease in serum iron levels in patients with COVID-19. It may trigger further cellular damage, which ultimately results in ferroptosis. In severe COVID-19, as a consequence of cell death and tissue damage, intracellular ferritin is released out of the cells, with excess ferritin accumulating in the body to form hyperferritinemia (Kell and Pretorius, 2014). Therefore, elevated serum ferritin levels are typically linked to systemic inflammation. Methemoglobinemia is largely considered to be an indicator of severe COVID-19 correlation. In hospitalized COVID-19 patients, the risk of death increases roughly nine-fold when blood ferritin levels exceed 300 μg/L (Goldberg et al., 2020).

3.2.3 Antioxidant system in SARS-CoV-2 infection

Endogenous GSH deficiency may be closely related to factors such as age, gender, and concurrent chronic. Viral replication accelerates cysteine depletion, and COVID-19 patients are vulnerable to endogenous GSH depletion which has been demonstrated to function as a critical player in specific viral infections (Polonikov, 2020). A study showed that a decrease in GSH was linked to more ROS and complications, so patients with increased GSH levels had reduced ROS production and faster recovery (Horowitz et al., 2020). As an important antioxidant and free radical scavenger in the body, GSH is synthesized in the liver and functions in hepatic biochemical metabolism. One of the key contributors to liver damage in COVID-19 may be the formation of lipid peroxides brought on by GSH shortage, which in turn accelerates GSH depletion and exacerbates endogenous GSH insufficiency. Besides, immune responses induced by SARS-CoV-2 infection may also contribute to liver damage as one of the common factors (Bangash et al., 2020).

An underlying study infected African green monkey kidney (Vero) cells with SARS-CoV-2 and found that SARS-CoV-2 resulted in a significant reduction in mRNA expression of endoplasmic reticulum-resident selenoproteins, which is strongly correlated with selenium by GPX4 expression or activity, so infection with SARS-CoV-2 may be related to suppression of GPX4 (Wang et al., 2021). Available data suggest that infecting with SARS-CoV-2 would induce low levels of GSH and decreased expression of GPX4 protein, both of which are essential aspects of ferroptosis (Dixon et al., 2012). Ferroptosis may explain the clinical phenomenon that severe COVID-19 patients without a background of renal disease nevertheless develop renal dysfunction or impairment (Cheng et al., 2020). Notably, GPX4-deficient T cells undergo rapid accumulation of lipid peroxide (Matsushita et al., 2015). Eventually, the T cells go into ferroptosis due to the lack of GPX4, resulting in a weakened body defense system unable to effectively defend against viral infections, which may be one of the crucial reasons for COVID-19 progressing to severity.

4 COVID-19 potential treatment based on ferroptosis

Using ferroptosis inhibitors to block the signaling pathway may reduce multi-organ damage from SARS-CoV-2 infection. Both

enzymatic and non-enzymatic processes in mammalian cells can generate ROS, leading to lipid peroxidation. The two primary categories of methods to block this process are oxidase inhibitors and lipid autoxidation inhibitors. Free iron is a crucial factor in the induction of ROS production, and controlling its levels *in vivo* is critical for preventing ferroptosis. Iron chelating agents and hepcidin inhibitors are two effective methods for reducing free iron levels. Additionally, maintaining appropriate levels of GSH and activity of GPX4 expression is crucial for the GPX4-GSH-cysteine axis to function effectively against ferroptosis. Some treatments for viral infections have also been found to inhibit ferroptosis, potentially reducing complications of COVID-19.

4.1 Inhibitors of lipid peroxidation

4.1.1 Oxidase inhibitors

In lipid peroxidation with the involvement of oxidases, oxidase inhibitors can reduce the production of ROS and inhibit ferroptosis. 15-LOX-1 inhibitors may block ferroptosis and have positive performance in treating ischemic and hemorrhagic stroke (Yigitkanli et al., 2013; Wenzel et al., 2017). This may offer an alternative direction for improving brain injury in COVID-19 patients. Currently, a variety of NOX inhibitors with new structures are emerging. However, due to the short research period, some NOX inhibitors are still in the preliminary research stage, except for a few inhibitors under clinical trials. Recent studies, however, have revealed that AA metabolites of the LOX pathway have a signal link with NOX and can activate NOX-mediated ROS production in various cells (Cho et al., 2011). Consequently, we turned to the LOX pathway of AA and found a complex tissue-specific interaction between LOX and GPX4 (Brutsch et al., 2016). LOX has many isoforms. It has been reported that inhibition of multiple lipoxygenases is more protective for cells than targeted inhibition of a single lipoxygenase (Yang et al., 2016). Regrettably, more studies are necessary to validate how oxidase inhibitors impact ferroptosis.

As mentioned previously, ACSL4 is essential for the oxidation of AA by LOX. Therefore, the inhibition of ferroptosis could be achieved if ACSL4 is inhibited from interrupting the process of lipid peroxidation. Studies have shown significant resistance to ferroptosis for ACSL4-deficient cells even when the GPX4 gene was inactivated (Doll et al., 2017), adding to the conviction that ACSL4 may act as a target for ferroptosis inhibition. The peroxisome proliferator-activated receptor γ (PPARg) agonist, thiazolidinediones (TZDs), selectively inhibits ACSL4 (Kim et al., 2001). TZDs like rosiglitazone (Rosi), pioglitazone (PIO), and troglitazone (Tro), show significant inhibition in a model of ferroptosis cells induced by the ferroptosis inducer RSL-3. Both ACSL4-deficient and Acsl4-non-deficient cells treated with Rosi demonstrated a decrease in AA/AdA-PE (Doll et al., 2017). By inhibiting ACSL4, TZDs are believed to reduce the availability of substrates and prevent lipid peroxidation. It has been reported that the ACSL4 inhibitor Rosi mitigated pathological kidney and lung injury based on inhibiting cellular ferroptosis (Xu Y. et al., 2020; Wang et al., 2022), which may give hope for the treatment of COVID-19 complicated by multi-organ injury. Moreover, TZDs have been developed as an insulin sensitizer and may be optional for COVID-19 patients with underlying diabetes. More clinical trials are expected to validate the safety and efficacy of TZDs for ferroptosis inhibition.

4.1.2 Lipid autoxidation inhibitors

In non-enzymatic lipid peroxidation, lipid autoxidation inhibitors represented by RTAs protect lipids from autoxidation. RTAs are compounds that can interact with chain-carrying radicals. They are also referred to as chain-breaking antioxidants. α-Tocopherol (α-Toc), the most biologically active form of vitamin E, is a characterization of the activity in RTAs (Burton and Ingold, 2002). α-Toc is a typical antioxidant that traps peroxyl radicals and exceeds the ability of other lipid substrates to be oxidized by peroxyl radicals. Interestingly, vitamin E has recently been reported to have another possible function - direct inhibition of lipoxygenases, which may be achieved by competing for the substrate binding site with lipoxygenases (Kagan et al., 2017). As COVID-19 therapeutic agents, vitamin E supplements can reduce the damage caused by ferroptosis with several organs, including the lungs, kidneys, liver, intestines, heart, and nervous system. Furthermore, phenprocoumon, a vitamin K antagonist, was shown to significantly exacerbate ferroptotic cell death *in vitro* and significantly worsen the course of AKI in mice (Kolbrink et al., 2022). Vitamin K, as an antioxidant, can also prevent lipid peroxidation and thus inhibit ferroptosis, which has a therapeutic effect in COVID-19 patients with AKI.

In addition, ferroportin-1 (Fer-1) and Liproxstatin-1 (Lip-1) have been recognized in recent years as RTAs that effectively inhibit ferroptosis because of their ability to trap peroxyl radicals with acyl chains in lipid bilayers, having a strong activity to slow down the accumulation of lipid peroxides (Zilka et al., 2017). Fer-1 and Lip-1 are more potent in terminating lipid peroxidation compared to α-Toc. It may attribute to the fact that they are subsequently converted to nitrogen oxides, which are good RTAs (Haidasz et al., 2016). In the works of Krainz et al. (2016), Fer-1 and Lip-1 could inhibit ferroptosis in an *in vitro* cellular system. Lip-1 was the first Liproxstatin-like molecule to be identified, and it showed good pharmacological properties in the low nanomolar range with a short plasma half-life. In animal experiments, Lip-1 has been shown to effectively reduce liver and kidney-related disorders such as fatty liver and renal fibrosis by inhibiting ferroptosis (Zhang et al., 2021; Tong et al., 2023). Importantly, such molecule was shown to counteract acute renal failure in a Gpx4-deficient model and to have ferroptosis-inhibiting activity *in vivo* (Friedmann Angeli et al., 2014). Fer-1 eliminates lipid hydroperoxides in the presence of iron reduction. Fer-1 might interact with iron, as same as other antioxidants or complexing molecules, forming complexes to reduce lipid peroxidation formation. It has demonstrated that Fer-1 can effectively inhibit the oxidation of cell membranes and possess a notable protective effect on AKI (Skouta et al., 2014). Further studies are necessary to support the hypothesis that such inhibitors can reduce the complications of COVID-19. Although Fer-1 and Lip-1 are generally considered safe, there are limited studies on their potential adverse reactions. Therefore, it is imperative to exercise caution in the dose control of future *in vivo* trials.

4.2 Iron depletion methods

Free iron can catalyze the production of ROS in Fenton reaction, and excessive production of ROS in the presence of iron overload can lead to oxidative stress and damage DNA, lipids, and proteins (Evans et al., 2004). Therefore, excess iron can lead to cellular damage, which is harmful to the organism. The SARS-CoV-2 requires iron to replicate and function. As described previously in 3.3.2, LIP increases during the acute phase of infection by a mechanism involving the deprivation of additional iron from the pathogen. Currently, the treatment for iron overload is usually iron chelation therapy. This treatment uses iron complexing agents to compete with the body's natural chelator transferrin for iron and reduce LIP to interrupt the iron-catalyzed lipid peroxidation process. Desferrioxamine (DFO), deferiprone (L1), and deferasirox (DFX) are the three types of iron chelators most frequently used in the globe.

DFO is a clinically used iron chelator derived from *streptomyces* polymyxa and is a hexadentate complex that forms a 1:1 Fe^{3+}/DFO complex at physiological PH. DFO is generally administered intravenously for a prolonged period, requiring five to 7 days of infusion a week. For this reason, oral iron chelators have become a common choice (Franchini and Veneri, 2004). L1, an FDA-approved oral iron chelator, is a bidentate chelator that forms 3L1-1Fe complexes with iron and is comparable in efficacy to DFO. L1 is rapidly absorbed after oral administration, usually peaking 45 min after ingestion, and the widely adopted recommendation is to take three doses of L1 daily (Banerjee et al., 2019). Notably in COVID-9 patients, L1 can restore T cell resistance to the virus infection by increasing the expression of IFN-R2 on the surface of activated T cells (Regis et al., 2005; Perricone et al., 2020). DFX is also a commonly used oral iron chelator, a tridentate complex that can form 2DFX-1Fe complexes with iron, and its efficacy is also comparable to that of DFO. DFX reaches peak blood levels within one and a half to 4 h after oral administration, with a half-life ranging from 8 to 16 h, and is generally administered once daily (Stumpf, 2007). DFX and DFO have been reported to reduce tissue fibrosis by inhibiting free radical production and tissue infiltration of macrophages and significantly reducing IL-6 levels (Darwish et al., 2015). Therefore, DFX and DFO can treat COVID-19 patients with tissue damage caused by increased LIP and subsequent liver injury complicated by fibrosis. The mechanism of action differs between iron chelators, with DFO exerting a direct effect by inducing autophagy to promote ferritin degradation in the lysosome, while L1 and DFX may chelate intracellular free iron and take iron from ferritin before proteases break it down (Temraz et al., 2014).

Yet, iron complexation toxicity is a major problem, especially in patients with inadequate iron stores (Kolnagou et al., 2014). DFX is not recommended for iron-loaded patients with a serum ferritin below 500 μg/L. Patients receiving DFX are regularly monitored for renal function, with discontinuation of the drug recommended for patients with persistently elevated serum creatinine levels. DFO is relatively safe and has a much lower incidence of serious toxicities, but restrictions on the use of DFX still apply in patients with low iron stores. It is noted that ocular and auditory toxicity has also been reported with DFO when used for ophthalmic disease (Orton et al., 1985). The most serious reported toxicities of L1 are reversible granulocyte deficiency and neutropenia, for which blood counts are recommended every one to 2 weeks to prevent L1 toxicity. Besides, less severe toxic effects of L1 include gastric intolerance, joint pain, and zinc deficiency (Kolnagou et al., 2014). Notably, hepcidin plays a vital function, including iron regulation in SARS-CoV-2 infection as described earlier in 3.3.2. Studies have shown that the hepcidin inhibitor dalteparin improves symptoms in diabetic COVID-19 patients by properly regulating and reducing oxidative stress and inflammation (Zeinivand et al., 2022). This finding is beneficial for the prospect of developing dalteparin as a therapeutic agent for COVID-19 patients with the underlying diabetic disease.

4.3 GPX4-GSH-cysteine axis protector

SARS-CoV-2 infection disrupts the balance between the body's oxidative and antioxidant systems, preventing the timely clearance of ROS. As mentioned above, the GPX4-GSH-cysteine axis is one of the most critical antioxidant systems against ferroptosis, and selenium has a protective effect on GPX4 activity. However, COVID-19 patients with systemic inflammation have decreased hepatic selenase production, which lowers intraplasma selenium (Heller et al., 2021). Thus COVID-19 patients have GPX4 inhibition due to selenium deficiency, leading to ferroptosis. A related study showed that Ebselen was suggested as a low cytotoxic organoselenium compound for the clinical treatment of COVID-19 (Banerjee et al., 2021), as it could reduce the virus replication in the experiment. Furthermore, Ebselen can be used as a selenium supplement to maintain Gpx activity to enhance the antioxidant system. SARS-CoV-2 infection may lead to GSH deficiency, and patients with severe COVID-19 are often accompanied by liver damage by a mechanism related to ferroptosis. Maintaining GSH levels not only resists ferroptosis but also has great significance in protecting liver function itself. Since cysteine is a precursor of GSH synthesis, maintaining adequate cellular cysteine levels can hinder GSH depletion and enable GPX4 to scavenge lipid peroxidation products continuously (Stockwell et al., 2017). N-acetylcysteine (NAC) is a cysteine prodrug used to treat acetaminophen-induced liver failure, critically ill patients with sepsis, and mucus loss in chronic obstructive pulmonary disease. On the one hand, NAC can act as a precursor of GSH and exert an antiferroptosis effect by enhancing the Xc--glutathione--GPX4 axis. On the other hand, it has been shown that NAC can act as a free radical scavenger to counteract IL-6-induced ferroptosis in bronchial epithelial cells while possibly alleviating respiratory symptoms in COVID-19 patients (Han et al., 2021). Recently, there has been evidence that NAC is available for preventing and treating COVID-19 as an adjuvant drug (Shi and Puyo, 2020).

4.4 Others

Lactoferrin (LF) is a first-line defense protein that has a major role in the maturation and regulation of immune system function. Some studies suggested that LF enhances immunity against SARS–CoV–2 by enhancing intracellular antiviral mechanisms and could be a potential adjuvant therapy for COVID–19 (AlKhazindar and Elnagdy, 2020; Chang et al., 2020). In

addition, LF, as an iron-binding protein, possesses the ability to sequester free iron and prevent injury-induced oxidative stress that may be associated with ferroptosis, which can eventually lead to severe tissue necrosis. LF can be used for prophylaxis or as a therapeutic agent administered by multiple routes (including oral administration) to individuals at risk of SARS-CoV-2 infection, especially those with impaired innate immune function (Zimecki et al., 2021). Hypoxia-inducible factor (HIF), the effective substrate of HIF prolyl hydroxylase (HIF-PHD), similarly activates several genes involved in glucose metabolism, intracellular acidity regulation, vasculature, iron overload, mitosis, and other physiological processes (Wang and Semenza, 1995). Inhibitors of HIF-PHD can promote endogenous erythropoietin (EPO) by stabilizing and activating HIF and erythropoiesis (Joharapurkar et al., 2018). Since EPO treatment has anti-inflammatory and healing characteristics, people with moderate to severe COVID-19 are likely to benefit from it. Poloznikov et al. (2020) suggested that HIF-PHD inhibitors can counteract ferroptosis through various interactions with iron but also have the potential to cause greater damage. HIF-PHD inhibitors are a prospective therapy for COVID-19 adverse effects since they can inhibit ferroptosis as well as the entry of the virus into cells. Moreover, Coenzyme Q (CoQ), an essential antioxidant and anti-inflammatory compound in the body, is regarded as a lipophilic antioxidant that traps free radicals. As a CoQ reducer, ferroptosis suppressor protein 1 (FSP1) regenerates CoQ in the plasma membrane using NADPH. The Xc—glutathione—GPX4 axis is assumed to be a parallel system to the FSP1-CoQ10-NADPH pathway, and the two work together to combat ferroptosis and lipid peroxidation (Doll et al., 2019).

5 Discussion

COVID-19 is still spreading worldwide, negatively impacting human health and life. Severe patients are at high risk of complicated multi-organ failure and immune and coagulation dysfunction. Even mildly ill patients may still have persistent respiratory, cardiovascular, neurological, and digestive sequelae. It may be attributed to the wide distribution of ACE2 throughout the body, and SARS-CoV-2 damages multiple tissues and organs through ACE2. Besides, COVID-19 causes high systemic inflammation characterized by elevated ROS and cytokine storm (Girelli et al., 2021). The imbalance between oxidative and antioxidant systems triggered by SARS-CoV-2 infection causes elevated ROS, which exacerbates the corresponding acute/chronic inflammatory process, ultimately leading to multi-organ damage in the body. COVID-19 primarily affects multiple organs, including the lungs, heart, brain, liver, and gastrointestinal tract. Fatigue, dyspnea, cardiac arrhythmia, anxiety, insomnia, abdominal pain, diarrhea, and vomiting are among the symptoms. We are eager to discover new ways to reduce the complications of COVID-19, thereby easing the burden of life and gradually restoring social order as soon as possible. During our research, we discovered that ferroptosis could be a significant breakthrough.

Ferroptosis is a process that involves three primary metabolisms of thiols, lipids, and iron (Tang et al., 2021). It is a relatively passive process that results in cellular destruction or imbalance, mainly due to intracellular iron overload or disruption of normally active antioxidant mechanisms. This results in reactions of lipid peroxidation that depend on iron and the buildup of lipid peroxides. The GPX4-GSH-cysteine axis is the most crucial component of the antioxidant system that protects against ferroptosis. When GSH levels are low, this axis is inhibited, which indirectly inactivates GPX4. The inhibition of the antioxidant system leads cells can not clear the accumulated lipid peroxide, which compromises the cell membrane and ultimately results in ferroptosis.

There may be a crossover between the SARS-CoV-2 infection process and the ferroptosis pathway. Infection with SARS-CoV-2 triggered inflammation, and increased cytokines such as IL-6 promoted the synthesis of hepcidin and ferritin. While the high level of inflammation causes depletion of cells, resulting in the release of free iron from intracellular iron-storing ferritin, accompanied by accumulation of free iron in cells but the leakage of ferritin into the blood leads to hyperferritinemia. Iron is required for SARS-CoV-2 replication. The extracellular iron could be transported to the cell through the transporter protein, which eventually increases the intracellular LIP resulting in the active Fenton reaction and the production of lipid ROS. SARS-CoV-2 invades the cell by binding to ACE2, which leads to the downregulation of ACE2 and, therefore, the feedback increase of Ang II in circulation. Ang II triggers the activation of NOX, leading to oxidative stress. Clinical studies have shown that infection with SARS-CoV-2 leads to GSH deficiency and GPX4 inhibition in the body. Thus the antioxidant system is inhibited, and GSH is unable to reduce lipid peroxides in the presence of GPX4. In addition, oxidative stress promotes TF expression to initiate coagulation, and a hypercoagulable state, associated with thrombosis in patients with severe COVID-19, may be a marker of ferroptosis. Also, in the presence of cellular iron overload, hyperproteinemia in COVID-19 patients marks a worse prognosis and higher mortality in COVID-19 patients.

This paper discusses the possible therapeutic effects of lipid peroxidation inhibitors, iron complexing agents, and GPX4-GSH-cysteine axis protectors for patients based on the potential connection between COVID-19 complications and ferroptosis. Lipid peroxidation inhibitors are mainly divided into oxidase inhibitors and autoxidation inhibitors. As an ACSL4 inhibitor, TZDs not only interrupt the oxidation of AA or AdA to reduce the pathological damage caused by COVID-19 but also acts as an insulin sensitizer. Therefore, patients with severe COVID-19 with underlying diabetic disease may be considered to use hepcidin inhibitors or rosiglitazone to inhibit ferroptosis and mitigate the associated symptoms. Fer-1 and Lip-1 are currently commonly used ferroptosis inhibitors, and they have been shown to inhibit ferroptosis as RTAs. Regrettably, their effects on COVID-19 patients have not been clarified yet. The main treatment for iron overload is the use of iron chelators, which reduce ROS from the Fenton reaction by binding to free iron. Some studies have demonstrated the effect of iron chelators in reducing tissue fibrosis, which can prevent liver injury complicated by severe COVID-19 due to increased LIP. However, it has to be taken into account that iron levels in the patient should not be too low while using iron complexing agents. Hepcidin inhibitors can also treat iron overload, thereby reducing oxidative stress and inflammation. It has surprisingly been reported to improve the symptoms of COVID-19 in diabetic patients. GPX4-GSH-cysteine

axis protectors include selenium supplements and NAC, which together enhance the anti-ferroptosis effect of the GPX4-GSH-cysteine axis. Selenium supplements enhance the activity of Gpx4, and NAC not only scavenges free radicals but also acts as a precursor of GSH. GPX4-GSH-cysteine axis protectors include selenium supplements and NAC, which together act as anti-ferroptosis agents. GSH levels and Gpx4 activity are maintained to counteract the tissue and organ damage caused by SARS-CoV-2 infection and to reduce the severity of COVID-19. Other potential treatments for COVID-19-based ferroptosis include LF and HIF-PHD inhibitors. LF effectively enhances immunity to SARS-CoV-2, and HIF-PHD inhibitors are helpful in blocking virus entry into cells, prospective treatments for severe COVID-19 complications.

In conclusion, there is an association between ferroptosis and the multi-organ complications of COVID-19. Although partial inhibition of ferroptosis has been recorded clinically as adjuvant therapy for COVID-19 with desirable results (Shi and Puyo, 2020; Banerjee et al., 2021; Zeinivand et al., 2022), the definitive mechanism of ferroptosis inhibitors for preventing multi-organ damage in COVID-19 has not been illuminated. More clinical studies on the effects of inhibiting ferroptosis on COVID-19 are expected to emerge providing a new method to reduce COVID-19 complications.

Author contributions

QL, ZC, XZ, GL, and CZ participated in the literature review, analysis, and manuscript writing. YY guided manuscript writing and participated in manuscript revision. All authors contributed to the article and approved the submitted version.

Funding

This research is supported by the Key Research and Development Project of the Science & Technology Department of Sichuan Provincial, China (No. 2022YFS0059).

Acknowledgments

We acknowledge the support from Sichuan Academy of Medical Sciences & Sichuan Provincial People's Hospital, University of Electronic Science and Technology of China, Luxian People's Hospital, China Pharmaceutical University. And thank YY for his contribution to the paper.

Conflict of interest

The authors declare that the research was conducted in the absence of any commercial or financial relationships that could be construed as a potential conflict of interest.

Publisher's note

References

Ackermann, M., Verleden, S. E., Kuehnel, M., Haverich, A., Welte, T., Laenger, F., et al. (2020). Pulmonary vascular endothelialitis, thrombosis, and angiogenesis in covid-19. *N. Engl. J. Med.* 383 (2), 120–128. doi:10.1056/NEJMoa2015432

AlKhazindar, M., and Elnagdy, S. M. (2020). Can lactoferrin boost human immunity against COVID-19? *Pathog. Glob. Health* 114 (5), 234–235. doi:10.1080/20477724.2020.1779514

Amann, K., Boor, P., Wiech, T., Singh, J., Vonbrunn, E., Knoll, A., et al. (2021). COVID-19 effects on the kidney. *Pathologe* 42 (2), 183–187. doi:10.1007/s00292-020-00899-1

Andrews, N. C., and Schmidt, P. J. (2007). Iron homeostasis. *Annu. Rev. Physiol.* 69, 69–85. doi:10.1146/annurev.physiol.69.031905.164337

Banerjee, G., Sammaraiee, Y., and Werring, D. J. (2019). The role of deferiprone in iron chelation. *N. Engl. J. Med.* 380 (9), 891–892. doi:10.1056/NEJMc1817335

Banerjee, R., Perera, L., and Tillekeratne, L. M. V. (2021). Potential SARS-CoV-2 main protease inhibitors. *Drug Discov. Today* 26 (3), 804–816. doi:10.1016/j.drudis.2020.12.005

Bangash, M. N., Patel, J., and Parekh, D. (2020). COVID-19 and the liver: Little cause for concern. *Lancet Gastroenterol. Hepatol.* 5 (6), 529–530. doi:10.1016/S2468-1253(20)30084-4

Bellmann-Weiler, R., Lanser, L., Barket, R., Rangger, L., Schapfl, A., Schaber, M., et al. (2020). Prevalence and predictive value of anemia and dysregulated iron homeostasis in patients with COVID-19 infection. *J. Clin. Med.* 9 (8), 2429. doi:10.3390/jcm9082429

Boldrini, M., Canoll, P. D., and Klein, R. S. (2021). How COVID-19 affects the brain. *JAMA Psychiatry* 78 (6), 682–683. doi:10.1001/jamapsychiatry.2021.0500

Borges do Nascimento, I. J., Cacic, N., Abdulazeem, H. M., von Groote, T. C., Jayarajah, U., Weerasekara, I., et al. (2020). Novel coronavirus infection (COVID-19) in humans: A scoping review and meta-analysis. *J. Clin. Med.* 9 (4), 941. doi:10.3390/jcm9040941

Brussow, H., and Timmis, K. (2021). COVID-19: Long Covid and its societal consequences. *Environ. Microbiol.* 23 (8), 4077–4091. doi:10.1111/1462-2920.15634

Brutsch, S. H., Rademacher, M., Roth, S. R., Muller, K., Eder, S., Viertel, D., et al. (2016). Male subfertility induced by heterozygous expression of catalytically inactive glutathione peroxidase 4 is rescued *in vivo* by systemic inactivation of the Alox15 gene. *J. Biol. Chem.* 291 (45), 23578–23588. doi:10.1074/jbc.M116.738930

Burton, G. W., and Ingold, K. U. (2002). Vitamin E: Application of the principles of physical organic chemistry to the exploration of its structure and function. *Accounts Chem. Res.* 19 (7), 194–201. doi:10.1021/ar00127a001

Chang, R., Ng, T. B., and Sun, W. Z. (2020). Lactoferrin as potential preventative and adjunct treatment for COVID-19. *Int. J. Antimicrob. Agents* 56 (3), 106118. doi:10.1016/j.ijantimicag.2020.106118

Chen, N., Zhou, M., Dong, X., Qu, J., Gong, F., Han, Y., et al. (2020). Epidemiological and clinical characteristics of 99 cases of 2019 novel coronavirus pneumonia in wuhan, China: A descriptive study. *Lancet* 395 (10223), 507–513. doi:10.1016/S0140-6736(20)30211-7

Chen, X., Li, J., Kang, R., Klionsky, D. J., and Tang, D. (2021). Ferroptosis: Machinery and regulation. *Autophagy* 17 (9), 2054–2081. doi:10.1080/15548627.2020.1810918

Cheng, Y., Luo, R., Wang, K., Zhang, M., Wang, Z., Dong, L., et al. (2020). Kidney disease is associated with in-hospital death of patients with COVID-19. *Kidney Int.* 97 (5), 829–838. doi:10.1016/j.kint.2020.03.005

Cheung, K. S., Hung, I. F. N., Chan, P. P. Y., Lung, K. C., Tso, E., Liu, R., et al. (2020). Gastrointestinal manifestations of SARS-CoV-2 infection and virus load in fecal samples from a Hong Kong cohort: Systematic review and meta-analysis. *Gastroenterology* 159 (1), 81–95. doi:10.1053/j.gastro.2020.03.065

Chieffo, A., Stefanini, G. G., Price, S., Barbato, E., Tarantini, G., Karam, N., et al. (2020). EAPCI position statement on invasive management of acute coronary syndromes during the COVID-19 pandemic. *EuroIntervention* 16 (3), 233–246. doi:10.4244/EIJY20M05_01

Cho, K. J., Seo, J. M., and Kim, J. H. (2011). Bioactive lipoxygenase metabolites stimulation of NADPH oxidases and reactive oxygen species. *Mol. Cells* 32 (1), 1–5. doi:10.1007/s10059-011-1021-7

Darwish, S. F., El-Bakly, W. M., El-Naga, R. N., Awad, A. S., and El-Demerdash, E. (2015). Antifibrotic mechanism of deferoxamine in concanavalin A induced-liver fibrosis: Impact on interferon therapy. *Biochem. Pharmacol.* 98 (1), 231–242. doi:10.1016/j.bcp.2015.09.001

Dikalov, S. I., and Nazarewicz, R. R. (2013). Angiotensin II-induced production of mitochondrial reactive oxygen species: Potential mechanisms and relevance for cardiovascular disease. *Antioxid. Redox Signal* 19 (10), 1085–1094. doi:10.1089/ars.2012.4604

Dixon, S. J., Lemberg, K. M., Lamprecht, M. R., Skouta, R., Zaitsev, E. M., Gleason, C. E., et al. (2012). Ferroptosis: An iron-dependent form of nonapoptotic cell death. *Cell* 149 (5), 1060–1072. doi:10.1016/j.cell.2012.03.042

Doll, S., Freitas, F. P., Shah, R., Aldrovandi, M., da Silva, M. C., Ingold, I., et al. (2019). FSP1 is a glutathione-independent ferroptosis suppressor. *Nature* 575 (7784), 693–698. doi:10.1038/s41586-019-1707-0

Doll, S., Proneth, B., Tyurina, Y. Y., Panzilius, E., Kobayashi, S., Ingold, I., et al. (2017). ACSL4 dictates ferroptosis sensitivity by shaping cellular lipid composition. *Nat. Chem. Biol.* 13 (1), 91–98. doi:10.1038/nchembio.2239

Dolma, S., Lessnick, S. L., Hahn, W. C., and Stockwell, B. R. (2003). Identification of genotype-selective antitumor agents using synthetic lethal chemical screening in engineered human tumor cells. *Cancer Cell* 3 (3), 285–296. doi:10.1016/s1535-6108(03)00050-3

Evans, M., Dizdaroglu, M., and Cooke, M. S. (2004). Evans MD, dizdaroglu M, cooke MSOxidative DNA damage and disease: Induction, repair and significance. Mutat res 567:1-61. *Mutat. Research/Fundamental Mol. Mech. Mutagen.* 567 (1), 1–61.

Feng, H., and Stockwell, B. R. (2018). Unsolved mysteries: How does lipid peroxidation cause ferroptosis? *PLoS Biol.* 16 (5), e2006203. doi:10.1371/journal.pbio.2006203

Florez, A. F., and Alborzinia, H. (2021). *Ferroptosis: Mechanism and diseases*. Springer.

Franchini, M., and Veneri, D. (2004). Iron-chelation therapy: An update. *Hematol. J.* 5 (4), 287–292. doi:10.1038/sj.thj.6200407

Frazer, D. M., and Anderson, G. J. (2014). The regulation of iron transport. *Biofactors* 40 (2), 206–214. doi:10.1002/biof.1148

Friedmann Angeli, J. P., Schneider, M., Proneth, B., Tyurina, Y. Y., Tyurin, V. A., Hammond, V. J., et al. (2014). Inactivation of the ferroptosis regulator Gpx4 triggers acute renal failure in mice. *Nat. Cell Biol.* 16 (12), 1180–1191. doi:10.1038/ncb3064

Ganz, T. (2005). Cellular iron: Ferroportin is the only way out. *Cell Metab.* 1 (3), 155–157. doi:10.1016/j.cmet.2005.02.005

Gill, I., and Valivety, R. (1997). Polyunsaturated fatty acids, Part 1: Occurrence, biological activities and applications. *Trends Biotechnol.* 15 (10), 401–409. doi:10.1016/S0167-7799(97)01076-7

Girelli, D., Marchi, G., Busti, F., and Vianello, A. (2021). Iron metabolism in infections: Focus on COVID-19. *Semin. Hematol.* 58 (3), 182–187. doi:10.1053/j.seminhematol.2021.07.001

Goldberg, M. F., Goldberg, M. F., Cerejo, R., and Tayal, A. H. (2020). Cerebrovascular disease in COVID-19. *AJNR Am. J. Neuroradiol.* 41 (7), 1170–1172. doi:10.3174/ajnr.A6588

Guan, W. J., Ni, Z. Y., Hu, Y., Liang, W. H., Ou, C. Q., He, J. X., et al. (2020). Clinical characteristics of coronavirus disease 2019 in China. *N. Engl. J. Med.* 382 (18), 1708–1720. doi:10.1056/NEJMoa2002032

Guo, T., Fan, Y., Chen, M., Wu, X., Zhang, L., He, T., et al. (2020). Cardiovascular implications of fatal outcomes of patients with coronavirus disease 2019 (COVID-19). *JAMA Cardiol.* 5 (7), 811–818. doi:10.1001/jamacardio.2020.1017

Guo, Y., Luo, R., Wang, Y., Deng, P., Song, T., Zhang, M., et al. (2021). SARS-CoV-2 induced intestinal responses with a biomimetic human gut-on-chip. *Sci. Bull. (Beijing)* 66 (8), 783–793. doi:10.1016/j.scib.2020.11.015

Gupta, A., Madhavan, M. V., Sehgal, K., Nair, N., Mahajan, S., Sehrawat, T. S., et al. (2020). Extrapulmonary manifestations of COVID-19. *Nat. Med.* 26 (7), 1017–1032. doi:10.1038/s41591-020-0968-3

Hadian, K., and Stockwell, B. R. (2020). SnapShot: Ferroptosis. *Cell* 181 (5), 1188–1188 e1181. doi:10.1016/j.cell.2020.04.039

Haeggstrom, J. Z., and Funk, C. D. (2011). Lipoxygenase and leukotriene pathways: Biochemistry, biology, and roles in disease. *Chem. Rev.* 111 (10), 5866–5898. doi:10.1021/cr200246d

Haidasz, E. A., Meng, D., Amorati, R., Baschieri, A., Ingold, K. U., Valgimigli, L., et al. (2016). Acid is key to the radical-trapping antioxidant activity of nitroxides. *J. Am. Chem. Soc.* 138 (16), 5290–5298. doi:10.1021/jacs.6b00677

Han, F., Li, S., Yang, Y., and Bai, Z. (2021). Interleukin-6 promotes ferroptosis in bronchial epithelial cells by inducing reactive oxygen species-dependent lipid peroxidation and disrupting iron homeostasis. *Bioengineered* 12 (1), 5279–5288. doi:10.1080/21655979.2021.1964158

Han, Y., Zhu, J., Yang, L., Nilsson-Payant, B. E., Hurtado, R., Lacko, L. A., et al. (2022). SARS-CoV-2 infection induces ferroptosis of sinoatrial node pacemaker cells. *Circ. Res.* 130 (7), 963–977. doi:10.1161/CIRCRESAHA.121.320518

Heller, R. A., Sun, Q., Hackler, J., Seelig, J., Seibert, L., Cherkezov, A., et al. (2021). Prediction of survival odds in COVID-19 by zinc, age and selenoprotein P as composite biomarker. *Redox Biol.* 38, 101764. doi:10.1016/j.redox.2020.101764

Helms, J., Tacquard, C., Severac, F., Leonard-Lorant, I., Ohana, M., Delabranche, X., et al. (2020). High risk of thrombosis in patients with severe SARS-CoV-2 infection: A multicenter prospective cohort study. *Intensive Care Med.* 46 (6), 1089–1098. doi:10.1007/s00134-020-06062-x

Hendren, N. S., Drazner, M. H., Bozkurt, B., and Cooper, L. T., Jr. (2020). Description and proposed management of the acute COVID-19 cardiovascular syndrome. *Circulation* 141 (23), 1903–1914. doi:10.1161/CIRCULATIONAHA.120.047349

Hikmet, F., Mear, L., Edvinsson, A., Micke, P., Uhlen, M., and Lindskog, C. (2020). The protein expression profile of ACE2 in human tissues. *Mol. Syst. Biol.* 16 (7), e9610. doi:10.15252/msb.20209610

Horowitz, R. I., Freeman, P. R., and Bruzzese, J. (2020). Efficacy of glutathione therapy in relieving dyspnea associated with COVID-19 pneumonia: A report of 2 cases. *Respir. Med. Case Rep.* 30, 101063. doi:10.1016/j.rmcr.2020.101063

Iba, T., Levy, J. H., Raj, A., and Warkentin, T. E. (2019). Advance in the management of sepsis-induced coagulopathy and disseminated intravascular coagulation. *J. Clin. Med.* 8 (5), 728. doi:10.3390/jcm8050728

Imre, G. (2020). The involvement of regulated cell death forms in modulating the bacterial and viral pathogenesis. *Int. Rev. Cell Mol. Biol.* 353, 211–253. doi:10.1016/bs.ircmb.2019.12.008

Jacobs, W., Lammens, M., Kerckhofs, A., Voets, E., Van San, E., Van Coillie, S., et al. (2020). Fatal lymphocytic cardiac damage in coronavirus disease 2019 (COVID-19): Autopsy reveals a ferroptosis signature. *Esc. Heart Fail* 7 (6), 3772–3781. doi:10.1002/ehf2.12958

Jankun, J., Landeta, P., Pretorius, E., Skrzypczak-Jankun, E., and Lipinski, B. (2014). Unusual clotting dynamics of plasma supplemented with iron(III). *Int. J. Mol. Med.* 33 (2), 367–372. doi:10.3892/ijmm.2013.1585

Joharapurkar, A. A., Pandya, V. B., Patel, V. J., Desai, R. C., and Jain, M. R. (2018). Prolyl hydroxylase inhibitors: A breakthrough in the therapy of anemia associated with chronic diseases. *J. Med. Chem.* 61 (16), 6964–6982. doi:10.1021/acs.jmedchem.7b01686

Kagan, V. E., Mao, G., Qu, F., Angeli, J. P., Doll, S., Croix, C. S., et al. (2017). Oxidized arachidonic and adrenic PEs navigate cells to ferroptosis. *Nat. Chem. Biol.* 13 (1), 81–90. doi:10.1038/nchembio.2238

Kell, D. B., and Pretorius, E. (2014). Serum ferritin is an important inflammatory disease marker, as it is mainly a leakage product from damaged cells. *Metallomics* 6 (4), 748–773. doi:10.1039/c3mt00347g

Kell, D. B. (2010). Towards a unifying, systems biology understanding of large-scale cellular death and destruction caused by poorly liganded iron: Parkinson's, huntington's, alzheimer's, prions, bactericides, chemical toxicology and others as examples. *Arch. Toxicol.* 84 (11), 825–889. doi:10.1007/s00204-010-0577-x

Kim, J. H., Lewin, T. M., and Coleman, R. A. (2001). Expression and characterization of recombinant rat Acyl-CoA synthetases 1, 4, and 5. Selective inhibition by triacsin C and thiazolidinediones. *J. Biol. Chem.* 276 (27), 24667–24673. doi:10.1074/jbc.M010793200

Kolbrink, B., von Samson-Himmelstjerna, F. A., Messtorff, M. L., Riebeling, T., Nische, R., Schmitz, J., et al. (2022). Vitamin K1 inhibits ferroptosis and counteracts a detrimental effect of phenprocoumon in experimental acute kidney injury. *Cell Mol. Life Sci.* 79 (7), 387. doi:10.1007/s00018-022-04416-w

Kolnagou, A., Kontoghiorghe, C. N., and Kontoghiorghes, G. J. (2014). Transition of Thalassaemia and Friedreich ataxia from fatal to chronic diseases. *World J. Methodol.* 4 (4), 197–218. doi:10.5662/wjm.v4.i4.197

Koralnik, I. J., and Tyler, K. L. (2020). COVID-19: A global threat to the nervous system. *Ann. Neurol.* 88 (1), 1–11. doi:10.1002/ana.25807

Krainz, T., Gaschler, M. M., Lim, C., Sacher, J. R., Stockwell, B. R., and Wipf, P. (2016). A mitochondrial-targeted nitroxide is a potent inhibitor of ferroptosis. *ACS Cent. Sci.* 2 (9), 653–659. doi:10.1021/acscentsci.6b00199

Lechner-Scott, J., Levy, M., Hawkes, C., Yeh, A., and Giovannoni, G. (2021). Long COVID or post COVID-19 syndrome. *Mult. Scler. Relat. Disord.* 55, 103268. doi:10.1016/j.msard.2021.103268

Lee, M. H., Perl, D. P., Nair, G., Li, W., Maric, D., Murray, H., et al. (2021). Microvascular injury in the brains of patients with covid-19. *N. Engl. J. Med.* 384 (5), 481–483. doi:10.1056/NEJMc2033369

Li, M. Y., Li, L., Zhang, Y., and Wang, X. S. (2020). Expression of the SARS-CoV-2 cell receptor gene ACE2 in a wide variety of human tissues. *Infect. Dis. Poverty* 9 (1), 45. doi:10.1186/s40249-020-00662-x

Mao, L., Jin, H., Wang, M., Hu, Y., Chen, S., He, Q., et al. (2020). Neurologic manifestations of hospitalized patients with coronavirus disease 2019 in wuhan, China. *JAMA Neurol.* 77 (6), 683–690. doi:10.1001/jamaneurol.2020.1127

Matschke, J., Lutgehetmann, M., Hagel, C., Sperhake, J. P., Schroder, A. S., Edler, C., et al. (2020). Neuropathology of patients with COVID-19 in Germany: A post-mortem case series. *Lancet Neurol.* 19 (11), 919–929. doi:10.1016/S1474-4422(20)30308-2

Matsushita, M., Freigang, S., Schneider, C., Conrad, M., Bornkamm, G. W., and Kopf, M. (2015). T cell lipid peroxidation induces ferroptosis and prevents immunity to infection. *J. Exp. Med.* 212 (4), 555–568. doi:10.1084/jem.20140857

Megyeri, K., Dernovics, A., Al-Luhaibi, Z. I. I., and Rosztoczy, A. (2021). COVID-19-associated diarrhea. *World J. Gastroenterol.* 27 (23), 3208–3222. doi:10.3748/wjg.v27.i23.3208

Mehta, O. P., Bhandari, P., Raut, A., Kacimi, S. E. O., and Huy, N. T. (2020). Coronavirus disease (COVID-19): Comprehensive review of clinical presentation. *Front. Public Health* 8, 582932. doi:10.3389/fpubh.2020.582932

Merad, M., and Martin, J. C. (2020). Pathological inflammation in patients with COVID-19: A key role for monocytes and macrophages. *Nat. Rev. Immunol.* 20 (6), 355–362. doi:10.1038/s41577-020-0331-4

Neitemeier, S., Jelinek, A., Laino, V., Hoffmann, L., Eisenbach, I., Eying, R., et al. (2017). BID links ferroptosis to mitochondrial cell death pathways. *Redox Biol.* 12, 558–570. doi:10.1016/j.redox.2017.03.007

Ni, W., Yang, X., Liu, J., Bao, J., Li, R., Xu, Y., et al. (2020). Acute myocardial injury at hospital admission is associated with all-cause mortality in COVID-19. *J. Am. Coll. Cardiol.* 76 (1), 124–125. doi:10.1016/j.jacc.2020.05.007

Nishiga, M., Jahng, J. W. S., and Wu, J. C. (2022). Ferroptosis of pacemaker cells in COVID-19. *Circ. Res.* 130 (7), 978–980. doi:10.1161/CIRCRESAHA.122.320951

Organization, W. H. (2023). Coronavirus (COVID-19) dashboard data table *[Online]*. Available at: https://covid19.who.int (Accessed February 12, 2023).

Orton, R. B., de Veber, L. L., and Sulh, H. M. (1985). Ocular and auditory toxicity of long-term, high-dose subcutaneous deferoxamine therapy. *Can. J. Ophthalmol.* 20 (4), 153–156.

Owens, A. P., 3rd, Passam, F. H., Antoniak, S., Marshall, S. M., McDaniel, A. L., Rudel, L., et al. (2012). Monocyte tissue factor-dependent activation of coagulation in hypercholesterolemic mice and monkeys is inhibited by simvastatin. *J. Clin. Investig.* 122 (2), 558–568. doi:10.1172/JCI58969

Paizis, G., Tikellis, C., Cooper, M. E., Schembri, J. M., Lew, R. A., Smith, A. I., et al. (2005). Chronic liver injury in rats and humans upregulates the novel enzyme angiotensin converting enzyme 2. *Gut* 54 (12), 1790–1796. doi:10.1136/gut.2004.062398

Patel, S., Rauf, A., Khan, H., and Abu-Izneid, T. (2017). Renin-angiotensin-aldosterone (RAAS): The ubiquitous system for homeostasis and pathologies. *Biomed. Pharmacother.* 94, 317–325. doi:10.1016/j.biopha.2017.07.091

Perico, L., Benigni, A., and Remuzzi, G. (2020). Should COVID-19 concern nephrologists? Why and to what extent? The emerging impasse of angiotensin blockade. *Nephron* 144 (5), 213–221. doi:10.1159/000507305

Perricone, C., Bartoloni, E., Bursi, R., Cafaro, G., Guidelli, G. M., Shoenfeld, Y., et al. (2020). COVID-19 as part of the hyperferritinemic syndromes: The role of iron depletion therapy. *Immunol. Res.* 68 (4), 213–224. doi:10.1007/s12026-020-09145-5

Philpott, C. C. (2018). The flux of iron through ferritin in erythrocyte development. *Curr. Opin. Hematol.* 25 (3), 183–188. doi:10.1097/MOH.0000000000000417

Polonikov, A. (2020). Endogenous deficiency of glutathione as the most likely cause of serious manifestations and death in COVID-19 patients. *ACS Infect. Dis.* 6 (7), 1558–1562. doi:10.1021/acsinfecdis.0c00288

Poloznikov, A. A., Nersisyan, S. A., Hushpulian, D. M., Kazakov, E. H., Tonevitsky, A. G., Kazakov, S. V., et al. (2020). HIF prolyl hydroxylase inhibitors for COVID-19 treatment: Pros and cons. *Front. Pharmacol.* 11, 621054. doi:10.3389/fphar.2020.621054

Puelles, V. G., Lutgehetmann, M., Lindenmeyer, M. T., Sperhake, J. P., Wong, M. N., Allweiss, L., et al. (2020). Multiorgan and renal tropism of SARS-CoV-2. *N. Engl. J. Med.* 383 (6), 590–592. doi:10.1056/NEJMc2011400

Ratliff, B. B., Abdulmahdi, W., Pawar, R., and Wolin, M. S. (2016). Oxidant mechanisms in renal injury and disease. *Antioxid. Redox Signal* 25 (3), 119–146. doi:10.1089/ars.2016.6665

Regis, G., Bosticardo, M., Conti, L., De Angelis, S., Boselli, D., Tomaino, B., et al. (2005). Iron regulates T-lymphocyte sensitivity to the IFN-gamma/STAT1 signaling pathway *in vitro* and *in vivo*. *Blood* 105 (8), 3214–3221. doi:10.1182/blood-2004-07-2686

Ronco, C., Reis, T., and Husain-Syed, F. (2020). Management of acute kidney injury in patients with COVID-19. *Lancet Respir. Med.* 8 (7), 738–742. doi:10.1016/S2213-2600(20)30229-0

Rubin, R. (2022). From positive to negative to positive again-the mystery of why COVID-19 rebounds in some patients who take Paxlovid. *JAMA* 327 (24), 2380–2382. doi:10.1001/jama.2022.9925

Ryu, M. S., Zhang, D., Protchenko, O., Shakoury-Elizeh, M., and Philpott, C. C. (2017). PCBP1 and NCOA4 regulate erythroid iron storage and heme biosynthesis. *J. Clin. Investig.* 127 (5), 1786–1797. doi:10.1172/JCI90519

Santana-Codina, N., and Mancias, J. D. (2018). The role of NCOA4-mediated ferritinophagy in health and disease. *Pharm. (Basel)* 11 (4). doi:10.3390/ph11040114

Shah, R., Shchepinov, M. S., and Pratt, D. A. (2018). Resolving the role of lipoxygenases in the initiation and execution of ferroptosis. *ACS Cent. Sci.* 4 (3), 387–396. doi:10.1021/acscentsci.7b00589

Shi, Z., and Puyo, C. A. (2020). N-acetylcysteine to combat COVID-19: An evidence review. *Ther. Clin. Risk Manag.* 16, 1047–1055. doi:10.2147/TCRM.S273700

Skouta, R., Dixon, S. J., Wang, J., Dunn, D. E., Orman, M., Shimada, K., et al. (2014). Ferrostatins inhibit oxidative lipid damage and cell death in diverse disease models. *J. Am. Chem. Soc.* 136 (12), 4551–4556. doi:10.1021/ja411006a

Stockwell, B. R., Friedmann Angeli, J. P., Bayir, H., Bush, A. I., Conrad, M., Dixon, S. J., et al. (2017). Ferroptosis: A regulated cell death nexus linking metabolism, redox biology, and disease. *Cell* 171 (2), 273–285. doi:10.1016/j.cell.2017.09.021

Stumpf, J. L. (2007). Deferasirox. *Am. J. Health Syst. Pharm.* 64 (6), 606–616. doi:10.2146/ajhp060405

Sun, C., Han, Y., Zhang, R., Liu, S., Wang, J., Zhang, Y., et al. (2022). Regulated necrosis in COVID-19: A double-edged sword. *Front. Immunol.* 13, 917141. doi:10.3389/fimmu.2022.917141

Tang, D., Chen, X., Kang, R., and Kroemer, G. (2021). Ferroptosis: Molecular mechanisms and health implications. *Cell Res.* 31 (2), 107–125. doi:10.1038/s41422-020-00441-1

Temraz, S., Santini, V., Musallam, K., and Taher, A. (2014). Iron overload and chelation therapy in myelodysplastic syndromes. *Crit. Rev. Oncol. Hematol.* 91 (1), 64–73. doi:10.1016/j.critrevonc.2014.01.006

Tian, D., and Ye, Q. (2020). Hepatic complications of COVID-19 and its treatment. *J. Med. Virol.* 92 (10), 1818–1824. doi:10.1002/jmv.26036

Tong, J., Lan, X. T., Zhang, Z., Liu, Y., Sun, D. Y., Wang, X. J., et al. (2023). Ferroptosis inhibitor liproxstatin-1 alleviates metabolic dysfunction-associated fatty liver disease in mice: Potential involvement of PANoptosis. *Acta Pharmacol. Sin.* 44 (5), 1014–1028. doi:10.1038/s41401-022-01010-5

Ursini, F., Maiorino, M., Brigelius-Flohe, R., Aumann, K. D., Roveri, A., Schomburg, D., et al. (1995). Diversity of glutathione peroxidases. *Methods Enzymol.* 252, 38–53. doi:10.1016/0076-6879(95)52007-4

Violi, F., Oliva, A., Cangemi, R., Ceccarelli, G., Pignatelli, P., Carnevale, R., et al. (2020). Nox2 activation in covid-19. *Redox Biol.* 36, 101655. doi:10.1016/j.redox.2020.101655

von Bruhl, M. L., Stark, K., Steinhart, A., Chandraratne, S., Konrad, I., Lorenz, M., et al. (2012). Monocytes, neutrophils, and platelets cooperate to initiate and propagate venous thrombosis in mice *in vivo*. *J. Exp. Med.* 209 (4), 819–835. doi:10.1084/jem.20112322

Wang, G. L., and Semenza, G. L. (1995). Purification and characterization of hypoxia-inducible factor 1. *J. Biol. Chem.* 270 (3), 1230–1237. doi:10.1074/jbc.270.3.1230

Wang, Y., Huang, J., Sun, Y., Stubbs, D., He, J., Li, W., et al. (2021). SARS-CoV-2 suppresses mRNA expression of selenoproteins associated with ferroptosis, endoplasmic reticulum stress and DNA synthesis. *Food Chem. Toxicol.* 153, 112286. doi:10.1016/j.fct.2021.112286

Wang, Y., Zhang, M., Bi, R., Su, Y., Quan, F., Lin, Y., et al. (2022). ACSL4 deficiency confers protection against ferroptosis-mediated acute kidney injury. *Redox Biol.* 51, 102262. doi:10.1016/j.redox.2022.102262

Wenzel, S. E., Tyurina, Y. Y., Zhao, J., St Croix, C. M., Dar, H. H., Mao, G., et al. (2017). PEBP1 wardens ferroptosis by enabling lipoxygenase generation of lipid death signals. *Cell* 171 (3), 628–641 e626. doi:10.1016/j.cell.2017.09.044

Williamson, E. J., Walker, A. J., Bhaskaran, K., Bacon, S., Bates, C., Morton, C. E., et al. (2020). Factors associated with COVID-19-related death using OpenSAFELY. *Nature* 584 (7821), 430–436. doi:10.1038/s41586-020-2521-4

Xu, Y., Li, X., Cheng, Y., Yang, M., and Wang, R. (2020a). Inhibition of ACSL4 attenuates ferroptotic damage after pulmonary ischemia-reperfusion. *FASEB J.* 34 (12), 16262–16275. doi:10.1096/fj.202001758R

Xu, Z., Shi, L., Wang, Y., Zhang, J., Huang, L., Zhang, C., et al. (2020b). Pathological findings of COVID-19 associated with acute respiratory distress syndrome. *Lancet Respir. Med.* 8 (4), 420–422. doi:10.1016/S2213-2600(20)30076-X

Yang, W. S., Kim, K. J., Gaschler, M. M., Patel, M., Shchepinov, M. S., and Stockwell, B. R. (2016). Peroxidation of polyunsaturated fatty acids by lipoxygenases drives ferroptosis. *Proc. Natl. Acad. Sci. U. S. A.* 113 (34), E4966–E4975. doi:10.1073/pnas.1603244113

Yigitkanli, K., Pekcec, A., Karatas, H., Pallast, S., Mandeville, E., Joshi, N., et al. (2013). Inhibition of 12/15-lipoxygenase as therapeutic strategy to treat stroke. *Ann. Neurol.* 73 (1), 129–135. doi:10.1002/ana.23734

Yin, H., Xu, L., and Porter, N. A. (2011). Free radical lipid peroxidation: Mechanisms and analysis. *Chem. Rev.* 111 (10), 5944–5972. doi:10.1021/cr200084z

Yong, S. J. (2021). Long COVID or post-COVID-19 syndrome: Putative pathophysiology, risk factors, and treatments. *Infect. Dis. (Lond)* 53 (10), 737–754. doi:10.1080/23744235.2021.1924397

Zeinivand, M., Jamali-Raeufy, N., and Zavvari, F. (2022). The beneficial role of hepcidin peptide inhibitor in improved the symptoms of COVID-19 in diabetics: Anti-inflammatory and potential therapeutic effects. *J. Diabetes Metab. Disord.* 21 (2), 1797–1807. doi:10.1007/s40200-022-01053-9

Zhang, B., Chen, X., Ru, F., Gan, Y., Li, B., Xia, W., et al. (2021). Liproxstatin-1 attenuates unilateral ureteral obstruction-induced renal fibrosis by inhibiting renal tubular epithelial cells ferroptosis. *Cell Death Dis.* 12 (9), 843. doi:10.1038/s41419-021-04137-1

Zhao, K., Huang, J., Dai, D., Feng, Y., Liu, L., and Nie, S. (2020). Serum iron level as a potential predictor of coronavirus disease 2019 severity and mortality: A retrospective study. *Open Forum Infect. Dis.* 7 (7), ofaa250. doi:10.1093/ofid/ofaa250

Zhou, Y., Zhang, J., Guan, Q., Tao, X., Wang, J., and Li, W. (2022). The role of ferroptosis in the development of acute and chronic kidney diseases. *J. Cell Physiol.* 237 (12), 4412–4427. doi:10.1002/jcp.30901

Zilka, O., Shah, R., Li, B., Friedmann Angeli, J. P., Griesser, M., Conrad, M., et al. (2017). On the mechanism of cytoprotection by ferrostatin-1 and liproxstatin-1 and the role of lipid peroxidation in ferroptotic cell death. *ACS Cent. Sci.* 3 (3), 232–243. doi:10.1021/acscentsci.7b00028

Zimecki, M., Actor, J. K., and Kruzel, M. L. (2021). The potential for Lactoferrin to reduce SARS-CoV-2 induced cytokine storm. *Int. Immunopharmacol.* 95, 107571. doi:10.1016/j.intimp.2021.107571

Zou, X., Chen, K., Zou, J., Han, P., Hao, J., and Han, Z. (2020). Single-cell RNA-seq data analysis on the receptor ACE2 expression reveals the potential risk of different human organs vulnerable to 2019-nCoV infection. *Front. Med.* 14 (2), 185–192. doi:10.1007/s11684-020-0754-0

frontiers | Frontiers in Genetics

TYPE Original Research
PUBLISHED 08 June 2023
DOI 10.3389/fgene.2023.1199566

OPEN ACCESS

EDITED BY
Shaoqiu Chen,
University of Hawaii at Mānoa,
United States

REVIEWED BY
Qing Li,
Daping Hospital, China
Xuanming Guo,
St. Jude Children's Research Hospital,
United States

*CORRESPONDENCE
Jianying Zhou,
zjyzjhz@126.com

RECEIVED 03 April 2023
ACCEPTED 10 May 2023
PUBLISHED 08 June 2023

CITATION
Feng M, Wang J and Zhou J (2023), Unraveling the therapeutic mechanisms of dichloroacetic acid in lung cancer through integrated multi-omics approaches: metabolomics and transcriptomics.
Front. Genet. 14:1199566.
doi: 10.3389/fgene.2023.1199566

Unraveling the therapeutic mechanisms of dichloroacetic acid in lung cancer through integrated multi-omics approaches: metabolomics and transcriptomics

Malong Feng[1,2], Ji Wang[3] and Jianying Zhou[1]*

[1]Department of Respiratory and Critical Care Medicine, The First Affiliated Hospital of Zhejiang University School of Medicine, Hangzhou, Zhejiang, China, [2]Department of Respiration, Fenghua District People's Hospital of Ningbo, Ningbo, China, [3]Department of Infectious Diseases, Fenghua District People's Hospital of Ningbo, Ningbo, China

Objective: The aim of this study was to investigate the molecular mechanisms underlying the therapeutic effects of dichloroacetic acid (DCA) in lung cancer by integrating multi-omics approaches, as the current understanding of DCA's role in cancer treatment remains insufficiently elucidated.

Methods: We conducted a comprehensive analysis of publicly available RNA-seq and metabolomic datasets and established a subcutaneous xenograft model of lung cancer in BALB/c nude mice (n = 5 per group) treated with DCA (50 mg/kg, administered via intraperitoneal injection). Metabolomic profiling, gene expression analysis, and metabolite-gene interaction pathway analysis were employed to identify key pathways and molecular players involved in the response to DCA treatment. *In vivo* evaluation of DCA treatment on tumor growth and MIF gene expression was performed in the xenograft model.

Results: Metabolomic profiling and gene expression analysis revealed significant alterations in metabolic pathways, including the Warburg effect and citric acid cycle, and identified the MIF gene as a potential therapeutic target in lung cancer. Our analysis indicated that DCA treatment led to a decrease in MIF gene expression and an increase in citric acid levels in the treatment group. Furthermore, we observed a potential interaction between citric acid and the MIF gene, suggesting a novel mechanism underlying the therapeutic effects of DCA in lung cancer.

Conclusion: This study underscores the importance of integrated omics approaches in deciphering the complex molecular mechanisms of DCA treatment in lung cancer. The identification of key metabolic pathways and the novel finding of citric acid elevation, together with its interaction with the MIF gene, provide promising directions for the development of targeted therapeutic strategies and improving clinical outcomes for lung cancer patients.

KEYWORDS

lung cancer, dichloroacetic acid (DCA), multi-omics, metabolomics, gene expression, molecular mechanisms, therapeutic target, drug mechanism

Introduction

Lung cancer remains a formidable global health issue, accounting for a considerable percentage of cancer-related mortalities worldwide (Bunn, 2012). This complex and heterogeneous disease presents numerous challenges in terms of early diagnosis, treatment, and management. The late-stage detection of lung cancer often renders treatment less effective, emphasizing the need for improved diagnostic tools and screening methods to facilitate timely intervention (Hammerschmidt and Wirtz, 2009). Additionally, the high incidence of drug resistance and recurrence in lung cancer patients underscores the importance of developing novel therapeutic strategies. A comprehensive understanding of the molecular mechanisms underlying lung cancer is crucial to identifying innovative treatment options and overcoming the existing obstacles in lung cancer management (Mottaghitalab et al., 2019). Dichloroacetic acid (DCA), a small halogenated molecule, has recently emerged as a potential anti-cancer agent due to its ability to modulate cellular metabolism. The side effects and toxicities of DCA have been relatively well-documented. The most common side effects reported include peripheral neuropathy, which is reversible upon cessation of treatment, as well as liver enzyme abnormalities and gastrointestinal disturbances. In some cases, patients have experienced a mild and reversible cognitive decline. While these side effects are generally manageable, it is essential to balance the potential therapeutic benefits of DCA with the risk of adverse events (Farina et al., 2020). However, the precise mechanisms through which DCA exerts its therapeutic effects in lung cancer remain to be fully elucidated (Ma et al., 2018; Tataranni and Piccoli, 2019).

The utilization of multi-omics methodologies, incorporating metabolomics and transcriptomics, has demonstrated considerable potential in deciphering intricate biological systems

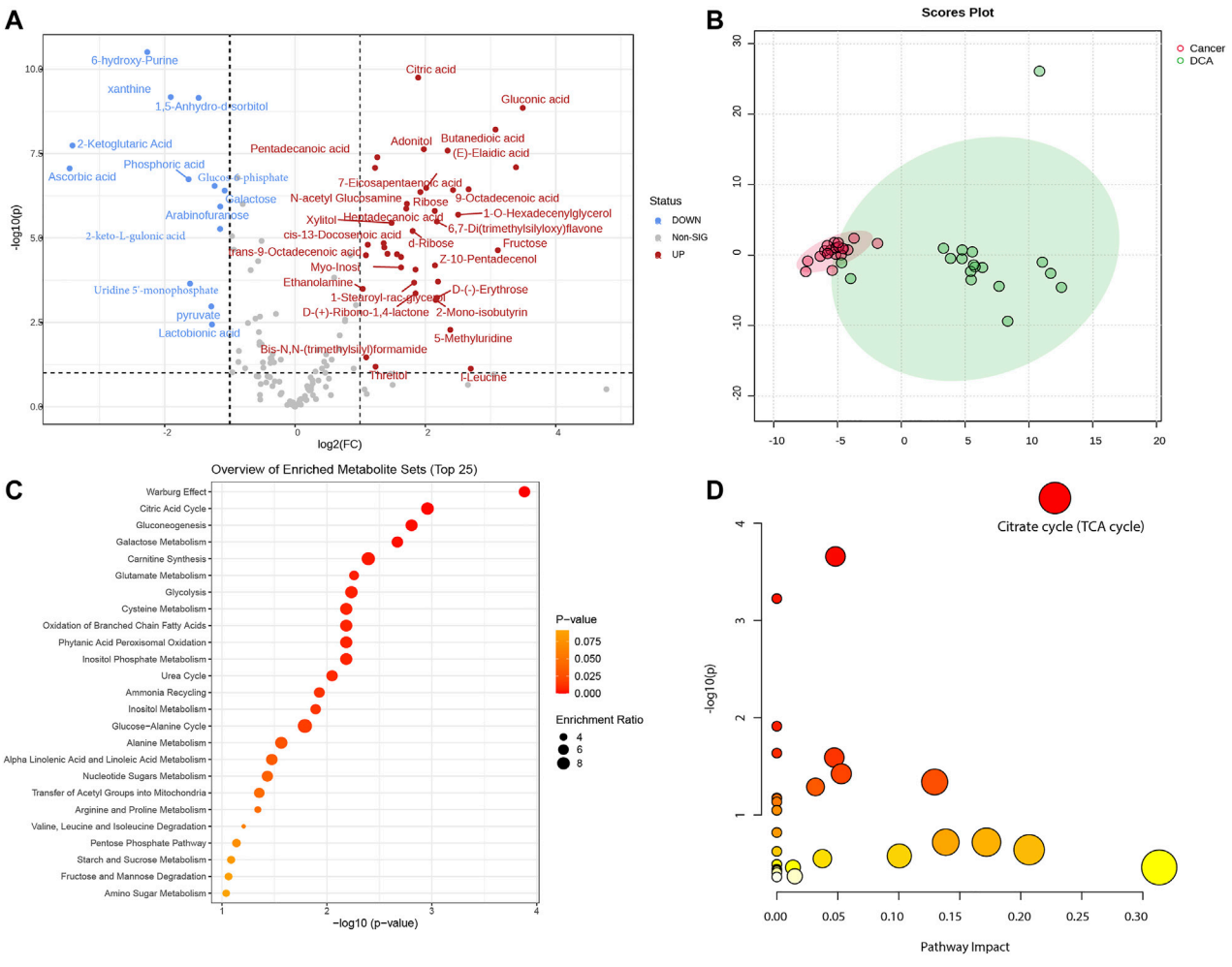

FIGURE 1
Metabolomic analysis of lung cancer control and DCA treatment groups. **(A)** Volcano plot displaying the differentially expressed metabolites between the lung cancer control group and the DCA treatment group. Red dots represent upregulated metabolites, while blue dots indicate downregulated metabolites. The threshold for differential expression is set at |log2(Fold change)|> 1 and -log10(P) > 1. **(B)** Principal component analysis (PCA) of the differentially expressed metabolites, showing a clear separation between the lung cancer control group (red) and the DCA treatment group (green). **(C)** Pathway enrichment analysis of the differentially expressed metabolites, with the Warburg effect and Citric acid cycle emerging as the most significantly enriched pathways. **(D)** Pathway impact analysis, revealing the Citrate cycle (TCA cycle) as the most significantly impacted pathway in the DCA treatment group.

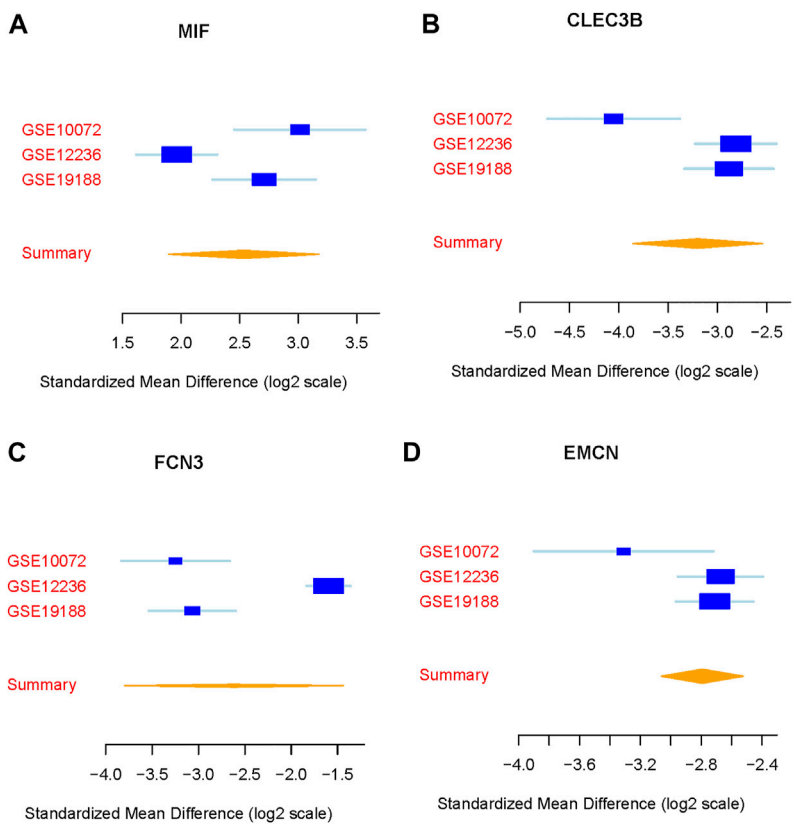

FIGURE 2
Identification of differentially expressed genes in lung cancer. **(A–D)** Expression patterns of the four highly significant differentially expressed genes (MIF, CLEC3B, FCN3, and EMCN) across the three public datasets GSE10072, GSE12236, and GSE19188.

and revealing previously unidentified therapeutic targets (Lefort et al., 2014). Metabolomics, the comprehensive analysis of endogenous small molecules within biological systems, can furnish valuable information on the metabolic ramifications of DCA administration. Concurrently, transcriptomics facilitates the examination of DCA-induced alterations in gene expression patterns. The amalgamation of these techniques can yield a more thorough understanding of DCA's mode of action in the context of lung cancer treatment (Tataranni and Piccoli, 2019).

In the present investigation, our objective was to shed light on the therapeutic mechanisms of DCA in lung cancer by employing an integrated multi-omics approach, which encompasses both metabolomic and transcriptomic analyses. We utilized gas chromatography-time-of-flight mass spectrometry (GC-TOF-MS) to characterize the metabolomic profile of lung cancer cells subjected to DCA treatment, while RNA sequencing generated the corresponding transcriptomic data. Through the integration of these datasets, we endeavored to unravel the molecular pathways influenced by DCA and pinpoint potential biomarkers indicative of treatment response. Our findings may enhance the understanding of the molecular foundations of DCA's therapeutic effects in lung cancer and offer invaluable insights for refining DCA-based treatment strategies. Moreover, the integrated multi-omics approach implemented in this research may serve as a template for subsequent inquiries into the mechanisms of other putative anti-cancer agents.

Materials and methods

Data collection and processing

We collected RNA-seq data from publicly available datasets. We extracted gene expression profiles from RNA-seq data in public datasets, including GSE10072, GSE12236, and GSE19188 (Lu et al., 2012; Zhang et al., 2018; Edginton-White et al., 2023). For transcriptomic data, we performed background correction, log2 transformation, and quantile normalization. For the metabolomic data, we applied missing value imputation, data transformation (log10), and autoscaling (mean-centering and dividing by the standard deviation) to obtain the normalized dataset. The primary purpose of using these datasets was to identify differentially expressed genes and potential biomarkers associated with DCA treatment in lung cancer. By integrating and analyzing the gene expression profiles from these datasets, we aimed to reveal the key molecular mechanisms underlying the therapeutic effects of DCA in lung cancer.

Quantitative real-time PCR (qRT-PCR) analysis

Total RNA was extracted from tumor tissues using TRIzol reagent (Invitrogen, United States) following the manufacturer's instructions. The quality of the extracted RNA was assessed using a NanoDrop spectrophotometer (Thermo Scientific, United States) and an Agilent 2100 Bioanalyzer (Agilent Technologies, United States). cDNA synthesis was performed using the RevertAid First Strand cDNA Synthesis Kit (Thermo Fisher Scientific, United States) according to the manufacturer's instructions. Quantitative real-time PCR (qRT-PCR) was conducted using the PowerUp SYBR Green Master Mix (Thermo Fisher Scientific, United States) on a QuantStudio 6 Flex Real-Time PCR System (Applied Biosystems, United States). The primer sequences used in the study are as follows:

MIF Forward: 5′- GAACCGCAACTACAGTAAGCTGC -3′
MIF Reverse: 5′- ACGTTGGCAGCGTTCATGTCGT -3′
GAPDH Forward: 5′- CATCACTGCCACCCAGAAGACTG -3′
GAPDH Reverse: 5′- ATGCCAGTGAGCTTCCCGTTCAG -3′

The relative expression levels of the MIF gene were calculated using the $2^{(-\Delta\Delta Ct)}$ method, with the reference gene (GAPDH) serving as an internal control for normalization.

Bioinformatics analysis

For the transcriptomic meta-analysis, we utilized the MetaIntegrator tool, a robust bioinformatics resource designed to integrate and analyze gene expression data from multiple studies (Haynes et al., 2017). The MetaIntegrator tool facilitated the identification of consistent gene expression signatures across diverse datasets, thereby enhancing the reliability of our findings. During the meta-analysis, both forward and backward searches were conducted to ensure a comprehensive assessment of the available data. Regarding the metabolomic analysis, we employed the MetaboAnalyst platform, a powerful and user-friendly web-based tool tailored for the interpretation of high-throughput metabolomics data (Chong et al., 2018). This platform enabled us to perform a series of advanced statistical analyses, including volcano plots to visualize the distribution of differentially expressed metabolites, principal component analysis (PCA) for dimensionality reduction and sample clustering, differential metabolite enrichment analysis to identify significantly altered metabolic features, and metabolic pathway analysis to investigate the biological functions and pathways impacted by DCA treatment. Additionally, we conducted metabolite-gene interaction analysis to explore the possible relationships between the identified metabolites and their corresponding genes, providing further insights into the molecular mechanisms underlying the therapeutic effects of DCA in lung cancer.

Animal handling and treatment

We established a subcutaneous xenograft model of lung cancer using BALB/c nude mice, which were purchased from the Shanghai Laboratory Animal Center of the Chinese Academy of Sciences (Shanghai, China). The mice were housed in a temperature-controlled environment with a 12-h light/dark cycle and were provided with standard rodent chow and water *ad libitum*. After acclimatization, the animals were injected subcutaneously with A549 cells to establish the lung cancer model. Once the tumors were successfully established, the mice were divided into two experimental groups: the lung cancer control group and the lung cancer treatment group. In the lung cancer treatment group, the mice received dichloroacetic acid (DCA) at a concentration of 2 g/L (DCAC2) in their drinking water, while the lung cancer control group was administered an equivalent volume of 0.9% saline solution as their drinking water. At the end of the treatment period, the mice were euthanized following approved ethical guidelines, and serum samples were collected for further analyses.

GC-TOF-MS

For the metabolomic profiling of mouse serum samples using gas chromatography-time-of-flight mass spectrometry (GC-TOF-MS), we adapted a published protocol with minor modifications to prepare and derivatize the samples. Initially, pooled quality control (QC) samples were created by combining 20 μL aliquots from each serum sample (Dunn et al., 2008). Subsequently, a 50 μL aliquot of serum sample was spiked with two internal standards (10 μL of L-2-chlorophenylalanine in water, 0.3 mg/mL; 10 μL of heptadecanoic acid in methanol, 1 mg/mL) and vortexed for 10 s. The mixed solution was extracted with 175 μL of methanol/chloroform (3:1) and vortexed for 30 s. After storing the samples for 10 min at −20°C, they were centrifuged at 8,000 rpm for 10 min. A 200 μL supernatant aliquot was transferred to a glass sampling vial and vacuum-dried at room temperature. The dried residue underwent a two-step derivatization process. First, 80 μL of methoxyamine (15 mg/mL in pyridine) was added to the vial, followed by incubation at 30°C for 90 min. Next, the samples were incubated with 80 μL of N,O-bis(trimethylsilyl)trifluoroacetamide (BSTFA, containing 1% trimethylchlorosilane (TMCS)) at 70°C for 60 min. Upon completion of the reaction, the samples were allowed to rest at room temperature for 1 h before proceeding with the GC-TOF-MS analysis.

Cell culture

The human lung cancer cell line A549 was procured from the Cell Bank of the Chinese Academy of Sciences (Shanghai, China). Cells were maintained in Dulbecco's Modified Eagle Medium (DMEM; Gibco, United States) supplemented with 10% fetal bovine serum (FBS; Gibco, United States) and 1% penicillin-streptomycin (Gibco, United States). Cultures were incubated at 37°C in a humidified atmosphere containing 5% CO_2.

Results

Metabolomic profiling

In this study, we utilized a total of 38 mice, comprising 18 in the DCA treatment group and 20 in the lung cancer control group. Based on our previously defined criteria for selecting differentially expressed metabolites, we set the threshold at |log2(Fold Change)|> 1 and -log10P) > 1. A total of 53 differentially expressed metabolites were

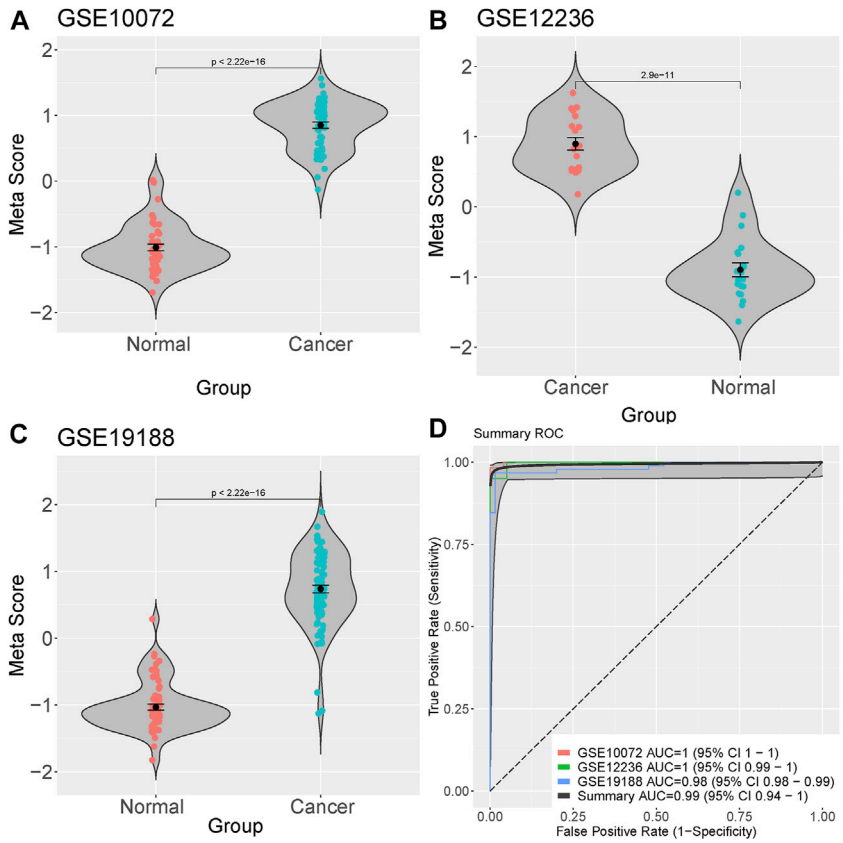

FIGURE 3
Diagnostic potential of the four identified genes in Lung cacner. **(A–C)** Meta-score generation by combining the expression levels of the four differentially expressed genes (MIF, CLEC3B, FCN3, and EMCN) in each sample. **(D)** Summary receiver operating characteristic (ROC) curve analysis demonstrating the diagnostic accuracy of the meta-score, with an area under the curve (AUC) of 0.99.

identified between the two groups (see Supplementary Table S1 for details). These metabolites were visualized using a volcano plot to demonstrate their differential expression (Figure 1A). We conducted a principal component analysis (PCA) on the differentially expressed metabolites between the lung cancer and DCA treatment groups. The PCA revealed a significant separation between the two groups (Figure 1B), indicating distinct metabolic profiles. Subsequently, we performed pathway enrichment analysis and pathway impact analysis on the differentially expressed metabolites. The pathway enrichment analysis revealed that the two most significantly enriched pathways were the Warburg effect and the Citric acid cycle (Figure 1C). In the pathway impact analysis, the Citrate cycle (TCA cycle) emerged as the most significantly impacted pathway (Figure 1D), suggesting a potential influence of DCA treatment on these metabolic processes in lung cancer.

Gene expression profiles in lung cancer

We integrated and analyzed RNA-seq data from three public datasets, including GSE10072, GSE12236, and GSE19188. Our analysis identified four highly significant differentially expressed genes in lung cancer, comprising MIF, CLEC3B, FCN3, and EMCN (Figures 2A–D). The consistent validation of these genes across multiple datasets suggests their potential importance in lung cancer. To further investigate the diagnostic potential of these four genes, we generated a meta-score by combining their expression levels in each sample (Figures 3A–C). We then used this meta-score to distinguish between lung cancer and normal control samples. The summary receiver operating characteristic (ROC) curve analysis revealed that the area under the curve (AUC) was 0.99, indicating high diagnostic accuracy for lung cancer (Figure 3D).

Metabolite-metabolite and metabolite-gene interaction pathway analysis

In order to explore the relationships between differentially expressed metabolites and their associated genes, as well as the interactions among the metabolites themselves, we conducted a series of analyses. First, we performed a metabolite-pathway interaction analysis on the 53 differentially expressed metabolites. In the resulting network, we observed interactions between the Warburg effect and Citric acid cycle pathways (Figure 4A). Subsequently, we investigated the interactions between metabolites and genes. Our analysis revealed a significant interaction between the core metabolite citric acid, which is involved in the Citric acid

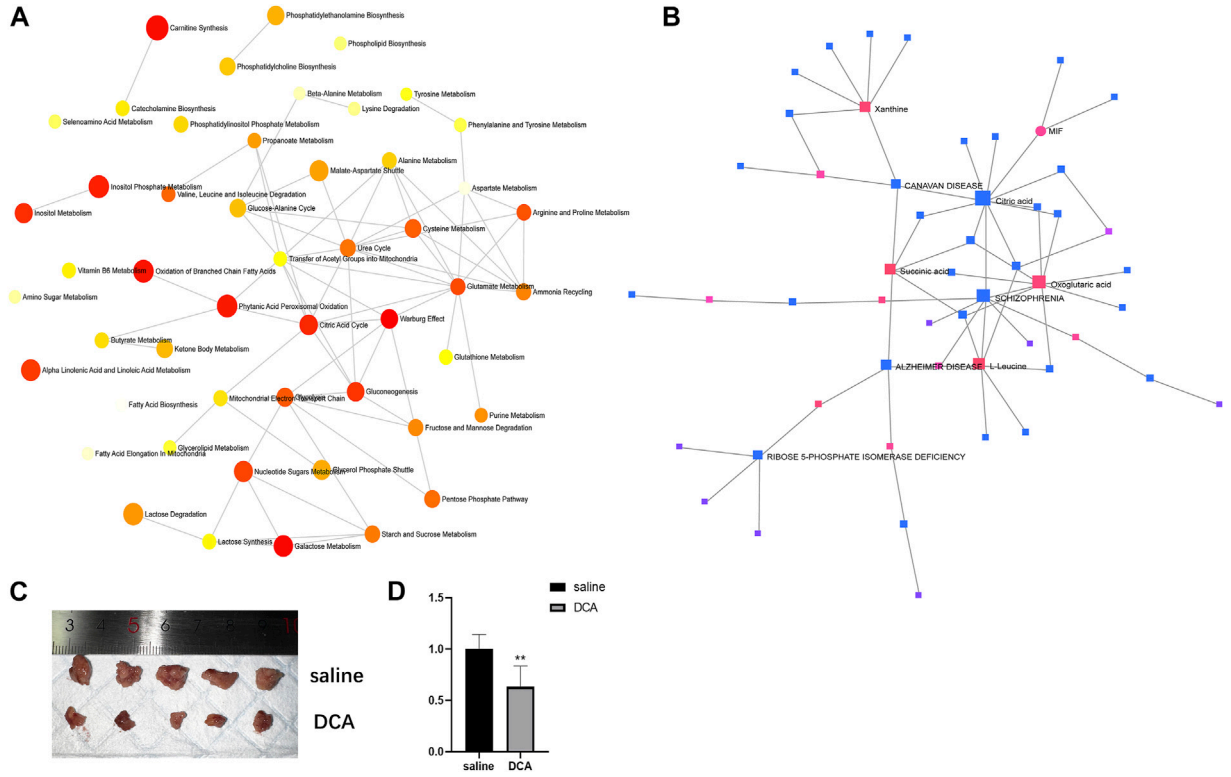

FIGURE 4
Interactions between metabolites and pathways, and *in vivo* evaluation of DCA treatment. **(A)** Network analysis of differentially expressed metabolites showing interactions between the Warburg effect and Citric acid cycle pathways. **(B)** Interaction between citric acid and MIF gene in lung cancer. **(C)** Representative images of subcutaneous xenograft tumors in the cancer control and DCA treatment groups, showing a significant difference in tumor size. **(D)** RT-PCR analysis of MIF gene expression in tumors from the cancer control and DCA treatment groups, demonstrating a significant reduction in MIF expression in the DCA-treated group.

cycle, and the differentially expressed gene MIF in lung cancer (Figure 4B). This finding suggests a potential link between the identified metabolites and genes in the context of lung cancer pathogenesis.

In vivo evaluation of DCA treatment on tumor growth and MIF gene expression

To assess the impact of DCA treatment on tumor growth *in vivo*, we compared the subcutaneous xenograft tumors in the cancer control group and the DCA treatment group. As depicted in Figure 4C, there was a significant difference in tumor size between the two groups, with the DCA treatment group exhibiting notably smaller tumors compared to the cancer control group, which received saline. We then performed RT-PCR analysis to examine the expression of the MIF gene in the tumors of both groups. The results, shown in Figure 4D, revealed a significant decrease in MIF gene expression in the DCA treatment group compared to the cancer control group. These findings suggest that DCA treatment may effectively suppress tumor growth and modulate MIF gene expression in the lung cancer xenograft model.

Discussion

In this study, we aimed to explore the effects of DCA treatment on lung cancer by integrating transcriptomic and metabolomic data, as well as validating our findings using an *in vivo* lung cancer xenograft model. Our comprehensive analysis not only provided insights into the molecular mechanisms underlying the therapeutic effects of DCA in lung cancer but also identified potential diagnostic biomarkers and therapeutic targets.

We found 53 differentially expressed metabolites between the DCA treatment and lung cancer control groups. Our pathway enrichment and impact analyses revealed that the Warburg effect and Citric acid cycle were the most significantly enriched and impacted metabolic pathways, respectively. Importantly, we observed a significant increase in citric acid levels in the DCA treatment group. Previous studies have reported that elevated citric acid can inhibit the growth of A549 cells (Zhou et al., 2015; Ji et al., 2020). Furthermore, our analysis indicated a potential interaction between citric acid and the MIF gene. These findings suggest a novel mechanism by which DCA may exert its anticancer effects, involving the modulation of citric acid levels and its subsequent interaction with the MIF gene.

The Warburg effect, a well-known metabolic alteration in cancer cells, is characterized by an increased rate of glycolysis even under nonmonic conditions, leading to lactate production instead of oxidative

phosphorylation in the mitochondria (Liberti and Locasale, 2016). Our findings suggest that DCA may exert its anticancer effects by targeting these key metabolic pathways and shifting the cancer cells' metabolism away from the Warburg effect towards oxidative phosphorylation, which ultimately leads to increased ROS production and subsequent cell death. This is in line with previous studies demonstrating that DCA can reverse the Warburg effect in cancer cells and promote apoptosis via the mitochondria-dependent pathway.

Our analysis also identified four highly significant differentially expressed genes in lung cancer, namely, MIF, CLEC3B, FCN3, and EMCN. Among these, MIF was found to interact significantly with the core metabolite citric acid in the Citric acid cycle. MIF, also known as macrophage migration inhibitory factor, is a pleiotropic cytokine implicated in various biological processes, including cell proliferation, angiogenesis, and immune regulation. Overexpression of MIF has been reported in several cancer types, including lung cancer, and is associated with tumor progression, metastasis, and poor prognosis (Verjans et al., 2009; Nobre et al., 2017; Penticuff et al., 2019). Our findings suggest that the therapeutic effects of DCA in lung cancer may be partially mediated through the regulation of MIF expression and its interaction with citric acid. Further investigation of MIF as a potential therapeutic target in lung cancer is warranted. Besides lung cancer, DCA has been investigated in numerous other cancer types, including breast cancer, glioblastoma, colorectal cancer, and prostate cancer. In addition to the Warburg effect reversal, DCA treatment has been shown to modulate other signaling pathways and cellular processes in various cancer types. For instance, in breast cancer, DCA has been found to inhibit the Akt/mTOR signaling pathway, leading to the suppression of cell proliferation and migration (Xiao et al., 2017). In glioblastoma, DCA has been reported to enhance the activity of the DNA repair enzyme O6-methylguanine-DNA methyltransferase (MGMT), thereby increasing the sensitivity of glioblastoma cells to temozolomide, a standard chemotherapeutic agent (Singh et al., 2021). In colorectal cancer, DCA has been shown to modulate the p53 signaling pathway, promoting cell cycle arrest and apoptosis (Zeng et al., 2015).

In our *in vivo* lung cancer xenograft model, we observed that DCA treatment significantly reduced tumor size and suppressed MIF gene expression. This corroborates our *in silico* findings and provides evidence for the potential therapeutic value of DCA in lung cancer treatment. Although DCA has been widely studied for its anticancer properties, clinical trials involving DCA for cancer treatment have yielded mixed results. Our study adds to the growing body of evidence supporting the potential of DCA as a therapeutic agent in lung cancer and provides a rationale for further investigation into the optimal dosing, treatment duration, and possible combination therapies with other anticancer agents to enhance its efficacy and minimize potential side effects.

In summary, our integrated transcriptomic and metabolomic analysis, together with *in vivo* validation, provided valuable insights into the molecular mechanisms underlying the therapeutic effects of DCA in lung cancer. We identified key metabolic pathways, including the novel finding of citric acid elevation and its interaction with the MIF gene, potential diagnostic biomarkers, as well as therapeutic targets, which may help guide future research and clinical management of lung cancer. Nevertheless, further studies with larger sample sizes and diverse cancer models are needed to confirm our findings and establish the clinical utility of DCA in the treatment of lung cancer. Additionally, investigations into the potential synergistic effects of DCA in combination with other anticancer agents may help optimize its therapeutic potential and overcome potential resistance mechanisms.

In conclusion, our study highlights the importance of integrated omics approaches in unraveling the complex molecular mechanisms underpinning the therapeutic effects of DCA in lung cancer. The identification of key metabolic pathways, including the novel finding of citric acid elevation and its interaction with the MIF gene, offers promising avenues for the development of targeted therapeutic strategies and the improvement of clinical outcomes for lung cancer patients.

Data availability statement

The original contributions presented in the study are included in the article/Supplementary Materials, further inquiries can be directed to the corresponding author.

Ethics statement

The animal study was reviewed and approved by the First Affiliated Hospital of Zhejiang University School of Medicine.

Author contributions

MF, JW, and JZ contributed to this study in several ways. MF contributed to the design of the study, the analysis and interpretation of data, and the drafting of the manuscript. JW contributed to the collection and analysis of data, the interpretation of results, and the critical revision of the manuscript. JZ contributed to the interpretation of data, the critical revision of the manuscript, and the final approval of the version to be published. All authors contributed to the article and approved the submitted version.

Conflict of interest

The authors declare that the research was conducted in the absence of any commercial or financial relationships that could be construed as a potential conflict of interest.

Publisher's note

Supplementary material

The Supplementary Material for this article can be found online at: https://www.frontiersin.org/articles/10.3389/fgene.2023.1199566/full#supplementary-material

References

Bunn, P. A., Jr (2012). Worldwide overview of the current status of lung cancer diagnosis and treatment. *Archives pathology laboratory Med.* 136, 1478–1481. doi:10.5858/arpa.2012-0295-SA

Chong, J., Soufan, O., Li, C., Caraus, I., Li, S., Bourque, G., et al. (2018). MetaboAnalyst 4.0: Towards more transparent and integrative metabolomics analysis. *Nucleic acids Res.* 46, W486–W494. doi:10.1093/nar/gky310

Dunn, W. B., Broadhurst, D., Ellis, D. I., Brown, M., Halsall, A., O'Hagan, S., et al. (2008). A GC-TOF-MS study of the stability of serum and urine metabolomes during the UK Biobank sample collection and preparation protocols. *Int. J. Epidemiol.* 37, i23–i30. doi:10.1093/ije/dym281

Edginton-White, B., Maytum, A., Kellaway, S. G., Goode, D. K., Keane, P., Pagnuco, I., et al. (2023). A genome-wide relay of signalling-responsive enhancers drives hematopoietic specification. *Nat. Commun.* 14, 267. doi:10.1038/s41467-023-35910-9

Farina, G. A., Cherubini, K., de Figueiredo, M. A. Z., and Salum, F. G. (2020). Deoxycholic acid in the submental fat reduction: A review of properties, adverse effects, and complications. *J. Cosmet. dermatology* 19, 2497–2504. doi:10.1111/jocd.13619

Hammerschmidt, S., and Wirtz, H. (2009). Lung cancer: Current diagnosis and treatment. *Dtsch. Ärzteblatt Int.* 106, 809–818. doi:10.3238/arztebl.2009.0809

Haynes, W. A., et al. (2017). *Pacific symposium on biocomputing 2017*, 144-153. World Scientific.

Ji, Z., Yin, Z., Jia, Z., and Wei, J. (2020). Carbon nanodots derived from urea and citric acid in living cells: Cellular uptake and antioxidation effect. *Langmuir* 36, 8632–8640. doi:10.1021/acs.langmuir.0c01598

Lefort, N., Brown, A., Lloyd, V., Ouellette, R., Touaibia, M., Culf, A. S., et al. (2014). ^{1}H NMR metabolomics analysis of the effect of dichloroacetate and allopurinol on breast cancers. *J. Pharm. Biomed. analysis* 93, 77–85. doi:10.1016/j.jpba.2013.08.017

Liberti, M. V., and Locasale, J. W. (2016). The Warburg effect: How does it benefit cancer cells? *Trends Biochem. Sci.* 41, 211–218. doi:10.1016/j.tibs.2015.12.001

Lu, T.-P., Tsai, M.-H., Hsiao, C. K., Lai, L.-C., and Chuang, E. Y. (2012). Expression and functions of semaphorins in cancer. *Transl. Cancer Res.* 1, 74–87.

Ma, W., Zhao, X., Wang, K., Liu, J., and Huang, G. (2018). Dichloroacetic acid (DCA) synergizes with the SIRT2 inhibitor Sirtinol and AGK2 to enhance anti-tumor efficacy in non-small cell lung cancer. *Cancer Biol. Ther.* 19, 835–846. doi:10.1080/15384047.2018.1480281

Mottaghitalab, F., Farokhi, M., Fatahi, Y., Atyabi, F., and Dinarvand, R. (2019). New insights into designing hybrid nanoparticles for lung cancer: Diagnosis and treatment. *J. Control. release* 295, 250–267. doi:10.1016/j.jconrel.2019.01.009

Nobre, C. C. G., de Araújo, J. M. G., Fernandes, T. A. A. d. M., Cobucci, R. N. O., Lanza, D. C. F., Andrade, V. S., et al. (2017). Macrophage migration inhibitory factor (MIF): Biological activities and relation with cancer. *Pathology Oncol. Res.* 23, 235–244. doi:10.1007/s12253-016-0138-6

Penticuff, J. C., Woolbright, B. L., Sielecki, T. M., Weir, S. J., and Taylor, J. A., III (2019). MIF family proteins in genitourinary cancer: Tumorigenic roles and therapeutic potential. *Nat. Rev. Urol.* 16, 318–328. doi:10.1038/s41585-019-0171-9

Singh, N., Miner, A., Hennis, L., and Mittal, S. (2021). Mechanisms of temozolomide resistance in glioblastoma-a comprehensive review. *Cancer drug Resist.* 4, 17–43. doi:10.20517/cdr.2020.79

Tataranni, T., and Piccoli, C. (2019). Dichloroacetate (DCA) and cancer: An overview towards clinical applications. *Oxidative Med. Cell. Longev. 2019* 2019, 8201079. doi:10.1155/2019/8201079

Verjans, E., Noetzel, E., Bektas, N., Schütz, A. K., Lue, H., Lennartz, B., et al. (2009). Dual role of macrophage migration inhibitory factor (MIF) in human breast cancer. *BMC cancer* 9, 230–318. doi:10.1186/1471-2407-9-230

Xiao, Y., Peng, H., Hong, C., Chen, Z., Deng, X., Wang, A., et al. (2017). PDGF promotes the Warburg effect in pulmonary arterial smooth muscle cells via activation of the PI3K/AKT/mTOR/HIF-1α signaling pathway. *Cell. Physiology Biochem.* 42, 1603–1613. doi:10.1159/000479401

Zeng, H., Claycombe, K. J., and Reindl, K. M. (2015). Butyrate and deoxycholic acid play common and distinct roles in HCT116 human colon cell proliferation. *J. Nutr. Biochem.* 26, 1022–1028. doi:10.1016/j.jnutbio.2015.04.007

Zhang, W., Fan, J., Chen, Q., Lei, C., Qiao, B., and Liu, Q. (2018). SPP1 and AGER as potential prognostic biomarkers for lung adenocarcinoma. *Oncol. Lett.* 15, 7028–7036. doi:10.3892/ol.2018.8235

Zhou, X., Chen, R., Yu, Z., Li, R., Li, J., Zhao, X., et al. (2015). Dichloroacetate restores drug sensitivity in paclitaxel-resistant cells by inducing citric acid accumulation. *Mol. Cancer* 14, 63–12. doi:10.1186/s12943-015-0331-3

frontiers | Frontiers in Genetics

TYPE Review
PUBLISHED 24 August 2023
DOI 10.3389/fgene.2023.1242711

OPEN ACCESS

EDITED BY
Jian Gao,
Shanghai Children's Medical Center, China

REVIEWED BY
Chen Qi,
Guizhou Provincial People's Hospital, China
Miao Yan,
Central South University, China

*CORRESPONDENCE
Hailin Liu,
liuhailinaa@126.com
Yong Yang,
yyxpower@163.com

†These authors have contributed equally to this work and share first authorship

‡These authors have contributed equally to this work and share last authorship

RECEIVED 19 June 2023
ACCEPTED 10 August 2023
PUBLISHED 24 August 2023

CITATION
Li G, Li Q, Zhang C, Yu Q, Li Q, Zhou X, Yang R, Yang X, Liu H and Yang Y (2023), The impact of gene polymorphism and hepatic insufficiency on voriconazole dose adjustment in invasive fungal infection individuals.
Front. Genet. 14:1242711.
doi: 10.3389/fgene.2023.1242711

The impact of gene polymorphism and hepatic insufficiency on voriconazole dose adjustment in invasive fungal infection individuals

Guolin Li[1,2†], Qinhui Li[3†], Changji Zhang[1,2], Qin Yu[4], Qi Li[1,5], Xiaoshi Zhou[1,5], Rou Yang[1,5], Xuerong Yang[1,5], Hailin Liu[6*‡] and Yong Yang[1,5*‡]

[1]Department of Pharmacy, Sichuan Academy of Medical Sciences and Sichuan Provincial People's Hospital, School of Medicine, University of Electronic Science and Technology of China, Chengdu, China, [2]School of Basic Medicine and Clinical Pharmacy, China Pharmaceutical University, Nanjing, China, [3]Department of Medical, Sichuan Academy of Medical Sciences and Sichuan Provincial People's Hospital, School of Medicine, University of Electronic Science and Technology of China, Chengdu, China, [4]College of Pharmacy, Southwest Medical University, Luzhou, China, [5]Personalized Drug Therapy Key Laboratory of Sichuan Province, School of Medicine, University of Electronic Science and Technology of China, Chengdu, China, [6]Department of Pharmacy, The People's Hospital of Chongqing Liangjiang New Area, Chongqing, China

Voriconazole (VRZ) is a broad-spectrum antifungal medication widely used to treat invasive fungal infections (IFI). The administration dosage and blood concentration of VRZ are influenced by various factors, posing challenges for standardization and individualization of dose adjustments. On the one hand, VRZ is primarily metabolized by the liver, predominantly mediated by the cytochrome P450 (CYP) 2C19 enzyme. The genetic polymorphism of CYP2C19 significantly impacts the blood concentration of VRZ, particularly the trough concentration (Ctrough), thereby influencing the drug's efficacy and potentially causing adverse drug reactions (ADRs). Recent research has demonstrated that pharmacogenomics-based VRZ dose adjustments offer more accurate and individualized treatment strategies for individuals with hepatic insufficiency, with the possibility to enhance therapeutic outcomes and reduce ADRs. On the other hand, the security, pharmacokinetics, and dosing of VRZ in individuals with hepatic insufficiency remain unclear, making it challenging to attain optimal Ctrough in individuals with both hepatic insufficiency and IFI, resulting in suboptimal drug efficacy and severe ADRs. Therefore, when using VRZ to treat IFI, drug dosage adjustment based on individuals' genotypes and hepatic function is necessary. This review summarizes the research progress on the impact of genetic polymorphisms and hepatic insufficiency on VRZ dosage in IFI individuals, compares current international guidelines, elucidates the current application status of VRZ in individuals with hepatic insufficiency, and discusses the influence of CYP2C19, CYP3A4, CYP2C9, and ABCB1 genetic polymorphisms on VRZ dose adjustments and Ctrough at the pharmacogenomic level. Additionally, a comprehensive summary and analysis of existing studies' recommendations on VRZ dose adjustments based on CYP2C19 genetic polymorphisms and hepatic insufficiency are provided, offering a more comprehensive reference for dose selection and adjustments of VRZ in this patient population.

KEYWORDS

voriconazole, genetic polymorphism, hepatic insufficiency, CYP2C19, invasive fungal infections, dose adjustment

1 Introduction

Invasive fungal infection (IFI) is a dangerous disease commonly seen in individuals with damaged immune function, such as individuals with acquired immune deficiency syndrome (AIDS), malignancy, and organ transplantation (Kullberg and Arendrup, 2015; Douglas et al., 2021). Individuals with hepatic insufficiency are vulnerable to IFI due to their low immune function and increased intestinal mucosal permeability, and IFI has a high mortality rate, which seriously affects patient prognosis, especially in immunosuppressed individuals, where the mortality rate may reach up to 90% (Yamada et al., 2018; Chen et al., 2021; Jenks et al., 2021). VRZ is a medication with broad-ranging antifungal properties extensively used to treat IFI (Ullmann et al., 2007). However, the pharmacokinetic parameters, efficacy, and safety of VRZ are influenced by various factors, such as genetic polymorphisms, liver function, and drug interactions (Liu and Mould, 2014; Lamoureux et al., 2016).

Gene polymorphism is one of the critical factors in the variability of pharmacokinetic parameters of VRZ. Gene polymorphism is when multiple versions of genes are present in a population, and these versions can result in different enzyme activities (Cheng et al., 2018). VRZ is primarily metabolized in the liver by CYP2C19 enzyme and partially by CYP3C4 and CYP2C9. CYP2C19 gene polymorphism affects the pharmacokinetic parameters and efficacy of VRZ (Hulin et al., 2011; Hamadeh et al., 2017). It has been found that the pharmacokinetic parameters of VRZ in mutant carriers such as CYP2C19*2 are significantly higher than those in wild-type carriers, while enhanced carriers such as CYP2C19*17 show the opposite trend (Pascual et al., 2008; Dolton et al., 2012). Therefore, individualized dose adjustment strategies are needed for different CYP2C19 genotypes to improve the efficacy and safety of VRZ (Pascual et al., 2012).

Hepatic insufficiency can also affect the pharmacokinetic parameters and efficacy of VRZ. Individuals with hepatic insufficiency experience difficulty breaking down and eliminating drugs from their system, and this causes the drug to remain in the body for an extended duration, leading to higher concentrations of the drug (Liu and Mould, 2014). Therefore, individuals with hepatic insufficiency should decrease their VRZ dosage to prevent ADRs caused by a potential overdose (Lamoureux et al., 2016). According to a study, the way VRZ works and its effects differ significantly for individuals with hepatic insufficiency compared to those with normal liver function (Tang et al., 2019; 2021). In addition, VRZ has a small margin of safety and has multiple ADRs, including neurotoxicity, hepatotoxicity, and visual impairment (Levine and Chandrasekar, 2016; Lem et al., 2019). Research has confirmed a meaningful connection between Ctrough and both the effectiveness of the treatment and the adverse drug reactions (Yang et al., 2022). As a result, medical professionals frequently suggest therapeutic drug monitoring (TDM) to enhance patient outcomes (Jin et al., 2016; Luong et al., 2016). The instructions provide dosage adjustment recommendations for individuals with mild to moderate liver impairment, utilizing exposure data from real-world usage of VRZ. However, there is a lack of comprehensive data on the safety, pharmacokinetics, and appropriate dosage for patients with severe hepatic insufficiency. It is crucial to develop individualized dose adjustment strategies for these patients to optimize the efficacy and safety of VRZ treatment.

Based on the above studies, the treatment of IFI involves a significant role for VRZ, but its pharmacokinetic parameters, efficacy and safety are influenced by several factors. Individualized dose adjustment strategies can enhance the effectiveness and safety of VRZ, but there are some differences in the results of different studies. Therefore, when developing dose adjustment strategies, the distribution of genetic polymorphisms and hepatic insufficiency in diverse populations should be considered, and the effects of multiple factors should be taken into account. However, there is not enough large-scale clinical research on personalized dosing for VRZ to confirm whether it is a safe and effective approach for guiding clinical practice. This paper focuses on how the CYP2C19 gene and hepatic insufficiency affect VRZ dose adjustment. From a pharmacogenomic perspective, we further investigate the influence of genetic polymorphisms in CYP3A4, CYP2C9, and ABCB1 on Ctrough. This information can help develop personalized treatment plans for VRZ use in individuals with IFI.

2 Voriconazole

Voriconazole (VRZ) was approved for marketing by the U.S. Food and Drug Administration (FDA) in 2002 and was introduced in China in 2005 (Pallet and Loriot, 2021). VRZ is a synthetic second-generation triazole antifungal drug derived from fluconazole and exhibits broad-spectrum antifungal activity. It is believed that the mechanism of action for triazole antifungal drugs involves inhibiting the fungal enzyme 14α-demethylase, which is responsible for converting lanosterol to ergosterol, thereby disrupting the synthesis of the cell membrane (Thompson and Lewis, 2010). The Infectious Diseases Society of America recommends VRZ as the primary treatment for invasive Aspergillosis (Chen et al., 2018). It is also effective against *Candida* spp. in treatment and prevention (Xing et al., 2017). The metabolic pathways of VRZ are influenced by multiple enzymes, with its primary circulating metabolite being Voriconazole N-oxide (Theuretzbacher et al., 2006; Voriconazole Pathway, Pharmacokinetics, n.d.) (Figure 1).

VRZ is used to treat invasive Aspergillosis, non-neutropenic Candidaemia individuals, and severe invasive infections caused by fluconazole-resistant *Candida*; however, VRZ may cause side effects such as hepatotoxicity, neurotoxicity, photosensitivity, visual disturbances, and osteochondritis with or without hyperfluorosis (Chau et al., 2014). Psychiatric disorders are common ADRs caused by VRZ, characterized by symptoms such as delirium, hallucinations, and emotional excitement (Benitez and Carver, 2019). A study suggested that these symptoms are associated

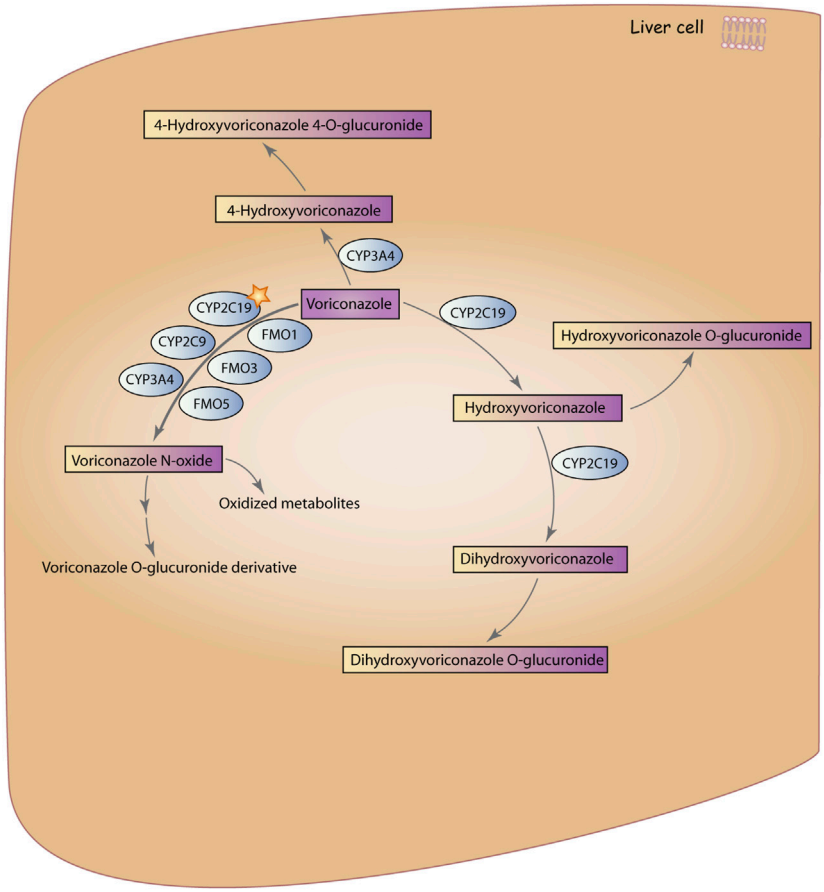

FIGURE 1
Metabolic pathways of VRZ. VRZ is primarily metabolized by the enzyme CYP2C19 to form Voriconazole N-oxide, with contributions from members of the CYP3A4, CYP2C9, and FMO families. Subsequently, Voriconazole N-oxide is further metabolized to voriconazole O-glucuronidated derivative and other oxidized metabolites. The second metabolic pathway involves hydroxylation of the methyl group of VRZ, in which VRZ is metabolized by CYP3A4 to 4-Hydroxyvoriconazole, which is then glucuronidated to form 4-Hydroxyvoriconazole 4-glucuronidate. The third pathway involves hydroxylation of the fluconazole ring of VRZ, in which VRZ is metabolized by CYP2C19 to hydroxyvoriconazole, which can further undergo hydroxylation by CYP2C19 to form dihydroxyvoriconazole. Finally, dihydroxyvoriconazole is glucuronidated to form dihydroxyvoriconazole O-glucuronidated. Voriconazole Pathway, Pharmacokinetics (Reproduced from PharmaGKB, licensed under CC BY-SA 4.0).

with the distribution and blood concentration of VRZ in the body; during its distribution in the body, VRZ can penetrate the blood-cerebrospinal fluid barrier, resulting in brain tissue concentrations that are 2–3 times higher than plasma concentrations (Ertem et al., 2022). ADRs associated with Ctrough also include hepatotoxicity and other neurological disorders (Hamada et al., 2012; Moriyama et al., 2017). Any form of VRZ can be excreted as a metabolite (98%) and as a prototype (2%) within 48 h of administration, so although it is not uncommon for VRZ to cause psychiatric disorders, psychiatric symptoms can rapidly improve or even disappear in a brief amount of time after discontinuation of the drug (Yi et al., 2017). In individuals with hepatic insufficiency combined with invasive aspergillosis, VRZ remains the drug of choice, but there is still much controversy regarding dose selection (Chen and Ning, 2022).

Reports suggest that VRZ can cause liver injury, but the mechanism of its occurrence is still unclear, and some studies suggest that it is mainly related to VRZ metabolism (Kyriakidis et al., 2017; Zhou et al., 2022). VRZ can be converted to active metabolites in the liver, and such functional products can cause mitochondrial damage directly or through inhibition of CYP proteins, leading to cellular dysfunction or necrosis, thus causing liver injury (Pessayre et al., 2012). There is controversy surrounding the impact of VRZ on liver injury, with some studies suggesting that VRZ-induced liver injury is a dose-dependent ADR, but others suggesting that liver injury does not correlate with drug concentration (Suzuki et al., 2013; Zonios et al., 2014).

The pharmacokinetic profile of VRZ in adults is nonlinear, with a significant increase in Ctrough with increasing medication administration. It is predominantly metabolized oxidatively by cytochrome P450 isoenzymes and secondarily by CYP3A4 and CYP2C9 enzymes, in addition to being a CYP3A4 inhibitor itself, so VRZ has more clinically significant drug interactions (Lee et al., 2022). Some studies have reported that the interaction of VRZ with carbamazepine, efavirenz, ritonavir, rifampin, phenobarbital, rifabutin, and nevirapine affects their pharmacokinetic parameters and efficacy (Chen et al., 2018). Therefore, attention needs to be paid to VRZ interactions with other drugs during treatment. VRZ pharmacokinetics are variable within and between individuals, with influencing factors including age, CYP2C19 gene polymorphisms, hepatic function status, drug

interactions, and ingestion, further adding to the concern of clinical response variability (Job et al., 2016; Li et al., 2017; You et al., 2018). In addition, Ctrough can significantly impact clinical response, and routine TDM of VRZ is recommended because of inter-patient variability in VRZ pharmacokinetics to avoid high Ctrough-related toxicity and treatment failure with low Ctrough (Denning et al., 2002).

3 Hepatic insufficiency combined with IFI

Hepatic insufficiency refers to the damage of liver cells by various hepatogenic factors, resulting in dysfunction of synthesis, degradation, detoxification, storage, secretion, and immunity, which may lead to jaundice, hemorrhage, infection, renal dysfunction, and hepatic encephalopathy (Verma et al., 2022). The advanced stage of hepatic insufficiency is generally called hepatic failure, and the main clinical manifestations are hepatic encephalopathy and hepatorenal syndrome (Rose et al., 2020; Vasques et al., 2022). Individuals with hepatic insufficiency are prone to complications of various infections due to impaired immune function, dysbiosis of intestinal flora, and reduced number of hepatic Kupffer cells, resulting in low immunity (Yamada et al., 2018). Moreover, the application of broad-spectrum, potent antimicrobial drugs and glucocorticoids, as well as invasive procedures, greatly raises the risk of opportunistic infections, especially in individuals with IFI, which are mostly single-site, but there are also cases of two or even multi-site disseminated infections (Hou et al., 2010; Lahmer et al., 2022). In critically ill individuals with hepatic insufficiency and IFI, the most frequent site of infection is the lung (37.0%–56.0%); other sites are the gastrointestinal tract (1.1%–20.2%), urinary tract (4.3%–15.9%), abdominal cavity (2.9%–14.4%) and bloodstream (0.7%–5.8%), and fungal infections of the thoracic cavity, biliary tract, and central nervous system are also seen (Fernández et al., 2018; Piano et al., 2019; Libera et al., 2023). When the liver is not functioning properly, it can affect the metabolism and excretion of VRZ; this may impact the drug's absorption and clearance rates from the body (Baririan et al., 2007; Verbeeck, 2008). Their Ctrough levels are significantly higher when they have hepatic insufficiency, which raises the risk of ADRs and can have a detrimental effect on their prognosis (Alffenaar et al., 2009; Ueda et al., 2009).

The most common pathogenic fungi of hepatic insufficiency combined with IFI are *Candida* spp. and Aspergillus spp. *Candida* spp. are mainly *Candida* albicans, accounting for more than 50%, and are the main pathogens of the intestinal tract, bloodstream, abdominal cavity, and urinary tract (Jenks et al., 2020; Silva et al., 2021; Hall et al., 2023). A multicenter study in Europe showed that fungal bloodstream infections were dominated by *Candida* albicans (54.4%), followed by *Candida* smooth (14.5%), *Candida* subsmooth (14.1%), *Candida tropicalis* (5.8%), *Candida* graminearum (2.5%), of which 34.9% of individuals suffered from septic shock (Bassetti et al., 2017; Medeiros et al., 2019). *Candida* albicans was also the main causative agent of fungal peritonitis (48.0%–81.8%), followed by *Candida klebsiella* (15.0%–25.0%), *Candida* smoothes (6.6%–20.0%), and novel Cryptococcus spp. were seen in some individuals (Tariq et al., 2019; Feldman et al., 2023). Pulmonary IFI is mainly caused by Aspergillus spp., with Aspergillus fumigatus being the most common, followed by Aspergillus flavus and Aspergillus niger; Aspergillus pyogenes and Aspergillus terreus are less frequently reported (Su et al., 2010; Jović et al., 2019; Lahmer et al., 2019). Cases of severe hepatic insufficiency combined with Pneumocystis pneumonia have also been reported to occur (Hadfield et al., 2019). In severe hepatic insufficiency, both natural and acquired immunity are severely impaired, resulting in decreased immunity, and often accompanied by intestinal dysfunction, intestinal mucosal edema, increased permeability, impaired intestinal barrier leading to flora translocation, intestinal microorganisms can enter the portal vein through the intestinal wall, coupled with serious damage to the liver mononuclear macrophage system, the ability to remove microorganisms is reduced, resulting in infection with bacteria, viruses and fungi and other pathogens the risk of infection with pathogens such as bacteria, viruses and fungi is significantly increased (Matsubara et al., 2016; Andrade et al., 2022). Therefore, individuals with hepatic insufficiency are more susceptible to developing IFI, and IFI usually occurs in the blood circulation and eventually causes systemic fungal infections, leading to conditions such as organ failure, sepsis, and fatal multi-organ dysfunction syndrome, for which VRZ is the first-line drug (Xing et al., 2017).

Severe hepatic insufficiency combined with IFI has an inadequate prognosis, with an upper morbidity and death rate, the clinical manifestations can be atypical, and diagnosing and treating it can be difficult. Antifungal drugs are mostly metabolized in the liver, which can cause highly toxic side effects (Cheong et al., 2009). According to relevant literature, individuals infected with *Candida* have a 30%–40% morbidity and mortality rate, while individuals infected with Aspergillus have an even higher rate of 50%–100% (Lahmer et al., 2016). *Candida* infection, invasive Aspergillus infection individuals to increase morbidity and mortality rate (Hwang et al., 2014). During liver transplantation, individuals who receive a new liver have an increased chance of getting fungal infections during and after the procedure (Kang et al., 2020). In recent years, prophylactic use of antifungal medications has helped to bring the overall prevalence of these infections down to 4%–8% (Lum et al., 2020; Khalid et al., 2021).

4 The impact of gene polymorphisms on VRZ

4.1 The impact of CYP2C19 on VRZ dose adjustment

VRZ is mainly metabolized in the liver and mediated by cytochrome P450 (CYP) 2C19 enzyme (Theuretzbacher et al., 2006). The CYP2C19 gene has genetic polymorphisms that can affect the pharmacokinetic characteristics of VRZ; in fact, these polymorphisms are responsible for 50% of the variability in VRZ. (Amsden and Gubbins, 2017). The gene that codes for CYP2C19 has more than 34 different versions, known as alleles; one of these alleles, called CYP2C19*17, has a mutation in the gene's promoter region, making it more active than usual (Lee et al., 2022). It was found that mutant genes such as CYP2C19*2 and CYP2C19*3 were connected to pharmacokinetic parameters of VRZ, and individuals carrying mutant genes such as CYP2C19*2 and CYP2C19*3 had a slower

TABLE 1 CYP2C19 phenotype classification.

Phenotype	Genotype	Effects on ctrough	Recommendations for adjustment from the CPIC
UMs (2–5%)	An individual with 2 increased function alleles (*17/*17)	The probability of attainment of therapeutic voriconazole Ctrough is small with standard dosing	Consider using an alternative agent, such as isavuconazole, liposomal amphotericin B, or posaconazole, as the primary therapy instead of voriconazole. These agents are not dependent on CYP2C19 metabolism
RMs (2–30%)	An individual with one common function allele and one increased function allele (*1/*17)	The probability of attainment of therapeutic voriconazole Ctrough is small with standard dosing	Consider using an alternative agent, such as isavuconazole, liposomal amphotericin B, or posaconazole, as the primary therapy instead of voriconazole. These agents are not dependent on CYP2C19 metabolism
NMs (35–50%)	An individual with 2 common function alleles (*1/*1)	Normal voriconazole metabolism	Start treatment with the recommended standard dosage
IMs (18–45%)	An individual with one common function allele and one no function allele or one no function allele and one increased function allele (*1/*2, *1/*3, *2/*17)	Higher dose-adjusted Ctrough of voriconazole compared with NMs	Start treatment with the recommended standard dosage
PMs (2–15%)	An individual with 2 no function alleles (*2/*2, *2/*3, *3/*3)	Higher dose-adjusted Ctrough of VRZ and may increase probability of adverse events	Consider using an alternative agent, such as isavuconazole, liposomal amphotericin B, or posaconazole, as the primary therapy instead of voriconazole. These agents are not dependent on CYP2C19 metabolism

UMs, CYP2C19 ultra-rapid metabolizers; RMs, CYP2C19 rapid metabolizers; NMs, CYP2C19 normal metabolizers; IMs, CYP2C19 intermediate metabolizers; PMs, CYP2C19 poor metabolizers.

clearance of VRZ, higher drug exposure, and greater fluctuations in drug concentration at the same dose (Hamadeh et al., 2017). It has been found that individualized adjustment of VRZ dose according to individuals' CYP2C19 genotypes can reduce drug exposure and decrease the incidence of ADRs while ensuring drug efficacy (Amsden and Gubbins, 2017; Zhang et al., 2021). Individualized dose adjustment of VRZ may be necessary for different CYP2C19 genotypes. The proper dosage can be determined using TDM in conjunction with pharmacogenetic testing (He et al., 2020; Li et al., 2021).

The Clinical Pharmacogenetics Implementation Consortium (CPIC) categorizes individuals into five groups based on their genotype for CYP2C19 (Moriyama et al., 2017). These groups include CYP2C19 ultrarapid metabolizers (UMs), CYP2C19 rapid metabolizers (RMs), CYP2C19 normal metabolizers (NMs), CYP2C19 intermediate metabolizers (IMs), and CYP2C19 poor metabolizers (PMs) (Lee et al., 2022) (See Table 1: CYP2C19 phenotype classification). The differences in CYP2C19 genes between individuals can greatly affect how they respond to VRZ medication, particularly for those with liver problems. Studies have shown that identifying a patient's CYP2C19 gene phenotype is essential in determining the appropriate VRZ dosage, as it can vary greatly from UMs to PMs (Ren et al., 2019). The impact of CYP2C19 is noted in the VRZ medication label approved by the FDA. However, there are currently no genetic variant-based dosing instructions available. To avoid potential problems, CPIC suggests utilizing antifungal medications that do not rely on the CYP2C19 enzyme metabolism for individuals with PMs/Ums, while standard VRZ dosing is recommended for other phenotypes, and the Dutch Pharmacogenetics Working Group (DPWG) recommends dose adjustment for both PMs and UMs phenotypes (García-García and Borobia, 2021; Maertens et al., 2021). The inconsistency and ambiguity of these guidelines may hinder clinicians' practical application of these drugs.

The CYP2C19*1/*17 and *17/*17 genotypes conferred higher enzymatic activity to the RMs and UMs phenotypes, respectively, compared to NMs (Sim et al., 2006). The *2 and *3 alleles were loss-of-function variations. IMs with one such variant had significantly lower enzyme activity compared to NMs. However, PMs with two such variants showed no enzyme activity. According to Hamadeh et al. (2017), CYP2C19 genotype significantly impacts the risk of VRZ underexposure, individuals with *17/*17 genotypes (UMs) and around 50% of those with *1/*17 genotypes (RMs) were unable to achieve a therapeutic Ctrough (2–6 mg/L) when VRZ was administered based on body weight. UMs showed a decrease in VRZ Ctrough, resulting in a delay in reaching the target Ctrough; on the other hand, PMs exhibited an increase in Ctrough, which puts them at a higher risk of ADRs (Walsh et al., 2018). Hence, compared to NMs, UMs and RMs may require an increase in the VRZ dosage, while PMs may necessitate a reduction in the VRZ dosage (Lamoureux et al., 2016) (See Table. 2: Recommendations for dose adjustment for different CYP2C19 phenotypes). It is important to be aware that medications like omeprazole and cimetidine, which inhibit CYP2C19, can increase Ctrough levels in VRZ; conversely, taking certain CYP450 enzyme inducers at the same time can cause Ctrough levels to drop below the necessary therapeutic levels, resulting in clinical failure (Mikus et al., 2006). Existing meta-analyses indicate that PMs taking VRZ are at an upper risk of experiencing ADRs compared to NMs and IMs; however, other meta-analyses have not found a significant correlation between the two (Li et al., 2016; Amsden and Gubbins, 2017). Therefore, we still require extensive, high-quality trials to confirm these findings.

Even though many studies have shown how the CYP2C19 gene polymorphisms affect VRZ dosage adjustment, specific details and controversies still exist. PMs/IMs lead to elevated VRZ blood levels that may result in toxicity, such as hepatotoxicity or neurotoxicity, but the link between PMs/IMs and hepatotoxicity has not been

TABLE 2 Recommendations for dose adjustment for different CYP2C19 phenotypes.

First author year	Study design	Sample size	Phenotype	Recommendations for dose adjustment
Zubiaur et al. (2021)	prospective observational study	106	UMs	3 times the standard dose
			RMs	2 times the standard dose
			NMs	the standard dose
			IMs	0.5 times the standard dose
			PMs	0.25 times the standard dose
Tanaka et al. (2020)	prospective observational study	19	IMs	Reduce the initial maintenance dose
			PMs	
Blanco-Dorado et al. (2020)	prospective observational study	78	RMs	Increase the initial maintenance dose
			UMs	
Li et al. (2020)	prospective observational study	93	RMs	PO 400 mg, twice a day
			NMs	PO 400 mg, twice a day
			IMs	PO 200 mg, twice a day
Hicks et al. (2020)	prospective observational study	202	UMs	VRZ is recommended to be avoided
			RMs	PO 300 mg, twice a day
			NMs, IMs, PMs	PO 200 mg, twice a day
Miao et al. (2019)	retrospective cohort study	105	NMs	the standard dose
			IMs	1.64 times the standard dose
			PMs	2.61 times the standard dose
Lin et al. (2018)	prospective observational study	105	RMs	IV 300 mg, twice a day
			IMs	IV 200 mg/Oral 350 mg, twice a day
			PMs	IV 150 mg/Oral 250 mg, twice a day
PharmGKB (2017)	NA	NA	UMs	1.5 times the standard dose
			IMs	the standard dose
			PMs	0.5 times the standard dose
Lamoureux et al. (2016)	retrospective study	35	UMs	IV 6.75 mg/kg, twice a day
			RMs	IV 3.94 mg/kg, twice a day
			NMs	IV 2.57 mg/kg, twice a day
Wang et al. (2014b)	prospective observational study	144	PMs	PO 200 mg, twice a day
			non-PMs	IV 200 mg/PO 300 mg, twice a day

UMs, CYP2C19 ultra-rapid metabolizers; RMs, CYP2C19 rapid metabolizers; NMs, CYP2C19 normal metabolizers; IMs, CYP2C19 intermediate metabolizers; PMs, CYP2C19 poor metabolizers; PO, oral administration; IV, intravenous injection; NA, not applicable.

established (Wang et al., 2014b). Additional investigation is necessary to fully comprehend the effects of CYP2C19*2 and CYP2C19*3 mutations on VRZ therapy response and hepatotoxicity. Differences in CYP2C19 genotype distribution in different populations may affect the applicability of dose adjustment strategies. For example, some studies have found a higher frequency of mutant phenotypes such as CYP2C19*2 in Asian populations, while enhanced phenotypes such as CYP2C19*17 predominate in European and American people, which may affect the accuracy and effectiveness of dose adjustment strategies (Mikus et al., 2011; Lee et al., 2021). Various studies indicate that the impact of CYP2C19 gene variations on the efficiency and security of VRZ may depend on the particular approach used for adjusting the dosage. For example, it has been suggested that individualized dose adjustment strategies may improve the efficacy and safety of VRZ more than conventional dose adjustment strategies in CYP2C19*2 and other mutant carriers (Hamada et al., 2013). Although CYP2C19 gene polymorphisms have an impact on the pharmacokinetic parameters and efficacy of VRZ, other causes, including individuals' liver and kidney function and drug interactions, need to be considered in actual clinical application. Special attention should be given to the impact of drug-induced

TABLE 3 Inhibitors and inducers of CYP2C19, CYP3A4, and CYP2C9.

Liver enzymes	Inhibitors	Inducers
CYP2C19	Esomeprazole, omeprazole, fluconazole, voriconazole, chloramphenicol, artemisinin, isoniazid, fluoxetine hydrochloride, indomethacin, valproate sodium, oxcarbazepine, fluvastatin, lovastatin, nicardipine, amiodarone, zafirlukast, oral contraceptives, etc	Rifampicin, ritonavir, dexamethasone, Ginkgo biloba preparation, etc
CYP2C9	Amiodarone, nifedipine, nicardipine, fenofibrate, fluvastatin, tamoxifen, cimetidine, fluoxetine, paroxetine, sertraline, fluvoxamine, isoniazid, ketoconazole, fluconazole, voriconazole, sulfamethoxazole, Leflunomide, sodium valproate, zafirlukast, fluorouracil, etc	Barbiturates, bosentan, carbamazepine, rifampicin, dexamethasone, ritonavir, etc
CYP3A4	Amiodarone, verapamil, cimetidine, doxycycline, enoxacin, Ciprofloxacin hydrochloride, erythromycin, clarithromycin, ketoconazole, miconazole, fluconazole, itraconazole, voriconazole, ritonavir, etc	Glucocorticoids, phenobarbital, phenytoin sodium, carbamazepine, oxcarbazepine, topiramate, rifampicin, pioglitazone, etc

enzyme reactions on the alteration of related drug plasma concentrations, particularly when co-administered with hepatic enzyme inducers or inhibitors, to avoid ADRs (Hakkola et al., 2020) (See Table 3: Inhibitors and inducers of CYP2C19, CYP3A4, and CYP2C9). Therefore, the dose adjustment strategy should consider various factors rather than being based solely on CYP2C19 genotype (Moriyama et al., 2017).

4.2 The impact of CYP3A on VRZ

CYP3A is the most prevalent metabolic enzyme in the liver and is engaged in the metabolism of 45%–60% of frequently used medications; CYP3A4 and CYP3A5 are the most significant drug-metabolizing enzymes in this regard (Wojnowski, 2004). CYP3A5 accounts for approximately 17%–60% of hepatic CYP3A and has a similar substrate specificity to CYP3A4; however, even with the same substrate, CYP3A4 exerts a higher metabolic efficiency (Klyushova et al., 2022). CYP3A4 is the main metabolic enzyme for VRZ hydroxylation metabolism, while CYP3A5 plays a relatively weak role in VRZ hydroxylation metabolism, and studies have shown that the hydroxylation metabolism of VRZ by CYP3A4 and CYP3A5 is relatively enhanced when CYP2C19 enzyme activity is diminished (Murayama et al., 2007). The CYP3A4 gene is a key enzyme in VRZ metabolism, and its genotype is associated with the pharmacokinetic and pharmacodynamic properties of VRZ. Still, compared with CYP2C19, CYP3A4 affects VRZ metabolism *in vivo* to a lesser extent, approximately 1/50th of CYP2C19(Hyland et al., 2003). Although CYP3A4 has been addressed in several previous studies, no genotypes explained the phenotype until two SNPs, rs4646437 and rs35599367, were found to be associated with the Ctrough of VRZ. The research findings reveal that the rs4646437 polymorphism significantly influences the mean blood drug concentration of VRZ, with the T variant allele being associated with higher blood drug concentrations (Gautier-Veyret et al., 2015; He et al., 2015). Walsh et al. found that polymorphisms such as CYP3A4*22 and CYP3A4*23 may impact the metabolism of VRZ, and CYP3A4 *22 was associated with higher VRZ concentrations compared to CYP3A4 *1/*1 (Walsh et al., 2018). Meanwhile, some studies indicate that genetic variations of CYP3A4 and CYP3A5 have little impact on the pharmacokinetics of VRZ (Lee et al., 2012; Chuwongwattana et al., 2020). Diverse studies' findings on how CYP3A4 genotype affects VRZ are equivocal; more research is required to determine how the two are related. Research on how CYP3A5 affects the pharmacokinetics of VRZ has also produced inconsistent results. According to Weiss et al., there is no apparent connection between CYP3A5*3 mutations and VRZ pharmacokinetics (Weiss et al., 2009). According to Levin et al. (2007), the amount of hepatic drug-metabolizing enzymes in the blood may indicate high levels of VRZ plasma concentration-induced liver toxicity; the study also discovered that the liver damage was not related to the CYP3A5*3 allele. However, a study conducted in a laboratory setting has demonstrated that individuals with the genetic variant CYP3A5*3/*3 experience a threefold increase in AUC when taking VRZ compared to those with at least one functional allele (Yamazaki et al., 2010).

4.3 The impact of CYP2C9 on VRZ

Studies have revealed that CYP2C19 is the primary enzyme responsible for the nitrogen-based oxidative metabolism of VRZ; however, CYP2C9 can also contribute to this process to a lesser extent (Dorji et al., 2019). Lee et al. (2002) showed that there is a link between the variability of VRZ blood concentration and the CYP2C9*2 and CYP2C9*3 alleles. The CYP2C9*13 allele is the first novel variant of CYP2C9 identified in Chinese and is important in determining the metabolic capacity of CYP2C9. Some studies indicate that the CYP2C9*13 gene variation can decrease drug clearance from the bloodstream (Si et al., 2004; Zhang et al., 2007). There are few conclusions regarding clinical aspects supporting the impact of different genotypes of CYP2C9 on VRZ metabolism, and there are some indications that CYP2C9 genotypes may not be associated with VRZ pharmacokinetics. The current research has made the function of CYP2C9 in VRZ metabolism somewhat controversial. According to Niwa et al., the CYP2C9 *2 allele results in less effective inhibition of CYP2C9 by VRZ compared to the CYP2C9 *1 and CYP2C9 *3 alleles (Niwa and Hata, 2016). It has been reported that the pharmacokinetic parameters of VRZ were not altered in individuals genotyped as CYP2C9 *2/*2 pure siblings (Liu and Mould, 2014). Furthermore, a study conducted on 35 healthy participants revealed that there was no impact of CYP2C9 on VRZ pharmacokinetic parameters, as

determined by a multiple regression analysis of VRZ pharmacokinetics (Weiss et al., 2009). In conclusion, there are varying results from different studies regarding the impact of CYP2C9 genotype on VRZ, further research is necessary to reach a definitive conclusion.

4.4 The impact of ABCB1 on VRZ

P-glycoprotein (ABCB1) is one of the crucial transporter proteins in the human body and is essential for maintaining biological barriers (Tulsyan et al., 2016). Currently, there have been over 50 SNPs documented in the ABCB1 gene (Tanabe et al., 2001). According to Cascorbi et al., a specific variation, rs1045642, in exon 26 of the ABCB1 gene can lead to a decrease in protein function (Cascorbi et al., 2001). ABCB1 also has genetic polymorphisms that affect its transport activity and, thus, the pharmacokinetic parameters of its transported substrates (Sauna et al., 2007). It was found that VRZ can interact with CaMdr1p, a homolog of yeast P-glycoprotein and that VRZ can mildly inhibit the activity of P-glycoprotein, corroborating that VRZ may be a substrate of ABCB1(Wakieć et al., 2007). Few studies have been conducted on the effects of ABCB1 gene polymorphisms on VRZ metabolism, and no clear conclusions have been obtained. One study found that ABCB1 gene polymorphism has an impact on VRZ clearance (Weiss et al., 2009). It has been shown that the AA allele of the rs1045642 polymorphic locus carrying the ABCB1 gene is associated with reduced VRZ metabolism in healthy individuals compared to the GG genotype (Weiss et al., 2009; Allegra et al., 2018). However, Recent studies have shown that the ABCB1 gene polymorphism does not significantly impact blood concentrations of VRZ (Chuwongwattana et al., 2020). Therefore, To fully understand the impact of ABCB1 gene variations on VRZ metabolism, it is necessary to conduct studies using larger sample sizes encompassing different races.

4.5 The impact of other gene polymorphisms on VRZ

In addition to the genetic involvement of CYP2C19, CYP3A4, CYP2C9, and ABCB1, several other genetic variants may also broadly affect VRZ concentrations in individuals. According to the study, subjects carrying the rs3781727 variant of the SLCO2B1 gene had reduced and delayed oral absorption of VRZ, and genotype CC + CT was associated with reduced VRZ exposure in healthy individuals compared to genotype TT (Lee et al., 2020). The presence of the AA genotype at the rs2461817 polymorphic site in the NR1I2 gene is associated with a decrease in VRZ concentrations; furthermore, the presence of the GG allele at the rs6785049 polymorphic site and the CC allele at the rs3814057 polymorphic site in the NR1I2 gene, the AA allele at the rs2266780 polymorphic site in the FMO3 gene, and the AA allele at the rs2266780 polymorphic site in the POR gene, as well as the GG allele at the rs10954732 polymorphic site in the POR gene, is correlated with an increase in VRZ concentrations (Zeng et al., 2020). Regression analysis confirmed the potential function of the rs4149117 GT/TT genotype group of the SLCO1B3 gene in predicting Ctrough reduction by VRZ, and one study showed that individuals carrying the GT + TT allele of the rs4149117 polymorphic locus of the SLCO1B3 gene were associated with reduced Ctrough in children (Allegra et al., 2018). The ABCC2 gene encodes a transporter protein that has a tremendous impact on the transport and clearance of VRZ, and the rs717620 polymorphic locus CT + TT allele carrying the ABCC2 gene and the rs13120400 polymorphic locus CC allele carrying the ABCG2 gene were also associated with elevated Ctrough in children (Allegra et al., 2018).

Overall, among the genetic influences on VRZ dose adjustment, CYP2C19 gene polymorphisms were the most influential, accounting for approximately 50% of VRZ variability (Amsden and Gubbins, 2017). Although CYP3A4 is associated with the pharmacokinetic and pharmacodynamic properties of VRZ, the effect of CYP3A4 on the metabolism of VRZ *in vivo* is less than that of CYP2C19, which is about 1/50 of CYP2C19 (Hyland et al., 2003; Murayama et al., 2007). The effect of CYP2C9 on the dose adjustment of VRZ is more slight, and it is only involved in a small part of the nitrogen oxidation metabolism of VRZ (Dorji et al., 2019). Although several studies have shown that CYP3A5, ABCB1, SLCO2B1, NR1I2, FMO3 and other genes have an effect on VRZ metabolism, these effects are relatively small compared with CYP2C19, CYP3A4, and CYP2C9. Moreover, there is a considerable amount of confounding factors and a lack of consistent conclusions in these studies, warranting further research in this area.

5 The recommended dose of VRZ in individuals with IFI

The recommended dose of VRZ for treating IFI in adults varies between countries and regions. Thus, it is important to adjust the dosage for each individual (See Table 4: Comparison of recommended doses in different countries). Overall, the recommended doses varied somewhat between countries. Still, all had the same intravenous loading dose and maintenance dose, and there was less variation between countries in oral dosing, and all recommended inter-individual dose adjustments based on Ctrough.

Different countries have varying Ctrough levels. For instance, Chinese guidelines suggest a minimum of 0.5 mg/L and a maximum of 5 mg/L for VRZ target Ctrough (Chen et al., 2018). The Japanese guidelines state that Ctrough ≥12 mg/L can achieve clinical efficacy, and individuals with Ctrough >4–5 mg/L should be monitored for elevated related indicators (Roberts et al., 2012). According to the 2016 guidelines in the US, individuals should maintain a minimum requirement of 1–1.5 mg/L and a maximum requirement of 5–6 mg/L for Ctrough (Patterson et al., 2016). European 2017 guidelines recommend that the lower limit of Ctrough in individuals should be 1–1.5 mg/L, and the recommended Ctrough for severe infections is 2–6 mg/L (Ullmann et al., 2018). The British Society for Medical Mycology (BSMM) antifungal drug TDM guideline recommendation defines the VRZ treatment window as 2 ~ 6 mg/L (Ashbee et al., 2014).

In terms of dose adjustment, the "VRZ Personalized Medication Guidelines," published by the Chinese Pharmacology Society, recommend using a population pharmacokinetic model based on

TABLE 4 Comparison of recommended doses in different countries.

Country	Intravenous infusion		Oral administration		Recommendations for dose adjustment
	Loading dose	Maintenance dose	Loading dose	Maintenance dose	
China	6 mg/kg every 12 h	4 mg/kg every 12 h	weighing more than 40 kg: 400 mg every 12 h; weighing less than 40 kg: 200 mg every 12 h	weighing more than 40 kg: 200 mg every 12 h; weighing less than 40 kg: 100 mg every 12 h	The dosage should be modified for each patient based on weight, disease features, drug metabolism, liver, kidney, and Ctrough (Chen et al., 2018)
United States	6 mg/kg every 12 h	4 mg/kg every 12 h	6 mg/kg every 12 h (Intravenous infusion)	weighing more than 40 kg: 200 mg every 12 h; weighing less than 40 kg: 100/150 mg every 12 h	The prescribed dose interval should be modified according to the patient's medication metabolism, liver function, and renal function (Patterson et al., 2016)
EU	6 mg/kg every 12 h	4 mg/kg twice daily	weighing more than 40 kg: 400 mg every 12 h; weighing less than 40 kg: 200 mg every 12 h	Weighing more than 40 kg: 200 mg twice daily; weighing less than 40 kg: 100 mg twice daily	Individuals with compromised liver function and drug interactions should have their dosages customized based on their Ctrough levels (Ullmann et al., 2018)
United Kingdom	6 mg/kg every 12 h	4 mg/kg twice daily	weighing more than 40 kg: 400 mg every 12 h; weighing less than 40 kg: 200 mg every 12 h	weighing more than 40 kg: 200 mg twice daily; weighing less than 40 kg: 100 mg twice daily	The dosage should be adjusted accordingly, taking into consideration the patient's drug metabolism, potential drug interactions, as well as liver and kidney function (Ashbee et al., 2014)
Japan	6 mg/kg every 12 h	4 mg/kg twice daily	weighing more than 40 kg: 300 mg twice daily (For the first 2 days). weighing less than 40 kg: 150 mg twice daily (For the first 2 days)	weighing more than 40 kg: 150/200 mg twice daily; weighing less than 40 kg: 100 mg twice daily	Ctrough monitoring is advised, along with tailored dosage and dosing interval adjustments for VRZ based on genetic polymorphism and drug metabolism (Roberts et al., 2012)

the Chinese public to adjust VRZ dosing. For individuals with a steady-state Ctrough below the lower limit of the target Ctrough or poor efficacy, it is recommended that the VRZ maintenance dose be increased by 50% and then adjusted according to Ctrough; for individuals with a steady-state Ctrough above the upper limit of the target Ctrough and below 10 mg/L, and in the absence of grade 2 or higher adverse events, it is recommended that the VRZ maintenance dose be diminished by 20% and then adjusted according to Ctrough; For individuals with steady-state Ctrough above 10 mg/L or Grade 2 adverse events, then VRZ is recommended to be discontinued for one dose, followed by a maintenance dose reduction of 50%, followed by adjustment based on Ctrough (Chen et al., 2018).

6 VRZ dose adjustment in individuals with hepatic insufficiency

Individuals with hepatic insufficiency may face a higher risk of ADRs due to the potential accumulation of VRZ caused by decreased hepatic blood flow and enzyme activity. Individuals with hepatic insufficiency are advised to follow the VRZ instructions. For those with mild to moderate hepatic insufficiency (Child-Pugh A/B), a standard loading dose and a maintenance dose that is half the usual dosage are recommended (Chen and Chen, 2021). However, it is unclear what the proper dosing of VRZ should be for individuals with serious hepatic insufficiency (Child-Pugh C). Studies have indicated that the recommended VRZ loading dose and maintenance dose halving are not suitable and that reducing the maintenance dose by half can result in perilously high drug levels in these individuals (Wang et al., 2018b; Spernovasilis and Kofteridis, 2018). Therefore, conducting a pharmacokinetic study of VRZ in this particular population is crucial to develop suitable dosage schedules (See Table 5: Recommendations for dose adjustment in hepatic insufficiency).

The 12 studies have examined the use of VRZ in individuals with hepatic insufficiency. All have concluded that the currently recommended dose is unsuitable for these individuals and requires adjustment. Of these, 10 studies provided specific recommendations for dose adjustments, but only 5 gave both loading and maintenance doses, while the other 5 only provided maintenance doses. 8 retrospective multisample studies and 1 case report have shown that the standard loading dose and maintenance dose for individuals with hepatic insufficiency may not be appropriate, particularly for those in Child-Pugh class B and C. This is because of their higher Ctrough levels, which increase the risk of serious ADRs. To prevent elevated Ctrough levels and associated ADRs, it is advisable to consider lower doses, longer dosing intervals, and early TDM for these patients.

In individuals with hepatic dysfunction, total bilirubin has been identified as a crucial factor in predicting the pharmacokinetic parameters of VRZ. Optimizing the VRZ dosage to align with the total bilirubin levels can enhance treatment effectiveness. A prospective observational study categorized individuals with hepatic insufficiency into three levels based on total bilirubin levels and determined the optimal therapeutic dosage of VRZ for each bilirubin level (refer to Table 5); additionally, the study found that the pharmacokinetics of VRZ can be appropriately described using a one-compartment model with first-order absorption and elimination in individuals with hepatic dysfunction (Tang et al., 2021). These findings align with former retrospective studies and the research conducted by Pascual et al. (2012) and Wang et al. (2014a)

TABLE 5 Recommendations for dose adjustment in hepatic insufficiency.

First author year	Study design	Sample size	Liver function grading	Recommendations for dose adjustment
Cai et al. (2023)	retrospective study	308	Child-Pugh C	Loading dose: no recommendation Maintenance dose: 200 mg every 24 h
Lin et al. (2022)	prospective observational study	26	Child-Pugh A/B	Loading dose:5 mg/kg every 12 h
				Maintenance dose: 100 mg every 12 h/200 mg every 24 h
			Child-Pugh C	Loading dose:5 mg/kg every 12 h
				Maintenance dose: 50 mg every 12 h/100 mg every 24 h
Zhao et al. (2021)	prospective observational study	43	Child-Pugh C	Loading dose:200 mg every 24 h
				Maintenance dose: 100 mg every 24 h
Wang et al. (2021)	Retrospective study	120	Child-Pugh A/B	Loading dose: 200 mg every 12 h
				Maintenance dose: 75 mg every 12 h/150 mg every 24 h
			Child-Pugh C	Loading dose:200 mg every 12 h
				Maintenance dose: 50 mg every 12 h/100 mg every 24 h
Tang et al. (2021)	prospective observational study	51	TBIL-1	Loading dose:200 mg every 12 h
				Maintenance dose: 100 mg every 12 h
			TBIL-2	Loading dose:200 mg every 12 h
				Maintenance dose: 50 mg every 12 h/100 mg every 24 h
			TBIL-3	Loading dose: 200 mg every 12 h
				Maintenance dose: 50 mg every 24 h
Ren et al. (2019)	retrospective study	180	Child-Pugh A/B	Loading dose: no recommendation Maintenance dose: 75 mg every 12 h
			Child-Pugh C	Loading dose: no recommendation
				Maintenance dose: 100 mg every 24 h
Zhao et al. (2019)	retrospective study	117	Child-Pugh C	Loading dose: no recommendation
				Maintenance dose: 100 mg every 12 h
Yamada et al. (2018)	retrospective study	6	Child-Pugh C	Loading dose: no recommendation Maintenance dose: 100–130 mg every 24 h
Wang et al. (2018b)	Retrospective Study	78	Child-Pugh B/C	The recommended maintenance dose (200 mg every 12 h) and halved maintenance dose (100 mg every 12 h) result in high Ctrough
Wang et al. (2018a)	Retrospective Study	34	Child-Pugh C	Maintenance doses (100 mg every 12 h/200 mg every 24 h) result in high Ctrough
Gao et al. (2018)	retrospective study	20	Acute Chronic Liver Failure	Loading dose: 200 mg every 12 h
				Maintenance dose: 100 mg every 24 h
Liu et al. (2017)	case report	1	Child-Pugh C	Loading dose: no recommendation
				Maintenance dose: 100 mg every 24 h

TBIL-1, TBIL <51 μmol/L; TBIL-2, 51 μmol/L ≤ TBIL <171 μmol/L; TBIL-3, TBIL ≥171 μmol/L.

on the pharmacokinetics of VRZ in individuals. A population-based pharmacokinetic modeling study showed that individuals with Ctrough >5.12 mg/L were more likely to experience VRZ-related ADRs, and individuals with hepatic insufficiency should receive a reduced half-load dose regimen compared with individuals with normal liver function, and the VRZ maintenance dose should be reduced to one-third for Child-Pugh A/B individuals and one-quarter for Child-Pugh C individuals (Wang et al., 2021). CYP2C19 phenotype plays a crucial role in selecting VRZ treatment regimens in individuals with liver insufficiency. When CYP2C19 activity is reduced, individuals with the same degree of liver insufficiency can further reduce the dose of VRZ. The results of a dosing regimen optimization based on MonteCarlo simulation showed that the maintenance dose of VRZ should be decreased to less than 50% in individuals with mild to moderate hepatic insufficiency with extensive CYP2C19 metabolism and o 1/4 in individuals with moderate to severe hepatic insufficiency (Ren et al., 2019). Dote et al. found that taking glucocorticoids alongside VRZ

lowers plasma levels, while taking proton pump inhibitors increases plasma levels (Dote et al., 2016). Some studies have indicated that steroids are a hazard element for fungal infections in individuals with liver failure; Liu et al. (2017) found that VRZ is safe in individuals with fungal pneumonia and that low-maintenance doses of VRZ (100 mg/d) can achieve effective Ctrough without causing liver damage, but Ctrough of VRZ should be carefully monitored. A prospective observational study has shown that the regular VRZ dose can be increased by 50 mg in individuals with hepatic insufficiency at a MIC of 1 mg/L, but Ctrough needs to be monitored carefully to avoid severe ADRs; When the MIC is ≥ 2 mg/L, other alternative drugs are recommended, and depending on the type of fungal pathogen and its susceptibility to VRZ, lower doses or longer dosing intervals should be recommended to individuals with hepatic insufficiency (Lin et al., 2022).

7 Discussion

VRZ, a widely used broad-spectrum antifungal medication for treating fungal infections, shows significant variability in its pharmacokinetics and pharmacodynamics among individuals. This is due to the involvement of multiple metabolic pathways and influencing factors. More and more research has emphasized the significance of genetic polymorphisms and hepatic insufficiency in determining appropriate VRZ dosage adjustments for individuals with IFI. Recent studies have investigated the potential relationship between genetic variations, such as CYP2C19, CYP3A4, ABCB1, ABCC2, FMO3, and POR, and the pharmacokinetics and pharmacodynamics of VRZ. Among these genes, CYP2C19 has the strongest impact on VRZ metabolism and clearance, followed by CYP3A4. Certain variants, like CYP2C19*2 and CYP2C19*3, reduce the enzymatic activity of CYP2C19, which results in higher drug exposure. On the contrary, variants such as CYP2C19*17 enhance CYP2C19 activity, resulting in faster VRZ metabolism and reduced drug exposure. ABCB1 and ABCC2 genotypes may influence VRZ transport and distribution, while FMO3 and POR genotypes could potentially impact its metabolism and clearance. However, it is important to note that the findings from different studies are not always consistent, warranting further research to understand the specific effects of each genotype on VRZ.

The treatment of patients with hepatic insufficiency complicated by IFI is a clinical challenge and a topic of great interest. While existing pharmacokinetic studies, clinical trials, and post-marketing safety data of available antifungal agents can assist clinicians in optimizing antifungal treatment regimens in patients with mild to moderate hepatic insufficiency and IFI, the recommended dosage adjustments for patients with severe hepatic insufficiency remain unclear in most current guidelines. Furthermore, the majority of dose adjustment studies for VRZ in patients with hepatic insufficiency have primarily focused on maintenance doses, with limited recommendations for loading doses. Moreover, there are discrepancies in the recommended adjustment doses across different studies, highlighting the lack of consensus. Therefore, further pharmacokinetic and clinical research is warranted to guide the use of VRZ in patients with hepatic insufficiency. Additionally, TDM of antifungal agents should be strengthened in clinical practice for patients with hepatic insufficiency and IFI to prevent or promptly identify hepatic and renal impairment, thereby avoiding adverse clinical outcomes. Furthermore, there is limited evidence and research on the dose adjustment of antifungal agents based on genotype and phenotype in patients with hepatic insufficiency, necessitating more extensive investigation in this aspect.

The current recommendations in guidelines and package inserts regarding patients with mild to moderate hepatic insufficiency (Child-Pugh A and B) who are prescribed VRZ suggest standard loading doses and halved maintenance doses, but this approach is likely to result in high Ctrough levels in patients, making it potentially inappropriate. Several ADRs associated with VRZ use have been found to directly correlate with Ctrough levels (Zonios et al., 2008; Tang et al., 2021). A meta-analysis conducted to assess the utility of TDM revealed a significantly higher frequency of toxic adverse events in patients with Ctrough levels ranging from 4.0 to 6.0 mg/L compared to those with lower Ctrough levels (Luong et al., 2016). Furthermore, a review of plasma monitoring studies for VRZ demonstrated that maintaining a treatment window of >1–2 mg/L and <5–5.5 mg/L was associated with improved efficacy and reduced toxicity (Karthaus et al., 2015). Additionally, a randomized controlled trial evaluating the utility of TDM in patients receiving VRZ treatment for IFI found that patients undergoing TDM exhibited a significant increase in complete or partial treatment response, with fewer discontinuations due to adverse events (Park et al., 2012). Moreover, the "VRZ personalized dosing guideline" strongly recommends Ctrough monitoring for patients with hepatic insufficiency, those co-administering drugs that affect VRZ pharmacokinetics, patients with CYP2C19 gene mutations, patients experiencing VRZ-related adverse events or suboptimal treatment efficacy, and critically ill patients with life-threatening fungal infections (Chen et al., 2018). It is evident that conducting Ctrough monitoring in hepatic insufficiency patients using VRZ is highly necessary. TDM should be initiated early when administering VRZ, and if steady-state Ctrough falls below the lower limit or if treatment efficacy is suboptimal, dosage adjustments should be made according to the dose adjustment scheme outlined in the "VRZ personalized dosing guideline." Additionally, the CYP2C19 gene phenotype plays a crucial role in determining VRZ dosage in patients with hepatic insufficiency. When making dosage adjustments, special attention should be given to the impact of CYP2C19 gene phenotype in hepatic insufficiency patients on VRZ dosage adjustments (Tang et al., 2019).

From an individualized dosing perspective, hepatic insufficiency and genetic polymorphisms are two important factors influencing the administration dosage of VRZ in patients. In terms of the genetic impact on VRZ dose adjustments, the majority of the influence is attributed to the involvement of CYP2C19, CYP3A4, and CYP2C9, with CYP2C19 being particularly significant (accounting for approximately 50% of VRZ variability). Therefore, it is crucial to focus on the impact of CYP2C19, CYP3A4, and CYP2C9 gene phenotypes in hepatic insufficiency patients on VRZ plasma concentrations, as this holds positive implications for the successful treatment of hepatic insufficiency with concomitant invasive fungal infections. Other genes such as CYP3A5, ABCB1, SLCO2B1, NR1I2, and FMO3, which have lesser impact, may also be considered to some extent. To validate the safety and efficacy of VRZ dose adjustment strategies based on genotypes and liver function, future research should further investigate how to optimize the

therapeutic approach of VRZ and better utilize genetic testing and clinical practice guidelines to guide VRZ dosage adjustments. This includes expanding the sample size and enhancing comparative studies among different populations, which can further elucidate the influence of genetic polymorphisms on VRZ pharmacokinetics and pharmacodynamics. Furthermore, since hepatic insufficiency patients often present with other diseases and receive concurrent medication, these factors may also impact VRZ pharmacokinetics and dose adjustments. Lastly, further research is necessary to examine the influence of genetic polymorphisms on ADRs, in order to guide clinical drug use and personalized treatment.

In conclusion, pharmacogenomics-based VRZ dose adjustment offers accurate and personalized treatment for hepatic insufficiency, improving outcomes and reducing ADRs. Compared to those with normal liver function, patients with hepatic insufficiency require lower drug doses and longer dosing intervals. Early TDM is crucial to mitigate potential adverse events. Additionally, the impact of CYP2C19, CYP3A4, and CYP2C9 genes on hepatic insufficiency patients with IFI should be carefully considered. Future high-quality pharmacogenomics trials are urgently needed to enhance evidence-based medicine and pharmacology for the diagnosis and treatment of hepatic insufficiency patients with IFI.

Author contributions

GL, QnL, CZ, QY, QiL, XZ, RY, and XY participated in the literature review, analysis, and manuscript writing. HL and YY guided manuscript writing and participated in manuscript revision. All authors contributed to the article and approved the submitted version.

Funding

This study was supported by research grants from the Chongqing Science and Health Joint Medical Research Project (No. 2022MSXM110).

Acknowledgments

We acknowledge the support from Sichuan Academy of Medical Sciences & Sichuan Provincial People's Hospital, China Pharmaceutical University, University of Electronic Science and Technology of China, Southwest Medical University. And thank YY for his contribution to the paper.

Conflict of interest

The authors declare that the research was conducted in the absence of any commercial or financial relationships that could be construed as a potential conflict of interest.

Publisher's note

References

Alffenaar, J.-W. C., de Vos, T., Uges, D. R. A., and Daenen, S. M. G. J. (2009). High voriconazole trough levels in relation to hepatic function: how to adjust the dosage? *Br. J. Clin. Pharmacol.* 67, 262–263. doi:10.1111/j.1365-2125.2008.03315.x

Allegra, S., Fatiguso, G., Francia, S. D., Pirro, E., Carcieri, C., Cusato, J., et al. (2018). Pharmacogenetic of voriconazole antifungal agent in pediatric patients. *Pharmacogenomics* 19, 913–925. doi:10.2217/pgs-2017-0173

Amsden, J. R., and Gubbins, P. O. (2017). Pharmacogenomics of triazole antifungal agents: implications for safety, tolerability and efficacy. *Expert Opin. Drug Metab. Toxicol.* 13, 1135–1146. doi:10.1080/17425255.2017.1391213

Andrade, J. C., Kumar, S., Kumar, A., Černáková, L., and Rodrigues, C. F. (2022). Application of probiotics in candidiasis management. *Crit. Rev. Food Sci. Nutr.* 62, 8249–8264. doi:10.1080/10408398.2021.1926905

Ashbee, H. R., Barnes, R. A., Johnson, E. M., Richardson, M. D., Gorton, R., and Hope, W. W. (2014). Therapeutic drug monitoring (TDM) of antifungal agents: guidelines from the British society for medical Mycology. *J. Antimicrob. Chemother.* 69, 1162–1176. doi:10.1093/jac/dkt508

Baririan, N., Van Obbergh, L., Desager, J.-P., Verbeeck, R. K., Wallemacq, P., Starkel, P., et al. (2007). Alfentanil-induced miosis as a surrogate measure of alfentanil pharmacokinetics in patients with mild and moderate liver cirrhosis. *Clin. Pharmacokinet.* 46, 261–270. doi:10.2165/00003088-200746030-00006

Bassetti, M., Peghin, M., Carnelutti, A., Righi, E., Merelli, M., Ansaldi, F., et al. (2017). Clinical characteristics and predictors of mortality in cirrhotic patients with candidemia and intra-abdominal candidiasis: a multicenter study. *Intensive Care Med.* 43, 509–518. doi:10.1007/s00134-017-4717-0

Benitez, L. L., and Carver, P. L. (2019). Adverse effects associated with long-term administration of azole antifungal agents. *Drugs* 79, 833–853. doi:10.1007/s40265-019-01127-8

Blanco-Dorado, S., Maroñas, O., Latorre-Pellicer, A., Rodríguez Jato, M. T., López-Vizcaíno, A., Gómez Márquez, A., et al. (2020). Impact of CYP2C19 genotype and drug interactions on voriconazole plasma concentrations: a Spain pharmacogenetic-pharmacokinetic prospective multicenter study. *Pharmacotherapy* 40, 17–25. doi:10.1002/phar.2351

Cai, X., Li, W., Yang, J., Wu, G., Song, J., Gong, X., et al. (2023). Is halving maintenance of voriconazole safe and efficient in patients suffering from invasive fungal infections with serious hepatic dysfunction? *Infect. Drug Resist.* 16, 1–8. doi:10.2147/IDR.S390026

Cascorbi, I., Gerloff, T., Johne, A., Meisel, C., Hoffmeyer, S., Schwab, M., et al. (2001). Frequency of single nucleotide polymorphisms in the P-glycoprotein drug transporter MDR1 gene in white subjects. *Clin. Pharmacol. Ther.* 69, 169–174. doi:10.1067/mcp.2001.114164

Chau, M. M., Kong, D. C. M., van Hal, S. J., Urbancic, K., Trubiano, J. A., Cassumbhoy, M., et al. (2014). Consensus guidelines for optimising antifungal drug delivery and monitoring to avoid toxicity and improve outcomes in patients with haematological malignancy, 2014. *Intern. Med. J.* 44, 1364–1388. doi:10.1111/imj.12600

Chen, D. L., and Chen, J. (2021). Antifungal therapy for severe liver disease complicated with invasive fungal disease. *Liver* 26, 804–807. doi:10.14000/j.carolcarrollnki.Issn1008-1704.2021.07.025

Chen, D., Qian, Z., Su, H., Meng, Z., Lv, J., Huang, Y., et al. (2021). Invasive pulmonary aspergillosis in acute-on-chronic liver failure patients: short-term outcomes and antifungal options. *Infect. Dis. Ther.* 10, 2525–2538. doi:10.1007/s40121-021-00524-5

Chen, K., Zhang, X., Ke, X., Du, G., Yang, K., and Zhai, S. (2018). Individualized medication of voriconazole: a practice guideline of the division of therapeutic drug monitoring, Chinese pharmacological society. *Ther. Drug Monit.* 40, 663–674. doi:10.1097/FTD.0000000000000561

Chen, T., Ning, Q., Chen, L., Chen, Z., Wang, B., and Zhou, D. (2022). The effects of fructose diphosphate on routine coagulation tests *in vitro*. *J. Clin. Hepatobiliary Dis.* 38, 304–310. doi:10.1038/s41598-021-04263-y

Cheng, Y., Wang, L., Iacono, L., Zhang, D., Chen, W., Gong, J., et al. (2018). Clinical significance of CYP2C19 polymorphisms on the metabolism and pharmacokinetics of

11β-hydroxysteroid dehydrogenase type-1 inhibitor BMS-823778. *Br. J. Clin. Pharmacol.* 84, 130–141. doi:10.1111/bcp.13421

Cheong, H. S., Kang, C. I., Lee, J. A., Moon, S. Y., Joung, M. K., Chung, D. R., et al. (2009). Clinical significance and outcome of nosocomial acquisition of spontaneous bacterial peritonitis in patients with liver cirrhosis. *Clin. Infect. Dis.* 48 (9), 1230–1236. doi:10.1086/597585

Chuwongwattana, S., Jantararoungtong, T., Prommas, S., Medhasi, S., Puangpetch, A., and Sukasem, C. (2020). Impact of CYP2C19, CYP3A4, ABCB1, and FMO3 genotypes on plasma voriconazole in Thai patients with invasive fungal infections. *Pharmacol. Res. Perspect.* 8, e00665. doi:10.1002/prp2.665

Denning, D. W., Ribaud, P., Milpied, N., Caillot, D., Herbrecht, R., Thiel, E., et al. (2002). Efficacy and safety of voriconazole in the treatment of acute invasive aspergillosis. *Clin. Infect. Dis.* 34, 563–571. doi:10.1086/324620

Dolton, M. J., Ray, J. E., Chen, S. C.-A., Ng, K., Pont, L. G., and McLachlan, A. J. (2012). Multicenter study of voriconazole pharmacokinetics and therapeutic drug monitoring. *Antimicrob. Agents Chemother.* 56, 4793–4799. doi:10.1128/AAC.00626-12

Dorji, P. W., Tshering, G., and Na-Bangchang, K. (2019). CYP2C9, CYP2C19, CYP2D6 and CYP3A5 polymorphisms in south-east and east asian populations: A systematic review. *J. Clin. Pharm. Ther.* 44, 508–524. doi:10.1111/jcpt.12835

Dote, S., Sawai, M., Nozaki, A., Naruhashi, K., Kobayashi, Y., and Nakanishi, H. (2016). A retrospective analysis of patient-specific factors on voriconazole clearance. *J. Pharm. Health Care Sci.* 2, 10. doi:10.1186/s40780-016-0044-9

Douglas, A. P., Smibert, O. C., Bajel, A., Halliday, C. L., Lavee, O., McMullan, B., et al. (2021). Consensus guidelines for the diagnosis and management of invasive aspergillosis, 2021. *Intern. Med. J.* 51 (7), 143–176. doi:10.1111/imj.15591

Ertem, O., Tufekci, O., Oren, H., Tuncok, Y., Ergon, M. C., and Gumustekin, M. (2022). Evaluation of voriconazole related adverse events in pediatric patients with hematological malignancies. *J. Oncol. Pharm. Pract.* 29, 861–873. doi:10.1177/10781552221086887

Feldman, E. B., Bellinghausen, A. L., Vodkin, I. E., Abeles, S. R., and Kamdar, B. B. (2023). Secondary peritonitis in a patient with cirrhosis involving Hyphopichia burtonii, an emerging fungal pathogen. *IDCases* 31, e01730. doi:10.1016/j.idcr.2023.e01730

Fernández, J., Acevedo, J., Wiest, R., Gustot, T., Amoros, A., Deulofeu, C., et al. (2018). Bacterial and fungal infections in acute-on-chronic liver failure: prevalence, characteristics and impact on prognosis. *Gut* 67, 1870–1880. doi:10.1136/gutjnl-2017-314240

Gao, J., Zhang, Q., Wu, Y., Li, Y., Qi, T., Zhu, C., et al. (2018). Improving survival of acute-on-chronic liver failure patients complicated with invasive pulmonary aspergillosis. *Sci. Rep.* 8, 876. doi:10.1038/s41598-018-19320-2

García-García, I., and Borobia, A. M. (2021). Current approaches and future strategies for the implementation of pharmacogenomics in the clinical use of azole antifungal drugs. *Expert Opin. Drug Metab. Toxicol.* 17, 509–514. doi:10.1080/17425255.2021.1890715

Gautier-Veyret, E., Fonrose, X., Tonini, J., Thiebaut-Bertrand, A., Bartoli, M., Quesada, J.-L., et al. (2015). Variability of voriconazole plasma concentrations after allogeneic hematopoietic stem cell transplantation: impact of cytochrome p450 polymorphisms and comedications on initial and subsequent trough levels. *Antimicrob. Agents Chemother.* 59, 2305–2314. doi:10.1128/AAC.04838-14

Hadfield, N. J., Selvendran, S., and Johnston, M. P. (2019). Fatal Pneumocystis jirovecii pneumonia in a non-immunocompromised patient with alcohol-related liver cirrhosis. *Scott. Med. J.* 64, 148–153. doi:10.1177/0036933019872629

Hakkola, J., Hukkanen, J., Turpeinen, M., and Pelkonen, O. (2020). Inhibition and induction of CYP enzymes in humans: an update. *Arch. Toxicol.* 94, 3671–3722. doi:10.1007/s00204-020-02936-7

Hall, V. G., Tang, K., Kumar, D., Rotstein, C., Chow, S., Chan, S. M., et al. (2023). Breakthrough invasive fungal infection after coadministration of venetoclax and voriconazole. *Open Forum Infect. Dis.* 10, ofad134. doi:10.1093/ofid/ofad134

Hamada, Y., Seto, Y., Yago, K., and Kuroyama, M. (2012). Investigation and threshold of optimum blood concentration of voriconazole: a descriptive statistical meta-analysis. *J. Infect. Chemother.* 18, 501–507. doi:10.1007/s10156-011-0363-6

Hamada, Y., Tokimatsu, I., Mikamo, H., Kimura, M., Seki, M., Takakura, S., et al. (2013). Practice guidelines for therapeutic drug monitoring of voriconazole: a consensus review of the Japanese Society of Chemotherapy and the Japanese Society of Therapeutic Drug Monitoring. *J. Infect. Chemother.* 19 (3), 381–392. doi:10.1007/s10156-013-0607-8

Hamadeh, I. S., Klinker, K. P., Borgert, S. J., Richards, A. I., Li, W., Mangal, N., et al. (2017). Impact of the CYP2C19 genotype on voriconazole exposure in adults with invasive fungal infections. *Pharmacogenet. Genomics* 27, 190–196. doi:10.1097/FPC.0000000000000277

He, H.-R., Sun, J.-Y., Ren, X.-D., Wang, T.-T., Zhai, Y.-J., Chen, S.-Y., et al. (2015). Effects of CYP3A4 polymorphisms on the plasma concentration of voriconazole. *Eur. J. Clin. Microbiol. Infect. Dis.* 34, 811–819. doi:10.1007/s10096-014-2294-5

He, L., Chen, S., Li, J., Xie, X., Huang, L., Kuang, Y., et al. (2020). Genetic and phenotypic frequency distribution of CYP2C9, CYP2C19 and CYP2D6 in over 3200 Han Chinese. *Clin. Exp. Pharmacol. Physiol.* 47, 1659–1663. doi:10.1111/1440-1681.13357

Hicks, J. K., Quilitz, R. E., Komrokji, R. S., Kubal, T. E., Lancet, J. E., Pasikhova, Y., et al. (2020). Prospective CYP2C19-guided voriconazole prophylaxis in patients with neutropenic acute myeloid leukemia reduces the incidence of subtherapeutic antifungal plasma concentrations. *Clin. Pharmacol. Ther.* 107, 563–570. doi:10.1002/cpt.1641

Hou, Z., Tan, D., Liu, G., Xie, Y., Li, C., Xie, J., et al. (2010). Clinical characteristics and therapeutic analysis of invasive fungal infection in chronic severe hepatitis patients. *Zhong Nan Da Xue Xue Bao Yi Xue Ban.* 35, 537–542. doi:10.3969/j.issn.1672-7347.2010.06.001

Hulin, A., Dailly, E., and Le Guellec, C.Groupe Suivi Therapeutique Pharmacologique de la Societe Francaise de Pharmacologie et de Therapeutique (2011). Level of evidence for therapeutic drug monitoring of voriconazole. *Therapie* 66, 109–114. doi:10.2515/therapie/2011009

Hwang, S. Y., Yu, S. J., Lee, J. H., Kim, J. S., Yoon, J. W., Kim, Y. J., et al. (2014). Spontaneous fungal peritonitis: a severe complication in patients with advanced liver cirrhosis. *Eur. J. Clin. Microbiol. Infect. Dis.* 33, 259–264. doi:10.1007/s10096-013-1953-2

Hyland, R., Jones, B. C., and Smith, D. A. (2003). Identification of the cytochrome P450 enzymes involved in the N-oxidation of voriconazole. *Drug Metab. Dispos. Biol. Fate Chem.* 31, 540–547. doi:10.1124/dmd.31.5.540

Jenks, J. D., Cornely, O. A., Chen, S. C.-A., Thompson, G. R., and Hoenigl, M. (2020). Breakthrough invasive fungal infections: who is at risk? *Mycoses* 63, 1021–1032. doi:10.1111/myc.13148

Jenks, J. D., Nam, H. H., and Hoenigl, M. (2021). Invasive aspergillosis in critically ill patients: review of definitions and diagnostic approaches. *Mycoses* 64, 1002–1014. doi:10.1111/myc.13274

Jin, H., Wang, T., Falcione, B. A., Olsen, K. M., Chen, K., Tang, H., et al. (2016). Trough concentration of voriconazole and its relationship with efficacy and safety: a systematic review and meta-analysis. *J. Antimicrob. Chemother.* 71, 1772–1785. doi:10.1093/jac/dkw045

Job, K. M., Olson, J., Stockmann, C., Constance, J. E., Enioutina, E. Y., Rower, J. E., et al. (2016). Pharmacodynamic studies of voriconazole: informing the clinical management of invasive fungal infections. *Expert Rev. Anti Infect. Ther.* 14, 731–746. doi:10.1080/14787210.2016.1207526

Jović, Z., Janković, S. M., Ružić Zečević, D., Milovanović, D., Stefanović, S., Folić, M., et al. (2019). Clinical pharmacokinetics of second-generation triazoles for the treatment of invasive aspergillosis and candidiasis. *Eur. J. Drug Metab. Pharmacokinet.* 44, 139–157. doi:10.1007/s13318-018-0513-7

Kang, W.-H., Song, G.-W., Lee, S.-G., Suh, K.-S., Lee, K.-W., Yi, N.-J., et al. (2020). A multicenter, randomized, open-label study to compare micafungin with fluconazole in the prophylaxis of invasive fungal infections in living-donor liver transplant recipients. *J. Gastrointest. Surg.* 24, 832–840. doi:10.1007/s11605-019-04241-w

Karthaus, M., Lehrnbecher, T., Lipp, H.-P., Kluge, S., and Buchheidt, D. (2015). Therapeutic drug monitoring in the treatment of invasive aspergillosis with voriconazole in cancer patients—an evidence-based approach. *Ann. Hematol.* 94, 547–556. doi:10.1007/s00277-015-2333-z

Khalid, M., Neupane, R., Anjum, H., and Surani, S. (2021). Fungal infections following liver transplantation. *World J. Hepatol.* 13, 1653–1662. doi:10.4254/wjh.v13.i11.1653

Klyushova, L. S., Perepechaeva, M. L., and Grishanova, A. Y. (2022). The role of CYP3A in Health and disease. *Biomedicines* 10, 2686. doi:10.3390/biomedicines10112686

Kullberg, B. J., and Arendrup, M. C. (2015). Invasive candidiasis. *N. Engl. J. Med.* 373, 1445–1456. doi:10.1056/NEJMra1315399

Kyriakidis, I., Tragiannidis, A., Munchen, S., and Groll, A. H. (2017). Clinical hepatotoxicity associated with antifungal agents. *Expert Opin. Drug Saf.* 16, 149–165. doi:10.1080/14740338.2017.1270264

Lahmer, T., Brandl, A., Rasch, S., Baires, G. B., Schmid, R. M., Huber, W., et al. (2019). Prevalence and outcome of invasive pulmonary aspergillosis in critically ill patients with liver cirrhosis: an observational study. *Sci. Rep.* 9, 11919. doi:10.1038/s41598-019-48183-4

Lahmer, T., Brandl, A., Rasch, S., Schmid, R. M., and Huber, W. (2016). Fungal peritonitis: underestimated disease in critically ill patients with liver cirrhosis and spontaneous peritonitis. *PloS One* 11, e0158389. doi:10.1371/journal.pone.0158389

Lahmer, T., Peçanha-Pietrobom, P. M., Schmid, R. M., and Colombo, A. L. (2022). Invasive fungal infections in acute and chronic liver impairment: A systematic review. *Mycoses* 65, 140–151. doi:10.1111/myc.13403

Lamoureux, F., Duflot, T., Woillard, J.-B., Metsu, D., Pereira, T., Compagnon, P., et al. (2016). Impact of CYP2C19 genetic polymorphisms on voriconazole dosing and exposure in adult patients with invasive fungal infections. *Int. J. Antimicrob. Agents* 47, 124–131. doi:10.1016/j.ijantimicag.2015.12.003

Lee, C. R., Goldstein, J. A., and Pieper, J. A. (2002). Cytochrome P450 2C9 polymorphisms: a comprehensive review of the *in-vitro* and human data. *Pharmacogenetics* 12, 251–263. doi:10.1097/00008571-200204000-00010

Lee, C. R., Luzum, J. A., Sangkuhl, K., Gammal, R. S., Sabatine, M. S., Stein, C. M., et al. (2022). Clinical pharmacogenetics implementation Consortium guideline for CYP2C19 genotype and clopidogrel therapy: 2022 update. *Clin. Pharmacol. Ther.* 112, 959–967. doi:10.1002/cpt.2526

Lee, J., Ng, P., Hamandi, B., Husain, S., Lefebvre, M. J., and Battistella, M. (2021). Effect of therapeutic drug monitoring and cytochrome P450 2C19 genotyping on clinical outcomes of voriconazole: A systematic review. *Ann. Pharmacother.* 55, 509–529. doi:10.1177/1060028020948174

Lee, S., Kim, B.-H., Nam, W.-S., Yoon, S. H., Cho, J.-Y., Shin, S.-G., et al. (2012). Effect of CYP2C19 polymorphism on the pharmacokinetics of voriconazole after single and multiple doses in healthy volunteers. *J. Clin. Pharmacol.* 52, 195–203. doi:10.1177/0091270010395510

Lee, S. W., Oh, J., Kim, A. H., Ji, S. C., Park, S.-I., Yoon, S. H., et al. (2020). Oral absorption of voriconazole is affected by SLCO2B1 c*396T>C genetic polymorphism in CYP2C19 poor metabolizers. *Pharmacogenomics J.* 20, 792–800. doi:10.1038/s41397-020-0166-1

Lem, J., Younus, M., Aram, J. A., Moosavi, S., Freivogel, K., Lewis, A., et al. (2019). Evaluation of the effectiveness of additional risk minimization measures for voriconazole in the EU: findings and lessons learned from a healthcare professional survey. *Pharm. Med.* 33, 121–133. doi:10.1007/s40290-019-00273-4

Levin, M.-D., den Hollander, J. G., van der Holt, B., Rijnders, B. J., van Vliet, M., Sonneveld, P., et al. (2007). Hepatotoxicity of oral and intravenous voriconazole in relation to cytochrome P450 polymorphisms. *J. Antimicrob. Chemother.* 60, 1104–1107. doi:10.1093/jac/dkm330

Levine, M. T., and Chandrasekar, P. H. (2016). Adverse effects of voriconazole: over a decade of use. *Clin. Transpl.* 30, 1377–1386. doi:10.1111/ctr.12834

Li, S., Wu, S., Gong, W., Cao, P., Chen, X., Liu, W., et al. (2021). Application of population pharmacokinetic analysis to characterize CYP2C19 mediated metabolic mechanism of voriconazole and support dose optimization. *Front. Pharmacol.* 12, 730826. doi:10.3389/fphar.2021.730826

Li, X., Frechen, S., Moj, D., Lehr, T., Taubert, M., Hsin, C.-H., et al. (2020). A physiologically based pharmacokinetic model of voriconazole integrating time-dependent inhibition of CYP3A4, genetic polymorphisms of CYP2C19 and predictions of drug-drug interactions. *Clin. Pharmacokinet.* 59, 781–808. doi:10.1007/s40262-019-00856-z

Li, X., Yu, C., Wang, T., Chen, K., Zhai, S., and Tang, H. (2016). Effect of cytochrome P450 2C19 polymorphisms on the clinical outcomes of voriconazole: a systematic review and meta-analysis. *Eur. J. Clin. Pharmacol.* 72, 1185–1193. doi:10.1007/s00228-016-2089-y

Li, Z.-W., Peng, F.-H., Yan, M., Liang, W., Liu, X.-L., Wu, Y.-Q., et al. (2017). Impact of CYP2C19 genotype and liver function on voriconazole pharmacokinetics in renal transplant recipients. *Ther. Drug Monit.* 39, 422–428. doi:10.1097/FTD.0000000000000425

Libera, R., Dimala, C. A., Oakes, K., and Moss, C. (2023). Cryptococcal peritonitis in a patient with decompensated liver cirrhosis. *J. Community Hosp. Intern. Med. Perspect.* 13, 51–53. doi:10.55729/2000-9666.1139

Lin, X.-B., Li, Z.-W., Yan, M., Zhang, B.-K., Liang, W., Wang, F., et al. (2018). Population pharmacokinetics of voriconazole and CYP2C19 polymorphisms for optimizing dosing regimens in renal transplant recipients. *Br. J. Clin. Pharmacol.* 84, 1587–1597. doi:10.1111/bcp.13595

Lin, X.-B., Lui, K. Y., Guo, P.-H., Liu, X.-M., Liang, T., Hu, X.-G., et al. (2022). Population pharmacokinetic model-guided optimization of intravenous voriconazole dosing regimens in critically ill patients with liver dysfunction. *Pharmacotherapy* 42, 23–33. doi:10.1002/phar.2634

Liu, P., and Mould, D. R. (2014). Population pharmacokinetic-pharmacodynamic analysis of voriconazole and anidulafungin in adult patients with invasive aspergillosis. *Antimicrob. Agents Chemother.* 58, 4727–4736. doi:10.1128/AAC.02809-13

Liu, X., Su, H., Tong, J., Chen, J., Yang, H., Xiao, L., et al. (2017). Significance of monitoring plasma concentration of voriconazole in a patient with liver failure: A case report. *Med. Baltim.* 96, e8039. doi:10.1097/MD.0000000000008039

Lum, L., Lee, A., Vu, M., Strasser, S., and Davis, R. (2020). Epidemiology and risk factors for invasive fungal disease in liver transplant recipients in a tertiary transplant center. *Transpl. Infect. Dis.* 22, e13361. doi:10.1111/tid.13361

Luong, M.-L., Al-Dabbagh, M., Groll, A. H., Racil, Z., Nannya, Y., Mitsani, D., et al. (2016). Utility of voriconazole therapeutic drug monitoring: a meta-analysis. *J. Antimicrob. Chemother.* 71, 1786–1799. doi:10.1093/jac/dkw099

Maertens, J. A., Rahav, G., Lee, D.-G., Ponce-de-León, A., Ramírez Sánchez, I. C., Klimko, N., et al. (2021). Posaconazole versus voriconazole for primary treatment of invasive aspergillosis: a phase 3, randomised, controlled, non-inferiority trial. *Lancet lond. Engl.* 397, 499–509. doi:10.1016/S0140-6736(21)00219-1

Matsubara, V. H., Bandara, H. M. H. N., Mayer, M. P. A., and Samaranayake, L. P. (2016). Probiotics as antifungals in mucosal candidiasis. *Clin. Infect. Dis.* 62, 1143–1153. doi:10.1093/cid/ciw038

Medeiros, M. A. P., Melo, A. P. V., Bento, A. O., Souza, L. B. F. C., Neto, F. A. B., Garcia, J. B. L., et al. (2019). Epidemiology and prognostic factors of nosocomial candidemia in northeast Brazil: A six-year retrospective study. *PloS One* 14, e0221033. doi:10.1371/journal.pone.0221033

Miao, Q., Tang, J.-T., van Gelder, T., Li, Y.-M., Bai, Y.-J., Zou, Y.-G., et al. (2019). Correlation of CYP2C19 genotype with plasma voriconazole exposure in South-western Chinese Han patients with invasive fungal infections. *Med. Baltim.* 98, e14137. doi:10.1097/MD.0000000000014137

Mikus, G., Scholz, I. M., and Weiss, J. (2011). Pharmacogenomics of the triazole antifungal agent voriconazole. *Pharmacogenomics* 12, 861–872. doi:10.2217/pgs.11.18

Mikus, G., Schöwel, V., Drzewinska, M., Rengelshausen, J., Ding, R., Riedel, K.-D., et al. (2006). Potent cytochrome P450 2C19 genotype-related interaction between voriconazole and the cytochrome P450 3A4 inhibitor ritonavir. *Clin. Pharmacol. Ther.* 80, 126–135. doi:10.1016/j.clpt.2006.04.004

Moriyama, B., Obeng, A. O., Barbarino, J., Penzak, S. R., Henning, S. A., Scott, S. A., et al. (2017). Clinical pharmacogenetics implementation Consortium (CPIC) guidelines for CYP2C19 and voriconazole therapy. *Clin. Pharmacol. Ther.* 102, 45–51. doi:10.1002/cpt.583

Murayama, N., Imai, N., Nakane, T., Shimizu, M., and Yamazaki, H. (2007). Roles of CYP3A4 and CYP2C19 in methyl hydroxylated and N-oxidized metabolite formation from voriconazole, a new anti-fungal agent, in human liver microsomes. *Biochem. Pharmacol.* 73, 2020–2026. doi:10.1016/j.bcp.2007.03.012

Niwa, T., and Hata, T. (2016). The effect of genetic polymorphism on the inhibition of azole antifungal agents against CYP2C9-mediated metabolism. *J. Pharm. Sci.* 105, 1345–1348. doi:10.1016/j.xphs.2016.01.007

Pallet, N., and Loriot, M. A. (2021). Voriconazole pharmacogenetics. *Lancet lond. Engl.* 398, 578. doi:10.1016/S0140-6736(21)00879-5

Park, W. B., Kim, N.-H., Kim, K.-H., Lee, S. H., Nam, W.-S., Yoon, S. H., et al. (2012). The effect of therapeutic drug monitoring on safety and efficacy of voriconazole in invasive fungal infections: a randomized controlled trial. *Clin. Infect. Dis.* 55, 1080–1087. doi:10.1093/cid/cis599

Pascual, A., Calandra, T., Bolay, S., Buclin, T., Bille, J., and Marchetti, O. (2008). Voriconazole therapeutic drug monitoring in patients with invasive mycoses improves efficacy and safety outcomes. *Clin. Infect. Dis.* 46, 201–211. doi:10.1086/524669

Pascual, A., Csajka, C., Buclin, T., Bolay, S., Bille, J., Calandra, T., et al. (2012). Challenging recommended oral and intravenous voriconazole doses for improved efficacy and safety: population pharmacokinetics-based analysis of adult patients with invasive fungal infections. *Clin. Infect. Dis.* 55, 381–390. doi:10.1093/cid/cis437

Patterson, T. F., Thompson, G. R., Denning, D. W., Fishman, J. A., Hadley, S., Herbrecht, R., et al. (2016). Practice guidelines for the diagnosis and management of aspergillosis: 2016 update by the infectious diseases society of America. *Clin. Infect. Dis.* 63, e1–e60. doi:10.1093/cid/ciw326

Pessayre, D., Fromenty, B., Berson, A., Robin, M.-A., Lettéron, P., Moreau, R., et al. (2012). Central role of mitochondria in drug-induced liver injury. *Drug Metab. Rev.* 44, 34–87. doi:10.3109/03602532.2011.604086

PharmGKB (2017). Voriconazole pathway, pharmacokinetics. Available at: https://www.pharmgkb.org/pathway/PA166160640 (Accessed June 5, 2023).

Piano, S., Singh, V., Caraceni, P., Maiwall, R., Alessandria, C., Fernandez, J., et al. (2019). Epidemiology and effects of bacterial infections in patients with cirrhosis worldwide. *Gastroenterology* 156, 1368–1380.e10. doi:10.1053/j.gastro.2018.12.005

Ren, Q.-X., Li, X.-G., Mu, J.-S., Bi, J.-F., Du, C.-H., Wang, Y.-H., et al. (2019). Population pharmacokinetics of voriconazole and optimization of dosage regimens based on Monte Carlo simulation in patients with liver cirrhosis. *J. Pharm. Sci.* 108, 3923–3931. doi:10.1016/j.xphs.2019.09.019

Roberts, J. D., Wells, G. A., Le May, M. R., Labinaz, M., Glover, C., Froeschl, M., et al. (2012). Point-of-care genetic testing for personalisation of antiplatelet treatment (RAPID GENE): a prospective, randomised, proof-of-concept trial. *Lancet lond. Engl.* 379, 1705–1711. doi:10.1016/S0140-6736(12)60161-5

Rose, C. F., Amodio, P., Bajaj, J. S., Dhiman, R. K., Montagnese, S., Taylor-Robinson, S. D., et al. (2020). Hepatic encephalopathy: novel insights into classification, pathophysiology and therapy. *J. Hepatol.* 73, 1526–1547. doi:10.1016/j.jhep.2020.07.013

Sauna, Z. E., Kim, I.-W., and Ambudkar, S. V. (2007). Genomics and the mechanism of P-glycoprotein (ABCB1). *J. Bioenerg. Biomembr.* 39, 481–487. doi:10.1007/s10863-007-9115-9

Si, D., Guo, Y., Zhang, Y., Yang, L., Zhou, H., and Zhong, D. (2004). Identification of a novel variant CYP2C9 allele in Chinese. *Pharmacogenetics* 14, 465–469. doi:10.1097/01.fpc.0000114749.08559.e4

Silva, J. T., Ruiz-Camps, I., and Aguado, J. M. (2021). Invasive fungal infection over the last 30 years. *Rev. Iberoam. Micol.* 38, 47–51. doi:10.1016/j.riam.2021.03.003

Sim, S. C., Risinger, C., Dahl, M.-L., Aklillu, E., Christensen, M., Bertilsson, L., et al. (2006). A common novel CYP2C19 gene variant causes ultrarapid drug metabolism relevant for the drug response to proton pump inhibitors and antidepressants. *Clin. Pharmacol. Ther.* 79, 103–113. doi:10.1016/j.clpt.2005.10.002

Spernovasilis, N., and Kofteridis, D. P. (2018). Pre-existing liver disease and toxicity of antifungals. *J. Fungi Basel Switz.* 4, 133. doi:10.3390/jof4040133

Su, H.-B., Wang, H.-F., Yan, T., Lin, F., Zhao, H., Li, L., et al. (2010). The clinical characteristics of hepatic failure with aspergillosis. *Zhonghua Gan Zang Bing Za Zhi* 18, 520–522. doi:10.3760/cma.j.issn.1007-3418.2010.07.012

Suzuki, Y., Tokimatsu, I., Sato, Y., Kawasaki, K., Sato, Y., Goto, T., et al. (2013). Association of sustained high plasma trough concentration of voriconazole with the incidence of hepatotoxicity. *Clin. Chim. Acta Int. J. Clin. Chem.* 424, 119–122. doi:10.1016/j.cca.2013.05.025

Tanabe, M., Ieiri, I., Nagata, N., Inoue, K., Ito, S., Kanamori, Y., et al. (2001). Expression of P-glycoprotein in human placenta: relation to genetic polymorphism of the multidrug resistance (MDR)-1 gene. *J. Pharmacol. Exp. Ther.* 297, 1137–1143. doi:10.1023/A:1011583210549

Tanaka, R., Fujioka, T., Suzuki, Y., Iwao, M., and Itoh, H. (2020). A prospective study on the usefulness of initial voriconazole dose adjustment based on CYP2C19 gene polymorphism analysis. *Chemotherapy* 65, 59–64. doi:10.1159/000509970

Tang, D., Song, B.-L., Yan, M., Zou, J.-J., Zhang, M., Zhou, H.-Y., et al. (2019). Identifying factors affecting the pharmacokinetics of voriconazole in patients with liver dysfunction: a population pharmacokinetic approach. *Basic Clin. Pharmacol. Toxicol.* 125, 34–43. doi:10.1111/bcpt.13208

Tang, D., Yan, M., Song, B.-L., Zhao, Y.-C., Xiao, Y.-W., Wang, F., et al. (2021). Population pharmacokinetics, safety and dosing optimization of voriconazole in patients with liver dysfunction: a prospective observational study. *Br. J. Clin. Pharmacol.* 87, 1890–1902. doi:10.1111/bcp.14578

Tariq, T., Irfan, F. B., Farishta, M., Dykstra, B., Sieloff, E. M., and Desai, A. P. (2019). Spontaneous fungal peritonitis: micro-organisms, management and mortality in liver cirrhosis-A systematic review. *World J. Hepatol.* 11, 596–606. doi:10.4254/wjh.v11.i7.596

Theuretzbacher, U., Ihle, F., and Derendorf, H. (2006). Pharmacokinetic/pharmacodynamic profile of voriconazole. *Clin. Pharmacokinet.* 45, 649–663. doi:10.2165/00003088-200645070-00002

Thompson, G. R., and Lewis, J. S. (2010). Pharmacology and clinical use of voriconazole. *Expert Opin. Drug Metab. Toxicol.* 6, 83–94. doi:10.1517/17425250903463878

Tulsyan, S., Mittal, R. D., and Mittal, B. (2016). The effect of ABCB1 polymorphisms on the outcome of breast cancer treatment. *Pharmacogenomics Pers. Med.* 9, 47–58. doi:10.2147/PGPM.S86672

Ueda, K., Nannya, Y., Kumano, K., Hangaishi, A., Takahashi, T., Imai, Y., et al. (2009). Monitoring trough concentration of voriconazole is important to ensure successful antifungal therapy and to avoid hepatic damage in patients with hematological disorders. *Int. J. Hematol.* 89, 592–599. doi:10.1007/s12185-009-0296-3

Ullmann, A. J., Aguado, J. M., Arikan-Akdagli, S., Denning, D. W., Groll, A. H., Lagrou, K., et al. (2018). Diagnosis and management of Aspergillus diseases: executive summary of the 2017 ESCMID-ECMM-ERS guideline. *Clin. Microbiol. Infect.* 24 (1), e1–e38. doi:10.1016/j.cmi.2018.01.002

Ullmann, A. J., Lipton, J. H., Vesole, D. H., Chandrasekar, P., Langston, A., Tarantolo, S. R., et al. (2007). Posaconazole or fluconazole for prophylaxis in severe graft-versus-host disease. *N. Engl. J. Med.* 356, 335–347. doi:10.1056/NEJMoa061098

Vasques, F., Cavazza, A., and Bernal, W. (2022). Acute liver failure. *Curr. Opin. Crit. Care* 28, 198–207. doi:10.1097/MCC.0000000000000923

Verbeeck, R. K. (2008). Pharmacokinetics and dosage adjustment in patients with hepatic dysfunction. *Eur. J. Clin. Pharmacol.* 64, 1147–1161. doi:10.1007/s00228-008-0553-z

Verma, N., Singh, S., Singh, M., Chauhan, A., Pradhan, P., Jaiswal, N., et al. (2022). Global epidemiological burden of fungal infections in cirrhosis patients: a systematic review with meta-analysis. *Mycoses* 65, 266–284. doi:10.1111/myc.13387

Wakieć, R., Prasad, R., Morschhäuser, J., Barchiesi, F., Borowski, E., and Milewski, S. (2007). Voriconazole and multidrug resistance in Candida albicans. *Mycoses* 50, 109–115. doi:10.1111/j.1439-0507.2006.01327.x

Walsh, T. J., Moriyama, B., Penzak, S. R., Klein, T. E., and Caudle, K. E. (2018). Response to "impact of CYP3A4 genotype on voriconazole exposure: new insights into the contribution of CYP3A4*22 to metabolism of voriconazole". *Clin. Pharmacol. Ther.* 103, 187. doi:10.1002/cpt.811

Wang, T., Chen, S., Sun, J., Cai, J., Cheng, X., Dong, H., et al. (2014a). Identification of factors influencing the pharmacokinetics of voriconazole and the optimization of dosage regimens based on Monte Carlo simulation in patients with invasive fungal infections. *J. Antimicrob. Chemother.* 69, 463–470. doi:10.1093/jac/dkt369

Wang, T., Yan, M., Tang, D., Dong, Y., Zhu, L., Du, Q., et al. (2021). Using child-pugh class to optimize voriconazole dosage regimens and improve safety in patients with liver cirrhosis: insights from a population pharmacokinetic model-based analysis. *Pharmacotherapy* 41, 172–183. doi:10.1002/phar.2474

Wang, T., Yan, M., Tang, D., Xue, L., Zhang, T., Dong, Y., et al. (2018a). A retrospective, multicenter study of voriconazole trough concentrations and safety in patients with Child-Pugh class C cirrhosis. *J. Clin. Pharm. Ther.* 43, 849–854. doi:10.1111/jcpt.12724

Wang, T., Yan, M., Tang, D., Xue, L., Zhang, T., Dong, Y., et al. (2018b). Therapeutic drug monitoring and safety of voriconazole therapy in patients with child–pugh class B and C cirrhosis: a multicenter study. *Int. J. Infect. Dis.* 72, 49–54. doi:10.1016/j.ijid.2018.05.009

Wang, T., Zhu, H., Sun, J., Cheng, X., Xie, J., Dong, H., et al. (2014b). Efficacy and safety of voriconazole and CYP2C19 polymorphism for optimised dosage regimens in patients with invasive fungal infections. *Int. J. Antimicrob. Agents* 44, 436–442. doi:10.1016/j.ijantimicag.2014.07.013

Weiss, J., Ten Hoevel, M. M., Burhenne, J., Walter-Sack, I., Hoffmann, M. M., Rengelshausen, J., et al. (2009). CYP2C19 genotype is a major factor contributing to the highly variable pharmacokinetics of voriconazole. *J. Clin. Pharmacol.* 49, 196–204. doi:10.1177/0091270008327537

Wojnowski, L. (2004). Genetics of the variable expression of CYP3A in humans. *Ther. Drug Monit.* 26, 192–199. doi:10.1097/00007691-200404000-00019

Xing, Y., Chen, L., Feng, Y., Zhou, Y., Zhai, Y., and Lu, J. (2017). Meta-analysis of the safety of voriconazole in definitive, empirical, and prophylactic therapies for invasive fungal infections. *BMC Infect. Dis.* 17, 798. doi:10.1186/s12879-017-2913-8

Yamada, T., Imai, S., Koshizuka, Y., Tazawa, Y., Kagami, K., Tomiyama, N., et al. (2018). Necessity for a significant maintenance dosage reduction of voriconazole in patients with severe liver cirrhosis (Child-Pugh class C). *Biol. Pharm. Bull.* 41, 1112–1118. doi:10.1248/bpb.b18-00164

Yamazaki, H., Nakamoto, M., Shimizu, M., Murayama, N., and Niwa, T. (2010). Potential impact of cytochrome P450 3A5 in human liver on drug interactions with triazoles. *Br. J. Clin. Pharmacol.* 69, 593–597. doi:10.1111/j.1365-2125.2010.03656.x

Yang, L., Wang, C., Zhang, Y., Wang, Q., Qiu, Y., Li, S., et al. (2022). Central nervous system toxicity of voriconazole: risk factors and threshold - a retrospective cohort study. *Infect. Drug Resist.* 15, 7475–7484. doi:10.2147/IDR.S391022

Yi, W. M., Schoeppler, K. E., Jaeger, J., Mueller, S. W., MacLaren, R., Fish, D. N., et al. (2017). Voriconazole and posaconazole therapeutic drug monitoring: a retrospective study. *Ann. Clin. Microbiol. Antimicrob.* 16, 60. doi:10.1186/s12941-017-0235-8

You, H., Dong, Y., Zou, Y., Zhang, T., Lei, J., Chen, L., et al. (2018). Voriconazole therapeutic drug monitoring: factors associated with supratherapeutic and subtherapeutic voriconazole concentrations. *Int. J. Clin. Pharmacol. Ther.* 56, 239–246. doi:10.5414/CP203184

Zeng, G., Wang, L., Shi, L., Li, H., Zhu, M., Luo, J., et al. (2020). Variability of voriconazole concentrations in patients with hematopoietic stem cell transplantation and hematological malignancies: influence of loading dose, procalcitonin, and pregnane X receptor polymorphisms. *Eur. J. Clin. Pharmacol.* 76, 515–523. doi:10.1007/s00228-020-02831-1

Zhang, Y., Hou, K., Liu, F., Luo, X., He, S., Hu, L., et al. (2021). The influence of CYP2C19 polymorphisms on voriconazole trough concentrations: systematic review and meta-analysis. *Mycoses* 64, 860–873. doi:10.1111/myc.13293

Zhang, Y., Si, D., Chen, X., Lin, N., Guo, Y., Zhou, H., et al. (2007). Influence of CYP2C9 and CYP2C19 genetic polymorphisms on pharmacokinetics of gliclazide MR in Chinese subjects. *Br. J. Clin. Pharmacol.* 64, 67–74. doi:10.1111/j.1365-2125.2007.02846.x

Zhao, Q. G., Ren, Q. X., Du, C. H., and Wang, Y. H. (2019). Analysis of monitoring results of voriconazole plasma concentration in Child-Pugh class C patients. *Drug Use Monit. China* 16, 11–14. doi:10.3969/j.issn.1672-8157.2019.01.003

Zhao, Y., Hou, J., Xiao, Y., Wang, F., Zhang, B., Zhang, M., et al. (2021). Predictors of voriconazole trough concentrations in patients with child-pugh class C cirrhosis: a prospective study. *Antibiot. Basel Switz.* 10, 1130. doi:10.3390/antibiotics10091130

Zhou, Z.-X., Yin, X.-D., Zhang, Y., Shao, Q.-H., Mao, X.-Y., Hu, W.-J., et al. (2022). Antifungal drugs and drug-induced liver injury: a real-world study leveraging the FDA adverse event reporting system database. *Front. Pharmacol.* 13, 891336. doi:10.3389/fphar.2022.891336

Zonios, D. I., Gea-Banacloche, J., Childs, R., and Bennett, J. E. (2008). Hallucinations during voriconazole therapy. *Clin. Infect. Dis.* 47, e7–e10. doi:10.1086/588844

Zonios, D., Yamazaki, H., Murayama, N., Natarajan, V., Palmore, T., Childs, R., et al. (2014). Voriconazole metabolism, toxicity, and the effect of cytochrome P450 2C19 genotype. *J. Infect. Dis.* 209, 1941–1948. doi:10.1093/infdis/jiu017

Zubiaur, P., Kneller, L. A., Ochoa, D., Mejía, G., Saiz-Rodríguez, M., Borobia, A. M., et al. (2021). Evaluation of voriconazole CYP2C19 phenotype-guided dose adjustments by physiologically based pharmacokinetic modeling. *Clin. Pharmacokinet.* 60, 261–270. doi:10.1007/s40262-020-00941-8

frontiers | Frontiers in Genetics

TYPE Original Research
PUBLISHED 28 August 2023
DOI 10.3389/fgene.2023.1234263

OPEN ACCESS

EDITED BY
Shaoqiu Chen,
University of Hawaii at Mānoa,
United States

REVIEWED BY
Yuanyuan Luo,
Chongqing University, China
Dan Zi,
Guizhou Provincial People's Hospital,
China

*CORRESPONDENCE
Shuwen Sun,
rockoshu@163.com

RECEIVED 04 June 2023
ACCEPTED 04 August 2023
PUBLISHED 28 August 2023

CITATION
Huang Z, Jing H, Lv J, Chen Y, Huang Y and Sun S (2023), Investigating Doxorubicin's mechanism of action in cervical cancer: a convergence of transcriptomic and metabolomic perspectives.
Front. Genet. 14:1234263.
doi: 10.3389/fgene.2023.1234263

Investigating Doxorubicin's mechanism of action in cervical cancer: a convergence of transcriptomic and metabolomic perspectives

Zhuo Huang[1,2,3], Huining Jing[2,3,4], Juanjuan Lv[1,2], Yan Chen[1,2], YuanQiong Huang[5] and Shuwen Sun[1,2]*

[1]Department of Pediatrics, West China Second University Hospital, Sichuan University, Chengdu, China, [2]Key Laboratory of Birth Defects and Related Diseases of Women and Children, Ministry of Education, West China Second University Hospital, Sichuan University, Chengdu, China, [3]Department of Medical Genetics, West China Second University Hospital, Sichuan University, Chengdu, China, [4]Department of Obstetrics and Gynecology, West China Second University Hospital, Sichuan University, Chengdu, China, [5]Department of Oncology, Luzhou Hospital of Traditional Chinese Medicine, Luzhou, China

Introduction: Cervical cancer remains a significant global health burden, and Doxorubicin is a crucial therapeutic agent against this disease. However, the precise molecular mechanisms responsible for its therapeutic effects are not fully understood.

Methods: In this study, we employed a multi-omics approach that combined transcriptomic and metabolomic analyses with cellular and *in vivo* experiments. The goal was to comprehensively investigate the molecular landscape associated with Doxorubicin treatment in cervical cancer.

Results: Our unbiased differential gene expression analysis revealed distinct alterations in gene expression patterns following Doxorubicin treatment. Notably, the ANKRD18B gene exhibited a prominent role in the response to Doxorubicin. Simultaneously, our metabolomic analysis demonstrated significant perturbations in metabolite profiles, with a particular focus on L-Ornithine. The correlation between ANKRD18B gene expression and L-Ornithine levels indicated a tightly controlled gene-metabolite network. These results were further confirmed through rigorous cellular and *in vivo* experiments, which showed reductions in subcutaneous tumor size and significant changes in ANKRD18B, L-Ornithine, and Doxorubicin concentration.

Discussion: The findings of this study underscore the intricate interplay between transcriptomic and metabolomic changes in response to Doxorubicin treatment. These insights could have implications for the development of more effective therapeutic strategies for cervical cancer. The identification of ANKRD18B and L-Ornithine as key components in this process lays the groundwork for future research aiming to unravel the complex molecular networks that underlie Doxorubicin's therapeutic mechanism. While this study provides a solid foundation, it also highlights the necessity for further investigation to fully grasp these interactions and their potential implications for cervical cancer treatment.

KEYWORDS

cervical cancer, Doxorubicin, transcriptomics, metabolomics, ANKRD18B, L-Ornithine, multi-omics integration

Introduction

Cervical cancer, an intricate health concern worldwide, predominantly afflicts women and stands as the fourth most common malignancy in the female population (Ginsburg et al., 2017). The global burden of cervical cancer is colossal, with an estimated 604,000 new cases and around 342,000 deaths reported in 2022, according to the World Health Organization (Tan et al., 2022). Despite the advent of novel diagnostic techniques and preventative strategies such as the human papillomavirus (HPV) vaccination, the morbidity and mortality rates remain daunting, particularly in low- and middle-income countries where healthcare resources and infrastructure are limited (Bosch et al., 2013). It is widely acknowledged that persistent infection with certain types of human papillomavirus (HPV) is the most important risk factor for cervical cancer. Indeed, HPV is detected in more than 90% of cervical cancer cases, with HPV types 16 and 18 being the most prevalent. HPV, a small DNA virus, has over 100 types, of which about 40 can infect the genital tract. Among these, approximately 15 types are considered high-risk for the development of cervical cancer and other anogenital cancers (Ahmed et al., 2023). Prolonged infection with these high-risk types, particularly HPV 16 and HPV 18, can lead to the formation of precancerous lesions, which may progress to invasive cervical cancer if not treated (Cascardi et al., 2022). Despite the availability of prophylactic HPV vaccines, cervical cancer incidence remains high due to factors such as limited vaccine coverage and the long period between HPV infection and cancer development. Furthermore, the vaccines do not have therapeutic effects on existing HPV infections or HPV-associated lesions. As such, understanding the molecular mechanisms underlying cervical cancer progression and response to treatment, as explored in this study, is of utmost importance.

The standard therapeutic approach for cervical cancer encompasses a combination of surgery, radiation therapy, and chemotherapy, tailored according to the stage and extent of the disease (Yessaian et al., 2004). Doxorubicin, a potent anthracycline chemotherapy drug, has been employed as a primary or adjuvant treatment modality in various stages of cervical cancer (Koning et al., 2010). It operates primarily by intercalating into DNA, inhibiting the topoisomerase II enzyme, thus impeding DNA replication and transcription, culminating in cell death. Nevertheless, the precise molecular and metabolic pathways influenced by Doxorubicin in cervical cancer remain to be comprehensively elucidated. Recent advancements in high-throughput technologies have made it feasible to explore the complex landscape of biological systems at multiple levels, from genes to metabolites (Yessaian et al., 2004).

Transcriptomics and metabolomics, two integral components of systems biology, provide profound insights into the functional elements of the genome and the downstream metabolic processes, respectively (Zampieri et al., 2019; Jamil et al., 2020). These methodologies have empowered the scientific community to probe into the molecular intricacies of disease mechanisms, drug responses, and personalized therapeutics (Naylor and Chen, 2010; Beckmann and Lew, 2016). In the realm of cervical cancer, an integrative analysis of transcriptomic and metabolomic data may unveil the precise molecular and metabolic alterations induced by Doxorubicin. Such comprehensive understanding could aid in the optimization of treatment strategies, identification of potential therapeutic targets, and prediction of treatment response (Fleisher et al., 2017; Niu et al., 2019). This study leverages the synergistic potential of transcriptomics and metabolomics to investigate the mechanism of action of Doxorubicin in cervical cancer, paving the way for innovative and personalized treatment options in the future.

Materials and methods

Public data retrieval and preprocessing

Transcriptomic data for this study were obtained from the publicly available dataset GSE160234 (Demir et al., 2021). The experimental design encompassed HeLa cells that were incubated for 6 days without treatment (group Normal, $n = 3$), treated with 300 nM doxorubicin for 72 h and then incubated for an additional 72 h without treatment (group Cancer, $n = 3$), or treated with 300 nM doxorubicin for 72 h. These data were preprocessed and normalized according to the standard pipelines to ensure the accuracy and reliability of subsequent analyses.

Metabolomics analysis

For the metabolomic study, cells under the same treatment conditions were harvested, and metabolites were extracted using a cold methanol-acetonitrile-water solution (2:2:1 v/v/v). The extracts were then analyzed using an Agilent 1290 Infinity II LC system coupled with an Agilent 6545 Q-TOF mass spectrometer (Agilent Technologies, Santa Clara, CA, United States). The chromatographic separation was carried out on a Waters ACQUITY UPLC BEH Amide column (2.1 mm × 100 mm, 1.7 μm). The raw data were processed and analyzed using Agilent MassHunter Qualitative Analysis software (B.06.00).

Quantitative polymerase chain reaction (qPCR)

Quantitative polymerase chain reaction (qPCR) was performed to validate the expression of the ANKRD18B gene. RNA was extracted from the cells using the RNeasy Mini Kit (Qiagen, Valencia, CA, United States), and cDNA was synthesized using the iScript cDNA Synthesis Kit (Bio-Rad, Hercules, CA, United States). Real-time PCR was performed using the SYBR Green Master Mix (Applied Biosystems, Foster City, CA, United States) on a StepOnePlus Real-Time PCR System (Applied Biosystems, Foster City, CA, United States). The primer sequences for ANKRD18B were: forward, 5′- CTCGCTCTATCACCAGTCTGGA -3′; reverse, 5′- ATG GTCGCATGTGCCTGTTGTC -3′. Beta-actin was used as the reference gene, with the following primer sequences: forward, 5′- CACCATTGGCAATGAGCGGTTC -3′; reverse, 5′- AGGTCT TTGCGGATGTCCACGT -3′.

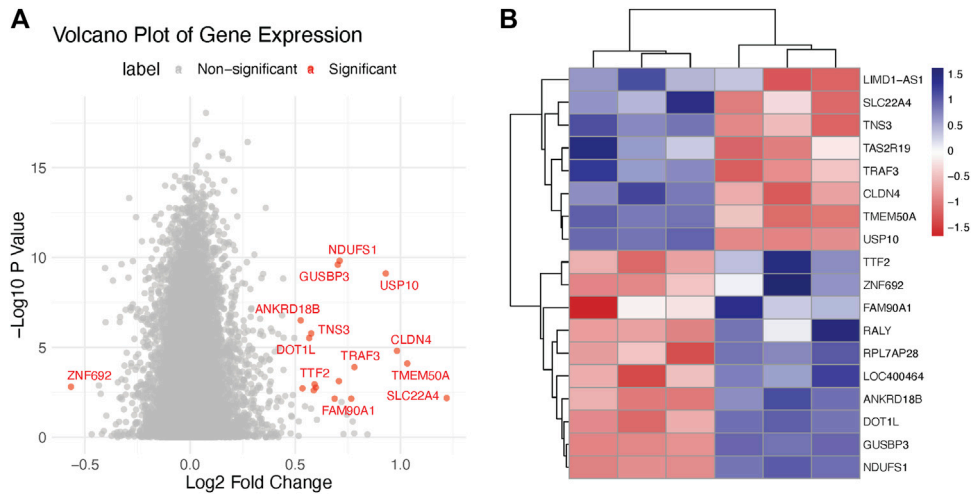

FIGURE 1
Transcriptomics analysis of doxorubicin-treated and control Hela cells. **(A)** Volcano plot illustrating the differential expression of genes in Hela cells treated with doxorubicin versus control. The X-axis represents the log2 fold change (FC) and the Y-axis represents the −log10 adjusted *p*-values. **(B)** Heatmap showing the clustering of significantly differentially expressed genes (DEGs) in doxorubicin-treated and control Hela cells.

In vivo mouse model experiments

The nude mice were inoculated subcutaneously with HeLa cells (ATCC® CCL-2™) to generate xenograft tumors. Post-inoculation, the mice were intraperitoneally treated with either doxorubicin (CAS 25316-40-9, Sigma-Aldrich, St. Louis, MO, United States) at varying doses between 2 and 3 mg/kg, or normal saline (CAS 7647-14-5, Sigma-Aldrich, St. Louis, MO, United States) at doses between 10 and 12 mg/kg, twice a week. The treatments started from the seventh day post-inoculation, and the experiment lasted for 28 days.

Statistical analysis

All statistical analyses were performed using the R programming language (version 4.0.2). Descriptive statistics were used to summarize the transcriptomics and metabolomics data. The Normal and Cancer groups were compared using Student's *t*-test for normally distributed data or the Mann-Whitney U test for non-normally distributed data. A *p*-value of less than 0.05 was considered statistically significant. Correlation analyses between the transcriptomics and metabolomics data were conducted using Pearson's correlation coefficient or Spearman's rank correlation coefficient as appropriate. The most significant genes and metabolites were selected based on the correlation coefficients. Differential expression analyses for the transcriptomics data were conducted using the DESeq2 package (Love et al., 2014). Genes with an adjusted *p*-value (Benjamini-Hochberg procedure) less than 0.05 and a log2 fold-change greater than 1 or less than −1 were considered differentially expressed. For the qPCR and *in vivo* mouse model experiment data, one-way analysis of variance (ANOVA) followed by Tukey's multiple comparisons test was used to compare the groups. Data visualization was performed using the ggplot2 package in R. Heatmaps were generated using the pheatmap package (Kolde and Kolde, 2018). Boxplots were used to visualize the expression levels of the most significant genes and metabolites.

Results

Revealing altered gene expression landscape in cervical cancer cells treated with Doxorubicin: a comprehensive transcriptomic analysis

As part of our endeavor to characterize the molecular mechanisms that underpin the therapeutic effect of Doxorubicin on cervical cancer, we began with a deep dive into the transcriptomic changes it instigates. We carried out an unbiased differential gene expression analysis to discern the molecular patterns associated with Doxorubicin treatment. Our analysis led us to the discovery of several genes that displayed marked expression differences between the Normal and Cancer groups. The ensuing volcano plot—Figure 1A—brings into stark relief the multitude of differentially expressed genes. Notably, the distribution of these genes followed an interesting pattern, suggesting potential stratification of gene expression alterations. Moreover, to zero in on the most significantly altered genes, we constructed a heatmap using those with an adjusted *p*-value < 0.05 and |log2 fold-change| > 1 (Figure 1B). This analysis unveiled clusters of genes with distinct expression patterns, giving us valuable insights into the potential molecular programs disrupted by Doxorubicin (Supplementary Table S1).

Doxorubicin's therapeutic action is accompanied by perturbations in metabolite profiles: an in-depth metabolomic analysis

Concurrent with our transcriptomic analysis, we undertook an exhaustive metabolomic analysis to unravel any accompanying metabolic perturbations associated with Doxorubicin treatment. Interestingly, like our transcriptomic analysis, many metabolites

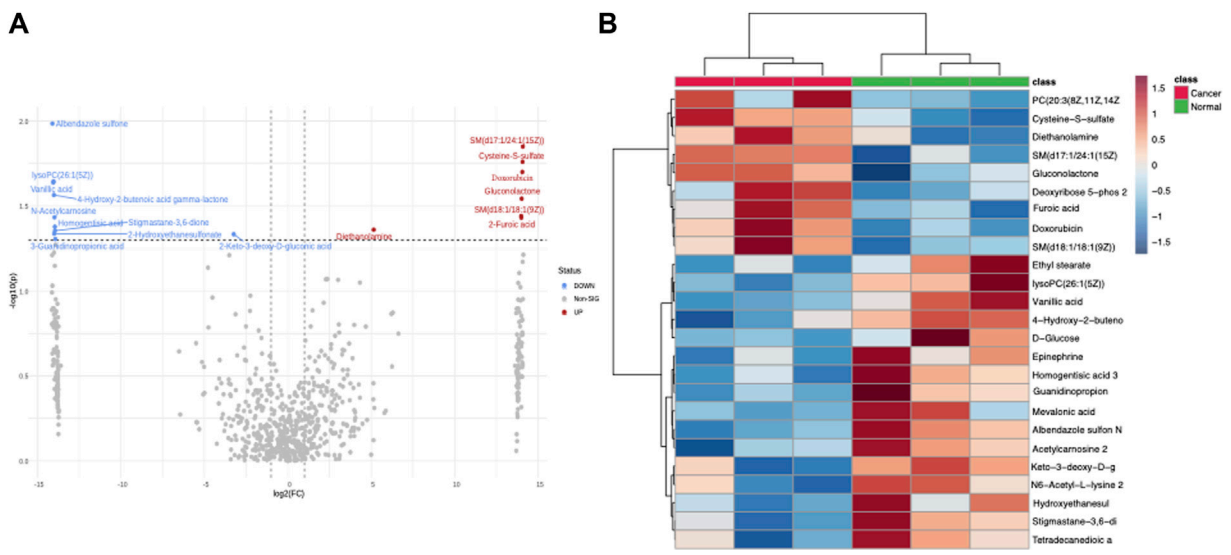

FIGURE 2
Metabolomics analysis of doxorubicin-treated and control Hela cells. **(A)** Volcano plot depicting the differential metabolite levels in Hela cells treated with doxorubicin versus control. The X-axis shows the log2 FC and the Y-axis represents the −log10 adjusted *p*-values. **(B)** Heatmap demonstrating the clustering of significantly different metabolites in doxorubicin-treated and control Hela cells.

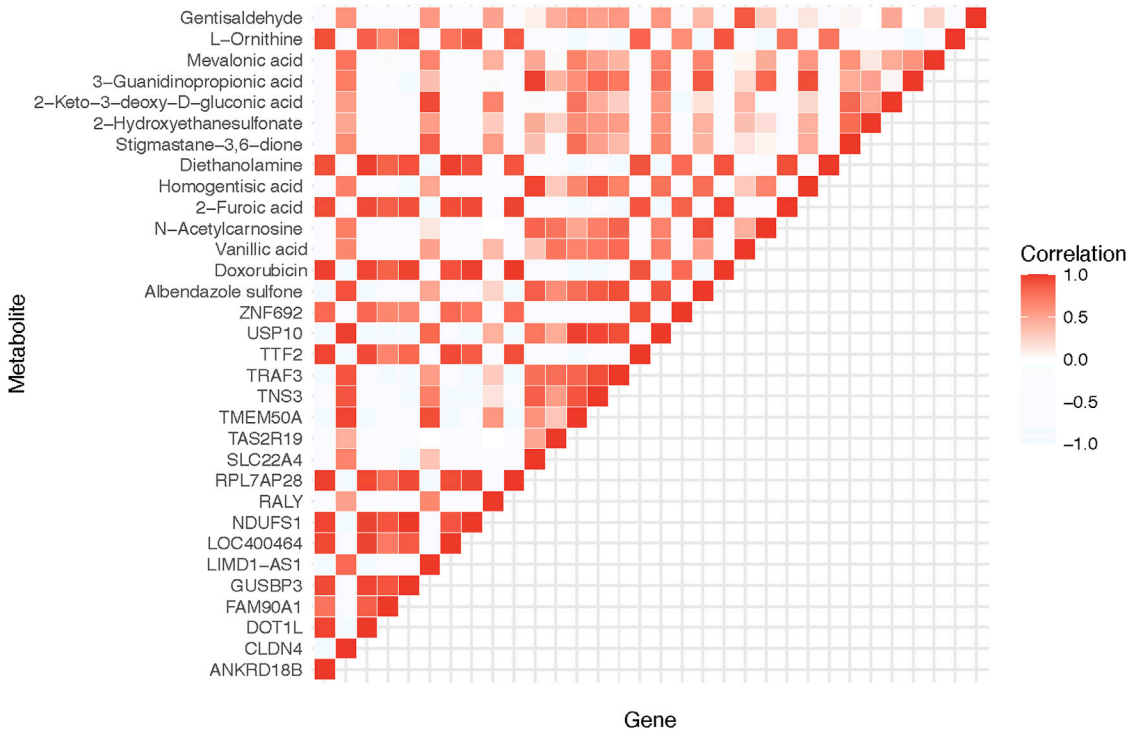

FIGURE 3
Correlation analysis of significantly differential genes and metabolites. The heatmap demonstrates the correlation between the DEGs and the significantly different metabolites. ANKRD18B and L-Ornithine are found to have a significant correlation.

exhibited significantly differential levels between the Normal and Cancer groups. The ensuing volcano plot (Figure 2A) clearly illustrates this widespread metabolic perturbation. To provide a finer granularity of these metabolic changes, we charted a heatmap using the most significantly altered metabolites. The heatmap in Figure 2B depicts an intricate metabolic landscape, suggesting a

10.3389/fgene.2023.1234263

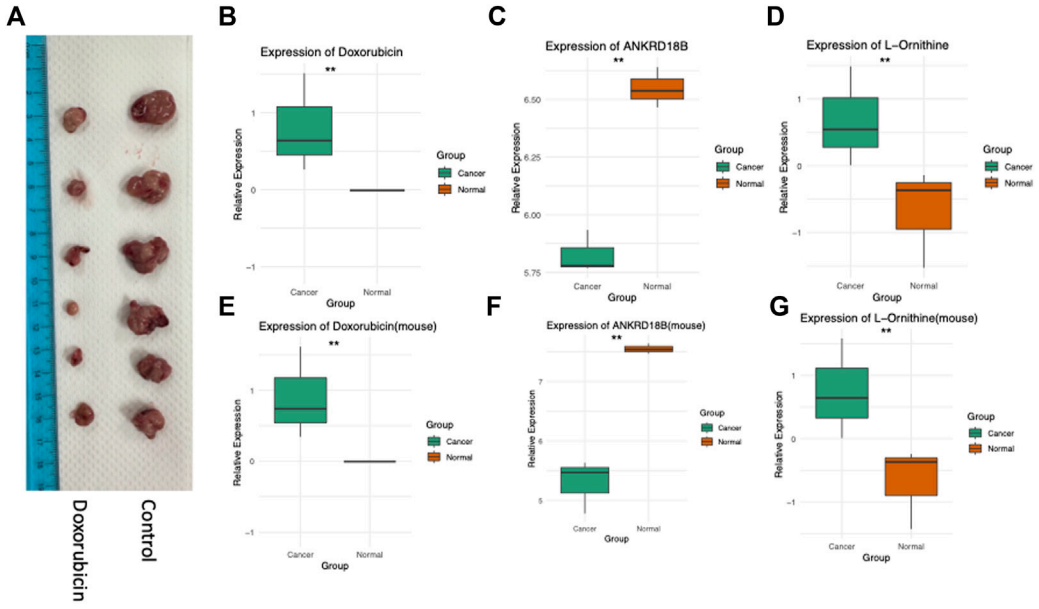

FIGURE 4
Experimental validation in cells and *in vivo*. **(A)** Doxorubicin inhibits the growth of Hela cell-derived subcutaneous tumors in mice. **(B)** ANKRD18B gene expression, **(C)** doxorubicin concentration, and **(D)** L-Ornithine concentration in cell cultures. **(E)** ANKRD18B gene expression, **(F)** doxorubicin concentration, and **(G)** L-Ornithine concentration in tumor tissues. *$p < 0.05$; **$p < 0.01$.

complex remodeling of metabolic pathways in response to Doxorubicin treatment (Supplementary Table S2).

A symbiotic relationship between transcriptomic and metabolomic alterations: integrated correlation analysis

With the wealth of data generated from our omics analyses, we sought to tease apart any possible relationships between the transcriptomic and metabolomic changes. In doing so, we uncovered a strong correlation between the gene ANKRD18B and the metabolite L-Ornithine, both of which showed marked changes in response to Doxorubicin treatment. As shown in Figure 3, this result illustrates the intimate interplay between gene expression and metabolite levels, potentially pointing towards a tightly controlled gene-metabolite network affected by Doxorubicin.

From cells to mice: experimental validation of omics findings

Complementing our multi-omics analyses, we conducted a series of rigorous cellular and *in vivo* experiments to validate our findings. The effect of Doxorubicin treatment on tumor growth was assessed in a mouse model, where we observed a significant decrease in subcutaneous tumor size (Figure 4A). Furthermore, cellular and tissue experiments corroborated the crucial roles of ANKRD18B and L-Ornithine in mediating the action of Doxorubicin. As evident from Figures 4B, E, ANKRD18B expression levels were significantly different in both the cell and tissue experiments, aligning with our omics data. Similarly, the intracellular concentrations of Doxorubicin (Figures 4C, F) and L-Ornithine (Figures 4D, G) were also found to vary significantly in line with the corresponding omics results. Collectively, these data provide compelling evidence for the involvement of ANKRD18B and L-Ornithine in the therapeutic mechanism of Doxorubicin, thus enriching our understanding. In our analysis of the TCGA-CESC (Cervical Squamous Cell Carcinoma and Endocervical Adenocarcinoma) dataset, ANKRD18B emerged as a gene of significant interest (Supplementary Figure S1). We found that the expression of ANKRD18B was significantly elevated in tumor tissues compared to their normal counterparts ($p < 0.05$). This upregulation in tumor tissues suggests a potential role of ANKRD18B in cervical cancer progression. However, when we examined the impact of ANKRD18B expression on overall survival, the results were not statistically significant (logrank $p = 0.45$).

Discussion

In this study, we embarked on a comprehensive investigation to elucidate the molecular underpinnings of the therapeutic action of Doxorubicin on cervical cancer. Our approach involved an integration of transcriptomic and metabolomic analyses, paired with rigorous cellular and *in vivo* experiments. This multi-pronged strategy led us to the discovery of ANKRD18B and L-Ornithine as significant players in the Doxorubicin treatment

response. The observed positive correlation between ANKRD18B and L-Ornithine is of special interest and warrants further investigation to unravel the intricacies of their joint impact on the disease process.

ANKRD18B, part of the Ankyrin repeat domain-containing protein family, has been previously implicated in various biological processes, albeit the exact mechanism of action of ANKRD18B is not fully understood (Sundar et al., 2017). Recent studies have shed light on the potential role of ANKRD18B in cellular processes such as cell cycle regulation and apoptosis, both of which are key mechanisms exploited by chemotherapeutic drugs like Doxorubicin (Al-Alem, 2011). The marked upregulation of ANKRD18B in response to Doxorubicin treatment, as revealed by our transcriptomic analysis, points towards a potential mechanistic role of this gene in the anti-tumor action of Doxorubicin. Moreover, the fact that its expression pattern is in sync with Doxorubicin concentration underscores its potential importance in Doxorubicin-mediated therapeutic effect. Although the exact role of ANKRD18B in this process is still unclear, its significant alteration following Doxorubicin treatment, as shown in our study, suggests that it may be implicated in the response to therapy in HPV-positive cervical cancers. On the other hand, L-Ornithine, a key player in the urea cycle, has been linked to multiple cancer-related processes (You et al., 2018). Several studies have implicated aberrant metabolism, including alterations in the urea cycle, as a hallmark of cancer (Erbaş et al., 2015; Wang et al., 2022). In cervical cancer, metabolic reprogramming often manifests as alterations in amino acid metabolism, of which the urea cycle is an integral part. Thus, our finding of significant alterations in L-Ornithine levels in response to Doxorubicin treatment is noteworthy. Given the critical role of metabolic remodeling in cancer progression and response to therapy, the observed L-Ornithine changes might signify an important metabolic response to Doxorubicin. Additionally, the fact that L-Ornithine levels mirrored those of ANKRD18B and Doxorubicin concentration points to a potential gene-metabolite network at play.

Interestingly, the positive correlation between ANKRD18B and L-Ornithine highlights a potential intricate interplay between gene expression and metabolite levels. Such an interaction could potentially contribute to the complex adaptive response of cancer cells to chemotherapy, thereby impacting the therapeutic outcome. The discovery of this correlation underscores the importance of integrative multi-omics analyses in unveiling complex molecular networks. While it necessitates further exploration, it provides a promising direction for future research aimed at a more comprehensive understanding of the therapeutic mechanism of Doxorubicin.

Our study is still with some limitations. While we have uncovered promising candidates that might be pivotal in the therapeutic response to Doxorubicin, the precise nature of their interaction and the resulting molecular cascade remains to be elucidated. Future work should focus on deciphering these molecular networks using techniques like gene knockdown or overexpression studies and metabolic flux analysis. Nonetheless, our findings lay a solid foundation for future research in this direction and can potentially aid the design of improved therapeutic strategies. Although our multi-omics approach has provided valuable insights into the molecular mechanisms of Doxorubicin, it is important to note some limitations of our study. One of these is the inability of our metabolomics equipment to differentiate between the D and L forms of metabolites. This is a significant limitation as the D and L forms can have different biological activities. Future studies with equipment capable of distinguishing between these forms would provide a more comprehensive understanding of the changes in the metabolome following Doxorubicin treatment.

In conclusion, our study highlights the intricate changes in gene expression and metabolic profiles in response to Doxorubicin treatment in cervical cancer. We provide compelling evidence pointing towards a crucial role of ANKRD18B and L-Ornithine in mediating the action of Doxorubicin. While our findings paint a complex picture of the molecular landscape associated with Doxorubicin treatment, they open new avenues for a deeper.

Data availability statement

The raw data supporting the conclusion of this article will be made available by the authors, without undue reservation.

Ethics statement

The studies involving humans were approved by the West China Second University Hospital, Sichuan University. The studies were conducted in accordance with the local legislation and institutional requirements. Written informed consent for participation was not required from the participants or the participants' legal guardians/next of kin in accordance with the national legislation and institutional requirements. The animal study was approved by the West China Second University Hospital, Sichuan University. The study was conducted in accordance with the local legislation and institutional requirements.

Author contributions

SS and ZH conceptualized and designed the study and performed the transcriptomics and metabolomics analysis. HJ and JL contributed to the data acquisition and interpretation, as well as the qPCR experiments. YC participated in the *in vivo* mouse model experiments and data interpretation. YH provided substantial help with data analysis and visualization. ZH provided significant advice on experimental design and data interpretation. SS, as the corresponding author, oversaw the entire project, provided guidance and feedback, and finalized the manuscript. All authors contributed to the article and approved the submitted version.

Conflict of interest

The authors declare that the research was conducted in the absence of any commercial or financial relationships that could be construed as a potential conflict of interest.

Publisher's note

Supplementary material

The Supplementary Material for this article can be found online at: https://www.frontiersin.org/articles/10.3389/fgene.2023.1234263/full#supplementary-material

SUPPLEMENTARY FIGURE S1

(A) Differential expression of ANKRD18B in TCGA-CESC dataset. This bar graph represents the expression levels of ANKRD18B in paired tumor (T) and normal (N) tissues from the TCGA-CESC dataset. The expression of ANKRD18B was significantly elevated in tumor tissues compared to their normal counterparts ($p < 0.05$). Error bars denote standard error of the mean (SEM). **(B)** Kaplan-Meier survival analysis of cervical cancer patients based on ANKRD18B expression. The survival curves represent the overall survival of cervical cancer patients stratified by the expression level of ANKRD18B (high vs. low). Despite the observed difference in survival times, the log-rank test did not reveal a significant difference ($p = 0.45$).

References

Ahmed, W., Zaib, S., Ullah, S., Fatima, A., Zaib, Z., Haseeb Azam, M. A., et al. (2023). Role of human papillomavirus in various cancers: epidemiology, screening and prevention. *Mini Rev. Med. Chem.* 23, 1079–1089. doi:10.2174/1389557523666230213140641

Al-Alem, L. F. (2011). *Unraveling the effects of Thiazolidinediones and peroxisome proliferator-activated receptor gamma 1 on ovarian cancer*. United Kingdom: University of Kentucky.

Beckmann, J. S., and Lew, D. (2016). Reconciling evidence-based medicine and precision medicine in the era of big data: challenges and opportunities. *Genome Med.* 8, 134–211. doi:10.1186/s13073-016-0388-7

Bosch, F. X., Broker, T. R., Forman, D., Moscicki, A.-B., Gillison, M. L., Doorbar, J., et al. (2013). Comprehensive control of human papillomavirus infections and related diseases. *Vaccine* 31, H1–H31. doi:10.1016/j.vaccine.2013.10.003

Cascardi, E., Cazzato, G., Daniele, A., Silvestris, E., Cormio, G., Di Vagno, G., et al. (2022). Association between cervical microbiota and HPV: could this be the key to complete cervical cancer eradication? *Biology* 11, 1114. doi:10.3390/biology11081114

Demir, Y. D. Ş., Özdemir, A., Sucularlı, C., Benhür, E., and Ark, M. (2021). The implication of ROCK 2 as a potential senotherapeutic target via the suppression of the harmful effects of the SASP: do senescent cancer cells really engulf the other cells? *Cell. Signal.* 84, 110007. doi:10.1016/j.cellsig.2021.110007

Erbaş, H., Oğuz, B., and Cakir, E. (2015). Effect of rosuvastatin on arginase enzyme activity and polyamine production in experimental breast cancer. *Balkan Med. J.* 32, 89–95. doi:10.5152/balkanmedj.2015.15611

Fleisher, B., Brown, A. N., and Ait-Oudhia, S. (2017). Application of pharmacometrics and quantitative systems pharmacology to cancer therapy: the example of luminal a breast cancer. *Pharmacol. Res.* 124, 20–33. doi:10.1016/j.phrs.2017.07.015

Ginsburg, O., Bray, F., Coleman, M. P., Vanderpuye, V., Eniu, A., Kotha, S. R., et al. (2017). The global burden of women's cancers: a grand challenge in global health. *Lancet* 389, 847–860. doi:10.1016/S0140-6736(16)31392-7

Jamil, I. N., Remali, J., Azizan, K. A., Nor Muhammad, N. A., Arita, M., Goh, H.-H., et al. (2020). Systematic multi-omics integration (MOI) approach in plant systems biology. *Front. plant Sci.* 11, 944. doi:10.3389/fpls.2020.00944

Kolde, R., and Kolde, M. R. (2018). Lecture de textes latins et mitic font BON MÉNAGE: quelques considérations sur L'ENSEIGNEMENT du Latin en suisse romande. *R. package* 1. doi:10.7202/1047800ar

Koning, G. A., Eggermont, A. M., Lindner, L. H., and ten Hagen, T. L. (2010). Hyperthermia and thermosensitive liposomes for improved delivery of chemotherapeutic drugs to solid tumors. *Pharm. Res.* 27, 1750–1754. doi:10.1007/s11095-010-0154-2

Love, M. I., Huber, W., and Anders, S. (2014). Moderated estimation of fold change and dispersion for RNA-seq data with DESeq2. *Genome Biol.* 15 (12), 550. doi:10.1186/s13059-014-0550-8

Naylor, S., and Chen, J. Y. (2010). Unraveling human complexity and disease with systems biology and personalized medicine. *Pers. Med.* 7, 275–289. doi:10.2217/pme.10.16

Niu, J., Straubinger, R. M., and Mager, D. E. (2019). Pharmacodynamic drug–drug interactions. *Clin. Pharmacol. Ther.* 105, 1395–1406. doi:10.1002/cpt.1434

Sundar, I. K., Yin, Q., Baier, B. S., Yan, L., Mazur, W., Li, D., et al. (2017). DNA methylation profiling in peripheral lung tissues of smokers and patients with COPD. *Clin. epigenetics* 9, 38–18. doi:10.1186/s13148-017-0335-5

Tan, F., Chen, J., Du, Z., Zhao, F., Liu, Y., Zhang, Q., et al. (2022). MIR17HG: a cancerogenic long-noncoding RNA in different cancers. *Curr. Pharm. Des.* 28, 1272–1281. doi:10.2174/1381612828666220310144500

Wang, Q., Tan, Y., Jiang, T., Wang, X., Li, Q., Li, Y., et al. (2022). Metabolic reprogramming and its relationship to survival in hepatocellular carcinoma. *Cells* 11, 1066. doi:10.3390/cells11071066

Yessaian, A., Magistris, A., Burger, R. A., and Monk, B. J. (2004). Radical hysterectomy followed by tailored postoperative therapy in the treatment of stage IB2 cervical cancer: feasibility and indications for adjuvant therapy. *Gynecol. Oncol.* 94, 61–66. doi:10.1016/j.ygyno.2004.04.016

You, J., Chen, W., Chen, J., Zheng, Q., Dong, J., and Zhu, Y. (2018). The oncogenic role of ARG1 in progression and metastasis of hepatocellular carcinoma. *BioMed Res. Int.* 2018, 2109865. doi:10.1155/2018/2109865

Zampieri, G., Vijayakumar, S., Yaneske, E., and Angione, C. (2019). Machine and deep learning meet genome-scale metabolic modeling. *PLoS Comput. Biol.* 15, e1007084. doi:10.1371/journal.pcbi.1007084

frontiers | Frontiers in Genetics

TYPE Original Research
PUBLISHED 14 September 2023
DOI 10.3389/fgene.2023.1231682

OPEN ACCESS

EDITED BY
Shaoqiu Chen,
University of Hawaii at Mānoa,
United States

REVIEWED BY
Guoqian He,
Sichuan University, China
Gregorio Martínez-Sánchez,
University of Havana, Cuba

*CORRESPONDENCE
Shu Ou,
ssw7162021@163.com

†These authors have contributed equally to this work

RECEIVED 30 May 2023
ACCEPTED 18 August 2023
PUBLISHED 14 September 2023

CITATION
Yang X, Chen C, Wang K, Chen M, Wang Y, Chen Z, Zhao W and Ou S (2023), Elucidating the molecular mechanisms of ozone therapy for neuropathic pain management by integrated transcriptomic and metabolomic approach.
Front. Genet. 14:1231682.
doi: 10.3389/fgene.2023.1231682

Elucidating the molecular mechanisms of ozone therapy for neuropathic pain management by integrated transcriptomic and metabolomic approach

Xiaolan Yang[1†], Chaoming Chen[1†], Keyang Wang[1], Min Chen[1], Yong Wang[1], Zhengping Chen[1], Wang Zhao[2] and Shu Ou[1*]

[1]Department of Neurology, The Fengjie People's Hospital, Fengjie Branch of the Second Affiliated Hospital of Chongqing Medical University, Chongqing, China, [2]Department of Neurology, Yongchuan Hospital Affiliated to Chongqing Medical University, Chongqing, China

Introduction: Neuropathic pain remains a prevalent and challenging condition to treat, with current therapies often providing inadequate relief. Ozone therapy has emerged as a promising treatment option; however, its mechanisms of action in neuropathic pain remain poorly understood.

Methods: In this study, we investigated the effects of ozone treatment on gene expression and metabolite levels in the brainstem and hypothalamus of a rat model, using a combined transcriptomic and metabolomic approach.

Results: Our findings revealed significant alterations in key genes, including DCST1 and AIF1L, and metabolites such as Aconitic acid, L-Glutamic acid, UDP-glucose, and Tyrosine. These changes suggest a complex interplay of molecular pathways and region-specific mechanisms underlying the analgesic effects of ozone therapy.

Discussion: Our study provides insights into the molecular targets of ozone treatment for neuropathic pain, laying the groundwork for future research on validating these targets and developing novel therapeutic strategies.

KEYWORDS

ozone therapy, neuropathic pain, transcriptomics, metabolomics, mechanism of action, multi-omics

Introduction

Neuropathic pain, a complex and debilitating condition, originates from dysfunction or damage to the somatosensory system, affecting approximately 7%–10% of the global population (Colloca et al., 2017). It is characterized by persistent pain, burning sensations, allodynia, and hyperalgesia, significantly impacting the quality of life for those affected. Conventional pharmacological treatments for neuropathic pain, such as opioids, anticonvulsants, and antidepressants, often provide limited relief and are associated with numerous side effects, including addiction, dizziness, and sedation. Consequently, there is an urgent need to explore novel, safe, and effective therapeutic interventions for neuropathic pain management (Raja et al., 2020).

Ozone therapy, an emerging alternative treatment, has recently gained attention for its potential in neuropathic pain management. It involves the administration of ozone, a highly reactive molecule comprising three oxygen atoms, through various routes, including intramuscular, intradiscal, and intraperitoneal injections. Studies have demonstrated the therapeutic benefits of ozone therapy in reducing pain and inflammation, improving blood flow and oxygenation, and promoting tissue healing (Clavo et al., 2021; Masan et al., 2021). However, despite these promising findings, the precise mechanisms underlying the effectiveness of ozone therapy for neuropathic pain remain largely unknown.

A comprehensive understanding of the molecular pathways involved in ozone therapy-induced pain relief is essential for optimizing this treatment modality and ensuring its safe and effective application. Transcriptomics and metabolomics are powerful tools that can facilitate the elucidation of these mechanisms by providing a global view of gene expression and metabolic changes in response to ozone treatment. Through the integration of transcriptomic and metabolomic data, researchers can identify key regulatory genes and metabolic pathways that contribute to the therapeutic effects of ozone therapy on neuropathic pain (Vassallo, 2012; Ma et al., 2020).

In this study, we employ a systems biology approach, leveraging both transcriptomic and metabolomic techniques, to investigate the molecular mechanisms underlying ozone therapy in the treatment of neuropathic pain. We aim to identify the key genes and metabolic pathways involved in ozone-induced pain relief, which could ultimately inform the development of more targeted and effective therapeutic interventions for neuropathic pain management.

Methods

Rat husbandry and ozone exposures

Adult male Sprague-Dawley rats were housed in temperature- and humidity-controlled rooms with a 12-h light/dark cycle and had free access to food and water. The rats were acclimated to their environment for 1 week prior to the experiments. Whole-body exposures to filtered air or ozone (0.8 ppm) were conducted for 4 h (0700–1100 AM). Ozone was generated using a silent arc discharge generator and directed to the exposure chambers with the aid of mass flow controllers. The concentration of ozone was continuously monitored and maintained at 0.800 ± 0.04 ppm using photometric analyzers. The exposure chamber conditions, including temperature, relative humidity, and airflow, were carefully regulated, and recorded hourly.

Blood collection and serum preparation

Before conducting the surgeries, blood samples were collected from the rats to obtain serum for further analyses. Rats were anesthetized using isoflurane (Piramal Critical Care, Bethlehem, PA, United States; Cat. No. NDC0409-1964-64) to minimize stress and discomfort during the procedure. Blood samples were collected from the tail vein using a sterile needle and placed in BD Vacutainer Serum Separator Tubes (BD Biosciences, San Jose, CA, United States; Cat. No. 367988). The tubes were then allowed to clot at room temperature for 30 min before centrifugation at 2000 × g for 10 min at 4°C. The obtained serum was carefully aliquoted and stored at −80°C for further analysis.

Rat surgery

Following blood collection, rats underwent surgery under aseptic conditions. Anesthesia was induced and maintained with isoflurane (Piramal Critical Care, Bethlehem, PA, United States; Cat. No. NDC0409-1964-64) during the surgery. Once the rats were adequately anesthetized, their surgical site was shaved and disinfected with iodine solution (Betadine, Avrio Health L.P., Stamford, CT, United States; Cat. No. NDC67618-150-02) and 70% ethanol (Decon Labs, Inc., King of Prussia, PA, United States; Cat. No. 2701-4). Sterile surgical instruments were used throughout the procedure. The surgery was conducted following standard procedures for the specific experimental requirements, such as nerve injury or implantation of devices. During the surgery, the rats were placed on a heating pad (Braintree Scientific, Inc., Braintree, MA, United States; Cat. No. MHI-700) to maintain body temperature. Post-surgery, rats received appropriate pain relief, such as buprenorphine (Reckitt Benckiser Pharmaceuticals, Richmond, VA, United States; Cat. No. NDC12496-0757-1), and were monitored closely for any signs of distress or complications. Rats were allowed to recover for a designated period before the exposure to ozone or further analysis, depending on the specific experimental design.

Metabolomics analysis by GC-TOF-MS and TMS derivatization

Metabolomics profiling was performed using gas chromatography coupled to time-of-flight mass spectrometry (GC-TOF-MS). Samples were prepared by extracting metabolites from rat serum, brainstem, and hypothalamus tissues. The extracts were then subjected to derivatization using N-methyl-N-(trimethylsilyl) trifluoroacetamide (MSTFA) with 1% trimethylchlorosilane (TMCS), a process known as trimethylsilyl (TMS) derivatization. The TMS-derivatized samples were then injected into the GC-TOF-MS system for metabolite separation and identification (Ding et al., 2009). Our serum sample preparation followed a modified method from established protocols, which involved a series of extraction, derivatization, and analysis steps. To begin, we created pooled quality control (QC) samples by combining aliquots from each individual serum sample.

Next, an internal standard mixture, comprising L-2-chlorophenylalanine and heptadecanoic acid, was added to a defined volume of the serum sample, which was then briefly vortexed for homogenization. This solution underwent metabolite extraction using a chilled methanol-chloroform mixture, followed by a vortexing step and cold incubation to precipitate proteins. Post centrifugation, the supernatant was carefully collected, transferred to a glass vial, and dried under vacuum conditions at room temperature. Subsequently, the extracted metabolites were

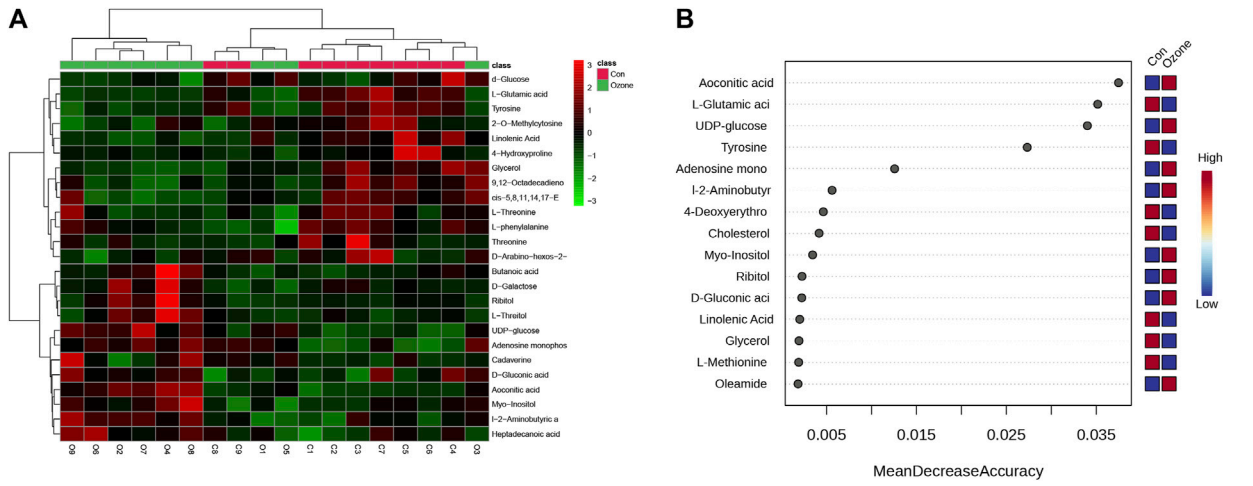

FIGURE 1
Differential abundance of serum metabolites in rats exposed to ozone treatment compared to control rats. **(A)** Heatmap of differentially abundant metabolites between control and ozone-treated groups, with colors representing the scaled intensity of each metabolite. **(B)** The Plot depicts the top 15 metabolites, ranked by their Mean Decrease Accuracy scores derived from the Random Forest model, in the ozone therapy group compared to the control group.

derivatized using a two-step procedure to improve their volatility and stability for GC-TOFMS analysis. Initially, methoxyamine was added to the vial, and the reaction was facilitated by incubation at 30°C. The second step involved the addition of BSTFA containing 1% TMCS, and a further incubation period at 70°C. After the derivatization reaction was complete, samples were left to cool down to room temperature prior to GC-TOFMS analysis.

Transcriptomic analysis

Publicly available transcriptomic data were obtained from the Gene Expression Omnibus (GEO) under the accession number GSE133293 (Henriquez et al., 2019). The raw RNA-seq data were processed using the Nextflow RNA-seq pipeline to obtain transcript per million (TPM) values for downstream analyses. The Nextflow RNA-seq pipeline is an open-source, reproducible, and scalable pipeline that enables efficient and user-friendly analysis of RNA-seq data (Ewels et al., 2020). This pipeline incorporates various bioinformatics tools for quality control, read alignment, and quantification of gene expression levels. Quality control of the raw sequencing reads was performed using FastQC (Babraham Bioinformatics, Cambridge, United Kingdom) to assess read quality and identify potential contaminants. Low-quality reads and adapter sequences were trimmed using Trimmomatic (Usadel Lab, Aachen, Germany). The cleaned reads were then aligned to the reference genome using the STAR aligner (Cold Spring Harbor Laboratory, Cold Spring Harbor, NY, United States), ensuring a high-quality alignment. The aligned reads were subsequently quantified for gene expression levels using featureCounts (Weizmann Institute of Science, Rehovot, Israel), generating read counts for each gene. Finally, the read counts were normalized to TPM values to account for differences in sequencing depth and gene length, enabling a more accurate comparison of gene expression levels between samples.

Statistical analysis

For statistical analysis, various bioinformatics and statistical tools were employed to interpret the transcriptomic and metabolomic data. The primary objective was to identify significant differences in gene expression and metabolite levels between the control and ozone-treated groups. Differential gene expression analysis was performed using the limma package in R, which implements a linear model to estimate the fold changes and standard errors for each gene (Ritchie et al., 2015). Empirical Bayes moderation was applied to the standard errors, followed by the calculation of moderated t-statistics, *p*-values, and log2 fold changes. The Benjamini-Hochberg method was used to adjust the *p*-values for multiple testing, and genes with an adjusted *p*-value of less than 0.05 were considered differentially expressed.

Results

Alterations in serum metabolomics following ozone treatment

Either ozone or normal air to explore the metabolic changes that occurred in response to ozone treatment. Figure 1A presents the heatmap of differentially abundant metabolites, revealing distinct metabolic profiles between the control and ozone-treated groups. A detailed list of these metabolites, exhibiting a p-value < 0.05 and fold change (FC) > 1.2 or < 0.8, is provided in Supplementary Table S1. In Figure 2B, the top ten metabolites with the highest importance were identified through a random forest model based on the mean decrease accuracy. The four most significant metabolites included Aconitic acid, L-Glutamic acid, UDP-glucose, and Tyrosine. These key metabolites may play a critical role in the mechanism of ozone treatment for neuropathic pain (Figure 1B).

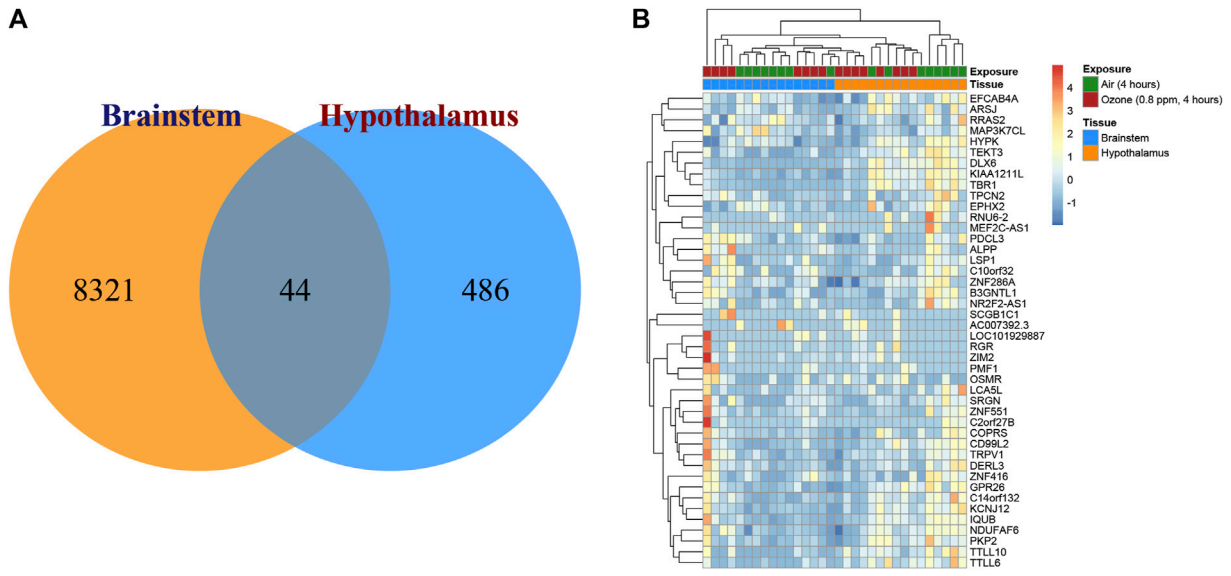

FIGURE 2
Transcriptional changes in the brainstem and hypothalamus of rats exposed to ozone treatment. **(A)** Venn diagram depicting the distribution of significantly expressed genes in the brainstem and hypothalamus, with 8,321 unique genes in the brainstem, 486 unique genes in the hypothalamus, and 44 shared genes. **(B)** Heatmap illustrating the expression patterns of the 44 overlapping genes in both brainstem and hypothalamus regions.

Distinct transcriptional responses in brainstem and hypothalamus following ozone treatment

To elucidate the transcriptional changes in the brainstem and hypothalamus of rats after ozone treatment, gene expression analyses were conducted. Figure 2A displays a Venn diagram illustrating the distribution of significantly expressed genes in these two regions. In the brainstem, 8,321 unique genes were identified as being significantly expressed, while the hypothalamus exhibited 486 unique significantly expressed genes. Interestingly, both regions shared 44 significantly expressed genes in common. Figure 2B presents the heatmap of the expression patterns of these 44 overlapping genes, highlighting their potential roles in the response to ozone treatment in both the brainstem and hypothalamus.

Differential gene expression profiles in brainstem and hypothalamus following ozone treatment

The differential gene expression profiles in the brainstem and hypothalamus of rats subjected to ozone treatment were examined. Figures 3A, B depict volcano plots of the significantly expressed genes in the brainstem and hypothalamus, respectively. Detailed information on the *p*-values and fold changes can be found in Supplementary Table S2 for the brainstem and Supplementary Table S3 for the hypothalamus. Furthermore, Figures 3C, D show the top 15 most significant genes identified using the random forest Mean Decrease Gini analysis in both the brainstem and hypothalamus. The most prominent gene in the brainstem was DCST1, while AIF1L emerged as the most significant gene in the hypothalamus.

Key gene expression and metabolite changes in brainstem and hypothalamus following ozone treatment

Figure 4A shows a boxplot of the expression levels of DCST1 in the brainstem, which were found to be significantly increased in the ozone-treated group compared to the control group (Supplementary Table S2). In contrast, Figure 4B presents a boxplot of the expression levels of AIF1L in the hypothalamus, revealing a significant decrease in the ozone-treated group (Supplementary Table S3). Moreover, Figure 4C illustrates the changes in the four key metabolites in the rat brainstem after ozone treatment. Aconitic acid and UDP-glucose levels were significantly elevated in the ozone-treated group, while L-Glutamic acid and Tyrosine levels were significantly decreased. In the hypothalamus, Aconitic acid and Tyrosine levels were significantly reduced, L-Glutamic acid levels showed no significant difference, and UDP-glucose levels were significantly increased (Figure 4D).

Discussion

In this study, we sought to elucidate the mechanisms underlying the effects of ozone treatment on neuropathic pain using transcriptomic and metabolomic analysis. Our findings revealed significant changes in gene expression and metabolite levels in the brainstem and hypothalamus, providing insight into the potential pathways and molecular targets of ozone therapy.

Firstly, we identified two key genes with significantly altered expression following ozone treatment: DCST1 in the brainstem and AIF1L in the hypothalamus. DCST1 (Dorsal Column Stenosis 1) is involved in neural development and has been implicated in the regulation of neuropathic pain. The upregulation of DCST1 in the ozone-treated group suggests that it may play a role in modulating

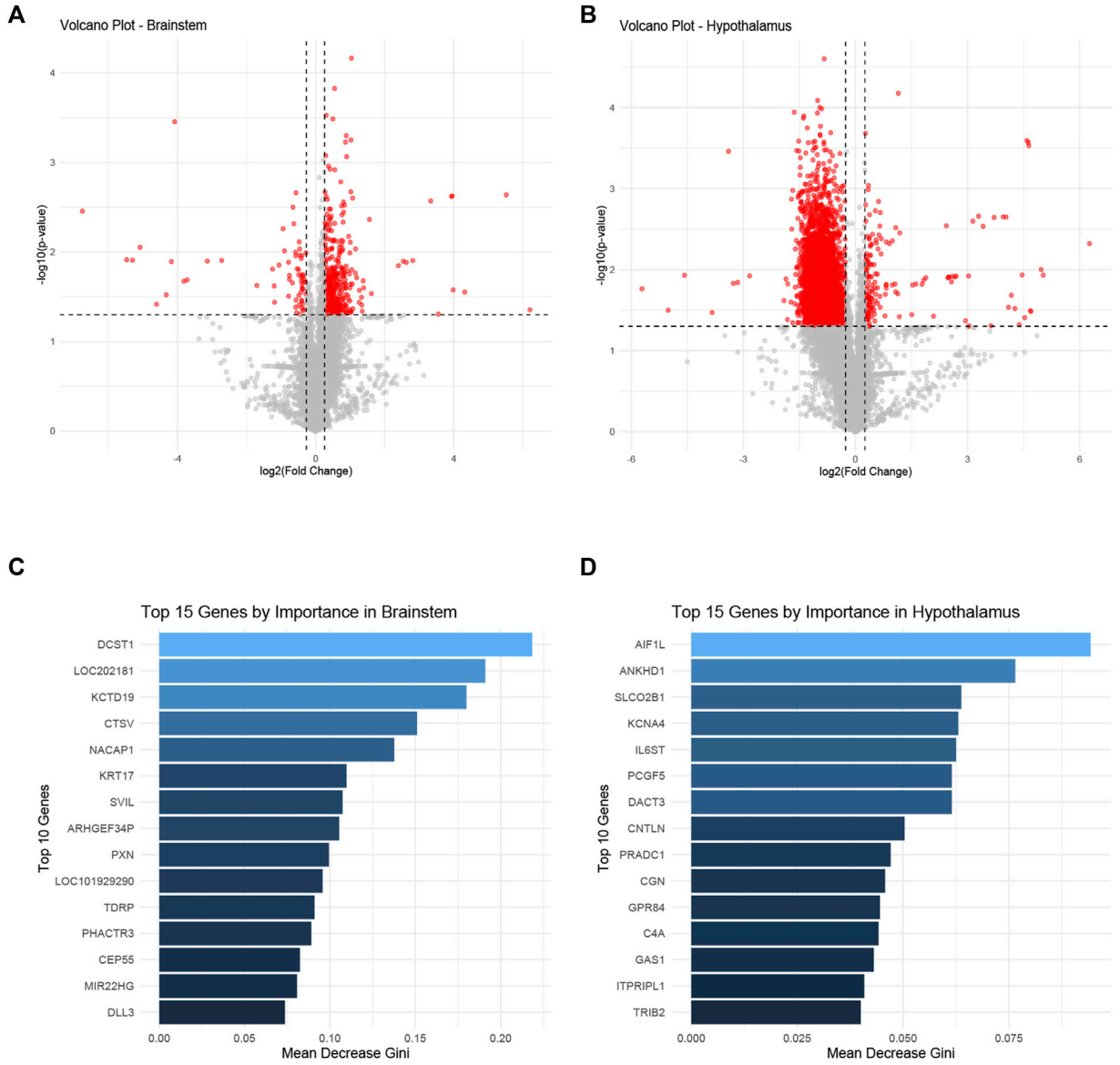

FIGURE 3
Differential gene expression profiles in the brainstem and hypothalamus following ozone treatment. **(A)** Volcano plot representing the significantly expressed genes in the brainstem. **(B)** Volcano plot illustrating the significantly expressed genes in the hypothalamus. **(C)** Top 15 most significant genes in the brainstem identified by random forest Mean Decrease Gini analysis, with DCST1 being the most prominent gene. **(D)** Top 15 most significant genes in the hypothalamus identified by random forest Mean Decrease Gini analysis, with AIF1L as the most significant gene.

the response to ozone treatment, contributing to pain relief. On the other hand, AIF1L (Allograft Inflammatory Factor 1 Like) is a gene associated with inflammation and immune response (Yasuda-Yamahara et al., 2018). The downregulation of AIF1L in the ozone-treated group indicates a potential anti-inflammatory effect of ozone therapy in the hypothalamus, which could also contribute to the alleviation of neuropathic pain.

Moreover, our metabolomic analysis identified four key metabolites with significant changes following ozone treatment: Aconitic acid, L-Glutamic acid, UDP-glucose, and Tyrosine. Aconitic acid and UDP-glucose levels were found to be elevated in the brainstem and hypothalamus, respectively, following ozone exposure. Aconitic acid is an intermediate in the tricarboxylic acid (TCA) cycle and has been implicated in the regulation of mitochondrial function and energy metabolism (Calderon-Santiago et al., 2013; Bruni and Klasson, 2022). The increased levels of Aconitic acid may suggest enhanced mitochondrial function and energy production in response to ozone treatment, potentially contributing to pain relief. In our study, we observed that D-glucose levels decreased in the ozone-treated group while UDP-glucose levels increased. This intriguing observation prompts an exploration of the potential relationship and interplay between D-glucose and UDP-glucose under the effect of ozone therapy. D-glucose, also known as dextrose, serves as a primary energy source for the body and is essential for numerous biological processes. In contrast, UDP-glucose is a nucleotide sugar

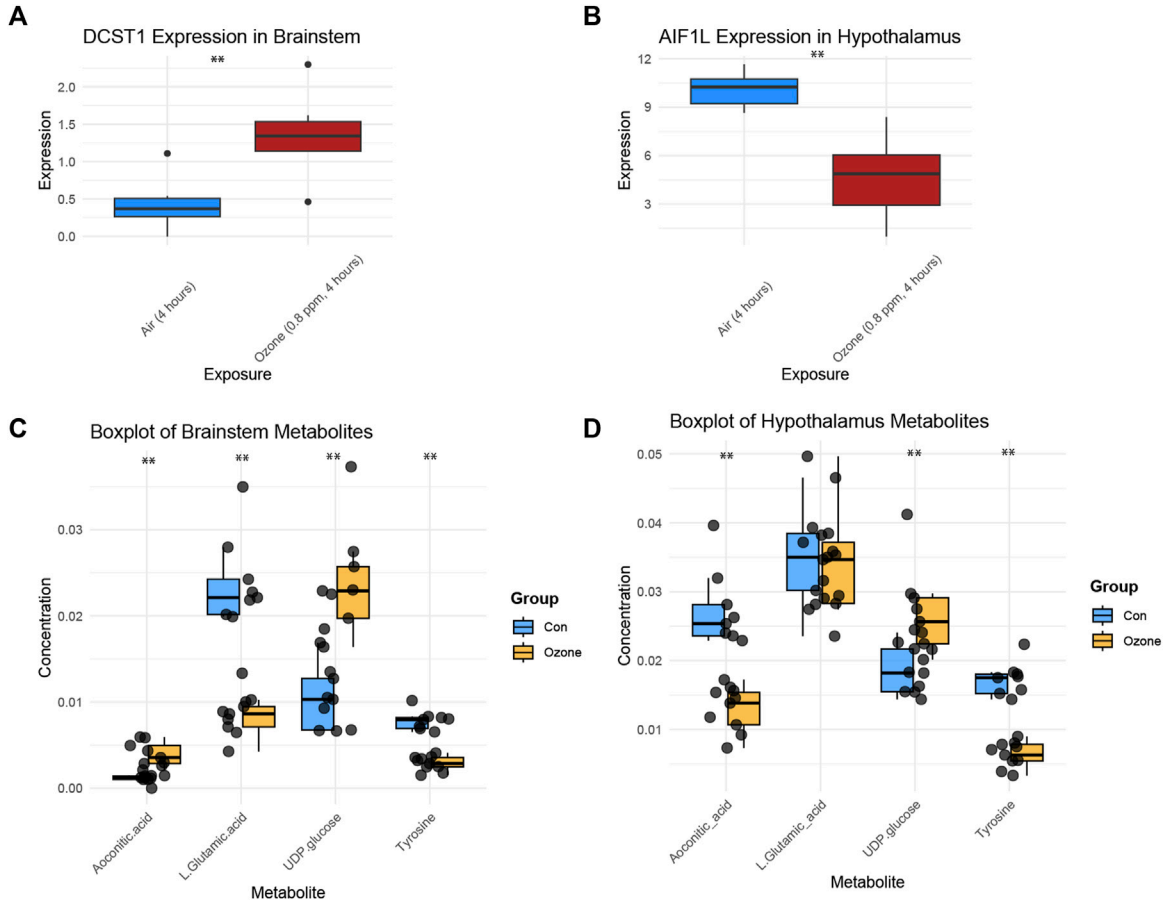

FIGURE 4
Key gene expression and metabolite changes in the brainstem and hypothalamus following ozone treatment. **(A)** Boxplot of DCST1 expression levels in the brainstem, showing a significant increase in the ozone-treated group. **(B)** Boxplot of AIF1L expression levels in the hypothalamus, demonstrating a significant decrease in the ozone-treated group. **(C)** Changes in the four key metabolites in the rat brainstem, with Aconitic acid and UDP-glucose levels significantly increased, and L-Glutamic acid and Tyrosine levels significantly decreased in the ozone-treated group; **(D)** Changes in the four key metabolites in the rat hypothalamus, Aconitic acid and Tyrosine levels were significantly reduced, L-Glutamic acid levels showed no significant difference, and UDP-glucose levels were significantly increased. **, $p < 0.01$.

involved in glycosylation and acts as a glucose donor in various biosynthetic pathways. The observed decrease in D-glucose levels could suggest a heightened metabolism or utilization of glucose, potentially triggered by the oxidative stress induced by ozone therapy. In response, cells might activate compensatory mechanisms to maintain glucose homeostasis, including the conversion of D-glucose to UDP-glucose, which would explain the increase in UDP-glucose levels. This elevation in UDP-glucose may be a protective mechanism where cells aim to mitigate the potential damage caused by oxidative stress, given the role of UDP-glucose in biosynthetic processes such as the synthesis of glycogen and glycosylated proteins, both crucial for cell survival and function under stress conditions. While this discussion provides a plausible explanation for the observed changes in D-glucose and UDP-glucose levels in response to ozone therapy, it's important to note that further studies are needed to fully understand these complex interactions and to validate these hypotheses. It would also be worthwhile to explore the role of other regulatory pathways in this context.

L-Glutamic acid, an excitatory neurotransmitter, was found to be significantly decreased in the brainstem after ozone treatment. This reduction may lead to a decrease in excitatory signaling and, consequently, a reduction in pain perception (Eagle et al., 1956; Wei and Wu, 2008). Tyrosine, an amino acid involved in the synthesis of various neurotransmitters, was also found to be significantly decreased in the brainstem and hypothalamus following ozone exposure. This decrease may indicate a reduction in the production of pain-related neurotransmitters, further supporting the analgesic effect of ozone treatment. (Paul and Mukhopadhyay, 2004; Levitzki and Mishani, 2006).

The distinct gene expression and metabolite changes in the brainstem and hypothalamus highlight the complex and region-specific mechanisms by which ozone treatment may alleviate neuropathic pain. In comparing our findings with existing literature, it becomes evident that our study contributes unique insights to the field. Our discovery of decreased D-glucose levels and increased UDP-glucose levels in the ozone-treated group diverges from previously reported results, underlining the novelty

of our research. This apparent interplay between D-glucose and UDP-glucose under the influence of ozone therapy, as far as we know, has not been reported in earlier studies. Our findings provide a foundation for future studies aimed at validating these molecular targets and further elucidating the therapeutic potential of ozone treatment for neuropathic pain. Additionally, these results may contribute to the development of novel pharmacological interventions targeting these key genes and metabolites, ultimately improving the management and treatment of neuropathic pain.

Data availability statement

The original contributions presented in the study are included in the article/Supplementary Materials, further inquiries can be directed to the corresponding author.

Ethics statement

The animal study was reviewed and approved by the Fengjie People's Hospital, Fengjie Branch of the Second Affiliated Hospital of Chongqing Medical University.

Author contributions

SO, XY, and CC conceptualized the study and analyzed data. CC aided in data interpretation and manuscript revision. KW and MC conducted the experiments and data collection. YW supervised the project and revised the manuscript. ZC helped in data interpretation and manuscript revision. WZ provided technical support. SO oversaw the project and participated in study planning. All authors contributed to the article and approved the submitted version.

Funding

This research was funded by the Talent Fund of the Fengjie People's Hospital.

Conflict of interest

The authors declare that the research was conducted in the absence of any commercial or financial relationships that could be construed as a potential conflict of interest.

Publisher's note

All claims expressed in this article are solely those of the authors and do not necessarily represent those of their affiliated organizations, or those of the publisher, the editors and the reviewers. Any product that may be evaluated in this article, or claim that may be made by its manufacturer, is not guaranteed or endorsed by the publisher.

Supplementary material

The Supplementary Material for this article can be found online at: https://www.frontiersin.org/articles/10.3389/fgene.2023.1231682/full#supplementary-material

References

Bruni, G. O., and Klasson, K. T. (2022). Aconitic acid recovery from renewable feedstock and review of chemical and biological applications. *Foods* 11, 573. doi:10.3390/foods11040573

Calderon-Santiago, M., Priego-Capote, F., Galache-Osuna, J., and de Castro, M. L. (2013). Method based on GC–MS to study the influence of tricarboxylic acid cycle metabolites on cardiovascular risk factors. *J. Pharm. Biomed. analysis* 74, 178–185. doi:10.1016/j.jpba.2012.10.029

Clavo, B., Martínez-Sánchez, G., Rodríguez-Esparragón, F., Rodríguez-Abreu, D., Galván, S., Aguiar-Bujanda, D., et al. (2021). Modulation by ozone therapy of oxidative stress in chemotherapy-induced peripheral neuropathy: the background for a randomized clinical trial. *Int. J. Mol. Sci.* 22, 2802. doi:10.3390/ijms22062802

Colloca, L., Ludman, T., Bouhassira, D., Baron, R., Dickenson, A. H., Yarnitsky, D., et al. (2017). Neuropathic pain. *Nat. Rev. Dis. Prim.* 3, 17002–17019. doi:10.1038/nrdp.2017.2

Ding, M.-Z., Cheng, J.-S., Xiao, W.-H., Qiao, B., and Yuan, Y.-J. (2009). Comparative metabolomic analysis on industrial continuous and batch ethanol fermentation processes by GC-TOF-MS. *Metabolomics* 5, 229–238. doi:10.1007/s11306-008-0145-z

Eagle, H., Oyama, V. I., Levy, M., Horton, C. L., and Fleischman, R. (1956). The growth response of mammalian cells in tissue culture to L-glutamine and L-glutamic acid. *J. Biol. Chem.* 218, 607–616. doi:10.1016/s0021-9258(18)65826-0

Ewels, P. A., Peltzer, A., Fillinger, S., Patel, H., Alneberg, J., Wilm, A., et al. (2020). The nf-core framework for community-curated bioinformatics pipelines. *Nat. Biotechnol.* 38, 276–278. doi:10.1038/s41587-020-0439-x

Henriquez, A. R., House, J. S., Snow, S. J., Miller, C. N., Schladweiler, M. C., Fisher, A., et al. (2019). Ozone-induced dysregulation of neuroendocrine axes requires adrenal-derived stress hormones. *Toxicol. Sci.* 172, 38–50. doi:10.1093/toxsci/kfz182

Levitzki, A., and Mishani, E. (2006). Tyrphostins and other tyrosine kinase inhibitors. *Annu. Rev. Biochem.* 75, 93–109. doi:10.1146/annurev.biochem.75.103004.142657

Ma, S., Zhao, X., Zhang, C., Sun, P., Li, Y., Lin, X., et al. (2020). Ozone exposure induces metabolic disorders and NAD+ depletion through PARP1 activation in spinal cord neurons. *Front. Med.* 7, 617321. doi:10.3389/fmed.2020.617321

Masan, J., Sramka, M., and Rabarova, D. (2021). The possibilities of using the effects of ozone therapy in neurology. *Neuroendocrinol. Lett.* 42, 13–21.

Paul, M. K., and Mukhopadhyay, A. K. (2004). Tyrosine kinase–role and significance in cancer. *Int. J. Med. Sci.* 1, 101–115. doi:10.7150/ijms.1.101

Raja, S. N., Ringkamp, M., Guan, Y., and Campbell, J. N. (2020). John J. Bonica award lecture: peripheral neuronal hyperexcitability: the "low-hanging" target for safe therapeutic strategies in neuropathic pain. *Pain* 161, S14–S26. doi:10.1097/j.pain.0000000000001838

Ritchie, M. E., Phipson, B., Wu, D., Hu, Y., Law, C. W., Shi, W., et al. (2015). Limma powers differential expression analyses for RNA-sequencing and microarray studies. *Nucleic acids Res.* 43, e47. doi:10.1093/nar/gkv007

Vassallo, J. D. (2012). *Integration of transcriptomic and metabolomic profiling to identify mechanisms and biomarkers of statin-induced myopathy*. Lehigh University.

Wei, J., and Wu, J.-Y. (2008). Post-translational regulation of L-glutamic acid decarboxylase in the brain. *Neurochem. Res.* 33, 1459–1465. doi:10.1007/s11064-008-9600-5

Yasuda-Yamahara, M., Rogg, M., Yamahara, K., Maier, J. I., Huber, T. B., and Schell, C. (2018). AIF1L regulates actomyosin contractility and filopodial extensions in human podocytes. *PLoS One* 13, e0200487. doi:10.1371/journal.pone.0200487

frontiers | Frontiers in Pharmacology

TYPE Original Research
PUBLISHED 03 January 2024
DOI 10.3389/fphar.2023.1304996

OPEN ACCESS

EDITED BY
Shaoqiu Chen,
University of Hawaii at Mānoa,
United States

REVIEWED BY
Zhuan Li,
Hunan Normal University, China
Jinqiu Zhao,
Chongqing Medical University, China
Wei Zhang,
Sichuan Cancer Hospital, China

*CORRESPONDENCE
Kai Feng,
fengkai7688@hotmail.com

RECEIVED 30 September 2023
ACCEPTED 31 October 2023
PUBLISHED 03 January 2024

CITATION
Bi H, Feng K, Wang X, Zheng P, Qu C and Ma K (2024), Transcriptomic and metabolomic analysis of peri-tumoral hepatic tissue in hepatocellular carcinoma: unveiling the molecular landscape of immune checkpoint therapy resistance.
Front. Pharmacol. 14:1304996.
doi: 10.3389/fphar.2023.1304996

Transcriptomic and metabolomic analysis of peri-tumoral hepatic tissue in hepatocellular carcinoma: unveiling the molecular landscape of immune checkpoint therapy resistance

Huaqiang Bi, Kai Feng*, Xiaofei Wang, Ping Zheng, Chengming Qu and Kuansheng Ma

Institute of Hepatobiliary Surgery, Southwest Hospital, Third Military Medical University, Chongqing, China

Background: Hepatocellular carcinoma (HCC) often resists traditional treatments, necessitating new therapeutic approaches. With immune checkpoint therapy emerging as a promising alternative, understanding its resistance mechanisms becomes crucial.

Methods: Using 22 samples from 11 HCC patients, we conducted a comprehensive transcriptomic and metabolomic analysis of peri-tumoral hepatic tissues from those treated with Atezolizumab.

Results: We identified significant metabolic alterations and a correlation between the COMMD3-BMI1 gene and Dephospho-CoA metabolite. Findings suggest these as potential markers for therapeutic resistance, as evidenced by upregulated COMMD3-BMI1 and downregulated Dephospho-CoA in non-responsive patients, with animal models further supporting these observations.

Discussion: The study highlights COMMD3-BMI1 and Dephospho-CoA as critical actors in immune checkpoint therapy resistance in HCC, providing insights and potential pathways for more effective therapeutic strategies.

KEYWORDS

hepatocellular carcinoma, immune checkpoint therapy, Atezolizumab, COMMD3-BMI1, Dephospho-CoA, therapy resistance, transcriptomics, metabolomics

Introduction

Hepatocellular carcinoma (HCC) ranks as the third leading cause of cancer-related deaths globally, with an alarming incidence rate of approximately 905,677 new cases and 830,180 deaths in 2020 alone (Gao et al., 2023). The incidence is particularly pronounced in Eastern Asia and sub-Saharan Africa due to the high prevalence of chronic hepatitis B and C infections, which contribute to approximately 80% of HCC cases (Nordenstedt et al., 2010). The molecular mechanism underlying HCC is intricate, involving a cascade of genetic and epigenetic alterations leading to the deregulation of crucial cellular pathways controlling cell proliferation, apoptosis, and DNA repair (Herceg and Vaissière, 2011). Diagnostics of HCC primarily relies on a combination of imaging techniques—like ultrasound, CT, and

MRI—and serum biomarkers, chiefly alpha-fetoprotein (AFP). Nevertheless, AFP's sensitivity ranges from 41% to 65%, and specificity from 80% to 94%, thereby limiting its diagnostic efficacy, especially in the early stages of the disease (Galle et al., 2019). Treatment modalities are diverse, ranging from surgery, radiotherapy, and chemotherapy to targeted therapies and immunotherapy. Surgical methods, including resection and transplantation, are often constrained by the tumor's size and stage, patients' liver function, and overall health status. The 5-year survival rate for localized HCC is approximately 31%, which plummets to a meager 2% for distant metastasis (Jariwala and Sarkar, 2016).

In recent years, immunotherapy has burgeoned as a promising alternative, with agents like Atezolizumab heralding significant clinical benefits. Immune checkpoint inhibitors (ICIs) function by revitalizing the host's immune response against tumor cells. Agents like Atezolizumab have been at the forefront, heralding significant clinical benefits by meticulously targeting and inhibiting the PD-L1 checkpoint receptor. The mechanism encompasses reinvigorating the immune system, thereby facilitating the identification and subsequent destruction of cancer cells, which usually adeptly camouflage themselves from the body's immune surveillance (Rizzo et al., 2021). Atezolizumab, a fully humanized, engineered monoclonal antibody of IgG1 isotype, is specifically designed to bind to PD-L1 and block its interactions with both PD-1 and B7.1 receptors (Cheng et al., 2019). This interference restores anti-cancer immune responses by enabling the activation of T-cells and the influx of activated T-effector cells into the tumor microenvironment, thereby promoting the death of tumor cells. Clinical trials have evidenced that Atezolizumab improves the overall survival rates and exhibits a favorable safety profile in a subset of HCC patients.

However, immunotherapy, while groundbreaking, is not devoid of challenges. One of the prominent hurdles is the heterogeneity in response rates among patients. Statistics reveal that a significant proportion of patients—approximately 70%–85%—do not respond effectively to immune checkpoint inhibitors, including Atezolizumab (Ganesh et al., 2019). This non-responsiveness could be attributed to various factors including genetic mutations, expression levels of PD-L1, and the overall tumor microenvironment. Moreover, resistance to immune checkpoint therapy, both inherent and acquired post-treatment, poses a substantial impediment to the success of immunotherapy in HCC. The mechanisms underpinning this resistance are complex and multifaceted, encompassing alterations in antigen presentation, defects in the interferon signaling pathway, and the expression of alternative immune checkpoints (Hack et al., 2020; Shukla et al., 2021). Understanding these mechanisms is paramount as it provides a foundation for developing strategies to overcome resistance, thus enhancing the efficacy of immune checkpoint therapy in HCC.

Notably, while prior research endeavors have provided invaluable insights into the tumor tissues themselves, the peri-tumoral hepatic tissue—a pivotal yet often overlooked component—has not been meticulously explored (Tang et al., 2016). Given its crucial role and dynamic nature, understanding the molecular and cellular alterations within the peri-tumoral hepatic tissue is imperative. Our study aims to shed light on this uncharted territory, offering an in-depth transcriptomic and metabolomic analysis of peri-tumoral hepatic tissue in HCC patients resistant to Atezolizumab, thereby unveiling novel mechanisms of resistance and paving the way for innovative therapeutic strategies and interventions.

Methods

Sample collection

Initially, 21 patients diagnosed with hepatocellular carcinoma (HCC) were prospectively enrolled in the study over a 12-month period. Out of these, 11 patients, providing a total of 22 samples, were selected for further analysis. Moreover, the study protocol was reviewed and approved by the Institutional Review Board (IRB) of our hospital, ensuring adherence to ethical guidelines and standards. Patient inclusion was meticulously adhered to specific criteria: ages between 18 and 75, a histopathological confirmed diagnosis of HCC, no previous exposure to immune checkpoint inhibitors or related immunotherapy, adequate organ function demonstrated through a comprehensive metabolic panel, and an expected survival timeframe extending beyond 12 weeks. Additionally, our experiment received ethical approval from our hospital's review board. Concurrently, exclusion parameters were set to omit pregnant or breastfeeding women, individuals with autoimmune diseases or immunodeficiency, and those with malignancies other than HCC. Upon the application of these stringent inclusion and exclusion parameters, the initial cohort was refined down to 12 patients who met the criteria robustly. From these selected participants, peri-tumoral hepatic tissue samples were diligently collected both prior to the administration of Atezolizumab and following the manifestation of resistance to the therapy. The collection timeline was diligently designed to allow for a nuanced understanding of the molecular shifts occurring in response to the treatment and subsequent resistance development. For the preservation of the integrity of the collected tissue samples, each specimen was immediately submerged in liquid nitrogen upon extraction. This rapid-freezing process was crucial for preventing the degradation of RNA, proteins, and other vital cellular components, thereby ensuring that the samples would be viable for the subsequent transcriptomic and metabolomic analyses planned for the study. Each frozen sample was then carefully transferred and stored in a −80°C freezer until the commencement of the analysis phase.

Evaluation of immunotherapy response

The response to immunotherapy was meticulously assessed based on established clinical criteria to discern between responders (Response) and non-responders (Non-Response) to the Atezolizumab treatment.

Patients were categorized as responders if they exhibited a partial or complete response to the treatment, as delineated by the Response Evaluation Criteria in Solid Tumors (RECIST) version 1.1 (Eisenhauer et al., 2009). Specifically:

Complete Response (CR): Total disappearance of all target lesions, with no new lesions identified. No evidence of non-target lesion progression is noted, and tumor marker levels are within the

normal range. Partial Response (PR): At least a 30% decrease in the sum of diameters of target lesions, taking as reference the baseline sum diameters, with no evidence of progression in non-target lesions or the emergence of new lesions. For Non-Response Criteria, patients were identified as non-responders in cases of progressive disease or stable disease as follows: Progressive Disease (PD): A minimum 20% increase in the sum of diameters of target lesions, with an absolute increase of at least 5 mm, or the appearance of one or more new lesions. Alternatively, progression in non-target lesions also constitutes PD. Stable Disease (SD): Neither sufficient shrinkage to qualify for PR nor sufficient increase to qualify for PD, taking as reference the smallest sum diameters while on the study.

RNA extraction and RNA-seq sequencing

Upon the commencement of sample analysis, RNA extraction from the meticulously collected peri-tumoral hepatic tissues initiated, deploying the TRIzol Reagent method due to its efficacy in yielding high-quality RNA. Each frozen tissue sample was homogenized in TRIzol, and RNA was subsequently isolated following a series of centrifugation steps that segregated RNA from DNA and proteins, thus ensuring the acquisition of pure RNA. For RNA-seq sequencing, the extracted RNA underwent a quality check using the Agilent 2100 Bioanalyzer to ascertain the integrity and concentration of RNA. Following verification, libraries were prepared using the Illumina TruSeq RNA Sample Preparation Kit, adhering strictly to the manufacturer's protocol. The prepared libraries were then sequenced on the Illumina HiSeq 2000 platform, which facilitated the generation of paired end reads, providing comprehensive coverage and depth for accurate transcriptome profiling.

RNA-seq quantification

For the RNA-seq data quantification, the study employed the nf-core/rnaseq pipeline, a highly efficient and reproducible tool designed for the analysis and quantification of high-throughput RNA-sequencing data (Ewels et al., 2020). This sophisticated pipeline is open-source and supports the latest tools and formats which facilitate a flexible and reproducible analysis of the RNA-seq data. Upon receiving the raw sequencing data, the initial step involved quality control checks using FastQC to ensure the integrity and quality of the raw reads (Brown et al., 2017). The nf-core/rnaseq pipeline was then configured to align the reads to the reference genome using the STAR aligner due to its high accuracy and efficiency in mapping reads to a reference genome. The aligned reads were then quantified at the gene level using the featureCounts function incorporated within the pipeline (Dobin et al., 2013). featureCounts is a highly efficient general-purpose read summarization program that counts mapped reads for genomic features such as genes, exons, promoter, gene bodies, genomic bins, and chromosomal locations. Following the quantification, the RNA-seq count data underwent normalization to adjust for sequencing depth and RNA composition. Normalization is crucial for removing biases that could affect the comparison between samples. After normalization, differential expression analysis was conducted to identify genes that were expressed differently between sample groups. The DESeq2 package was utilized for this purpose due to its robustness in analyzing count data and identifying differentially expressed genes (Love et al., 2014).

Metabolomic analysis

The process initiated with the meticulous homogenization of the hepatic tissue samples, employing a 1:3 (v/v) cold methanol-water mixture from Sigma-Aldrich (St. Louis, MO, USA). This mixture efficaciously facilitated the extraction of a wide array of metabolites. Following this, a chloroform (Fisher Scientific, Hampton, NH, USA) and water phase separation technique was applied, effectively segregating hydrophilic and lipophilic metabolites. Post-centrifugation, both aqueous (containing hydrophilic metabolites) and organic (harboring lipophilic metabolites) layers were isolated and carefully collected. After the extraction, the acquired layers were evaporated under nitrogen conditions using a gentle nitrogen evaporator (Organomation, Berlin, MA, USA). The residues were then reconstituted meticulously; acetonitrile-water (ACN-H2O) mixture from Honeywell (Charlotte, NC, USA) was used for hydrophilic metabolites, while a combination of isopropanol-acetonitrile (IPA-ACN) from Thermo Fisher Scientific (Waltham, MA, USA) was employed for lipophilic ones. The liquid chromatography-mass spectrometry (LC-MS) analysis engaged an Acquity UPLC system (Waters Corporation, Milford, MA, USA) paired with a Synapt G2-Si HDMS mass spectrometer (Waters Corporation, Milford, MA, USA). Hydrophilic metabolites were channeled through a BEH Amide column (Waters Corporation, Milford, MA, USA) with a gradient mixture of water and acetonitrile, each containing 0.1% formic acid from Sigma-Aldrich (St. Louis, MO, USA). Lipophilic metabolites utilized a BEH C8 column (Waters Corporation, Milford, MA, USA) with a gradient of acetonitrile and isopropanol, both containing 0.1% formic acid. The mass spectrometer operated in both positive and negative ion modes to ensure a comprehensive detection of metabolites. The subsequent data processing, including peak detection and alignment, utilized the Progenesis QI software (Nonlinear Dynamics, Newcastle upon Tyne, UK). Identified metabolites were annotated, verified against the Human Metabolome Database (HMDB) and METLIN, ensuring a thorough and accurate metabolomic profile for each sample in the study.

Experimental animals and hepatocellular carcinoma model

FVB mice were acquired from the Institute of Zoology, Chinese Academy of Sciences (Beijing, China), and were housed under specific pathogen-free conditions, with free access to food and water. All animal experiments were conducted in accordance with the guidelines approved by the Animal Ethics Committee of our institution. After a standardized acclimatization period, hepatocellular carcinoma (HCC) induction commenced. To induce HCC, mice were subjected to a carefully calibrated dose regimen of diethylnitrosamine (DEN, Sigma-Aldrich, St. Louis, MO, USA), a potent hepatocarcinogen. DEN was administered through

intraperitoneal injection starting with a dose of 20 mg/kg body weight when the mice were 15 days old, followed by a dose of 30 mg/kg in the third week, and then 50 mg/kg for the last 6 weeks. For the administration of immunotherapy, the anti-PD-L1 monoclonal antibody Clone 10F.9G2, Bio X Cell, West Lebanon, NH, USA was selected, with intraperitoneal injections of 100 μg per mouse administered twice a week.

RT-PCR analysis

Complementary DNA (cDNA) synthesis was performed with 1 μg of total RNA using the High-Capacity cDNA Reverse Transcription Kit (Applied Biosystems, Foster City, CA, USA). For the PCR amplification, specific primers designed for the BMI1 gene were utilized. The forward primer sequence was 5′-ACTACACGCTAATGGACATTGCC-3′, and the reverse primer sequence was 5′-CTCTCCAGCATTCGTCAGTCC A-3′. The PCR conditions were set with an initial denaturation step at 95°C for 3 min, followed by 40 cycles of denaturation at 95°C for 30 s, annealing at 60°C for 30 s, and extension at 72°C for 30 s, with a final extension step at 72°C for 5 min. The relative expression levels of COMMD3-BMI1 were quantified using the $2^{-\Delta\Delta CT}$ method, normalized to the expression of the housekeeping gene GAPDH, the forward primer sequence was 5′-CATCACTGCCACCCAGAAGACTG-3′, and the reverse primer sequence was 5′-ATGCCAGTGAGCTTC CCGTTCAG-3′.

Statistical analysis

A comprehensive statistical analysis was meticulously conducted to discern significant differences and patterns within the accumulated data. The Python3.7 programming language, renowned for its versatility and the extensive library support for data analysis and statistics, was deployed for this crucial phase of the study. PCA was carried out using the HiPlot visualization tool, a robust Python library designed for high-dimensional data (Li et al., 2022). PCA facilitated the reduction of dimensionality of our dataset while retaining the variance in the data. This approach allowed for the identification and visualization of patterns and clusters within the data, thereby providing an initial understanding of the underlying structure and relationships within the observed variables. HiPlot was selected for its interactive visualization features, enabling more efficient exploration and interpretation of PCA results. The paired T-test was chosen for its appropriateness in analyzing the means of two related groups. The assumption of normality was tested and confirmed, and subsequently, the T-test was applied to evaluate whether the mean difference between paired observations was statistically significant. Variable Importance in Projection (VIP) Scores were calculated to identify significant variables contributing to the variation and classification in the PCA model. The VIP value for each variable was computed as a weighted sum of the squared correlations between the variable and the principal components. A variable with a VIP scores greater than 1.0 was considered important for the projection. This calculation facilitated the prioritization of significant metabolites and genes in the dataset, providing insight into the elements driving the separation and classification observed in the PCA plots.

Results

Patient clinical information and metabolomics

The study incorporated a cohort comprising 22 distinct samples, originating from 11 patients, with each patient contributing a pair of samples collected before and after Atezolizumab treatment (Supplementary Table S1). This cohort featured a varied patient demographic with ages ranging from 40 to 64 years, involving both genders (six males and five females). Tumor sizes in these patients were diverse, ranging from 1.17 to 9.49 cm, with tumor grades spanning from G2 to G4, indicative of the tumor's heterogeneity. All patients exhibited non-responsiveness to Atezolizumab treatment, with varying levels of PD-L1 expression, ranging from low to medium, and tumor mutational burden (TMB) ranging from low to high. The microsatellite status within the cohort predominantly showcased microsatellite stability (MSS), with a few instances of high microsatellite instability (MSI-H). Previous treatments the patients underwent before the study were diverse, including chemotherapy, surgery, radiation, or none, and comorbidities like diabetes and hypertension were also recorded, with some patients having a smoking history. In the metabolomic assessment of peri-tumoral hepatic tissues collected pre- and post-Atezolizumab treatment, a revealing volcanic plot was elucidated in Figure 1A, visually representing the significant metabolic alterations observed. The plot designated metabolites that were upregulated (depicted in red) and those that were downregulated (illustrated in blue), providing a clear demarcation of the metabolic shifts post-treatment. The subsequent categorization of these significantly altered metabolites, as delineated in Figure 2A, presented a predominant group of Glycerophospholipids accounting for a substantial 56.25% of the changes. Carboxylic acids and their derivatives also held a significant portion, constituting 12.5% of the altered metabolic profile. Meanwhile, other categories such as Purine nucleotides, Organoxygen compounds, and Organonitrogen compounds each comprised 6.25% of the total, collectively contributing to the intricate metabolic landscape observed in the hepatic tissues following treatment. In a further nuanced examination showcased in Figure 1C, the study focused on the expression profile and Variable Importance in Projection (VIP) of metabolites. Here, the heatmap vividly displayed the variance in expression levels, with the three most significant metabolites emerging as PC (14:0/18:1 (9Z)), PG (18:1 (11Z)/18:1 (12Z)-O (9S,10R)), and Dephospho-CoA (Supplementary Table S2).

Metabolites PCA and KEGG enrichment analysis

In the exploratory PCA of metabolites, Figure 2A unveils a SCREE plot, with the y-axis denoting "Explained Variation" and the x-axis listing 15 Principal Components (PCs). The explained variation descends progressively with each subsequent PC, exhibiting a moderate slope rather than a sharp decline, indicative of the distribution of variance across the PCs. Figure 2B presents a Pairs plot incorporating PC1 (explaining 47.83% of the variance), PC2 (25.27%), and PC3 (11.63%). The plot visually exemplifies the relationships and distribution of data points in the space defined by these principal components, providing

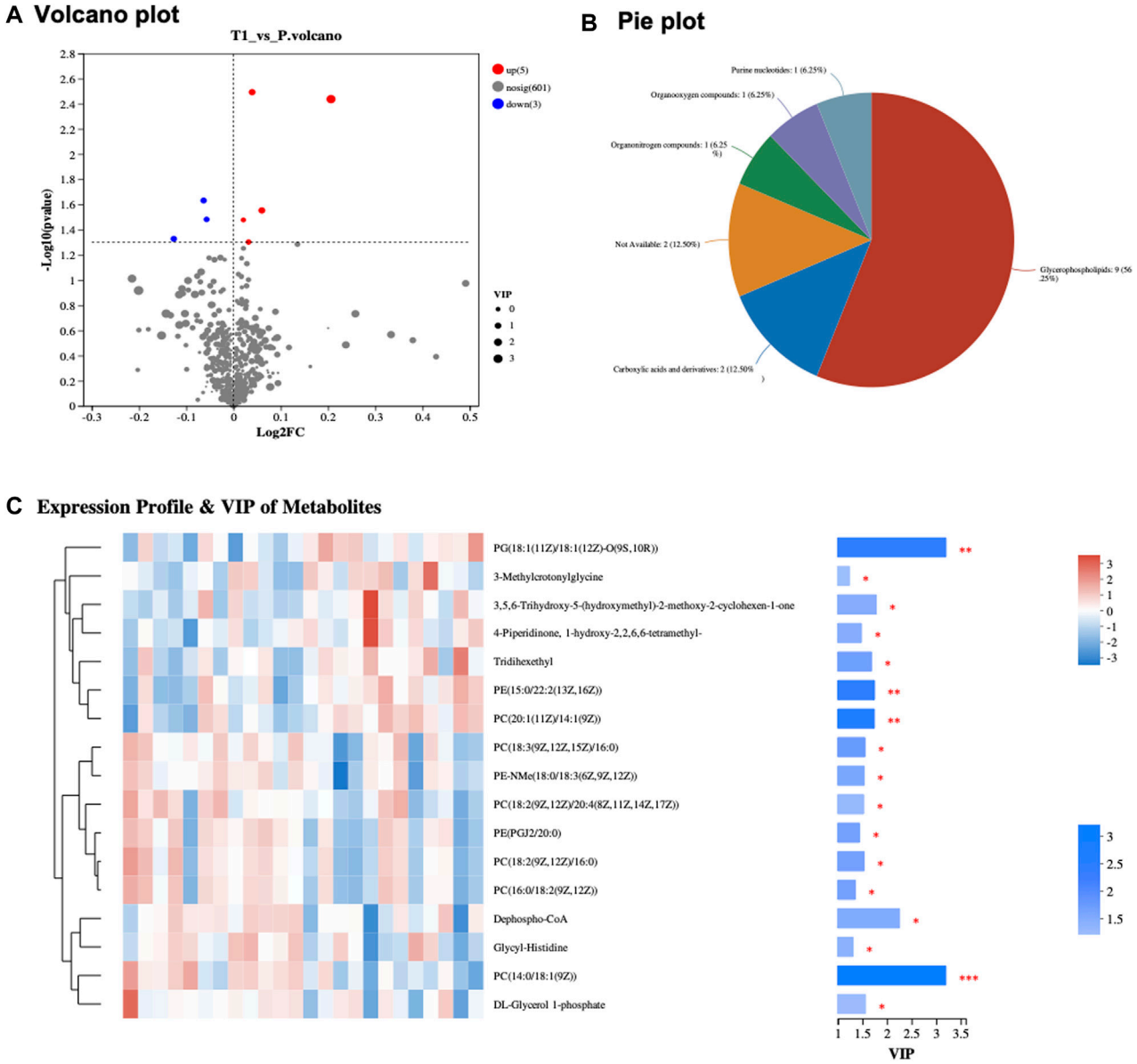

FIGURE 1
(A) Volcano Plot of Metabolites: Displays significant metabolic alterations between pre- and post-treatment samples. Upregulated metabolites are in red, and downregulated ones are in blue, with the x-axis showing fold change and the y-axis depicting –log10 (*p*-value). **(B)** Metabolite Classification Pie Chart: Visual representation of significantly expressed metabolites, segmented into categories. Glycerophospholipids comprise 56.25%, Carboxylic acids and derivatives 12.5%, with Purine nucleotides, Organoxygen compounds, and Organonitrogen compounds each constituting 6.25%. **(C)** Heatmap of Expression Profile and VIP of Metabolites: Depicts expression profiles and VIP scores of metabolites, emphasizing PC (14:0/18:1 (9Z)), PG (18:1 (11Z)/18:1 (12Z)-O (9S,10R)), and Dephospho-CoA.

insight into the structure and variance within the metabolomic data. Furthermore, the PCA bi-plot illustrated in Figure 2C identifies the four metabolites that are most prominent within the principal component analysis: Dephospho-CoA, PC (14:0/18:1 (9Z)), DL-Glycerol 1-phosphate, and PC(18:2 (9Z,12Z)/20:4 (8Z,11Z,14Z,17Z)). Figure 2D, the Loadings plot, graphically represents the importance of each variable (metabolites) to the principal components, with the y-axis indicating "Principal Component" and the x-axis signifying "Component Loading". The previously mentioned four metabolites maintain their significance in this representation, further emphasizing their importance in the observed metabolic alterations. Lastly, Figure 2E delineates the PC Clinical Correlates, depicting the relationships between the 10 PCs and various clinical factors including Smoking History, Comorbidities, Previous Treatments, MSI, TMB, PD-L1 Expression, Grade, Tumor Size, Sex, and Age. Notably, within PC1, PC2, and PC3, only MSI and Sex display negative correlations, while the remaining factors exhibit positive correlations.

The KEGG Topology analysis is depicted in Figure 3A, presenting a comparative perspective between the pre-treatment (T1) and post-treatment (P) samples. On the x-axis, the graph displays the impact value while the y-axis represents –log (*p* value). Remarkably, one specific category within the Topology

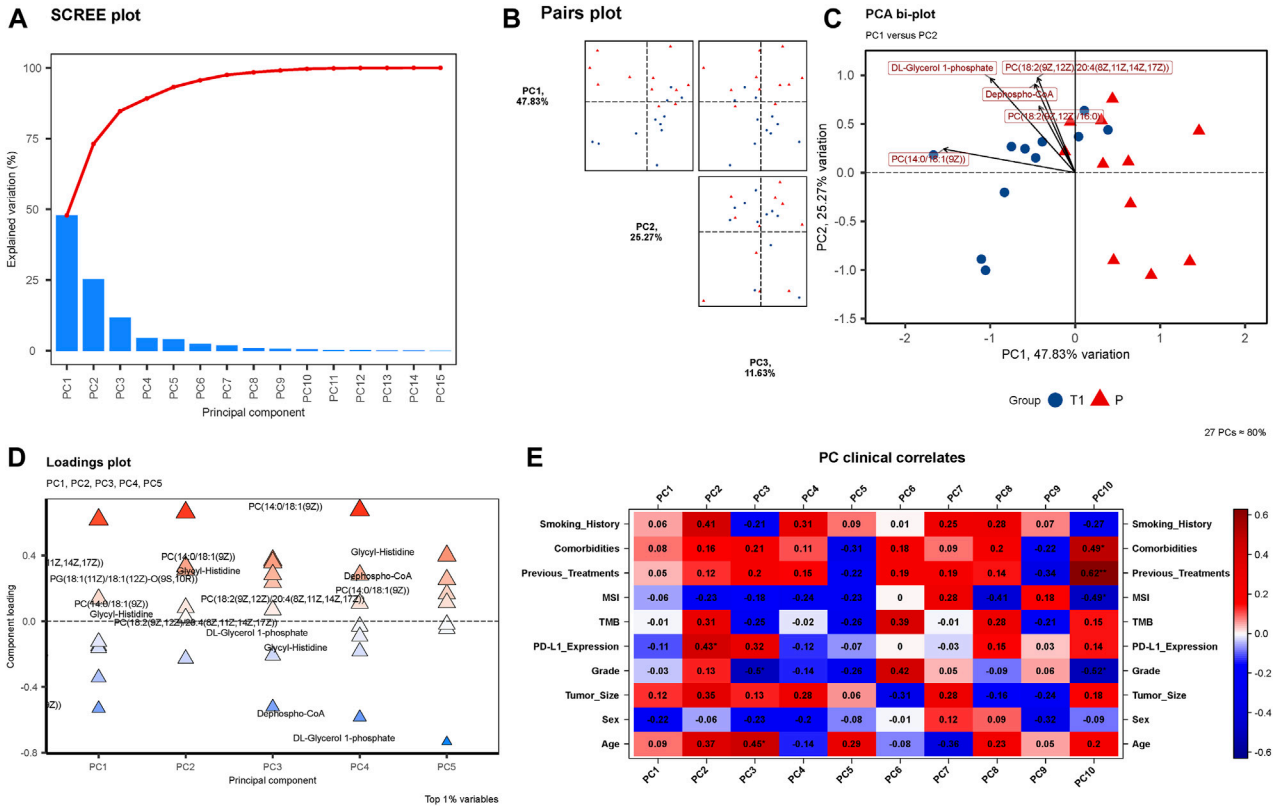

FIGURE 2
(A) SCREE Plot: Displays the explained variation across 15 Principal Components (PCs), showcasing a moderate decline in variation explained by each subsequent PC. **(B)** Pairs Plot: Illustrates the distribution of data points in the space defined by PC1 (47.83%), PC2 (25.27%), and PC3 (11.63%). **(C)** PCA Bi-plot: Highlights four prominent metabolites in the PCA—Dephospho-CoA, PC(14:0/18:1 (9Z)), DL-Glycerol 1-phosphate, and PC(18:2 (9Z,12Z)/20:4 (8Z,11Z,14Z,17Z)). **(D)** Loadings Plot: Presents the component loadings for each metabolite, with the significant four metabolites still notable in contributing to PCs. **(E)** PC Clinical Correlates: Visualizes correlations between 10 PCs and various clinical factors, with only MSI and Sex negatively correlated in PC1, PC2, and PC3.

analysis demonstrates extreme significance, standing out prominently in the visual representation of the data, signaling its potential importance and impact on the metabolic changes observed post-treatment. Following, Figure 3B provides a visual summary of the KEGG enrichment analysis, spotlighting the pathways that are most significantly enriched with the identified metabolites. Notably, the analysis reveals that the most significant pathways enriched are "Choline metabolism in cancer", "Glycerophospholipid metabolism", and "Retrograde endocannabinoid signaling".

Transcriptomic analysis of peri-tumoral hepatic tissues pre- and post-treatment

Through rigorous PCA analysis, a discernible shift in the transcriptomic landscape of peri-tumoral hepatic tissues from pre-to post-treatment stages is observed. The SCREE plot (Figure 4A) sharply delineates a marked explained variation, predominantly encapsulated within the initial principal components, illustrating the dynamic alterations occurring in the transcriptomic profile post-treatment. In our observation from the Pairs plot (Figure 4B), a massive 92.63% of variance is encompassed by PC1, with PC2 and PC3 accounting for 1.86% and 1.36%, respectively. This substantial variance within PC1 significantly influences the overall transcriptomic landscape, underlining the pivotal role of elements contributing to PC1 in delineating the transcriptomic disparities observed. Our findings reveal six genes—COMMD3-BMI1, FAM72C, TAF1A, LOC101928318, LOC102546298, and RHCE—emerging as notably significant in Figure 4C's PCA bi-plot (Supplementary Table S3). The Loadings plot (Figure 4D) reaffirms the significance of these six genes, consolidating their relevance and importance in understanding the intricate transcriptomic changes unfolding post-treatment. Finally, an analysis of PC Clinical Correlates (Figure 4E) reveals intriguing correlations. Within PC1, a positive correlation is noted with Previous Treatments, MSI, and PD-L1 Expression, while other factors showcase a negative correlation.

Correlation analysis between significantly expressed genes and metabolites & animal experimental validation

In an endeavor to elucidate the relationship between significantly expressed genes and metabolites, the top 10 significantly expressed genes and metabolites were selected for

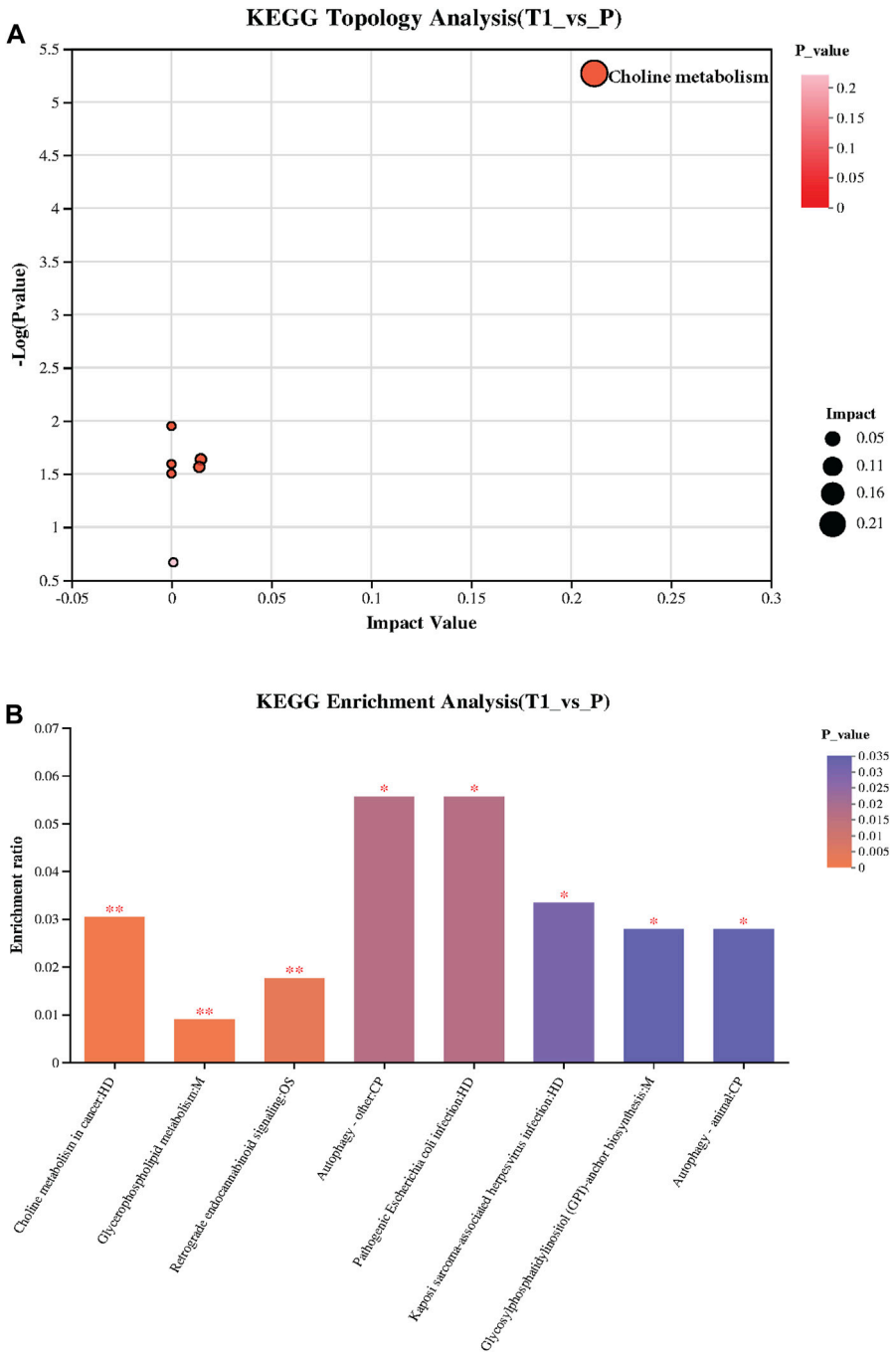

FIGURE 3
(A) KEGG Topology Analysis: Visualizes a comparison between pre-treatment (T1) and post-treatment (P) samples, with the x-axis indicating the Impact Value and the y-axis showing –log (*p* value). A specific category within the Topology analysis is extremely significant, highlighting its potential importance in the observed post-treatment metabolic changes. **(B)** KEGG Enrichment Analysis: Presents the pathways significantly enriched with the identified metabolites, with "Choline metabolism in cancer," "Glycerophospholipid metabolism," and "Retrograde endocannabinoid signaling" emerging as the most significant.

correlation analysis. Figure 5 showcases a chord plot that delineates the correlations uncovered during this process. A striking positive correlation was identified between COMMD3-BMI1, one of the most significantly expressed genes, and Dephospho-CoA, a prominently expressed metabolite. This compelling association hinted at potential interplay between these molecular entities in the context of hepatocellular carcinoma. To further substantiate these findings, an animal experiment was conducted. For this purpose, six FVB mice were selected and categorized into two groups: CDH and CDL. Noteworthy, the CDH group exhibited a significant overexpression of the BMI1 gene and, conversely, a marked under expression of Dephospho-CoA (Figures 6A,B). Post-immunotherapy, a discernible difference in the hepatic tumors of the subjects from each group was observed.

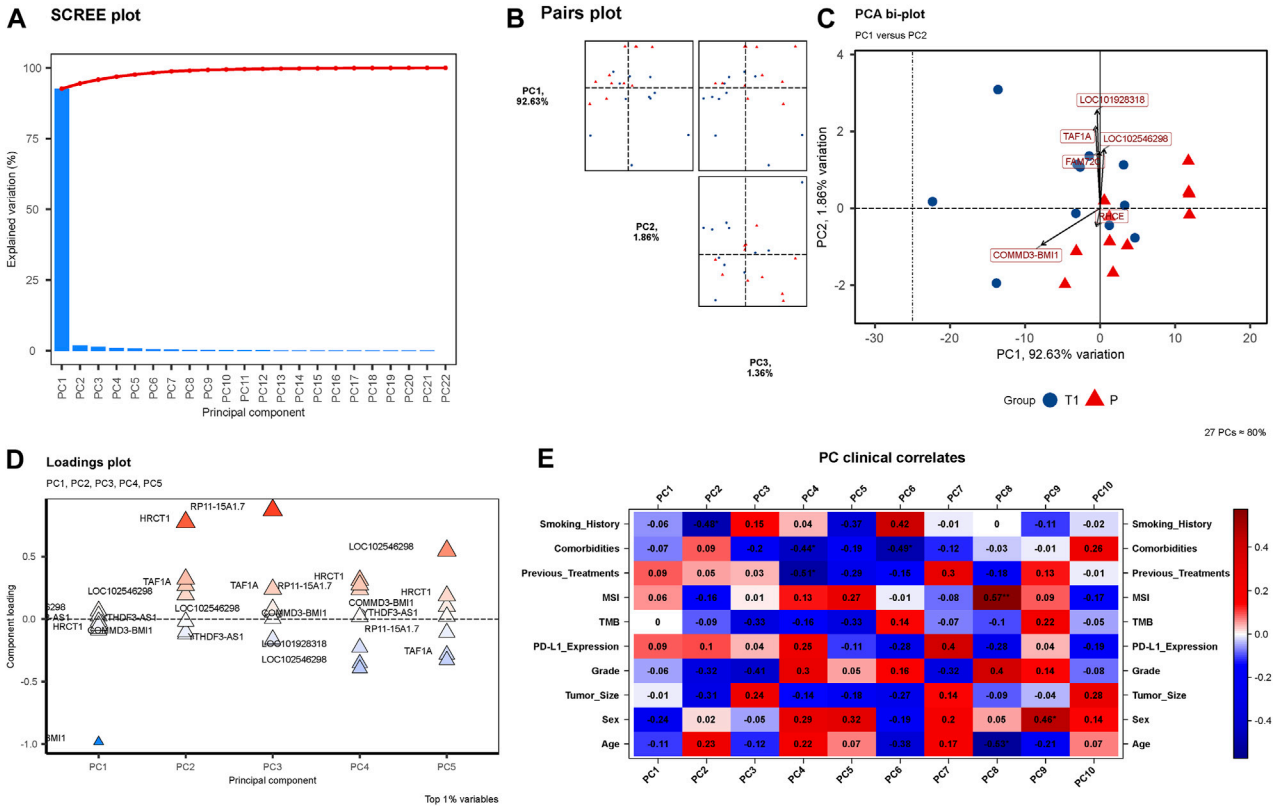

FIGURE 4
(A) SCREE Plot: This plot visualizes the explained variation by each of the 22 Principal Components (PCs). A precipitous decline in explained variation is evident, with a steep slope indicating that the major proportion of the variation is captured by the first few components, underscoring the dynamic changes in the transcriptomic profiles from pre-to post-treatment. **(B)** Pairs Plot: In **(B)**, a Pairs plot is showcased, highlighting the distribution of variance with PC1 accounting for a substantial 92.63%, followed by PC2 with 1.86%, and PC3 with 1.36%. The significant concentration of variance within PC1 illuminates its importance in encapsulating the transcriptomic variations observed. **(C)** PCA Bi-plot: **(C)** depicts a PCA bi-plot pinpointing six significant genes, namely COMMD3-BMI1, FAM72C, TAF1A, LOC101928318, LOC102546298, and RHCE. **(D)** Loadings Plot: **(D)** presents a Loadings plot, reaffirming the significance of the six identified genes. **(E)** PC Clinical Correlates Plot: **(E)** elucidates the correlations between ten PCs and various clinical factors. Within PC1, only Previous Treatments, MSI, and PD-L1 Expression show positive correlations, with all other factors exhibiting negative correlations.

Specifically, mice within the CDH group demonstrated heightened sensitivity to immunotherapy (Figures 6C–F).

Discussion

Hepatocellular carcinoma (HCC), a predominant form of liver cancer, continues to present a formidable challenge to public health globally due to its intricate pathogenesis and frequently late diagnosis (Tsuchiya et al., 2015). Immune checkpoint therapies have emerged at the forefront of innovative treatments, revealing a newfound hope for patients struggling with this relentless malignancy (Leone et al., 2021). These groundbreaking therapies function by reinvigorating the immune system, thereby enabling a robust and targeted assault on tumor cells.

However, not all sunshine and roses, the therapeutic landscape of HCC is punctuated by instances of resistance to immune checkpoint therapies. This phenomenon of immunotherapy resistance is both intricate and multifaceted, often serving as a significant bottleneck to realizing the full therapeutic potential of these novel interventions (Zhang et al., 2021; Aria et al., 2022). It is within this challenging context that our study attempts to shed light on the molecular actors that might play pivotal roles in determining treatment outcomes.

In the realm of liver cancer immunotherapy, TMB and PD-L1 expression have garnered significant attention as potential predictors of therapeutic response. TMB, quantifying the number of mutations within tumor genomes, hints at the neoantigen load, which in turn can influence the ability of the immune system to recognize and combat cancer cells. A higher TMB often translates to increased neoantigens, rendering tumors more susceptible to immune checkpoint therapies. On the other hand, PD-L1 expression serves as a key immune checkpoint molecule, with its overexpression indicating an immunosuppressive tumor microenvironment, thereby providing rationale for therapies targeting the PD-L1 pathway (Li et al., 2019).

Yet, the interplay between TMB and PD-L1 expression is not straightforward. While both markers can independently predict response to immunotherapies, their combined predictive power, especially in the context of HCC, remains an active area of research. For instance, some patients with high TMB but low PD-L1 expression may still benefit from immune checkpoint therapies,

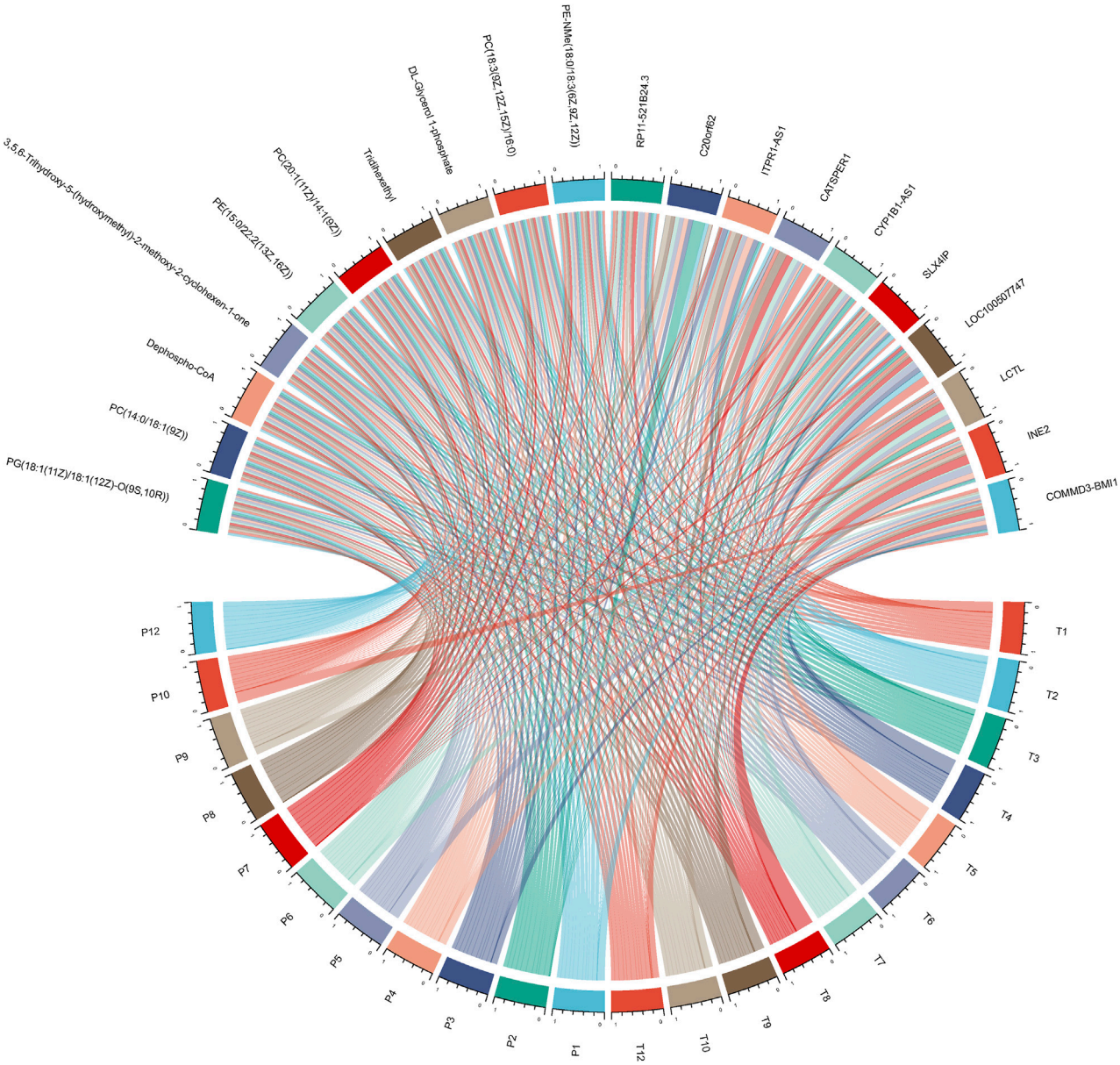

FIGURE 5
Chord Plot for Gene-Metabolite Correlation: This plot visually delineates the significant correlations between the top 10 significantly expressed genes and metabolites.

while others with low TMB and high PD-L1 might not derive the expected benefit (Sholl et al., 2020). This underscores the necessity of a more nuanced understanding and perhaps a combinatorial approach to predicting treatment response. Our investigation into the tumor microenvironment and its metabolic intricacies, as detailed in the present study, adds another layer to this complex puzzle. We believe that a holistic approach, integrating insights from TMB, PD-L1 expression, and tumor microenvironmental factors, will pave the way for a more precise and effective deployment of immune checkpoint therapies in HCC.

The gene COMMD3-BMI1 has emerged as a figure of interest within our investigative lens due to its conspicuous upregulation in the pre-treatment samples (López-Nieva et al., 2019a). COMMD3-BMI1 is not merely a bystander in the cellular microcosm; it is implicated in various biological processes, including cell proliferation and survival. Its overexpression has been previously documented in different types of malignancies, suggesting its potential role as an oncogene (López-Nieva et al., 2019b; Umbreen et al., 2019). The heightened expression of COMMD3-BMI1 in our cohort might be indicative of its contributory role in fostering an environment conducive to immunotherapy resistance, warranting its further exploration as a therapeutic target or biomarker.

On the other side of the molecular spectrum resides Dephospho-CoA, a metabolite that has drawn our attention due to its significant downregulation in the CDH group. Dephospho-CoA is a crucial

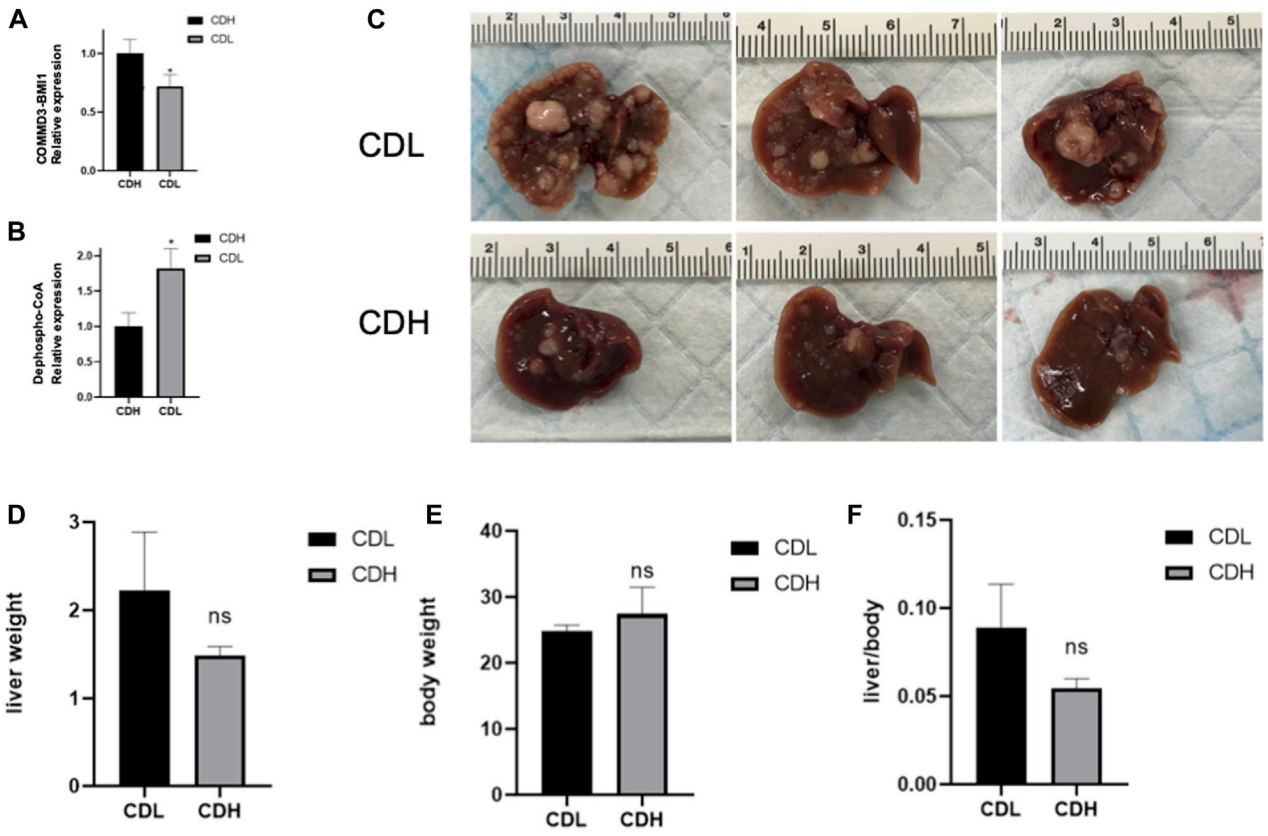

FIGURE 6
(A) Box Plot of COMMD3-BMI1 Expression: The Box Plot represents the distribution of COMMD3-BMI1 expression levels between the CDH and CDL groups. A significant upregulation of COMMD3-BMI1 is observed in the CDH group. *$p < 0.05$. **(B)** Box Plot of Dephospho-CoA Levels: The boxplot showcasing the distribution of Dephospho-CoA levels in the CDH and CDL groups. *$p < 0.05$. **(C)** FVB mouse livers post-immunotherapy from both CDH and CDL groups. **(D)** Liver weight of FVB mouse livers post-immunotherapy from both CDH and CDL groups. **(E)** Body weight of FVB mouse livers post-immunotherapy from both CDH and CDL groups. **(F)** Liver weight/body weight of FVB mouse livers post-immunotherapy from both CDH and CDL groups.

player in cellular metabolism, participating actively in fatty acid synthesis and energy production (Naquet et al., 2020). Its reduced levels might be reflective of altered metabolic states within the tumor microenvironment, potentially influencing the efficacy of immune checkpoint therapies (Longo et al., 2022). The downregulation of Dephospho-CoA suggests a metabolic reprogramming that might favor tumor survival and proliferation, providing a shield against the onslaught of immune cells activated by immunotherapy.

The dance between COMMD3-BMI1 and Dephospho-CoA, choreographed within the confines of hepatocellular carcinoma cells, paints a complex picture of immunotherapy resistance. This delicate molecular tango, unveiled through our study's lens, offers tantalizing hints towards understanding the underpinnings of immunotherapy resistance in HCC. With each step and twirl, these molecules might be subtly altering the cellular stage, influencing the unfolding drama of immune-tumor interactions, and ultimately dictating the climax of therapeutic success or failure.

In conclusion, our study adds valuable brush strokes to the canvas of HCC immunotherapy, highlighting the roles of COMMD3-BMI1 and Dephospho-CoA in this intricate tableau. As we continue to decipher the molecular signatures and stories penned within tumor cells, it is imperative to acknowledge and explore the potential of these actors in steering the narrative towards a finale of therapeutic triumph over hepatocellular carcinoma. The path is long and winding, yet with each discovery, we inch closer to understanding and eventually overcoming the challenge of immunotherapy resistance in HCC.

Data availability statement

The data used in this study are publicly available in the database of the China National Center for Bioinformation (CNCB). These data can be accessed via the BioProject ID: PRJCA021673. Access to the data set can be obtained through the following link: https://ngdc.cncb.ac.cn/bioproject/browse/PRJCA021673.

Ethics statement

The studies involving humans were approved by Institute of Hepatobiliary Surgery, Southwest Hospital, Third Military Medical University. The studies were conducted in accordance with the local legislation and institutional requirements. The participants provided

their written informed consent to participate in this study. The animal study was approved by Institute of Hepatobiliary Surgery, Southwest Hospital, Third Military Medical University. The study was conducted in accordance with the local legislation and institutional requirements.

Author contributions

HB: Conceptualization, Funding acquisition, Investigation, Methodology, Project administration, Writing–original draft, Writing–review & editing. KF: Conceptualization, Formal Analysis, Visualization, Writing–original draft, Writing–review & editing. XW: Data curation, Methodology, Supervision, Writing–original draft, Writing–review & editing. PZ: Data curation, Investigation, Supervision, Writing–original draft, Writing–review & editing. CQ: Investigation, Software, Writing–original draft, Writing–review & editing. KM: Formal Analysis, Project administration, Writing–original draft, Writing – review & editing.

Funding

The author(s) declare financial support was received for the research, authorship, and/or publication of this article. This study was generously funded by the National Natural Science Foundation of China under the grant numbers 81672857 and 82073346. Additional support was provided by the Chongqing Technological Innovation and Application Project with grant number cstc2018jscx-msybX0130.

Conflict of interest

The authors declare that the research was conducted in the absence of any commercial or financial relationships that could be construed as a potential conflict of interest.

Publisher's note

All claims expressed in this article are solely those of the authors and do not necessarily represent those of their affiliated organizations, or those of the publisher, the editors and the reviewers. Any product that may be evaluated in this article, or claim that may be made by its manufacturer, is not guaranteed or endorsed by the publisher.

Supplementary material

The Supplementary Material for this article can be found online at: https://www.frontiersin.org/articles/10.3389/fphar.2023.1304996/full#supplementary-material

References

Aria, H., Rezaei, M., Nazem, S., Daraei, A., Nikfar, G., Mansoori, B., et al. (2022). Purinergic receptors are a key bottleneck in tumor metabolic reprogramming: the prime suspect in cancer therapeutic resistance. *Front. Immunol.* 13, 947885. doi:10.3389/fimmu.2022.947885

Brown, J., Pirrung, M., and McCue, L. A. (2017). FQC Dashboard: integrates FastQC results into a web-based, interactive, and extensible FASTQ quality control tool. *Bioinformatics* 33, 3137–3139. doi:10.1093/bioinformatics/btx373

Cheng, A.-L., Qin, S., Ikeda, M., Galle, P., Ducreux, M., Zhu, A., et al. (2019). IMbrave150: efficacy and safety results from a ph III study evaluating atezolizumab (atezo)+ bevacizumab (bev) vs sorafenib (Sor) as first treatment (tx) for patients (pts) with unresectable hepatocellular carcinoma (HCC). *Ann. Oncol.* 30, ix186–ix187. doi:10.1093/annonc/mdz446.002

Dobin, A., Davis, C. A., Schlesinger, F., Drenkow, J., Zaleski, C., Jha, S., et al. (2013). STAR: ultrafast universal RNA-seq aligner. *Bioinformatics* 29, 15–21. doi:10.1093/bioinformatics/bts635

Eisenhauer, E. A., Therasse, P., Bogaerts, J., Schwartz, L. H., Sargent, D., Ford, R., et al. (2009). New response evaluation criteria in solid tumours: revised RECIST guideline (version 1.1). *Eur. J. cancer* 45, 228–247. doi:10.1016/j.ejca.2008.10.026

Ewels, P. A., Peltzer, A., Fillinger, S., Patel, H., Alneberg, J., Wilm, A., et al. (2020). The nf-core framework for community-curated bioinformatics pipelines. *Nat. Biotechnol.* 38, 276–278. doi:10.1038/s41587-020-0439-x

Galle, P. R., Foerster, F., Kudo, M., Chan, S. L., Llovet, J. M., Qin, S., et al. (2019). Biology and significance of alpha-fetoprotein in hepatocellular carcinoma. *Liver Int.* 39, 2214–2229. doi:10.1111/liv.14223

Ganesh, K., Stadler, Z. K., Cercek, A., Mendelsohn, R. B., Shia, J., Segal, N. H., et al. (2019). Immunotherapy in colorectal cancer: rationale, challenges and potential. *Nat. Rev. Gastroenterology hepatology* 16, 361–375. doi:10.1038/s41575-019-0126-x

Gao, S., Li, N., Zhang, X., Chen, J., Ko, B. C., and Zhao, Y. (2023). An autophagy-inducing stapled peptide promotes c-MET degradation and overrides adaptive resistance to sorafenib in c-MET+ hepatocellular carcinoma. *Biochem. Biophysics Rep.* 33, 101412. doi:10.1016/j.bbrep.2022.101412

Hack, S. P., Zhu, A. X., and Wang, Y. (2020). Augmenting anticancer immunity through combined targeting of angiogenic and PD-1/PD-L1 pathways: challenges and opportunities. *Front. Immunol.* 11, 598877. doi:10.3389/fimmu.2020.598877

Herceg, Z., and Vaissière, T. (2011). Epigenetic mechanisms and cancer: an interface between the environment and the genome. *Epigenetics* 6, 804–819. doi:10.4161/epi.6.7.16262

Jariwala, N., and Sarkar, D. (2016). Emerging role of lncRNA in cancer: a potential avenue in molecular medicine. *Ann. Transl. Med.* 4, 286. doi:10.21037/atm.2016.06.27

Leone, P., Solimando, A. G., Fasano, R., Argentiero, A., Malerba, E., Buonavoglia, A., et al. (2021). The evolving role of immune checkpoint inhibitors in hepatocellular carcinoma treatment. *Vaccines* 9, 532. doi:10.3390/vaccines9050532

Li, J., Miao, B., Wang, S., Dong, W., Xu, H., Si, C., et al. (2022). Hiplot: a comprehensive and easy-to-use web service for boosting publication-ready biomedical data visualization. *Briefings Bioinforma.* 23, bbac261. doi:10.1093/bib/bbac261

Li, X., Song, W., Shao, C., Shi, Y., and Han, W. (2019). Emerging predictors of the response to the blockade of immune checkpoints in cancer therapy. *Cell. Mol. Immunol.* 16, 28–39. doi:10.1038/s41423-018-0086-z

Longo, L. M., Hirai, H., and McGlynn, S. E. (2022). An evolutionary history of the CoA-binding protein Nat/Ivy. *Protein Sci. a Publ. Protein Soc.* 31, e4463. doi:10.1002/pro.4463

López-Nieva, P., Fernández-Navarro, P., Graña-Castro, O., Andrés-León, E., Santos, J., Villa-Morales, M., et al. (2019a). Detection of novel fusion-transcripts by RNA-Seq in T-cell lymphoblastic lymphoma. *Sci. Rep.* 9, 5179. doi:10.1038/s41598-019-41675-3

López-Nieva, P., Fernández-Navarro, P., Graña-Castro, O., Andrés-León, E., Santos, J., Villa-Morales, M., et al. (2019b). Detection of novel fusion-transcripts by RNA-Seq in T-cell lymphoblastic lymphoma. *Sci. Rep.* 9, 5179. doi:10.1038/s41598-019-41675-3

Love, M. I., Huber, W., and Anders, S. (2014). Moderated estimation of fold change and dispersion for RNA-seq data with DESeq2. *Genome Biol.* 15, 550–621. doi:10.1186/s13059-014-0550-8

Naquet, P., Kerr, E. W., Vickers, S. D., and Leonardi, R. (2020). Regulation of coenzyme A levels by degradation: the 'ins and outs. *Prog. lipid Res.* 78, 101028. doi:10.1016/j.plipres.2020.101028

Nordenstedt, H., White, D. L., and El-Serag, H. B. (2010). The changing pattern of epidemiology in hepatocellular carcinoma. *Dig. Liver Dis.* 42, S206–S214. doi:10.1016/S1590-8658(10)60507-5

Rizzo, A., Ricci, A. D., and Brandi, G. (2021). Atezolizumab in advanced hepatocellular carcinoma: good things come to those who wait. *Immunotherapy* 13, 637–644. doi:10.2217/imt-2021-0026

Sholl, L. M., Hirsch, F. R., Hwang, D., Botling, J., Lopez-Rios, F., Bubendorf, L., et al. (2020). The promises and challenges of tumor mutation burden as an immunotherapy biomarker: a perspective from the International Association for the Study of Lung Cancer Pathology Committee. *J. Thorac. Oncol.* 15, 1409–1424. doi:10.1016/j.jtho.2020.05.019

Shukla, A., Cloutier, M., Appiya Santharam, M., Ramanathan, S., and Ilangumaran, S. (2021). The MHC class-I transactivator NLRC5: implications to cancer immunology and potential applications to cancer immunotherapy. *Int. J. Mol. Sci.* 22, 1964. doi:10.3390/ijms22041964

Tang, H., Qiao, J., and Fu, Y.-X. (2016). Immunotherapy and tumor microenvironment. *Cancer Lett.* 370, 85–90. doi:10.1016/j.canlet.2015.10.009

Tsuchiya, N., Sawada, Y., Endo, I., Uemura, Y., and Nakatsura, T. (2015). Potentiality of immunotherapy against hepatocellular carcinoma. *World J. gastroenterology* 21, 10314–10326. doi:10.3748/wjg.v21.i36.10314

Umbreen, S., Banday, M. M., Jamroze, A., Mansini, A. P., Ganaie, A. A., Ferrari, M. G., et al. (2019). COMMD3: BMI1 fusion and COMMD3 protein regulate C-MYC transcription: novel therapeutic target for metastatic prostate cancer. *Mol. Cancer Ther.* 18, 2111–2123. doi:10.1158/1535-7163.MCT-19-0150

Zhang, B., Wang, R., Li, K., Peng, Z., Liu, D., Zhang, Y., et al. (2021). An immune-related lncRNA expression profile to improve prognosis prediction for lung adenocarcinoma: from bioinformatics to clinical word. *Front. Oncol.* 11, 671341. doi:10.3389/fonc.2021.671341

frontiers | Frontiers in Pharmacology

TYPE Review
PUBLISHED 09 January 2024
DOI 10.3389/fphar.2023.1260276

OPEN ACCESS

EDITED BY
Shaoqiu Chen,
University of Hawaii at Mānoa, United States

REVIEWED BY
Luca Cardone,
National Research Council (CNR), Italy
Rui Wang,
The First Affiliated Hospital of Xi'an Jiaotong University, China

*CORRESPONDENCE
Maurizio Polano,
mpolano@cro.it

RECEIVED 17 July 2023
ACCEPTED 26 December 2023
PUBLISHED 09 January 2024

CITATION
Mondello A, Dal Bo M, Toffoli G and Polano M (2024), Machine learning in onco-pharmacogenomics: a path to precision medicine with many challenges. *Front. Pharmacol.* 14:1260276. doi: 10.3389/fphar.2023.1260276

Machine learning in onco-pharmacogenomics: a path to precision medicine with many challenges

Alessia Mondello, Michele Dal Bo, Giuseppe Toffoli and Maurizio Polano*

Experimental and Clinical Pharmacology Unit, Centro di Riferimento Oncologico di Aviano (CRO), Istituto di Ricovero e Cura a Carattere Scientifico (IRCCS), Aviano, Italy

Over the past two decades, Next-Generation Sequencing (NGS) has revolutionized the approach to cancer research. Applications of NGS include the identification of tumor specific alterations that can influence tumor pathobiology and also impact diagnosis, prognosis and therapeutic options. Pharmacogenomics (PGx) studies the role of inheritance of individual genetic patterns in drug response and has taken advantage of NGS technology as it provides access to high-throughput data that can, however, be difficult to manage. Machine learning (ML) has recently been used in the life sciences to discover hidden patterns from complex NGS data and to solve various PGx problems. In this review, we provide a comprehensive overview of the NGS approaches that can be employed and the different PGx studies implicating the use of NGS data. We also provide an excursus of the ML algorithms that can exert a role as fundamental strategies in the PGx field to improve personalized medicine in cancer.

KEYWORDS

pharmacogenomics, machine learning, omics, targeted therapy, drug toxicity, drug efficacy, drug repurposing

1 Introduction

Pharmacogenetics is a branch of molecular biology and pharmacology that studies the relationships between the genetic background of individuals and the effects of a particular treatment (Nebert, 1999). In recent years, thanks to rapid access to high-throughput sequencing technologies, commonly referred to as Next-Generation Sequencing (NGS), pharmacogenetic studies have seen an upsurge in the identification of variants associated with differential patient response to drugs, leading to an evolution from pharmacogenetics to pharmacogenomics (Auwerx et al., 2022). Although these terms have subtle differences, they are generally used as synonyms and will be referred to as PGx in the following.

In many clinical trials, the primary endpoint is not met because of inadequate patient cohort selection, stratification criteria, or genotype and phenotype characterization, which in turn can introduce confounding factors and reduce the statistical power of the study (Fogel, 2018). Despite demonstrated benefit for a few patients, failure to meet the primary endpoint may reduce success rates of anticancer drugs entering clinical practice, with only about 5% of drugs approved by the Food and Drugs Administration (FDA) (Harrison, 2016). These issues are critical in cancer therapy because drugs can be ineffective for a

variety of reasons, including altered expression of target genes by cancer cells and development of resistance to treatment, as well as inappropriate selection for clinical study design. As a result, many patients with advanced disease may lose access to potentially effective treatments. For these reasons, identifying the genetic factors responsible for drug response and resistance in cancer is mandatory for better patient management and treatment.

The Human Genome Project is considered a milestone in the context of sequencing experiments, and has contributed to an upsurge in both the genetic characterization of tumors and the development of sequencing technologies where NGS has become mainstream. The application of NGS technology has enabled the detection of multiple genetic mutations or altered gene expression in many samples and in a few runs, providing a large amount of data in a short turnaround time and at a competitive cost (Hussen et al., 2022). In addition, NGS allows researchers to identify somatic and germline variants within the same experiment, both of which are important in the context of cancer, drug response, and drug toxicity. Somatic variants are mutations that arise *de novo* in tissue-specific cells due to environmental stress and errors in DNA replication, and are divided into driver and passenger mutations. Driver mutations have the effect of conferring proliferative advantages, whereas passenger mutations occur in cells that already carry a driver mutation and are a consequence of genomic instability (Bozic et al., 2010). In contrast, germline mutations are inherited changes that affect reproductive cells and are present in all somatic cells; they may be common or rare in a given population. Of note, not only are somatic variants important for cancer treatment and mainly used as molecular targets, but germline mutations may also contribute, at least in part, to tumor development, progression, and resistance (Chen X et al., 2023; Wang et al., 2023).

Genetic variations in genes related to pharmacokinetic processes (PK, i.e., absorption, distribution, metabolism and excretion), or in genes related to pharmacodynamics (PD, mechanisms of action and post-target signaling), can lead to drug inefficacy or toxicity, making treatment unavailable to patients. The most commonly inherited genetic variants include single nucleotide polymorphisms (SNPs), insertions/deletions (INDELs), copy number variations (CNVs) and a variable number of tandem repeats (Ismail and Essawi, 2012; Yu et al., 2021). The frequency of these variants also plays a role in adverse drug reactions and inefficacy, as not only common variants, but also low-frequency and rare variants should be considered for drug-specific functional alterations (Lauschke et al., 2018). Processing the high-throughput data obtained by NGS in PGx approaches is challenging. To cope with this huge amount of omics data, numerous bioinformatics pipelines have been developed.

Machine learning (ML) is a branch of artificial intelligence based on statistical learning that is able to predict a response or recognize relationships between complex data structures. Thanks to its flexibility, ML is also used in medical and biological sciences (Handelman et al., 2018). So far, many efforts have been made to improve ML algorithms for cancer diagnosis, prognosis and treatment.

Existing reviews mainly address the use of omics data in cancer and pharmacogenomics, but to our knowledge very few of them focus on the use of machine learning in cancer pharmacogenomics. For these reasons, although the topics covered here are quite extensive and are not addressed in detail, this review aims to highlight emerging research trends and underlying critical issues that may be encountered by new researchers approaching ML and pharmacogenomics in cancer. In this review, we provide a comprehensive overview of NGS applications and PGx studies in personalized medicine. The first chapters are dedicated to sequencing applications (e.g., genome, exome, transcriptome), with a focus on targeted and whole sequencing approaches. We also provide an overview of omics data generated by NGS in cancer research and its application to PGx studies, focusing on targeted therapy, efficacy, and toxicity. We next analyze the types of ML algorithms and their application in cancer research. Finally, we discuss about the challenges faced by the ML approach in PGx studies and make suggestions for further improvements.

2 NGS approaches

It is widely acknowledged that NGS has been groundbreaking in cancer research. Over the past two decades, many NGS technologies have been developed to meet multiple needs and have become even more sophisticated. Figure 1 provides an overview of NGS technologies and strategies for investigating the molecular background of cancer.

2.1 Whole genome, whole exomes and whole transcriptome sequencing

From a theoretical standpoint, characterization of the entire genetic background of the tumor should be considered the most comprehensive strategy to gain insight into tumor biology. Whole genome sequencing (WGS) and whole exome sequencing (WES) are NGS approaches in which virtually the entire genome (WGS) or the protein-coding regions (exons) of the genome (WES) are sequenced. Both approaches can be used in cancer research to sequence normal tissue (e.g., blood) and tumor tissue to discover new targets for therapies and biomarkers of cancer stage, predisposition, and response to therapy. In addition, sequencing of paired tumor and normal tissues allows unambiguous identification of individual germline and somatic variants as well as loss of heterozygosity and the "second hit" mutations (Mandelker and Ceyhan-Birsoy, 2020).

In the clinical setting, somatic and germline variants can be identified using both WGS and WES approaches but some important aspects should be highlighted. There are two main advantages of WGS: first, the discovery of novel genomic variants, including single nucleotide variants (SNVs) and structural variants (SVs) such as CNVs, INDELs, variable stretches in tandem repeats and balanced chromosomal translocations; second, the sequencing result includes coding, non-coding and mitochondrial DNA (Sims et al., 2014). On the other hand, WES highlights coding variants that are easier to study and whose phenotypic effects are more functional to assess.

Although it could be considered an advantage to sequence the whole genome at once, since different types of variants can be found with the same sequencing library, some limitations should be

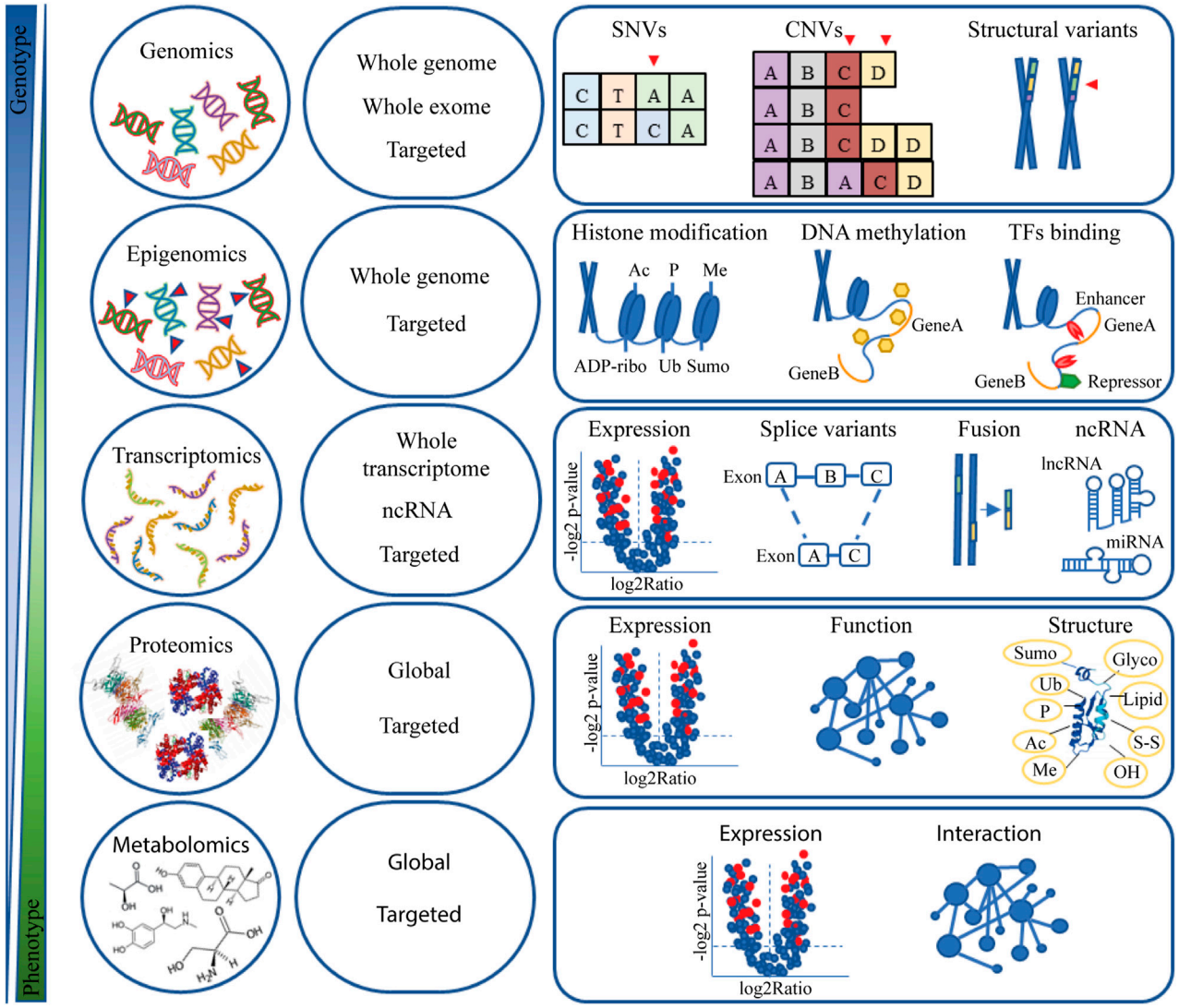

FIGURE 1
Omic data. Overview of NGS technology and applications in cancer research. Abbreviation: Ac, acetylation; ADP-ribo, ADP ribosylation; CNV, copy number variation; Glyco, glycosylation; Lipid, lipidation; lncRNA, long non-coding RNA; Me, methylation; miRNA, microRNA; ncRNA, non-coding RNA; OH, oxidrylic group; P, phosphorylation; SNV, single nucleotide variants; S-S, disulphide; Sumo, Sumoylation; TFs, transcription factors; Ub, ubiquitination.

considered. First, we need to distinguish between two key parameters in sequencing, coverage depth and coverage itself. Coverage depth is a measure of how often a particular base in a sequence is seen during sequencing and can be an indicator of the reliability of the results, while coverage is the percentage of the genome that is sequenced during the experiment. These parameters are closely related and must be weighed when researchers define the goal of their studies (Sims et al., 2014; Meienberg et al., 2016). Although the coverage of WGS is higher than that of WES, the average depth of coverage in WGS experiments may be low. In contrast, WES has a higher average depth of coverage compared to WGS because WES only covers the exons that account for about 2% of the genome. Another limitation is related to the data generated by sequencing, as WGS data are very huge, and processing and storing such amount of data requires adequate computational resources, which may be a limit in some contexts. Finally, the cost of WGS experiments is usually higher than WES, especially in clinical settings.

For these reasons, WES has long been considered the gold standard for detecting genetic variants. However, comparative WGS and WES studies have recently shown that WGS is more powerful than WES in exome variant detection, providing broader coverage and better variant detection, and costs are now decreasing (Belkadi et al., 2015). In addition, the latest WGS library preparation methods are PCR-free, while the WES library preparation methods still rely on PCR amplification. This could lead to GC content bias and misidentification of variants (Meienberg et al., 2016). In addition, WES does not really cover the whole exome, so some deleterious coding SNVs might be missed. As mentioned earlier, WES is not validated for the detection of structural variants, including CNVs and translocations, and finally, by definition, it does not include non-coding intron regions. Therefore, WGS has

become more attractive than WES for diagnostic purposes in recent years (Belkadi et al., 2015; Lionel et al., 2018; Hou et al., 2022).

Whole transcriptome sequencing (WTS) is an RNA-based sequencing strategy that captures the transcriptome repertoire, and its applications include quantification of gene expression, detection of alternative transcripts resulting from splice variants, detection of chromosomal rearrangements leading to chimeric gene fusions, and identification of the ever-growing family of non-coding RNAs (Lakhotia et al., 2020; Li and Wang, 2021). Depending on the research interest, total RNA extracted from samples should be treated to remove unwanted RNA species, which may be a limitation, especially in terms of time. On the other hand, the loss of valuable reads and the management of background noise are problems faced when no depletion is performed. Bulked WTS has been used in cancer research to identify pathways and genes involved in cancer development and, thanks to spatial transcriptomics and single-cell sequencing, also to understand tumor organization and interactions with the microenvironment (Chen TY et al., 2023).

2.2 Whole vs. targeted sequencing

Many companies that have developed high-throughput technologies have now launched numerous tumor-specific panels to study cancer. Targeted panels sequence only a small part of the genome because they are designed with probes targeting specifically regions of interest, such as sets of genes, in a specific/custom fashion. Depending on the size of the panel, they can achieve the depth of coverage required to highlight specific pathogenic variants (Lenahan et al., 2023). Targeted panels offer many advantages over WGS and WES approaches, including reduced hands-on time, ease of translation of raw data, profiling of specific tumor-associated genes and customization of the panel. These advantages can support the therapeutic decision-making process while reducing the time required (Bewicke-Copley et al., 2019).

For their part, WGS and WES approaches can be extremely useful in exploratory research and clinical trials, as they do not require "*a priori*" knowledge of disease mechanisms and can reveal novel molecular biomarkers. In this sense, the COGNITION study has shown that comprehensive molecular profiling using WGS and WES identifies a genomic signature in a subset of breast cancer patients at high risk of recurrence after neoadjuvant treatment, for whom targeted therapy solutions may be available (Pixberg et al., 2022).

On the other hand, targeted panels can also be employed in clinical trial design. In this case, panels could be used for many goals. First, to stratify the cohort according to known biomarkers, as in the case of the REGISTRI phase II clinical trial, in which a customized DNA panel was developed to specifically identify *KIT/PDGFRA* wildtype GIST patients eligible for regorafenib therapy (Martin-Broto et al., 2023); second, to support the discovery of new specific positive biomarkers, associated with response to therapy, as in the RELAY phase III trial, in which a targeted approach was used to assess ctDNA mutations and *EGFR* mutation dynamics after erlotinib with or without ramucirumab treatment in NSCLC patients (Garon et al., 2023); and finally, to identify actionable tumor alterations and candidate genes for molecular targeted therapies, as demonstrated in the MATCH study (Parsons et al., 2022). Of note, many targeted panels, known as PanCancer panels, are designed to cover many cancer-related genes, so the applications of these panels are widespread for many different goals.

Whole and targeted sequencing approaches can also be combined in clinical trials, as in the EVOLVE phase II study in which WES of tumor tissue and a targeted panel of cell-free DNA from blood were matched to discover novel genomic alterations responsible for resistance to PARP inhibitors in high-grade serous ovarian cancer (Lheureux et al., 2023).

In the clinical setting, things are different, as the cost of analysis is one of the limiting factors for sequencing. In this scenario, targeted panels are preferred because they have a lower cost per sample and an easier data management (Bewicke-Copley et al., 2019). Targeted panels are often designed to provide information on known biomarkers such as genomic instability score (GIS), loss of heterozygosity (LOH), microsatellite instability (MSI), and tumor mutation burden (TMB). The latter biomarker is of great interest in clinical practice, as pembrolizumab is the first FDA-approved agnostic cancer therapy that can be used in tumors with high TMB (Marcus et al., 2021); however, the sequencing method used to assess TMB may impact clinical outcomes, by excluding patients who might otherwise benefit from this treatment. Indeed, WGS, WES, and targeted-based panels have been used to measure TMB in cancer patients, with not only primary tumors but also circulating DNA in blood proposed as an alternative source material. In this context, WES of tumor and paired normal tissues is currently considered the most accurate approach to determine TMB, although this approach is both costly and time-consuming in the clinical setting (McGrail et al., 2021). On the other hand, an approach that uses targeted sequencing assays enriched in genes known to be involved in cancer appears to be more feasible in the clinic, particularly because these assays do not require paired tumor and normal samples to determine TMB. However, the type of cancer tested and the type of panel used to assess TMB can significantly affect the outcome (Merino et al., 2020). Among the many examples of targeted panels used in the clinical setting there are MyeloSeq, a 40-gene targeted panel used to determine variant and allele frequencies in patients with suspected hematologic malignancies (Barnell et al., 2021), the Oncomine Precision Assay, which tests 45 cancer-related genes (such as *EGFR, KRAS, ALK, RET, BRAF,* and others) used in screening for genomic alterations that can be treated with targeted therapy in NSCLC, colorectal cancer, melanoma, breast cancer, and other malignancies (Werner et al., 2022; Nindra et al., 2023), and other targeted panels such as the TruSight Oncology, the AmpliSeq, the FusionPlex, the QIASeq Multimodal Lung, which have demonstrated expertise in identifying genetic variants, and the *NTRK* gene fusion panel used to identify tumors sensitive to larotrectinib, an NTRK inhibitor (Drilon et al., 2018; Stockley et al., 2023).

In addition, there is also an ethical aspect to consider, as sequencing a larger portion of the genome may lead to the identification of unsolicited findings that should be better communicated to physicians and patients (Schoot et al., 2021). Targeted panels therefore have a lower chance of discovering new unsolicited findings, which facilitates clinical reports.

In summary, although WGS and WES sequencing are accurate and do not require "*a priori*" knowledge of disease mechanisms,

their introduction into clinical practice may not be feasible, mainly because of coping with the volume of data and the cost per sample. On the other hand, targeted sequencing may facilitate the introduction of bulk sequencing into routine clinical practice where testing of multiple molecular biomarkers has become common practice, as has been the case with TMB and NTRK gene fusions. Again, the best choice between the two strategies must be balanced between cost and application.

2.3 Epigenomics

Epigenomic sequencing has proliferated in recent years. Epigenetics is a branch of biology that studies the causal interactions between genes and their products. Basically, epigenetics studies all changes and phenotypes in gene expression that cannot be attributed to genetic causes. The most important changes can occur directly at the DNA, e.g., cytosine methylation, or at the chromatin proteins, e.g., acetylation, methylation, phosphorylation, and others (Kouzarides, 2007). The consequence of these changes is the modulation of the accessibility of the DNA sequence to enzymatic complexes, which determines the state of gene activation.

Sequencing of epigenetic modifications (epigenomics) identifies specific cancer signatures involved in tumorigenesis as well as cancer metastasis and recurrence (Huang et al., 2018; Malta et al., 2018; Sengupta et al., 2021). In particular, some histone modifications, such as reduced lysine acetylation and methylation, may act as prognostic biomarkers in breast cancer (Elsheikh et al., 2009; Zhou et al., 2022) or they may predict response to treatment, as in the case of immunotherapy (Peng et al., 2015; Hoffmann et al., 2023). In addition, dysregulation of genes involved in chromatin remodeling can also be a hallmark of a particular tumor. This is the case with mutations of histone deacetylase (HDAC) in multiple myeloma and lymphoma. HDAC inhibitors and DNA methylation inhibitors are anticancer drugs developed to target the aberrant activity of these molecules (Blumenschein et al., 2008; Galanis et al., 2009).

2.4 Proteomics and metabolomics

Proteomics and metabolomics are high-throughput screening of protein expression and metabolite abundance, respectively. Proteomics data can be considered a readout of the transcriptome, but it has been reported that only 40% of protein expression can be explained by a corresponding gene expression profile (Ideker et al., 2001; Vogel et al., 2010). Proteomic studies take pictures of the cellular protein repertoire that include protein abundance and turnover, post-translational modifications, subcellular localization, interactions with other proteins and structures, and finally protein involvement in metabolic pathways (Altelaar et al., 2013).

On the other hand, metabolomics studies investigate the presence of metabolites, their concentration and their interactions with biological systems. Unlike other "omics" approaches, metabolomics can reflect the actual biochemical activity and the state of cells and determine the true cellular phenotype (Patti et al., 2012; Tan et al., 2012).

In cancer research, proteomics and metabolomics strategies have been used not only to identify novel biomarkers involved in tumor resistance and signature that predicts treatment outcome (Dytfeld et al., 2016; Shrestha et al., 2021; Robles et al., 2022), but also to uncover cancer metabolic pathways and oncometabolites that may drive tumorigenesis and sustain tumor progression (Xu et al., 2011; Drusian et al., 2018).

3 Omics data in cancer personalized therapy

Over the past 20 years, molecular assessment of tumors has entered routine clinical practice and has been incorporated into the WHO classification criteria for tumor diagnosis, grading and prognosis (Organisation mondiale de la santé and Centre international de recherche sur le cancer, 2020; Sbaraglia et al., 2020; Louis et al., 2021).

As a result, the treatment of patients shifted mainly towards tailored therapies, and the development of new classes of anticancer drugs increased, defining the beginning of the molecular era of targeted therapy. The so-called "targeted therapy" refers to drugs that are aimed at interfere with specific molecular target that is thought to play an important role in tumor development and progression. One of the first and most successful examples of targeted therapy is imatinib, a small molecule receptor tyrosine kinase (RTK) inhibitor that targets a variety of RTKs. The use of imatinib in tumors harboring activating mutations of RTKs (e.g., gastrointestinal stromal tumors, dermatofibrosarcoma protuberans) or oncogenic RTK fusion proteins (e.g., chronic myeloid leukemia positive for the *BCR::ABL* fusion, myelodysplastic/myeloproliferative disorders associated with *PDGFR* gene rearrangements), leads to increased life expectancy for patients whose prognosis was previously very poor (Druker et al., 1996; Druker et al., 2001; Demetri et al., 2002).

The specificity of targeted therapies usually gives these drugs particularly high efficacy while reducing off-target toxicity to normal cells, but it is also responsible for mechanisms of tumor resistance. It is noteworthy that not only the presence of a mutated drug-responsive gene, but also the type of mutation on the same gene can play a role in drug response. The *EGFR* gene in particular can serve as an example. Most glioma tumors are dependent on EGFR signaling, making approved drugs targeting this gene attractive for precision oncology of gliomas. However, most clinical trials have failed to demonstrate the benefit of EGFR-targeted therapies in gliomas, as approved EGFR therapies have mainly focused on NSCLC *EGFR* gene alterations that are, however, distinct from those driving gliomagenesis (Lin et al., 2022). On the other hand, secondary resistance occurs when a fraction of cancer cells develops new acquired mutations or alterations in antigen presentation, which can also drastically affect the efficacy of targeted therapies. Transcriptional deregulation and de-repression of alternative RTK are also common strategies to facilitate adaptive evasion signaling, which is likely promoted by epigenetic changes (Jun et al., 2012; Akhavan et al., 2013). The presence of resistant cells forces clinicians to dose escalate with the risk of increased toxicity or to switch molecular targets with the risk of no new therapeutic options being available.

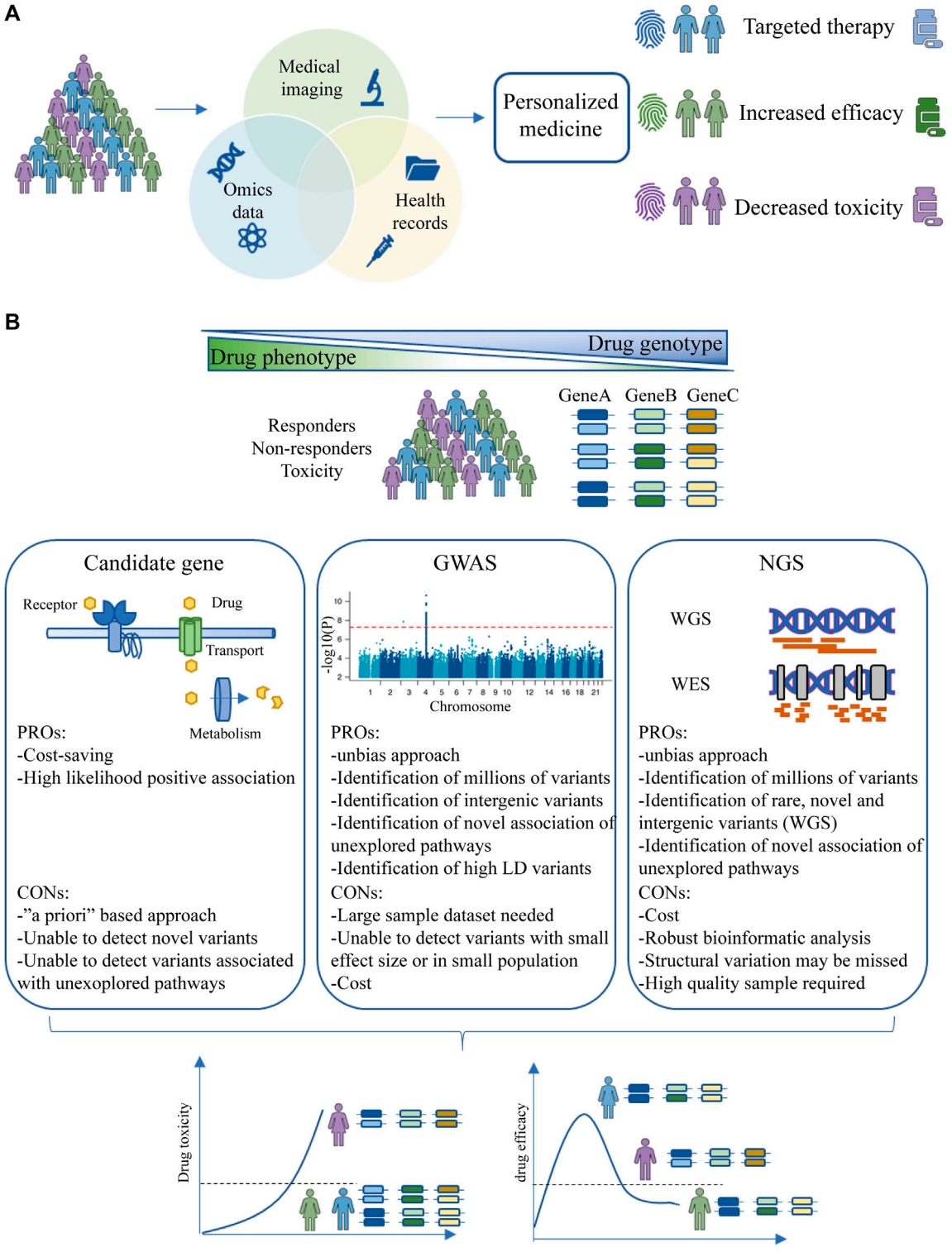

FIGURE 2
Personalized medicine and PGx studies. **(A)** Aims of personalized medicine. Patient data from multiple sources (health records, medical imaging and omics data) are combined to identify a patient-specific fingerprint that determines response to therapy, efficacy and toxicity. **(B)** PGx study design strategy. Three drug phenotypes will be identified (responders, non-responders and toxicity) and different populations will be studied to identify the genetic traits involved in particular drug phenotype. The strategies are divided into candidate genes, GWAS and NGS. The aim of PGx studies is to stratify the population based on genetic background to maximize drug efficacy and reduce toxicity. Abbreviations: GWAS, Genome-wide Association Study; NGS, Next-Generation Sequencing.

In the scenario of personalized cancer therapy, the assessment of the individual status of the tumor immune system also plays an important role and has led to the development of nanoparticles, monoclonal antibodies, and chimeric antigen receptor T-cell therapies (CAR-T) as well as antibody-drug conjugates. Some examples include the generation of third-generation CAR-T cells against the oncoembryonic antigen ROR1 (Meng et al., 2023) and the study of the chemokine expression signature that correlates with the characteristics of T-cell inflammation and potential response to immune checkpoint inhibitors in various cancers (Romero et al., 2023).

Another goal of precision medicine is to identify new molecular biomarkers that can monitor both disease stage and the efficacy of selective therapies. In this context, tumor molecules secreted in the bloodstream, such as microRNAs, non-coding RNAs, exosomes, and circulating tumor DNAs (ctDNAs) are of particular interest and can be detected without invasive procedures thanks to liquid biopsy. For example, the expression of circulating miR-221/222 correlates with response to and resistance to tamoxifen in the luminal subtype of breast cancer patients (Patellongi et al., 2023), circRNA_047733 can be used as a biomarker for risk assessment of lymph node metastasis in patients with oral squamous cell carcinoma (Deng et al., 2023), and baseline ctDNA mutation frequency can be used as a prognostic marker in patients with metastatic colorectal cancer (Bachet et al., 2023). In addition, measurement of ctDNA at specific time points by liquid biopsy can also be used as a biomarker of efficacy and toxicity to guide the dose and schedule of radiotherapy in cancer patients (McLaren and Aitman, 2023).

Finally, several cancer hospitals have interdisciplinary teams of experts, called molecular tumor boards, that recommend a patient-specific therapeutic strategy based on data from NGS profiling. A retrospective study of biliary tract tumor patients showed that comprehensive genomic profiling along with molecular targeted therapy discussed by the molecular tumor board resulted in a higher response rate and better overall survival for patients who received the recommended treatment (Zhang D et al., 2023). In addition, these molecular tumor boards can bridge the gap between research and the clinic by recruiting patients early for clinical trials (Weiss et al., 2023).

As discussed in the following section, various genetic polymorphisms that can be studied using omics experiments and that are located in genes associated with drugs PK and/or PD, can influence efficacy and toxicity.

3.1 Omics data in PGx studies

In addition to targeted therapy, NGS approaches can support the concept of personalized medicine by being included in PGx studies and linked to drug safety profiles (Figure 2A). Sequencing results can thus be associated with the identification of novel biomarkers related to drug efficacy and toxicity.

The three main research strategies for PGx biomarker discovery are candidate gene studies, Genome-Wide Associated Studies (GWAS), and NGS (Figure 2B). Candidate gene studies are based on genotyping or sequencing of genes known to be involved in PK and PD processes to uncover potential variants; this is the main approach taken so far. This approach is based on "*a priori*" knowledge, as genes are selected based on their membership in specific pathways (Malta et al., 2018; Kwok et al., 2022; Maeda et al., 2023). A limitation of this approach is that polymorphisms that are part of unexplored pathways and may alter the phenotype of the drug response are not detected. However, this approach may have higher statistical power than other approaches even with few samples (Chan et al., 2019).

On the contrary, GWAS discovers millions of SNPs across the genome and has the potential to find variants in unexplored genes and intergenic regions not previously thought to affect drug response (Uffelmann et al., 2021). One example is the germline variants in the *PRUNE2* and *BARD1* genes, which have prognostic potential in advanced colorectal cancer and ovarian cancer, respectively. In addition, the variants in the *AGAP1* gene may affect patient response to bevacizumab (Quintanilha et al., 2022b). Moreover, most of the SNPs detected are not the causal variants responsible for the observed phenotype, but are instead associated with the presence of functional variants in high linkage disequilibrium in a given population (Bei et al., 2010). One of the major limitations of this technique is the low statistical power in detecting associated signals for rare polymorphisms and thus the inability to find variants with small effect sizes, especially when a drug effect trait is not directly associated with drug effect or is population/region specific (Wang et al., 2019).

Finally, NGS approaches offer the possibility of generating a large amount of information on novel, common, or rare variants potentially associated with drug response, such as GWAS, but suffer less from the requirement of a large number of samples to achieve statistical power, overcoming the drawbacks of the other two SNP approaches (Sharma et al., 2014; Auwerx et al., 2022). However, NGS is not a panacea for identifying all inheritance patterns in PGx. The lack of standardization of NGS techniques and limitations in sample quality or quantity are issues that should be addressed to achieve comprehensive and robust detection and association of somatic and germline variants involved in individual drug response (Mu et al., 2019).

Although candidate gene studies, GWAS, and NGS enable the identification of variants potentially involved in individual drug response, the results obtained in these studies require internal and external validation before they can be adopted in clinical practice. Validation strategies include case/control studies, cross-validation based methods, and an independent series of patients to confirm results. In addition, orthogonal technical validation using low-throughput methods is required, with real-time PCR with TaqMan assay and pyrosequencing often being the first choice (Arbitrio et al., 2021; Hertz et al., 2021).

3.1.1 PGx in drug response: focus on efficacy

The efficacy of a drug is related to its plasmatic concentration, which is a surrogate for measuring the percentage of the administered dose that can reach the molecular target. Genetic variants in genes involved in PK or/and PD can affect the efficacy of a drug, as discussed below. Although much of the variation is due to PK (Roden et al., 2019), PD variations may also be important for treatment efficacy.

Classic examples of PGx in drug response involving PK mechanisms include glutathione S-transferase, cytochrome *P450* genes and *MDR1* gene polymorphisms. Glutathione S-transferase

(GST) is a class of metabolic enzymes that conjugates glutathione to xenobiotics for detoxification purposes. GST substrates include anthracyclines and cyclophosphamide, anticancer drugs used in breast cancer protocols. In particular, the GG genetic variant in the *GSTP1* gene (c.313A>G) appears to be associated with a lower risk of chemoresistance in breast cancer patients treated with doxorubicin (Romero et al., 2012) and a lower risk of death in patients treated with cyclophosphamide compared to patients with proficient-GST (Sweeney et al., 2003). One possible mechanism to explain these observations is that decreased GST activity leads to an increase in the systemic dose of active metabolites, which in turn results in a better therapeutic effect, even if this increases the risk of toxicity.

Cytochrome P450 is one of the most important enzyme classes involved in the metabolism of xenobiotics. This group includes the enzyme CYP2D6, which is involved in the conversion of tamoxifen to its more active metabolites, 4-hydroxytamoxifen and endoxifen. Genetic variants in the *CYP2D6* gene (*4, *5, *10 and *41) result in impaired enzyme activity, leading to lower production of active tamoxifen metabolites and shorter overall survival in cancer patients taking tamoxifen (Schroth et al., 2007).

Genetic variants affecting transporters may also play a role in altered drugs response. A silent polymorphism in the *MDR1* gene, one of the best-known efflux pump proteins involved in drug resistance mechanisms, has been shown to affect the timing of MDR1 mRNA translation into folded protein, thereby reducing total protein levels (Kimchi-Sarfaty et al., 2007).

Novel PK-related genetic variants have also been discovered. Germline polymorphisms in the *NT5C2* gene (e.g., rs72846714) were recently discovered in a GWAS study, and some of them have been linked to 6-mercaptopurine (6-MP) metabolism in patients with acute myeloid leukemia, as they are responsible for differential activation of 6-MP and thus its bioavailability (Jiang et al., 2021).

At PD, it can be speculated that any variant (germline or somatic) that affects the accessibility of the drug to its target or the affinity of the drug binding may result in altered drug efficacy. These scenarios include variants that alter the amino acid sequence at the core binding site between the drug and the target, thereby affecting binding affinity, variants that alter the spatial conformation of the protein and may lead to partial misfolding, and alterations in weakly bound bridges between individual nucleic bases. In NSCLC patients treated with the EGFR inhibitor gefitinib, patients with specific in-frame indel mutations in the *EGFR* gene were more sensitive to gefitinib, as these mutations increase the tumor's dependence on growth factor signaling, compared to patients without such mutations. Therefore, patients with these mutations respond better to gefitinib than patients who have other mutations (Lynch et al., 2004).

In glioblastoma, *EGFR* mutations and amplifications account for at least 50% of molecular alterations (Brennan et al., 2013). The EGFR variant III (EGFRvIII) is the product of the most common deletion in GBM, resulting from the deletion of exon 2-7 of the extracellular domain (ECD). This alteration occurs predominantly in cancer cells and in approximately one-third of GBM, making this variant an ideal epitope for immunotherapy. Rindopepimut is a peptide-based cancer vaccine that targets EGFRvIII. Although EGFRvIII is an extremely attractive therapeutic target, tumor cells escape this immune-mediated therapy by losing the EGFRvIII expression as a resistance mechanism (Binder et al., 2018).

Epigenetic changes may also affect PGx. Hypermethylation of *MLH1*, which is involved in the mismatch repair system, may affect the response to cancer therapy targeting this pathway (Wu F et al., 2015; Bukowski et al., 2020; Loukovaara et al., 2021). In addition, altered histone modifications that may occur during tumorigenesis and other pathological conditions may lead to heterogeneous expression of drug efflux proteins and thus affect PK (Kondo and Issa, 2004; Baker et al., 2005; Wu L-X et al., 2015). In particular, demethylation of the *ABCB1* gene in cancer cells can lead to a reduction in the accumulation of anticancer drugs in cancer cells, resulting in the acquisition of a resistant phenotype (Toth et al., 2012).

3.1.2 PGx in drug response: focus on toxicity

Drug toxicity refers to a variety of adverse effects associated with the use of a particular drug. The mechanisms of drug toxicity can vary widely and include four main aspects: on-target toxicity, off-target toxicity, hypersensitivity reactions and idiosyncratic reactions (Guengerich, 2011). Genetic polymorphisms may enhance or attenuate these reactions.

On-target toxicity refers to the adverse effect of a particular drug depending on its mechanism of action. This phenomenon is related to the binding of the drug to its therapeutic receptor, but in a different body compartment. Polymorphisms that enhance this type of response include rs9501929 of the *TUBB2A* gene, which encodes the β-tubulin protein. Although there are conflicting opinions about its clinical utility, rs9501929 may alter the toxicity profile of paclitaxel, an antimitotic drug that binds specifically to β-tubulin to arrest cell cycle progression. Patients carrying this variant have a higher risk of developing paclitaxel-induced neuropathy, a disease characterized by abnormal aggregation of microtubules in neurons (Abraham et al., 2014). This effect can be explained by the fact that β-tubulin is also targeted by paclitaxel in normal neurons, which is, by definition, an on-target toxicity. The lack of a selective and specific target for cancer cells is one of the major limitations of conventional chemotherapy such as paclitaxel.

Off-target toxicity refers to the adverse effects of a drug that binds to both its therapeutic and nontherapeutic receptors and is also related to mechanisms that are independent of the mechanisms of action (Rudmann, 2013). Some of these issues can be addressed in the preclinical stages of drug development by altering the structure of the drug to modulate its affinity to undesirable receptors. In addition, local administration, if applicable, may also partially help (Li M et al., 2022). Hypersensitivity reactions and idiosyncratic reactions depend on the activation of the immune system and the intrinsic characteristics of patients, respectively (Doña et al., 2014).

The best characterization of adverse reactions involves genes from PK processes. Individual variants in transporters and metabolic enzymes are responsible for most differences in drug response. In particular, polymorphisms in the gene *SLCO1B,* which encodes the OATP1B1 transporter responsible for cellular uptake of multiple substrates, can impair the availability of irinotecan and lead to drug toxicity (Nozawa et al., 2005; Di Martino et al., 2011). In addition, part of irinotecan is oxidized by CYP3A4, while another part of irinotecan is activated to SN-38 and its glucuronide conjugate SN-38G. These reactions are catalyzed by carboxylesterase and

UGT1A1, respectively. The genetic variant *UGT1A1*28* is associated with decreased glucuronidation activity, which in turn prolongs the mean half-life of the metabolite SN-38 and increases patient susceptibility to gastrointestinal and hematologic toxicity (Iyer et al., 2002; Innocenti et al., 2004; Peeters et al., 2023). Similar toxicities to irinotecan have been noted in patients carrying polymorphisms in the *ETS1* and *ABCG2* genes, which encode carboxylesterase and a membrane transporter, respectively (De With et al., 2023). The *UGT1A1*28* polymorphism, together with the *UGT1A1*60*, *UGT1A1*6*, and *UGT1A1*27* polymorphisms is associated with the metabolism of several anticancer drugs such as belinostat, an HDAC inhibitor, nilotinib and pazopanib, two RTK inhibitors. Thus, loss-of-function alleles are responsible for increased toxicities, such as neutropenia, thrombocytopenia and prolonged QTc intervals in patients treated with belinostat (Goey et al., 2016; Balasubramaniam et al., 2018).

Another example is 5-fluorouracil (5-FU), an antimetabolite that has long been used to treat tumors of the stomach, colon and rectum. Approximately 80% of 5-FU is converted to the inactive metabolite 5,6-dihydrofluorouracil by the rate-limiting enzyme DihydroPYrimidine Dehydrogenase (DPYD). Genetic mutations in the *DPYD* gene associated with lower DPYD activity, such as *2A, *13 and rs67376798, can lead to fluoropyrimidine toxicity (Caudle et al., 2013; Glewis et al., 2023; Lešnjaković et al., 2023).

Germline mutations in the *TPMT* gene, as well as in the *NUDT15* gene, may otherwise affect the metabolism of the thiopurines 6-mercaptopurine (6-MP) and 6-thioguanine (6-TG). In thiopurine metabolism, TPMT is a key enzyme that converts 6-MP and 6-TG to their inactive metabolites. Patients with loss of function alleles have higher circulating thiopurines levels, which increases the risk for developing myelosuppression, a common adverse effect of these drugs. In these patients, a lower starting dose is recommended to minimize toxicities (Wang et al., 2010). The same precautions should be observed in patients with loss-of-function alleles of the gene *NUDT15*, which is also involved in the metabolism of thiopurines (Moriyama et al., 2016). Genetic testing for *TPMT* and *NUDT15* genes has entered clinical practice and is strongly recommended for cancer patients who are to receive thiopurine therapeutics (Relling et al., 2019).

Some of the classic gene polymorphisms such as cytochrome *P450, DPYD, UGT, TPMT*, and *HLA* have already entered clinical practice. Panels of specific genes are routinely used to determine the optimal therapeutic window in cancer patients and their utility has been demonstrated. A recent multicenter implementation study evaluated a panel of 12 genes for pharmacogenetic testing in several European countries. The most important finding of this study, in addition to demonstrating that genotyping of this 12-gene panel leads to a reduction in the incidence of relevant adverse drug reactions, is the cross-national feasibility of these genetic tests, which paves the way for harmonization of genotyping (Swen et al., 2023).

In summary, PGx testing offers a number of benefits, including enhancing intended treatment benefits, reducing the likelihood of adverse effects and risk of dependence, reducing healthcare expenditures and the need for hospitalization in the event of severe adverse events, and shortening the time to achieve therapeutic effect. Although researchers and clinicians are increasingly aware of the importance of genetic testing for personalized oncology, global clinical implementation is still lacking, in part due to the need for standard procedures, cost reduction, but also support from healthcare systems, especially in less affluent countries.

4 Machine learning in cancer research

Machine learning (ML) is a subfield of artificial intelligence that aims to make predictions and inferences within a certain range of accuracy by analyzing multiple variables in input data, such as clinical and/or molecular data (Mitchell, 2013). In addition, without explicitly programming, ML can find hidden patterns and identify relationships between multiple variables to correctly predict the outcome.

Machine learning has indeed proven to be a powerful tool in cancer research, as it has the potential to improve cancer diagnosis, classification and prognosis (Kourou et al., 2015; Cui et al., 2022a). An example of the use of ML in cancer research is the study of medical imaging, where large amounts of data are available that are difficult to analyze. In particular, the emerging field of radiomics uses images routinely produced in clinical settings to evaluate patients undergoing treatment to develop a ML approach to disease detection (Lambin et al., 2012). Another example is radiogenomics, where key features extracted from radiological images can be linked to the genetic profile of the tumor. Thanks to the linkage of image and genotype highlighted by ML, radiogenomics offers the possibility of becoming a noninvasive surrogate for genetic testing (Meißner et al., 2022).

Other important approaches of ML in cancer research focus on treatment. Predicting how a particular tumor will respond to therapy, or which patient characteristics better predict response to therapy, is a fundamental goal of modern oncology that should ultimately lead to tailored treatment. For example, genetic profiles and clinical information of breast cancer patients from a complete study dataset were used to train a ML algorithm to predict the 5-year survival rate of these patients who underwent a specific medication (Tabl et al., 2019). In this context, genomic profiling can provide information about the role of biological pathways in cancer cells and their relationship with a specific medication, thus helping clinicians to tailor treatment for patients based on their molecular background.

4.1 Machine learning at a glance

A detailed description of ML is beyond the scope of this review; however, we provide here an overview of the main features of the algorithms of ML.

Supervised learning, unsupervised learning and reinforcement learning are three main types of machine learning approaches (Van Der Lee and Swen, 2023). A more classical classification based on the model built using this approach is divided into supervised, unsupervised and semi-supervised models based on the type of input data, i.e., whether it is labeled, unlabeled or a combination of both (Koteluk et al., 2021; Naik et al., 2023). A graphical representation of the concept is shown in Figure 3A.

In supervised models, which account for the majority of published ML methods, each data point contains an associated label (correct/expected response) for which a ML model must be

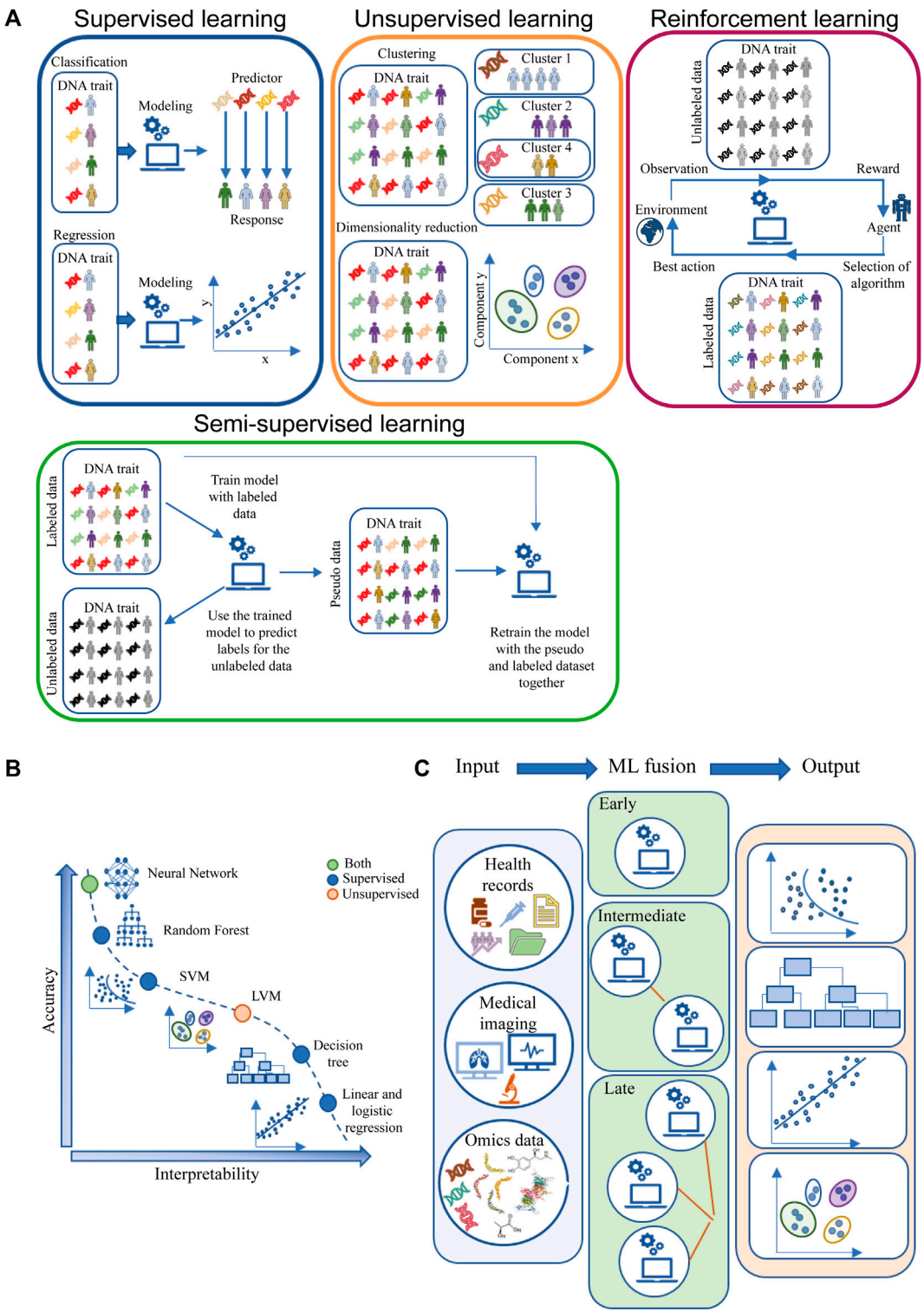

FIGURE 3
Machine learning algorithms. **(A)** ML main classification based on input data labels and possible outputs. **(B)** Trade-off between accuracy and interpretability for ML models grouped by supervised, unsupervised or both types of algorithms **(C)** ML fusion modeling. The light blue box represents the input data (health records, medical imaging and omics data), the green box represents the type of ML fusion: early fusion (top) computes a single ML model; intermediate ML fusion (middle) computes two or more ML models, with the final model using the output of previous model as input; late fusion (bottom) creates multiple ML models and then fuses the outputs of each model to produce the data output. The light red box represents examples of the outputs obtained through ML, from the top to the bottom: Classification, Decision Tree, Regression, Clustering. Abbreviation: LVM, latent variable model; SVM, support vector machine.

TABLE 1 ML algorithms in cancer research in the last 2 year. In this table, we summarize the most important research topics in cancer research using ML. For each publication, we describe the type of the ML algorithm used and the research outcome of the selected study. Publication years: 2021–2023.

Research topic	ML algorithm	Outcome	References
IC_{50} value	NN	*In silico* model that estimates IC_{50} values	Ma et al. (2022)
Structure-activity relationship	Decision tree	Analysis of SAR of HDAC1 inhibitors	Li et al. (2023)
Drug target prediction	SVM	Ligand- and structure-based identification of novel CDK9 inhibitors	Zhang et al. (2022)
Synergistic effect	RF	Synergistic drug combinations in CRC tumors using metabolomic data	Lv et al. (2022)
Pathway alteration	SVM	Identification of biological pathways involved in cancer drug response	Zhu and Dupuy (2022)
Treatment outcome	SVM	FOLFOXai signature identifies mCRC patients for whom oxalilplatin-containing therapies are less beneficial	Abraham et al. (2021)
Drug repurposing	SVM	Molecular simulation with approved drugs to identify molecules with RET inhibition profile	Ramesh et al. (2022)
Prognostic factors	LVM	Identification of somatic oncogenic mutations	Liu Y et al. (2022)
Prediction of benefits	Decision tree	Mutation signature predictive of the benefit of immunotherapy in NSCLC	Liu Z et al. (2022)
Efficacy predictors	SVM Regression	Prediction of the efficacy of anticancer drugs based on clinical and molecular features of OSCC	Brindha et al. (2022)
Toxicity predictors	RF	Identification of SNPs in the PI3K/AKT pathway associated with toxic effects during chemotherapy in LACC patients	Guo et al. (2023)
Multi-omics data integration	RF	Prediction of tumor recurrence and survival in PDAC patients based on multi-omics data from metastatic and non-metastatic microbiome patient signatures	Li S et al. (2022)
Medical imaging (radiomics)	Regression	Prediction of OS and PFS in patients with ESCC based on CT image radiomics signatures	Cui et al. (2022a)

Abbreviations: CRC, colorectal cancer; CT, computer tomography; ESCC, esophageal squamous cell carcinoma; FOLFOXai, folinic acid, fluorouracil, oxaliplatin artificial intelligence; LACC, locally advanced cervical cancer; LVM, latent variable model; mCRC, metastatic colorectal cancer; NN, neural network; NSCLC, non-small cell lung carcinoma; OS, overall survival; OSCC, oral squamous cell carcinoma; PDAC, pancreatic ductal adenocarcinoma; PFS, progression free survival; RF, random forest; SAR, structure-activity relationship; SNPs, single nucleotide polymorphisms; SVM, support vector machine.

developed. Typically, the data is split into two subsets: the training data and the testing data. The training data is used to tune and train the model (Shahin et al., 2023). The testing data is used to evaluate the generality of the model. In addition, supervised learning can be used to solve regression and classification problems. In regression problems, the labels are continuous values, while in classification problems labels are discrete values. Finally, the metrics used to assess the quality of the model depend on the nature of the problem and the type of application (Boyd, 2010; Sra et al., 2012; Orozco-Arias et al., 2020; Woodman and Mangoni, 2023).

In unsupervised models, the output label measurement is usually not available. In this case, the algorithm learns relationships from data structures to provide latent patterns that need to be evaluated for utility. However, this process still requires human intervention to validate the output variable. In general, unsupervised methods deal with clustering and dimensionality reduction, leading to the identification of subgroups with common features, which is one of the main applications of unsupervised ML (Sajda, 2006; Handelman et al., 2018).

Reinforcement learning is a type of learning where an agent learns to make decisions by interacting with an environment. The agent receives feedback in the form of rewards or penalties for its actions and learns to maximize the cumulative reward over time (Woodman and Mangoni, 2023). Unlike supervised and unsupervised learning, reinforcement learning does not require labeled data or a training set. This type of learning is often compared to a scenario where an agent learns through trial and error (Shahin et al., 2023). Reinforcement learning can be used to solve problems that deal with complex dynamics that are influenced by changing stimuli and conditions, such as in the real clinical world (Eckardt et al., 2021; Ryan et al., 2023). In particular, reinforcement learning could help physicians to select the right therapeutic regimens for a patient, and it is able to correct its predictions based on the observation of the adverse reaction resulting from the interaction between the agent and the environment (Niraula et al., 2021; Ryan et al., 2023).

Semi-supervised approach is a method in which there is a mixture of labeled and unlabeled data (Ge et al., 2020; Shi et al., 2021; Roy et al., 2022). There have been significant developments in the field of semi-supervised learning, as researchers have proposed various techniques to make effective use of the combination of labeled and unlabeled data. These techniques aim to overcome the challenges posed by the limited amount of labeled data and the growing volume of unlabeled data (Eckardt et al., 2022; Dou et al., 2023).

In ML it is important to note the differences between prediction and inference. These two terms, often used as synonyms, are used differently in ML algorithms. Prediction is about estimating or predicting unknown outcomes, while inference is about understanding the factors and relationships that contribute to those predictions. Both aspects are crucial in ML, as prediction

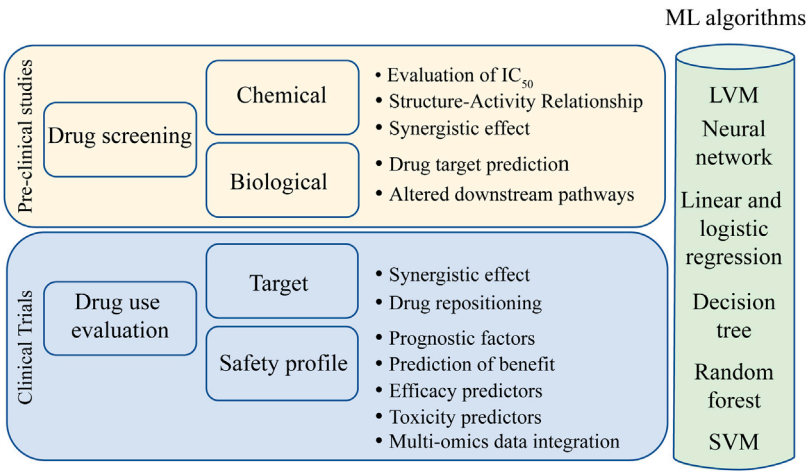

FIGURE 4
Main uses of ML algorithms in cancer research. Light yellow box represents preclinical studies where ML has been demonstrated to be effective. Light blue box represents the phases of drug utilization in target populations where ML has taken improvements. In the green light column, different ML algorithms that can be used for each research topic. Abbreviations: LVM, latent variable model; SVM, support vector machine.

enables useful forecasts, while inference helps to gain insights into the underlying mechanisms and to learn from the trained models (James et al., 2013). Depending on the objective, ML algorithms have been developed to make predictions, inferences or a combination of both.

An important issue to address when discussing ML is the trade-off between model accuracy and interpretability. Some approaches are easier to interpret, but are more rigid and less accurate, because they may be based on linear functions such as linear regression. Conversely, other ML models are more flexible in estimating the functional form of the function but can be difficult to explain (Eckardt et al., 2022; Kang et al., 2023). Figure 3B illustrates the trade-off between flexibility and interpretability for some of the most commonly used ML approaches.

ML input data can be of different origins, e.g., clinical data, medical imaging, omics, time series. The use of a single type of input data is characteristic of unimodal ML, while the use of different types of input data is a feature of multimodal ML. Each type of data can be modeled in different ways, resulting in early, intermediate and late fusion (Figure 3C). In early fusion, the input data types are merged at the beginning to create a single ML model. In intermediate fusion, ML models are created interlocked, each refining the previous model. Late fusion creates separate unimodal models that are combined into a final model. The multimodal ML provides more comprehensive and accurate predictions than unimodal models. Moreover, within the multimodal approaches, the intermediate and late fusion strategies achieve better results because they take complementarity information into account when training the model (Steinberg et al., 1999; Kline et al., 2022). In cancer research these multimodal approaches are considered very useful, but their application is not so obvious. ML late fusion strategies can be used to improve the oldest diagnosis criteria, tumor classification and subtype identification, as in the case of NSCLC, where a study shows that fusion of 5 different sources of information achieves the better performance in classification compared to algorithms using only single source information (Carrillo-Perez et al., 2022). In addition, they can be used to develop software for cancer theranostics, a cancer control strategy that combines early diagnosis, accurate molecular imaging, and personalized radiation treatment (in terms of chosen agent, dose, and timing) based on the individual omics profile.

4.2 Machine learning algorithms and deep learning applications

Numerous ML methods have been developed for medical research and recent applications of ML are summarized in Table 1. Here we give an overview of the main algorithms used in the field of oncology (Figure 4), namely, k-means clustering and hierarchical clustering, latent variable model, support vector machine, decision tree learning, and neural networks. For neural network algorithms, we focus on Deep Learning (DL), which is becoming increasingly important in cancer research.

In unsupervised learning, ML methods are not task-specific (i.e., they are not based on a specific predicted outcome, such as survival), provide general insights, and include methods such as k-means clustering and hierarchical clustering. These methods have been used in oncology to identify cancer subtypes, stratify patients, and create clusters from gene expression data to identify patterns and groupings (Eckardt et al., 2023). Another example of unsupervised learning is the latent variable model (LVM), which can capture unobserved variables that may affect the outcome. LVM can therefore be used to regress variables into one or more classes that would best explain the heterogeneity in the data (Miettunen et al., 2016).

Supervised methods include the support vector machine (SVM), which divides data into categories (two or more) to solve both regression and classification problems. It is based on kernel algorithms that can expand the feature space to make data more accessible. It is considered one of the most robust models to date (Tate et al., 2006; Pacurari et al., 2023).

Decision tree learning is a supervised model that is commonly used in clinical practice for decision-making processes. In this case, ML can help identify which variables have the highest separability to the desired categories and is used for both classification and regression (Podgorelec et al., 2002). Random Forest (RF) is an extension of decision tree learning that combines multiple randomly generated decision trees to improve decision making. Given the complexity of biology, data scientists usually prefer RF to decision tree (Breiman, 2001; Cui et al., 2022b).

Finally, neural networks (NNs) are models used in all three types of learning. NNs, which mimic the neural architecture of the human brain, can integrate multiple sources of information and process them in nodes and layers. Each node represents a specific feature with a specific weight, and nodes of the same level represent a layer. Moreover, nodes of different layers can be connected to each other. If the information stored in the node is valuable, the node weight exceeds a certain threshold, which means that the node is triggered and the network is active. During the training, the weight values and threshold are continuously adjusted to form the best combination of nodes and weights that results in the most informative NN (Kriegeskorte and Golan, 2019).

Deep Learning (DL) is one of the NN algorithms where the number of hidden layers and nodes is increased and the overall size of the network is very large, which allows better representation of complex relationships. The main advantage of DL is that it identifies hidden features as part of the learning process, making DL faster and more automated compared to ML (Erickson et al., 2017). These features also correlate with sensitivity and availability of cheaper computing power. Therefore, DL is now referred to as a specific subset of ML with its own algorithms and applications, and has become one of the most widely used approaches in cancer research. Thus, in the following part of this section, we discuss some applications of DL in cancer research.

The use of DL in oncology began with the analysis of medical images, because it is particularly good at identifying pathogenic features of the observed cells, and in certain cases the performance of DL is almost equal to human performance (LeCun et al., 2015; Jalloul et al., 2023). For example, the application MIA was developed to analyze images from microscopy and can be used for classification, object recognition, segmentation, and tracking (Körber, 2023). In addition, medical images of histopathological tumor sections were used to test whether DL can predict response to therapy in patients with adenocarcinoma of the gastroesophageal junction. In this work, researchers found that DL is able to distinguish patients who respond to neoadjuvant chemotherapy from those who do not by extracting certain features on the images before therapy initiation (Hörst et al., 2023). A Swedish study has developed a DL tool for detecting lymph node metastases in colorectal cancer that has excellent accuracy compared to human performance. This tool reduces the time required to assess lymph nodes, which in turn improves the diagnostic process and treatment decisions (Kindler et al., 2023). Another DL tool has been developed to assist clinicians in digital pathology by assessing the tumor cellularity of histopathologic hematoxylin and eosin sections (Altini et al., 2023). Apart from the importance that this algorithm may have in the clinical setting, it is important to point out that its use may also be useful in research, as it allows pathologists to share valuable information with researchers in an automated manner. A high percentage of tumor cells is an important requirement for researchers to perform NGS sequencing, as the biological material taken from the slice must be representative of the tumor in order to reduce the contribution of normal adjacent tissue, thereby reducing background noise and improving sequencing quality. In addition, DL has been successfully developed to predict optimal radiotherapy for patients with brain metastases using CT images and non-image clinical information (Cao et al., 2023). It has also been developed to predict pneumonitis risk in lung cancer patients treated with immune checkpoint inhibitors and to identify morphologic features that predict *ERBB2* status and trastuzumab efficacy in breast cancer patients (Bychkov et al., 2021; Cheng et al., 2023). In a retrospective multicenter study, a DL algorithm was developed to help radiologists diagnose breast cancer lesions and differentiate axillary lymph node metastases based on radiological features (Zhou et al., 2023).

Although medical imaging remains the foremost application of DL, it is also used in the analysis of genomics and transcriptomics data, including data from single-cell experiments that can improve variant detection calling at cell-specific resolution. DL improvements in single-cell sequencing could enhance the ability of researchers to understand intratumoral heterogeneity and identify previously unknown cell subpopulations, making this a particularly attractive area for molecular oncology (Erfanian et al., 2023; Halawani et al., 2023; Shen et al., 2023). DeepTTA is a DL model that uses transcriptomic data to predict anticancer drug response, which can shorten the preclinical phases of drug development and drug screening. In addition, DL models which can predict cancer drug response can also be used to identify new potential clinical applications of known drugs based on target affinity and mechanism of action (Douglass et al., 2022; Jiang et al., 2022; Park et al., 2023). DeepTAP is another DL algorithm capable of predicting sequence peptides that bind to tumor neoantigens, which may be of interest to the field of cancer immunotherapy (Zhang X et al., 2023). With this in mind, DL algorithms are being used in precision medicine to predict anticancer drug response in patient-derived cancer cell lines, as in the case of the DeepDRK framework, which is freely available (Wang Y et al., 2021). A method based on DL was developed to study the uptake of targeted nanoparticles in triple-negative breast cancer, which could be useful for proper dosing in clinical practice (Ali et al., 2022). A nanodiamond biosensor platform using DL was developed to rapidly assess individual specific sensitivity to oxidative phosphorylation inhibitors in patients with hepatocellular carcinoma (Xu et al., 2023).

Finally, network pharmacology is a new approach in drug development that aims to understand the network interactions of multiple drug combinations. In this context, the network algorithms of DL may be useful to identify synergistic combinations of multiple drugs targeting a specific network that can be used to improve cancer treatment (Noor et al., 2023). DeepDTnet, for example, is a DL method for network-based target identification that reveals novel therapeutic effects of known molecules, which in turn can accelerate drug repurposing, a process aimed at finding new uses for drugs that are approved or in trials (Zeng et al., 2020). The strategy of drug repurposing offers numerous advantages over developing a completely new drug, such as a lower risk of failure because safety and risk assessment have already been tested, cost and

time savings in the preclinical phases, and finally, phase I and II results are already available, thanks to sophisticated algorithms such as those used in DL and ML (Pushpakom et al., 2019). Based on this approach, many oncology and non-oncology drugs have been reviewed in recent years, and drug repurposing is particularly valuable in rare or late-stage diseases where the development of a new drug may be difficult in terms of patient recruitment and the time required for a complete clinical trial may be unreasonable.

In PGx studies, DL has also been used to predict the toxicity of specific medications. In recent works, DL methods were able to predict the toxicity of radiation-based therapy in four different cancer types (Tan et al., 2023) and identify SNP signatures associated with urinary symptoms and overall toxicity in prostate cancer patients treated with radiation therapy (Massi et al., 2020). An important implementation of DL in PGx studies may interest medical imaging with feature extraction that predicts drug response based on SNP signatures. However, this task is very difficult to accomplish because the DL algorithms used to scan medical images are designed to extract "abnormal" features, and PGx often refers to germline (i.e., "normal") variants. However, in this way, it would be possible to reduce the number of diagnostic tests a patient has to undergo, also in the context of the most appropriate choice of therapy after diagnosis.

The use of DL, as well as ML in general, can improve healthcare and assist clinicians by shortening the time required for diagnosis and staging and facilitating decision-making in drug selection and administration of the correct dose, thus contributing to the clinical translation of precision medicine in cancer.

4.3 Machine learning in PGx studies

PGx studies have gradually shifted from reactive testing on a single gene to proactive testing on multiple genes to improve treatment outcomes. This move has been made possible by the implementation of high-throughput data generation and analysis.

With the advent of ML and computer science in cancer research, it is now possible to discover previously unknown cancer-related features and latent signatures that impact tumor development, progression and recurrence. In addition, ML offers the opportunity to gain insight into failed clinical trials to understand their limitations and potential benefits, and to prevent toxicity and other drug effects that can impact patient quality of life and treatment efficacy (Harrer et al., 2019).

One of the first constraints in screening new drugs is selecting candidate molecules from the initial bulk of drug libraries. By combining genomic features of cell lines and chemical information of molecular compounds, researchers have been able to create *in silico* ML multi-drug models to predict IC_{50} values, saving cost and time (Menden et al., 2013). Furthermore, these *in silico* approaches enabled the identification of genomic events associated with altered drug sensitivity, optimizing drug trial design (Huang et al., 2017).

In cancer, multitherapy is often used not only to reduce the toxicity of a single anticancer agent and achieve synergistic effects, but also to overcome drug resistance (Dear et al., 2013; Lee et al., 2019; Kim et al., 2020). Screening to predict synergistic drug combinations is a computational approach that has been explored using ML technology. For example, screening multiple administrations of over 40 different drugs in melanoma cancer cells led to the identification of 11 validated, previously untested drug combinations that lead to different outcomes (Gayvert et al., 2017).

As mentioned earlier, there is growing evidence that optimal prediction of drug response relies on individualized molecular profiling (Bode and Dong, 2017). Many ML approaches in PGx studies have been developed to predict the best match between genetic alterations involved in the pathogenesis or recurrence of a given cancer and drugs targeting these alterations (Chang et al., 2018). From this perspective, therapeutic drug monitoring (TDM) is an experimental procedure that measures the plasmatic concentration of a given drug in a specific time window after administration. Recent work has shown that ML methods applied to TDM were able to predict the appropriate dosing for various drugs, e.g., lapatinib dose for patients with metastatic breast cancer (Yu et al., 2022) and cisplatin dose in cohort of patients with head and neck cancer to avoid cisplatin-related toxicity (Cauvin et al., 2022).

4.4 Multi-omics integration, ML and PGx

Integration of different omics information better captures the complexity of cancer through different molecular layers and therefore improves diagnosis, prognosis and treatment compared to using a single "omic" alone (Heo et al., 2021).

There are many examples of successful integration of multi-omics approaches. Whole genome and transcriptome data have been used to quantify the extent of specific genetic alterations at the mRNA level and derive quantitative trait loci (eQTLs). In this context, polymorphisms associated with specific phenotypes are found to be associated with eQTLs, and genetic risk factors associated with eQTLs can *bona fide* predict the level of the corresponding gene product (Nicolae et al., 2010).

Epigenomics and transcriptomics/proteomics data can be aligned to explain how epigenetic changes can affect protein turnover (Wang X et al., 2021). In addition, transcriptome sequencing has often been combined with miRNome sequencing to determine which microRNAs and non-coding RNAs may alter gene expression and modulate response to chemotherapy (Fazi et al., 2015; Cuttano et al., 2022). Many consortia and catalogs have been developed to promote the understanding of tumor processes with high-throughput data, such as the Clinical Proteomic Tumor Analysis Consortium (CPTAC), which integrates genomic and proteomic data to create a proteogenomic portrait of cancer toxicity and resistance (Ellis et al., 2013), the International Cancer Genome Consortium (ICGC), which provides cancer genomic, DNA methylation and gene expression data (Zhang et al., 2011), and The Cancer Genome Atlas (TCGA) program, which provides a collection of genomic, epigenomic, transcriptomic and proteomic data on 33 different cancer types (The Cancer Genome Atlas Research Network et al., 2013). These data collections are the tip of the iceberg of the various omics data consortia that have emerged to date, and they serve as a valuable resource for omics and ML modeling studies of cancer.

The application of ML with the integration of multi-omics data has resulted in several scores for risk prediction and diagnostic/

therapeutic potential, such as the polygenic risk score. The polygenic risk score considers all genetic inheritance variants known to be associated with a particular disease and measures the risk associated with the development of the disease under investigation, thereby improving risk stratification and screening (Akdeniz et al., 2023). Other examples include the BRECADA application, which uses genetic and nongenetic risk factors for early detection of breast cancer, and the OncoNPC signature, which classifies cancer of unknown primary and accordingly tailors initial palliative treatment intent, a strategy that often leads to better patient outcomes compared with cancer treated without querying the OncoNPC signature (Moon et al., 2023; Tao et al., 2023). In addition, some radiomics features have been extracted from images of brain metastases of extracranial primary tumors and correlated with the expression level of PD-L1, allowing stratification of patients according to their sensitivity to immune checkpoint inhibitors using a ML noninvasive classifier (Meißner et al., 2022).

The ability of ML to handle multiple data structures, namely, clinical, molecular and imaging data, allows to discover hidden correlations among different input data in PGx studies to make more accurate predictions and inferences. However, there are several crucial aspects to consider when managing and using multi-omics data that should be examined. First, collection of multi-omics data requires careful evaluation of the entire experimental workflow, from tissue collection and high-quality extraction of nucleic acids and proteins to sample preparation and sequencing. Second, data analysis pipelines need to be developed to integrate individual omics approaches. In this context, early, intermediate and late ML fusions help to address the management of multimodal approaches with positive impact on clinical cancer research. Third, the expertise required for analytical and bioinformatics analyses often requires the collaboration of multiple experts to properly mediate the integration of multi-omics data. Thus, building a multidisciplinary team is therefore challenging for the success of multimodal data integration, but the positive outcomes of multimodal approaches have already been demonstrated and adopted (Kwon et al., 2015; Jing et al., 2020).

4.5 Use of ML in clinical trials

Clinical trials are later phases of drug development and incur very high costs. Clinical trials in oncology have the highest overall failure rate, mainly due to poor trial design (Wong et al., 2019). Therefore, the use of ML in clinical trials could be an opportunity to increase success. However, most applications of ML have focused on preclinical studies rather than improving clinical trial design, possibly due to the significant regulatory challenges associated with the use of ML in a clinical context (Massella et al., 2022).

ML improvements in study design can be attributed to three main strategies: cohort composition to improve suitability by reducing cohort heterogeneity, patient recruitment to improve eligibility by maximizing patient-study match, and patient monitoring to improve adherence and endpoint detection to reduce dropout rates (Harrer et al., 2019; Van Der Lee and Swen, 2023).

As mentioned earlier, oncology clinical trials often fail to meet primary endpoints due to inadequate stratification criteria, poor recruitment and evidence of severe drug toxicity (Hwang et al., 2016; Kim et al., 2023). To address these issues, the RainForest algorithm was developed. The CAIRO2 clinical trial investigated the use of cetuximab in patients with metastatic colorectal cancer and concluded that there was no benefit to using this agent in the overall population. However, the RainForest algorithm was able to identify a small subset of patients who actually benefit from cetuximab treatment based on the SNP germline profile of patients (Ubels et al., 2020). The use of the RainForest algorithm in clinical trials can save enormous resources, as the cost of a single agent is estimated to be around 2.8 million US dollars in the final stages of approval (DiMasi et al., 2016).

Severe toxicity is another major issue in clinical trials, and changes or interruptions to treatment schedules account for at least 30% of failures in phases II and III (Harrison, 2016). ML has also supported the design of clinical trials in term of drug safety. A recent work has shown that SNPs signatures can serve as genetic predictors of toxicity in personalized medicine. The germline variant rs4864950 T>A in the *KDR* gene increased the risk of composite toxicity (occurrence of any of hypertension, diarrhea and dermatological reactions) in patients treated with the VEGFR TKIs sorafenib and regorafenib (Quintanilha et al., 2022a). In another work, the *ABCB1* rs9282564 was the variant most strongly associated with hypertension and nonhematological toxicities in ovarian cancer patients treated with bevacizumab, and SNPs in genes related to the biological oxidation pathway (*CYP3A4* rs28371763 and *CYP1B1* rs9341266) were the most significant variants associated with hematological toxicity in the same cohort (Polano et al., 2023).

Clinically relevant predictors of toxicity have also been found in many GWAS studies, e.g., SNPs predicting severe skin toxicity in patients with colorectal carcinoma treated with cetuximab (Baas et al., 2018) or predicting dysphagia in patients with nasopharyngeal carcinoma treated with radiotherapy (Wang et al., 2022) or predicting neurotoxicity and leukoencephalopathy in patients with lymphoblastic leukemia treated with methotrexate (Bhojwani et al., 2014). Many other correlations between SNPs and toxicity can be found in the literature. Most importantly, prediction of cancer-related toxicities can prevent deterioration in patients' quality of life and adherence to treatment and can be used to manage chemotherapy-related adverse effects in the clinical setting (On et al., 2022).

4.6 Challenges of ML in PGx

Incorporating assessment of somatic and germline variations into treatment decisions with FOLFIRI in elderly patients with metastatic colorectal cancer has been shown to be effective. This regimen requires assessment of *RAS* mutations as well as *DPYD* and *UGT* polymorphisms prior to treatment with the FOLFIRI protocol (Mathijssen et al., 2003; Morel et al., 2006; Sepulveda et al., 2017; Battaglin et al., 2018). Although PGx test guidelines have already been implemented in clinical practice, another important issue in this context is the implementation of ML in clinical practice. ML has demonstrated its usefulness in retrospectively classifying patients during clinical trials to assess drug safety and prognosis (Chang et al., 2018; Quintanilha et al., 2022a; Chen et al., 2022), but the

incorporation of ML into clinical trials and clinical practice is still up for debate. Standard guidelines and protocols need to be thoroughly regulated to obtain comparable information and a precise methodological approach, not only for the algorithms of ML, but also for PGx studies. It is worth noting that different ML models can be applied to the same given subject, as there is no universal applicability of ML algorithms and this could lead to different results in the same dataset.

Moreover, NGS has only recently been introduced into clinical practice to assess diagnosis and prognosis and to evaluate therapeutic strategies, but it is still a niche and there is room for improvement. In addition, sequencing of some parts of the genome remains challenging, e.g., highly polygenic regions, pseudogenes, triplet expansions, low complexity regions, short repetitive sequences, regions of high-similarity, and complex structural rearrangements (Treangen and Salzberg, 2012; Rojahn et al., 2022). It is estimated that approximately 14% of clinically relevant genetic tests are located in these genomic regions (Lincoln et al., 2021), and correct variant identification can be difficult. On the one hand, short tandem repeats and complex structural variants known to play a role in the pathogenesis of certain diseases can now be sequenced using a targeted approach with long reads sequencing technology, as longer reads are expected to generate appropriate sequence length that overlaps better during assembly (Stevanovski et al., 2022). On the other hand, these technical difficulties can be at least partially overcome by adapting NGS analysis workflows accordingly (Rojahn et al., 2022). However, detecting variants in these regions remains challenging and difficult to validate. Detection of rare and very rare mutations with low allele frequency should also be considered. Inclusion of all probes in the ML learning datasets can be helpful, because some isoforms are more informative than others, and pooling them into averages may lead to dilution or loss of this information. NGS and ML can lead to great improvements in PGx studies, as multiple samples and multiple genes can be tested simultaneously, and clinically relevant hidden patterns can be uncovered from complex data structures.

However, ML and DL also have their own limitations. In general, ML algorithms are not error-free: one of the biggest challenges is the learning model itself. Indeed, many ML approaches have problems with underfitting or overfitting, where the data follows the trained data or noise signals too closely, resulting in poor curve estimation. An appropriate size of the training dataset is also important for ML models to learn properly and make accurate predictions. The reliance on large datasets for developing accurate models is also a challenge due to the lack of sample availability. In addition, the relationship between bias and variance also plays a role in obtaining the best performance from ML models. On the other hand, the accessibility of the code used for ML in PGx studies is low (Huang et al., 2017). To further improve knowledge and sharing among distant researchers around the world, platforms for sharing data and code should be established. To this end, computer scientists could have the opportunity to address underestimated problems and find common resources to overcome them. In addition, the development and improvement of multimodal ML methods, such as late ML fusions, may encourage a more holistic view of specific patient characteristics across different input data types.

As previously reported, PGx testing has demonstrated its utility in many situations, and new variants of uncertain significance have been reported thanks to GWAS and NGS PGx studies. On the one hand, the impact of these new variants on PGx testing is still being evaluated. On the other hand, the clinical implementation of genotyping of genes known to be involved in individual drug response needs to be monitored. In particular, the development of genotyping panels should also be improved to enable the translation of new relevant findings into the clinical settings. One of the most important and unanswered questions related to the use of these genotyping panels is how representative they are of individual variability in drug response. Moreover, PGx studies often suffer from a lack of homogeneous tumor samples, which is particularly true for rare tumors and inconsistent sample ancestry origins and incomplete data are also common complaints. Harmonization of samples and data collection, as well as free and easy access to sample datasets, could facilitate PGx studies with ML. Finally, new and standardized scores to track NGS quality, ML accuracy and significance of PGx variants could also be developed to address new tasks.

5 Conclusions and future prospective

The molecular revolution in oncology continues to grow, with the paradigm flowing from pathological oncology based on morpho-histological assessment of tumor specimens to molecularly driven oncology, where precise individual molecular features are considered as part of diagnosis, grading and prognosis to tailor treatment to the individual. In this context, not only are targeted molecular therapy and patient genetic characteristics important factors in predicting therapeutic response, but drug repurposing can also be a valuable resource by using drugs approved for other diseases to treat cancer.

The therapeutic margin in cancer treatment is often small because the dose-toxicity curve is often close to the dose-response curve, so even small fluctuations in drug concentration can lead to severe side effects (Lowe and Lertora, 2012). Therapeutic drug monitoring (TDM) has already demonstrated its validity for assessing correct dosing, although its application is still limited to a small number of anticancer drugs (Knezevic and Clarke, 2020). Assessing genetic polymorphisms that may alter drug response can be beneficial for many reasons, including drug safety profile, patient adherence, and cost savings, not only in oncology, where PGx testing has been adopted more rapidly, but also in other areas (Roden et al., 2019). Therefore, proactive testing is becoming increasingly important for developing treatment strategies for patients based on individual genetic variability and needs, from the perspective of even more personalized medicine.

ML can improve understanding of data generated from PGx studies, increase understanding of clinical trial results, predict clinical outcomes, and discover new biomarkers even at very early stages of drug development to identify subgroups of patients who actually benefit from treatment, and subgroups of patients who do not benefit and may experience toxicity. Although the results of ML models derived from high-throughput data should be confirmed by classical functional studies, they offer researchers the opportunity to explore the extensive relationships that exist in biological processes.

Finally, ML can also be used in cancer theranostics, a combination of diagnostic and therapeutic procedures in which radioactive drugs are first used to identify the disease and then to deliver therapies. ML is a very innovative and versatile tool but the adoption of ML into routine

clinical practice is still unsettled and does not yet seem to be truly welcome. On the one hand, this feeling can be explained by the lack of standardization and the fact that specific guidelines for the use of ML have not yet been established. On the other hand, the lack of understanding of the hidden algorithms driving ML decisions may be perceived as a barrier to clinicians' skills and expertise. In addition, there is no single ML model that can solve a particular problem, so the use of a particular model is not tailored to the task at hand, which may increase the risk of complications in ML harmonization. Finally, patients should be informed and their data protected. Therefore, ethical aspects related to the security of individual data and the protection of privacy are a challenge and a mandatory requirement to gain patients' trust and prevent them from feeling threatened by ML. The innovation that the use of ML could bring to clinical practice is unquestionable and could help to improve cancer treatment towards a more personalized medicine.

Author contributions

AM: Formal Analysis, Writing–original draft, Writing–review and editing. MDB: Visualization, Writing–original draft, Writing–review and editing. GT: Visualization, Writing–original draft, Writing–review and editing, Funding acquisition. MP: Visualization, Writing–original draft, Writing–review and editing, Conceptualization, Supervision.

Funding

The author(s) declare financial support was received for the research, authorship, and/or publication of this article. This work is founded by the Progetto di Ricerca Finalizzata Regione Friuli Venezia Giulia Anno 2021 LR 13/2021, art. 8, c. 28-30 to GT (CUP J35F21002710002 of Centro di Riferimento Oncologico di Aviano, IRCCS), and by the Italian Ministry of Health (Ricerca Corrente).

Conflict of interest

The authors declare that the research was conducted in the absence of any commercial or financial relationships that could be construed as a potential conflict of interest.

Publisher's note

References

Abraham, J. E., Guo, Q., Dorling, L., Tyrer, J., Ingle, S., Hardy, R., et al. (2014). Replication of genetic polymorphisms reported to Be associated with taxane-related sensory neuropathy in patients with early breast cancer treated with paclitaxel. *Clin. Cancer Res.* 20, 2466–2475. doi:10.1158/1078-0432.CCR-13-3232

Abraham, J. P., Magee, D., Cremolini, C., Antoniotti, C., Halbert, D. D., Xiu, J., et al. (2021). Clinical validation of a machine-learning–derived signature predictive of outcomes from first-line oxaliplatin-based chemotherapy in advanced colorectal cancer. *Clin. Cancer Res.* 27, 1174–1183. doi:10.1158/1078-0432.CCR-20-3286

Akdeniz, B. C., Mattingsdal, M., Dominguez-Valentin, M., Frei, O., Shadrin, A., Puustusmaa, M., et al. (2023). A breast cancer polygenic risk score is feasible for risk stratification in the Norwegian population. *Cancers* 15, 4124. doi:10.3390/cancers15164124

Akhavan, D., Pourzia, A. L., Nourian, A. A., Williams, K. J., Nathanson, D., Babic, I., et al. (2013). De-repression of *PDGFRβ* transcription promotes acquired resistance to EGFR tyrosine kinase inhibitors in glioblastoma patients. *Cancer Discov.* 3, 534–547. doi:10.1158/2159-8290.CD-12-0502

Ali, R., Balamurali, M., and Varamini, P. (2022). Deep learning-based artificial intelligence to investigate targeted nanoparticles' uptake in TNBC cells. *IJMS* 23, 16070. doi:10.3390/ijms232416070

Altelaar, A. F. M., Munoz, J., and Heck, A. J. R. (2013). Next-generation proteomics: towards an integrative view of proteome dynamics. *Nat. Rev. Genet.* 14, 35–48. doi:10.1038/nrg3356

Altini, N., Puro, E., Taccogna, M. G., Marino, F., De Summa, S., Saponaro, C., et al. (2023). Tumor cellularity assessment of breast histopathological slides via instance segmentation and pathomic features explainability. *Bioengineering* 10, 396. doi:10.3390/bioengineering10040396

Arbitrio, M., Scionti, F., Di Martino, M. T., Caracciolo, D., Pensabene, L., Tassone, P., et al. (2021). Pharmacogenomics biomarker discovery and validation for translation in clinical practice. *Clin. Transl. Sci.* 14, 113–119. doi:10.1111/cts.12869

Auwerx, C., Sadler, M. C., Reymond, A., and Kutalik, Z. (2022). From pharmacogenetics to pharmaco-omics: milestones and future directions. *Hum. Genet. Genomics Adv.* 3, 100100. doi:10.1016/j.xhgg.2022.100100

Baas, J., Krens, L., Bohringer, S., Mol, L., Punt, C., Guchelaar, H.-J., et al. (2018). Genome wide association study to identify predictors for severe skin toxicity in colorectal cancer patients treated with cetuximab. *PLoS ONE* 13, e0208080. doi:10.1371/journal.pone.0208080

Bachet, J.-B., Laurent-Puig, P., Meurisse, A., Bouché, O., Mas, L., Taly, V., et al. (2023). Circulating tumour DNA at baseline for individualised prognostication in patients with chemotherapy-naïve metastatic colorectal cancer. An AGEO prospective study. *Eur. J. Cancer* 189, 112934. doi:10.1016/j.ejca.2023.05.022

Baker, E. K., Johnstone, R. W., Zalcberg, J. R., and El-Osta, A. (2005). Epigenetic changes to the MDR1 locus in response to chemotherapeutic drugs. *Oncogene* 24, 8061–8075. doi:10.1038/sj.onc.1208955

Balasubramaniam, S., Redon, C. E., Peer, C. J., Bryla, C., Lee, M.-J., Trepel, J. B., et al. (2018). Phase I trial of belinostat with cisplatin and etoposide in advanced solid tumors, with a focus on neuroendocrine and small cell cancers of the lung. *Anti-Cancer Drugs* 29, 457–465. doi:10.1097/CAD.0000000000000596

Barnell, E. K., Newcomer, K. F., Skidmore, Z. L., Krysiak, K., Anderson, S. R., Wartman, L. D., et al. (2021). Impact of a 40-gene targeted panel test on physician decision making for patients with acute myeloid leukemia. *JCO Precis. Oncol.* 5, 191–203. doi:10.1200/PO.20.00182

Battaglin, F., Puccini, A., Naseem, M., Schirripa, M., Berger, M. D., Tokunaga, R., et al. (2018). Pharmacogenomics in colorectal cancer: current role in clinical practice and future perspectives. *JCMT* 4, 12. doi:10.20517/2394-4722.2018.04

Bedon, L., Cecchin, E., Fabbiani, E., Dal Bo, M., Buonadonna, A., Polano, M., et al. (2022). Machine learning application in a phase I clinical trial allows for the identification of clinical-biomolecular markers significantly associated with toxicity. *Clin. Pharmacol. Ther.* 111, 686–696. doi:10.1002/cpt.2511

Bei, J.-X., Li, Y., Jia, W.-H., Feng, B.-J., Zhou, G., Chen, L.-Z., et al. (2010). A genome-wide association study of nasopharyngeal carcinoma identifies three new susceptibility loci. *Nat. Genet.* 42, 599–603. doi:10.1038/ng.601

Belkadi, A., Bolze, A., Itan, Y., Cobat, A., Vincent, Q. B., Antipenko, A., et al. (2015). Whole-genome sequencing is more powerful than whole-exome sequencing for detecting exome variants. *Proc. Natl. Acad. Sci. U.S.A.* 112, 5473–5478. doi:10.1073/pnas.1418631112

Bewicke-Copley, F., Arjun Kumar, E., Palladino, G., Korfi, K., and Wang, J. (2019). Applications and analysis of targeted genomic sequencing in cancer studies. *Comput. Struct. Biotechnol. J.* 17, 1348–1359. doi:10.1016/j.csbj.2019.10.004

Bhojwani, D., Sabin, N. D., Pei, D., Yang, J. J., Khan, R. B., Panetta, J. C., et al. (2014). Methotrexate-induced neurotoxicity and leukoencephalopathy in childhood acute lymphoblastic leukemia. *JCO* 32, 949–959. doi:10.1200/JCO.2013.53.0808

Binder, D. C., Ladomersky, E., Lenzen, A., Zhai, L., Lauing, K. L., Otto-Meyer, S. D., et al. (2018). Lessons learned from rindopepimut treatment in patients with EGFRvIII-expressing glioblastoma. *Transl. Cancer Res.* 7, S510–S513. doi:10.21037/tcr.2018.03.36

Blumenschein, G. R., Kies, M. S., Papadimitrakopoulou, V. A., Lu, C., Kumar, A. J., Ricker, J. L., et al. (2008). Phase II trial of the histone deacetylase inhibitor vorinostat (Zolinza™, suberoylanilide hydroxamic acid, SAHA) in patients with recurrent and/or metastatic head and neck cancer. *Invest. New Drugs* 26, 81–87. doi:10.1007/s10637-007-9075-2

Bode, A. M., and Dong, Z. (2017). Precision oncology-the future of personalized cancer medicine? *npj Precis. Onc* 1 (2), 2. doi:10.1038/s41698-017-0010-5

Boyd, S. (2010). Distributed optimization and statistical learning via the alternating direction method of multipliers. *FNT Mach. Learn.* 3, 1–122. doi:10.1561/2200000016

Bozic, I., Antal, T., Ohtsuki, H., Carter, H., Kim, D., Chen, S., et al. (2010). Accumulation of driver and passenger mutations during tumor progression. *Proc. Natl. Acad. Sci. U.S.A.* 107, 18545–18550. doi:10.1073/pnas.1010978107

Breiman, L. (2001). Random forest. *Mach. Learn.* 45, 5–32. doi:10.1023/A:1010933404324

Brennan, C. W., Verhaak, R. G. W., McKenna, A., Campos, B., Noushmehr, H., Salama, S. R., et al. (2013). The somatic genomic landscape of glioblastoma. *Cell* 155, 462–477. doi:10.1016/j.cell.2013.09.034

Brindha, G. R., Rishiikeshwer, B. S., Santhi, B., Nakendraprasath, K., Manikandan, R., and Gandomi, A. H. (2022). Precise prediction of multiple anticancer drug efficacy using multi target regression and support vector regression analysis. *Comput. Methods Programs Biomed.* 224, 107027. doi:10.1016/j.cmpb.2022.107027

Bukowski, K., Kciuk, M., and Kontek, R. (2020). Mechanisms of multidrug resistance in cancer chemotherapy. *IJMS* 21, 3233. doi:10.3390/ijms21093233

Bychkov, D., Linder, N., Tiulpin, A., Kücükel, H., Lundin, M., Nordling, S., et al. (2021). Deep learning identifies morphological features in breast cancer predictive of cancer ERBB2 status and trastuzumab treatment efficacy. *Sci. Rep.* 11, 4037. doi:10.1038/s41598-021-83102-6

Cao, Y., Kunaprayoon, D., and Ren, L. (2023). Interpretable AI-assisted Clinical Decision Making (CDM) for dose prescription in radiosurgery of brain metastases. *Radiotherapy Oncol.* 187, 109842. doi:10.1016/j.radonc.2023.109842

Carrillo-Perez, F., Morales, J. C., Castillo-Secilla, D., Gevaert, O., Rojas, I., and Herrera, L. J. (2022). Machine-learning-based late fusion on multi-omics and multi-scale data for non-small-cell lung cancer diagnosis. *JPM* 12, 601. doi:10.3390/jpm12040601

Caudle, K. E., Thorn, C. F., Klein, T. E., Swen, J. J., McLeod, H. L., Diasio, R. B., et al. (2013). Clinical pharmacogenetics implementation Consortium guidelines for dihydropyrimidine dehydrogenase genotype and fluoropyrimidine dosing. *Clin. Pharmacol. Ther.* 94, 640–645. doi:10.1038/clpt.2013.172

Cauvin, C., Bourguignon, L., Carriat, L., Mence, A., Ghipponi, P., Salas, S., et al. (2022). Machine-learning exploration of exposure-effect relationships of cisplatin in head and neck cancer patients. *Pharmaceutics* 14, 2509. doi:10.3390/pharmaceutics14112509

Chan, H. T., Chin, Y. M., and Low, S.-K. (2019). The roles of common variation and somatic mutation in cancer pharmacogenomics. *Oncol. Ther.* 7, 1–32. doi:10.1007/s40487-018-0090-6

Chang, Y., Park, H., Yang, H.-J., Lee, S., Lee, K.-Y., Kim, T. S., et al. (2018). Cancer drug response profile scan (CDRscan): a deep learning model that predicts drug effectiveness from cancer genomic signature. *Sci. Rep.* 8, 8857. doi:10.1038/s41598-018-27214-6

Chen, D., Liu, J., Zang, L., Xiao, T., Zhang, X., Li, Z., et al. (2022). Integrated machine learning and bioinformatic analyses constructed a novel stemness-related classifier to predict prognosis and immunotherapy responses for hepatocellular carcinoma patients. *Int. J. Biol. Sci.* 18, 360–373. doi:10.7150/ijbs.66913

Chen, T.-Y., You, L., Hardillo, J. A. U., and Chien, M.-P. (2023). Spatial transcriptomic technologies. *Cells* 12, 2042. doi:10.3390/cells12162042

Chen, X., Qian, X., Xiao, M., and Zhang, P. (2023). Survival outcomes and efficacy of platinum in early breast cancer patients with germline BRCA1 or BRCA2 mutation: a multicenter retrospective cohort study. *BCTT* 15, 671–682. doi:10.2147/BCTT.S423330

Cheng, M., Lin, R., Bai, N., Zhang, Y., Wang, H., Guo, M., et al. (2023). Deep learning for predicting the risk of immune checkpoint inhibitor-related pneumonitis in lung cancer. *Clin. Radiol.* 78, e377–e385. doi:10.1016/j.crad.2022.12.013

Cui, Y., Li, Z., Xiang, M., Han, D., Yin, Y., and Ma, C. (2022a). Machine learning models predict overall survival and progression free survival of non-surgical esophageal cancer patients with chemoradiotherapy based on CT image radiomics signatures. *Radiat. Oncol.* 17, 212. doi:10.1186/s13014-022-02186-0

Cui, Y., Wang, Q., Shi, X., Ye, Q., Lei, M., and Wang, B. (2022b). Development of a web-based calculator to predict three-month mortality among patients with bone metastases from cancer of unknown primary: an internally and externally validated study using machine-learning techniques. *Front. Oncol.* 12, 1095059. doi:10.3389/fonc.2022.1095059

Cuttano, R., Colangelo, T., Guarize, J., Dama, E., Cocomazzi, M. P., Mazzarelli, F., et al. (2022). miRNome profiling of lung cancer metastases revealed a key role for miRNA-PD-L1 axis in the modulation of chemotherapy response. *J. Hematol. Oncol.* 15, 178. doi:10.1186/s13045-022-01394-1

Dear, R. F., McGeechan, K., Jenkins, M. C., Barratt, A., Tattersall, M. H., and Wilcken, N. (2013). Combination versus sequential single agent chemotherapy for metastatic breast cancer. *Cochrane Database Syst. Rev.* 2013, CD008792. doi:10.1002/14651858.CD008792.pub2

Demetri, G. D., von Mehren, M., Blanke, C. D., Van den Abbeele, A. D., Eisenberg, B., Roberts, P. J., et al. (2002). Efficacy and safety of imatinib mesylate in advanced gastrointestinal stromal tumors. *N. Engl. J. Med.* 347, 472–480. doi:10.1056/NEJMoa020461

Deng, Q., Chen, Y., Lin, L., Lin, J., Wang, H., Qiu, Y., et al. (2023). Exosomal hsa_circRNA_047733 integrated with clinical features for preoperative prediction of lymph node metastasis risk in oral squamous cell carcinoma. *J. Oral Pathol. Med.* 52, 37–46. doi:10.1111/jop.13379

De With, M., Van Doorn, L., Kloet, E., Van Veggel, A., Matic, M., De Neijs, M. J., et al. (2023). Irinotecan-induced toxicity: a pharmacogenetic study beyond UGT1A1. *Clin. Pharmacokinet.* 62, 1589–1597. doi:10.1007/s40262-023-01279-7

Di Martino, M. T., Arbitrio, M., Leone, E., Guzzi, P. H., Saveria Rotundo, M., Ciliberto, D., et al. (2011). Single nucleotide polymorphisms of ABCC5 and ABCG1 transporter genes correlate to irinotecan-associated gastrointestinal toxicity in colorectal cancer patients: a DMET microarray profiling study. *Cancer Biol. Ther.* 12, 780–787. doi:10.4161/cbt.12.9.17781

DiMasi, J. A., Grabowski, H. G., and Hansen, R. W. (2016). Innovation in the pharmaceutical industry: new estimates of R&D costs. *J. Health Econ.* 47, 20–33. doi:10.1016/j.jhealeco.2016.01.012

Doña, I., Barrionuevo, E., Blanca-Lopez, N., Torres, M. J., Fernandez, T. D., Mayorga, C., et al. (2014). Trends in hypersensitivity drug reactions: more drugs, more response patterns, more heterogeneity. *J. Investig. Allergol. Clin. Immunol.* 24, 143–153. quiz 1 p following 153.

Dou, B., Zhu, Z., Merkurjev, E., Ke, L., Chen, L., Jiang, J., et al. (2023). Machine learning methods for small data challenges in molecular science. *Chem. Rev.* 123, 8736–8780. doi:10.1021/acs.chemrev.3c00189

Douglass, E. F., Allaway, R. J., Szalai, B., Wang, W., Tian, T., Fernández-Torras, A., et al. (2022). A community challenge for a pancancer drug mechanism of action inference from perturbational profile data. *Cell Rep. Med.* 3, 100492. doi:10.1016/j.xcrm.2021.100492

Drilon, A., Laetsch, T. W., Kummar, S., DuBois, S. G., Lassen, U. N., Demetri, G. D., et al. (2018). Efficacy of larotrectinib in *TRK* fusion–positive cancers in adults and children. *N. Engl. J. Med.* 378, 731–739. doi:10.1056/NEJMoa1714448

Druker, B. J., Sawyers, C. L., Kantarjian, H., Resta, D. J., Reese, S. F., Ford, J. M., et al. (2001). Activity of a specific inhibitor of the BCR-ABL tyrosine kinase in the blast crisis of chronic myeloid leukemia and acute lymphoblastic leukemia with the Philadelphia chromosome. *N. Engl. J. Med.* 344, 1038–1042. doi:10.1056/NEJM200104053441402

Druker, B. J., Tamura, S., Buchdunger, E., Ohno, S., Segal, G. M., Fanning, S., et al. (1996). Effects of a selective inhibitor of the Abl tyrosine kinase on the growth of Bcr–Abl positive cells. *Nat. Med.* 2, 561–566. doi:10.1038/nm0596-561

Drusian, L., Nigro, E. A., Mannella, V., Pagliarini, R., Pema, M., Costa, A. S. H., et al. (2018). mTORC1 upregulation leads to accumulation of the oncometabolite fumarate in a mouse model of renal cell carcinoma. *Cell Rep.* 24, 1093–1104. doi:10.1016/j.celrep.2018.06.106

Dytfeld, D., Luczak, M., Wrobel, T., Usnarska-Zubkiewicz, L., Brzezniakiewicz, K., Jamroziak, K., et al. (2016). Comparative proteomic profiling of refractory/relapsed multiple myeloma reveals biomarkers involved in resistance to bortezomib-based therapy. *Oncotarget* 7, 56726–56736. doi:10.18632/oncotarget.11059

Eckardt, J.-N., Bornhäuser, M., Wendt, K., and Middeke, J. M. (2022). Semi-supervised learning in cancer diagnostics. *Front. Oncol.* 12, 960984. doi:10.3389/fonc.2022.960984

Eckardt, J.-N., Röllig, C., Metzeler, K., Heisig, P., Stasik, S., Georgi, J.-A., et al. (2023). Unsupervised meta-clustering identifies risk clusters in acute myeloid leukemia based on clinical and genetic profiles. *Commun. Med.* 3, 68. doi:10.1038/s43856-023-00298-6

Eckardt, J.-N., Wendt, K., Bornhäuser, M., and Middeke, J. M. (2021). Reinforcement learning for precision oncology. *Cancers* 13, 4624. doi:10.3390/cancers13184624

Ellis, M. J., Gillette, M., Carr, S. A., Paulovich, A. G., Smith, R. D., Rodland, K. K., et al. (2013). Connecting genomic alterations to cancer biology with proteomics: the NCI clinical proteomic tumor analysis Consortium. *Cancer Discov.* 3, 1108–1112. doi:10.1158/2159-8290.CD-13-0219

Elsheikh, S. E., Green, A. R., Rakha, E. A., Powe, D. G., Ahmed, R. A., Collins, H. M., et al. (2009). Global histone modifications in breast cancer correlate with tumor phenotypes, prognostic factors, and patient outcome. *Cancer Res.* 69, 3802–3809. doi:10.1158/0008-5472.CAN-08-3907

Erfanian, N., Heydari, A. A., Feriz, A. M., Iañez, P., Derakhshani, A., Ghasemigol, M., et al. (2023). Deep learning applications in single-cell genomics and transcriptomics data analysis. *Biomed. Pharmacother.* 165, 115077. doi:10.1016/j.biopha.2023.115077

Erickson, B. J., Korfiatis, P., Akkus, Z., and Kline, T. L. (2017). Machine learning for medical imaging. *RadioGraphics* 37, 505–515. doi:10.1148/rg.2017160130

Fazi, B., Felsani, A., Grassi, L., Moles, A., D'Andrea, D., Toschi, N., et al. (2015). The transcriptome and miRNome profiling of glioblastoma tissues and peritumoral regions highlights molecular pathways shared by tumors and surrounding areas and reveals differences between short-term and long-term survivors. *Oncotarget* 6, 22526–22552. doi:10.18632/oncotarget.4151

Fogel, D. B. (2018). Factors associated with clinical trials that fail and opportunities for improving the likelihood of success: a review. *Contemp. Clin. Trials Commun.* 11, 156–164. doi:10.1016/j.conctc.2018.08.001

Galanis, E., Jaeckle, K. A., Maurer, M. J., Reid, J. M., Ames, M. M., Hardwick, J. S., et al. (2009). Phase II trial of vorinostat in recurrent glioblastoma multiforme: a north central cancer treatment group study. *JCO* 27, 2052–2058. doi:10.1200/JCO.2008.19.0694

Garon, E. B., Reck, M., Nishio, K., Heymach, J. V., Nishio, M., Novello, S., et al. (2023). Ramucirumab plus erlotinib versus placebo plus erlotinib in previously untreated EGFR-mutated metastatic non-small-cell lung cancer (RELAY): exploratory analysis of next-generation sequencing results. *ESMO Open* 8, 101580. doi:10.1016/j.esmoop.2023.101580

Gayvert, K. M., Aly, O., Platt, J., Bosenberg, M. W., Stern, D. F., and Elemento, O. (2017). A computational approach for identifying synergistic drug combinations. *PLoS Comput. Biol.* 13, e1005308. doi:10.1371/journal.pcbi.1005308

Ge, C., Gu, I.Y.-H., Jakola, A. S., and Yang, J. (2020). Deep semi-supervised learning for brain tumor classification. *BMC Med. Imaging* 20, 87. doi:10.1186/s12880-020-00485-0

Glewis, S., Lingaratnam, S., Krishnasamy, M., H Martin, J., Tie, J., Alexander, M., et al. (2023). Pharmacogenetics testing (DPYD and UGT1A1) for fluoropyrimidine and irinotecan in routine clinical care: perspectives of medical oncologists and oncology pharmacists. *J. Oncol. Pharm. Pract.* 2023, 107815522311675. doi:10.1177/10781552231167554

Goey, A. K. L., Sissung, T. M., Peer, C. J., Trepel, J. B., Lee, M., Tomita, Y., et al. (2016). Effects of *UGT1A1* genotype on the pharmacokinetics, pharmacodynamics, and toxicities of belinostat administered by 48-hour continuous infusion in patients with cancer. *J. Clin. Pharma* 56, 461–473. doi:10.1002/jcph.625

Guengerich, F. P. (2011). Mechanisms of drug toxicity and relevance to pharmaceutical development. *Drug Metabolism Pharmacokinet.* 26, 3–14. doi:10.2133/dmpk.DMPK-10-RV-062

Guo, L., Wang, W., Xie, X., Wang, S., and Zhang, Y. (2023). Machine learning for genetic prediction of chemotherapy toxicity in cervical cancer. *Biomed. Pharmacother.* 161, 114518. doi:10.1016/j.biopha.2023.114518

Halawani, R., Buchert, M., and Chen, Y.-P. P. (2023). Deep learning exploration of single-cell and spatially resolved cancer transcriptomics to unravel tumour heterogeneity. *Comput. Biol. Med.* 164, 107274. doi:10.1016/j.compbiomed.2023.107274

Handelman, G. S., Kok, H. K., Chandra, R. V., Razavi, A. H., Lee, M. J., and Asadi, H. (2018). eDoctor: machine learning and the future of medicine. *J. Intern Med.* 284, 603–619. doi:10.1111/joim.12822

Harrer, S., Shah, P., Antony, B., and Hu, J. (2019). Artificial intelligence for clinical trial design. *Trends Pharmacol. Sci.* 40, 577–591. doi:10.1016/j.tips.2019.05.005

Harrison, R. K. (2016). Phase II and phase III failures: 2013–2015. *Nat. Rev. Drug Discov.* 15, 817–818. doi:10.1038/nrd.2016.184

Heo, Y. J., Hwa, C., Lee, G.-H., Park, J.-M., and An, J.-Y. (2021). Integrative multi-omics approaches in cancer research: from biological networks to clinical subtypes. *Mol. Cells* 44, 433–443. doi:10.14348/molcells.2021.0042

Hertz, D. L., Arwood, M. J., Stocco, G., Singh, S., Karnes, J. H., and Ramsey, L. B. (2021). Planning and conducting a pharmacogenetics association study. *Clin Pharma Ther.* 110, 688–701. doi:10.1002/cpt.2270

Hoffmann, F., Franzen, A., De Vos, L., Wuest, L., Kulcsár, Z., Fietz, S., et al. (2023). CTLA4 DNA methylation is associated with CTLA-4 expression and predicts response to immunotherapy in head and neck squamous cell carcinoma. *Clin. Epigenet* 15, 112. doi:10.1186/s13148-023-01525-6

Hörst, F., Ting, S., Liffers, S.-T., Pomykala, K. L., Steiger, K., Albertsmeier, M., et al. (2023). Histology-based prediction of therapy response to neoadjuvant chemotherapy for esophageal and esophagogastric junction adenocarcinomas using deep learning. *JCO Clin. Cancer Inf.* 7, e2300038. doi:10.1200/CCI.23.00038

Hou, Y. C., Neidich, J. A., Duncavage, E. J., Spencer, D. H., and Schroeder, M. C. (2022). Clinical whole-genome sequencing in cancer diagnosis. *Hum. Mutat.* 43, 1519–1530. doi:10.1002/humu.24381

Huang, C., Mezencev, R., McDonald, J. F., and Vannberg, F. (2017). Open source machine-learning algorithms for the prediction of optimal cancer drug therapies. *PLoS ONE* 12, e0186906. doi:10.1371/journal.pone.0186906

Huang, X., Yan, J., Zhang, M., Wang, Y., Chen, Y., Fu, X., et al. (2018). Targeting epigenetic crosstalk as a therapeutic strategy for EZH2-aberrant solid tumors. *Cell* 175, 186–199. doi:10.1016/j.cell.2018.08.058

Hussen, B. M., Abdullah, S. T., Salihi, A., Sabir, D. K., Sidiq, K. R., Rasul, M. F., et al. (2022). The emerging roles of NGS in clinical oncology and personalized medicine. *Pathology - Res. Pract.* 230, 153760. doi:10.1016/j.prp.2022.153760

Hwang, T. J., Carpenter, D., Lauffenburger, J. C., Wang, B., Franklin, J. M., and Kesselheim, A. S. (2016). Failure of investigational drugs in late-stage clinical development and publication of trial results. *JAMA Intern Med.* 176, 1826–1833. doi:10.1001/jamainternmed.2016.6008

Ideker, T., Thorsson, V., Ranish, J. A., Christmas, R., Buhler, J., Eng, J. K., et al. (2001). Integrated genomic and proteomic analyses of a systematically perturbed metabolic network. *Science* 292, 929–934. doi:10.1126/science.292.5518.929

Innocenti, F., Undevia, S. D., Iyer, L., Xian Chen, P., Das, S., Kocherginsky, M., et al. (2004). Genetic variants in the *UDP-glucuronosyltransferase 1A1* gene predict the risk of severe neutropenia of irinotecan. *JCO* 22, 1382–1388. doi:10.1200/JCO.2004.07.173

Ismail, S., and Essawi, M. (2012). Genetic polymorphism studies in humans: Middle East. *J. Med. Genet.* 1, 57–63. doi:10.1097/01.MXE.0000415225.85003.47

Iyer, L., Das, S., Janisch, L., Wen, M., Ramírez, J., Karrison, T., et al. (2002). UGT1A1*28 polymorphism as a determinant of irinotecan disposition and toxicity. *Pharmacogenomics J.* 2, 43–47. doi:10.1038/sj.tpj.6500072

Jalloul, R., Chethan, H. K., and Alkhatib, R. (2023). A review of machine learning techniques for the classification and detection of breast cancer from medical images. *Diagnostics* 13, 2460. doi:10.3390/diagnostics13142460

James, G., Witten, D., Hastie, T., and Tibshirani, R. (2013). *An introduction to statistical learning: with applications in R* (New York: Springer). Springer texts in statistics.

Jiang, C., Yang, W., Moriyama, T., Liu, C., Smith, C., Yang, W., et al. (2021). Effects of *NT5C2* germline variants on 6-mecaptopurine metabolism in children with acute lymphoblastic leukemia. *Clin. Pharmacol. Ther.* 109, 1538–1545. doi:10.1002/cpt.2095

Jiang, L., Jiang, C., Yu, X., Fu, R., Jin, S., and Liu, X. (2022). DeepTTA: a transformer-based model for predicting cancer drug response. *Briefings Bioinforma.* 23, bbac100. doi:10.1093/bib/bbac100

Jing, Y., Liu, J., Ye, Y., Pan, L., Deng, H., Wang, Y., et al. (2020). Multi-omics prediction of immune-related adverse events during checkpoint immunotherapy. *Nat. Commun.* 11, 4946. doi:10.1038/s41467-020-18742-9

Jun, H. J., Acquaviva, J., Chi, D., Lessard, J., Zhu, H., Woolfenden, S., et al. (2012). Acquired MET expression confers resistance to EGFR inhibition in a mouse model of glioblastoma multiforme. *Oncogene* 31, 3039–3050. doi:10.1038/onc.2011.474

Kang, J., Chowdhry, A. K., Pugh, S. L., and Park, J. H. (2023). Integrating artificial intelligence and machine learning into cancer clinical trials. *Seminars Radiat. Oncol.* 33, 386–394. doi:10.1016/j.semradonc.2023.06.004

Kim, H., Lee, S. J., Lee, I. K., Min, S. C., Sung, H. H., Jeong, B. C., et al. (2020). Synergistic effects of combination therapy with AKT and mTOR inhibitors on bladder cancer cells. *IJMS* 21, 2825. doi:10.3390/ijms21082825

Kim, Y., Armstrong, T. S., Gilbert, M. R., and Celiku, O. (2023). A critical analysis of neuro-oncology clinical trials. *Neuro Oncol.* 25, 1658–1671. doi:10.1093/neuonc/noad036

Kimchi-Sarfaty, C., Oh, J. M., Kim, I.-W., Sauna, Z. E., Calcagno, A. M., Ambudkar, S. V., et al. (2007). A "silent" polymorphism in the *MDR* 1 gene changes substrate specificity. *Science* 315, 525–528. doi:10.1126/science.1135308

Kindler, C., Elfwing, S., Öhrvik, J., and Nikberg, M. (2023). A deep neural network–based decision support tool for the detection of lymph node metastases in colorectal cancer specimens. *Mod. Pathol.* 36, 100015. doi:10.1016/j.modpat.2022.100015

Kline, A., Wang, H., Li, Y., Dennis, S., Hutch, M., Xu, Z., et al. (2022). Multimodal machine learning in precision health: a scoping review. *npj Digit. Med.* 5, 171. doi:10.1038/s41746-022-00712-8

Knezevic, C. E., and Clarke, W. (2020). Cancer chemotherapy: the case for therapeutic drug monitoring. *Ther. Drug Monit.* 42, 6–19. doi:10.1097/FTD.0000000000000701

Kondo, Y., and Issa, J.-P. J. (2004). Epigenetic changes in colorectal cancer. *Cancer Metastasis Rev.* 23, 29–39. doi:10.1023/A:1025806911782

Körber, N. (2023). MIA is an open-source standalone deep learning application for microscopic image analysis. *Cell Rep. Methods* 3, 100517. doi:10.1016/j.crmeth.2023.100517

Koteluk, O., Wartecki, A., Mazurek, S., Kołodziejczak, I., and Mackiewicz, A. (2021). How do machines learn? Artificial intelligence as a new era in medicine. *JPM* 11, 32. doi:10.3390/jpm11010032

Kourou, K., Exarchos, T. P., Exarchos, K. P., Karamouzis, M. V., and Fotiadis, D. I. (2015). Machine learning applications in cancer prognosis and prediction. *Comput. Struct. Biotechnol. J.* 13, 8–17. doi:10.1016/j.csbj.2014.11.005

Kouzarides, T. (2007). Chromatin modifications and their function. *Cell* 128, 693–705. doi:10.1016/j.cell.2007.02.005

Kriegeskorte, N., and Golan, T. (2019). Neural network models and deep learning. *Curr. Biol.* 29, R231–R236. doi:10.1016/j.cub.2019.02.034

Kwok, W. C., Lam, D. C. L., Ip, M. S. M., Tam, T. C. C., and Ho, J. C. M. (2022). Association of genetic polymorphisms of CYP3A4 and CYP2D6 with gefitinib-induced toxicities. *Anti-Cancer Drugs* 33, 1139–1144. doi:10.1097/CAD.0000000000001360

Kwon, M.-S., Kim, Y., Lee, S., Namkung, J., Yun, T., Yi, S. G., et al. (2015). Integrative analysis of multi-omics data for identifying multi-markers for diagnosing pancreatic cancer. *BMC Genomics* 16, S4. doi:10.1186/1471-2164-16-S9-S4

Lakhotia, S. C., Mallick, B., and Roy, J. (2020). Non-coding RNAs: ever-expanding diversity of types and functions. *Rna-Based Regul. Hum. Health Dis.* 19, 5–57. doi:10.1016/B978-0-12-817193-6.00002-9

Lambin, P., Rios-Velazquez, E., Leijenaar, R., Carvalho, S., Van Stiphout, R. G. P. M., Granton, P., et al. (2012). Radiomics: extracting more information from medical images using advanced feature analysis. *Eur. J. Cancer* 48, 441–446. doi:10.1016/j.ejca.2011.11.036

Lauschke, V. M., Milani, L., and Ingelman-Sundberg, M. (2018). Pharmacogenomic biomarkers for improved drug therapy—recent progress and future developments. *AAPS J.* 20, 4. doi:10.1208/s12248-017-0161-x

LeCun, Y., Bengio, Y., and Hinton, G. (2015). Deep learning. *Nature* 521, 436–444. doi:10.1038/nature14539

Lee, J. O., Kang, M. J., Byun, W. S., Kim, S. A., Seo, I. H., Han, J.Ah., et al. (2019). Metformin overcomes resistance to cisplatin in triple-negative breast cancer (TNBC) cells by targeting RAD51. *Breast Cancer Res.* 21, 115. doi:10.1186/s13058-019-1204-2

Lenahan, A. L., Squire, A. E., and Miller, D. E. (2023). Panels, exomes, genomes, and more—finding the best path through the diagnostic odyssey. *Pediatr. Clin. N. Am.* 70, 905–916. doi:10.1016/j.pcl.2023.06.001

Lešnjaković, L., Ganoci, L., Bilić, I., Šimičević, L., Mucalo, I., Pleština, S., et al. (2023). *DPYD* genotyping and predicting fluoropyrimidine toxicity: where do we stand? *Pharmacogenomics* 24, 93–106. doi:10.2217/pgs-2022-0135

Lheureux, S., Prokopec, S. D., Oldfield, L. E., Gonzalez-Ochoa, E., Bruce, J. P., Wong, D., et al. (2023). Identifying mechanisms of resistance by circulating tumor DNA in EVOLVE, a phase II trial of cediranib plus olaparib for ovarian cancer at time of PARP inhibitor progression. *Clin. Cancer Res.* 29, 3706–3716. doi:10.1158/1078-0432.CCR-23-0797

Li, M., Mei, S., Yang, Y., Shen, Y., and Chen, L. (2022). Strategies to mitigate the on- and off-target toxicities of recombinant immunotoxins: an antibody engineering perspective. *Antib. Ther.* 5, 164–176. doi:10.1093/abt/tbac014

Li, R., Tian, Y., Yang, Z., Ji, Y., Ding, J., and Yan, A. (2023). Classification models and SAR analysis on HDAC1 inhibitors using machine learning methods. *Mol. Divers* 27, 1037–1051. doi:10.1007/s11030-022-10466-w

Li, X., and Wang, C.-Y. (2021). From bulk, single-cell to spatial RNA sequencing. *Int. J. Oral Sci.* 13, 36. doi:10.1038/s41368-021-00146-0

Lin, B., Ziebro, J., Smithberger, E., Skinner, K. R., Zhao, E., Cloughesy, T. F., et al. (2022). EGFR, the Lazarus target for precision oncology in glioblastoma. *Neuro-Oncology* 24, 2035–2062. doi:10.1093/neuonc/noac204

Lincoln, S. E., Hambuch, T., Zook, J. M., Bristow, S. L., Hatchell, K., Truty, R., et al. (2021). One in seven pathogenic variants can be challenging to detect by NGS: an analysis of 450,000 patients with implications for clinical sensitivity and genetic test implementation. *Genet. Med.* 23, 1673–1680. doi:10.1038/s41436-021-01187-w

Lionel, A. C., Costain, G., Monfared, N., Walker, S., Reuter, M. S., Hosseini, S. M., et al. (2018). Improved diagnostic yield compared with targeted gene sequencing panels suggests a role for whole-genome sequencing as a first-tier genetic test. *Genet. Med.* 20, 435–443. doi:10.1038/gim.2017.119

Li S, S., Yang, M., Ji, L., and Fan, H. (2022). A multi-omics machine learning framework in predicting the recurrence and metastasis of patients with pancreatic adenocarcinoma. *Front. Microbiol.* 13, 1032623. doi:10.3389/fmicb.2022.1032623

Liu, Y., Sun, J., Sun, H., and Chang, Y. (2022). Identification of key somatic oncogenic mutation based on a confounder-free causal inference model. *PLoS Comput. Biol.* 18, e1010529. doi:10.1371/journal.pcbi.1010529

Liu, Z., Lin, G., Yan, Z., Li, L., Wu, X., Shi, J., et al. (2022). Predictive mutation signature of immunotherapy benefits in NSCLC based on machine learning algorithms. *Front. Immunol.* 13, 989275. doi:10.3389/fimmu.2022.989275

Louis, D. N., Perry, A., Wesseling, P., Brat, D. J., Cree, I. A., Figarella-Branger, D., et al. (2021). The 2021 WHO classification of tumors of the central nervous system: a summary. *Neuro-Oncology* 23, 1231–1251. doi:10.1093/neuonc/noab106

Loukovaara, M., Pasanen, A., and Bützow, R. (2021). Mismatch repair protein and *MLH1* methylation status as predictors of response to adjuvant therapy in endometrial cancer. *Cancer Med.* 10, 1034–1042. doi:10.1002/cam4.3691

Lowe, E. S., and Lertora, J. J. L. (2012). "Dose–effect and concentration–effect analysis," in *Principles of clinical pharmacology* (Elsevier), 343–356. doi:10.1016/B978-0-12-385471-1.00020-9

Lv, B., Xu, R., Xing, X., Liao, C., Zhang, Z., Zhang, P., et al. (2022). Discovery of synergistic drug combinations for colorectal cancer driven by tumor barcode derived from metabolomics "big data.". *Metabolites* 12, 494. doi:10.3390/metabo12060494

Lynch, T. J., Bell, D. W., Sordella, R., Gurubhagavatula, S., Okimoto, R. A., Brannigan, B. W., et al. (2004). Activating mutations in the epidermal growth factor receptor underlying responsiveness of non–small-cell lung cancer to gefitinib. *N. Engl. J. Med.* 350, 2129–2139. doi:10.1056/NEJMoa040938

Ma, T., Liu, Q., Li, H., Zhou, M., Jiang, R., and Zhang, X. (2022). DualGCN: a dual graph convolutional network model to predict cancer drug response. *BMC Bioinforma.* 23, 129. doi:10.1186/s12859-022-04664-4

Maeda, A., Ando, H., Irie, K., Hashimoto, N., Morishige, J.-I., Fukushima, S., et al. (2023). Effects of *ABCB1* and *ABCG2* polymorphisms on the pharmacokinetics of abemaciclib metabolites (M2, M20, M18). *Anticancer Res.* 43, 1283–1289. doi:10.21873/anticanres.16275

Malta, T. M., Sokolov, A., Gentles, A. J., Burzykowski, T., Poisson, L., Weinstein, J. N., et al. (2018). Machine learning identifies stemness features associated with oncogenic dedifferentiation. *Cell* 173, 338–354.e15. doi:10.1016/j.cell.2018.03.034

Mandelker, D., and Ceyhan-Birsoy, O. (2020). Evolving significance of tumor-normal sequencing in cancer care. *Trends Cancer* 6, 31–39. doi:10.1016/j.trecan.2019.11.006

Marcus, L., Fashoyin-Aje, L. A., Donoghue, M., Yuan, M., Rodriguez, L., Gallagher, P. S., et al. (2021). FDA approval summary: pembrolizumab for the treatment of tumor mutational burden–high solid tumors. *Clin. Cancer Res.* 27, 4685–4689. doi:10.1158/1078-0432.CCR-21-0327

Martin-Broto, J., Valverde, C., Hindi, N., Vincenzi, B., Martinez-Trufero, J., Grignani, G., et al. (2023). REGISTRI: regorafenib in first-line of KIT/PDGFRA wild type metastatic GIST: a collaborative Spanish (GEIS), Italian (ISG) and French Sarcoma Group (FSG) phase II trial. *Mol. Cancer* 22, 127. doi:10.1186/s12943-023-01832-9

Massella, M., Dri, D. A., and Gramaglia, D. (2022). Regulatory considerations on the use of machine learning based tools in clinical trials. *Health Technol.* 12, 1085–1096. doi:10.1007/s12553-022-00708-0

Massi, M. C., Gasperoni, F., Ieva, F., Paganoni, A. M., Zunino, P., Manzoni, A., et al. (2020). A deep learning approach validates genetic risk factors for late toxicity after prostate cancer radiotherapy in a REQUITE multi-national cohort. *Front. Oncol.* 10, 541281. doi:10.3389/fonc.2020.541281

Mathijssen, R. H. J., Marsh, S., Karlsson, M. O., Xie, R., Baker, S. D., Verweij, J., et al. (2003). Irinotecan pathway genotype analysis to predict pharmacokinetics. *Clin. Cancer Res.* 9, 3246–3253.

McGrail, D. J., Pilié, P. G., Rashid, N. U., Voorwerk, L., Slagter, M., Kok, M., et al. (2021). High tumor mutation burden fails to predict immune checkpoint blockade response across all cancer types. *Ann. Oncol.* 32, 661–672. doi:10.1016/j.annonc.2021.02.006

McLaren, D. B., and Aitman, T. J. (2023). Redefining precision radiotherapy through liquid biopsy. *Br. J. Cancer* 129, 900–903. doi:10.1038/s41416-023-02398-5

Meienberg, J., Bruggmann, R., Oexle, K., and Matyas, G. (2016). Clinical sequencing: is WGS the better WES? *Hum. Genet.* 135, 359–362. doi:10.1007/s00439-015-1631-9

Meißner, A.-K., Gutsche, R., Galldiks, N., Kocher, M., Jünger, S. T., Eich, M.-L., et al. (2022). Radiomics for the noninvasive prediction of the BRAF mutation status in patients with melanoma brain metastases. *Neuro-Oncology* 24, 1331–1340. doi:10.1093/neuonc/noab294

Menden, M. P., Iorio, F., Garnett, M., McDermott, U., Benes, C. H., Ballester, P. J., et al. (2013). Machine learning prediction of cancer cell sensitivity to drugs based on genomic and chemical properties. *PLoS ONE* 8, e61318. doi:10.1371/journal.pone.0061318

Meng, S., Li, M., Qin, L., Lv, J., Wu, D., Zheng, D., et al. (2023). The onco-embryonic antigen ROR1 is a target of chimeric antigen T cells for colorectal cancer. *Int. Immunopharmacol.* 121, 110402. doi:10.1016/j.intimp.2023.110402

Merino, D. M., McShane, L. M., Fabrizio, D., Funari, V., Chen, S.-J., White, J. R., et al. (2020). Establishing guidelines to harmonize tumor mutational burden (TMB): *in silico* assessment of variation in TMB quantification across diagnostic platforms: phase I of the Friends of Cancer Research TMB Harmonization Project. *J. Immunother. Cancer* 8, e000147. doi:10.1136/jitc-2019-000147

Miettunen, J., Nordström, T., Kaakinen, M., and Ahmed, A. O. (2016). Latent variable mixture modeling in psychiatric research – a review and application. *Psychol. Med.* 46, 457–467. doi:10.1017/S0033291715002305

Mitchell, T. M. (2013). "Machine learning, nachdr," in *McGraw-hill series in computer science* (New York: McGraw-Hill).

Moon, I., LoPiccolo, J., Baca, S. C., Sholl, L. M., Kehl, K. L., Hassett, M. J., et al. (2023). Machine learning for genetics-based classification and treatment response prediction in cancer of unknown primary. *Nat. Med.* 29, 2057–2067. doi:10.1038/s41591-023-02482-6

Morel, A., Boisdron-Celle, M., Fey, L., Soulie, P., Craipeau, M. C., Traore, S., et al. (2006). Clinical relevance of different dihydropyrimidine dehydrogenase gene single nucleotide polymorphisms on 5-fluorouracil tolerance. *Mol. Cancer Ther.* 5, 2895–2904. doi:10.1158/1535-7163.MCT-06-0327

Moriyama, T., Nishii, R., Perez-Andreu, V., Yang, W., Klussmann, F. A., Zhao, X., et al. (2016). NUDT15 polymorphisms alter thiopurine metabolism and hematopoietic toxicity. *Nat. Genet.* 48, 367–373. doi:10.1038/ng.3508

Mu, W., Li, B., Wu, S., Chen, J., Sain, D., Xu, D., et al. (2019). Detection of structural variation using target captured next-generation sequencing data for genetic diagnostic testing. *Genet. Med.* 21, 1603–1610. doi:10.1038/s41436-018-0397-6

Naik, K., Goyal, R. K., Foschini, L., Chak, C. W., Thielscher, C., Zhu, H., et al. (2023). Current status and future directions: the application of artificial intelligence/machine learning (AI/ML) for precision medicine. *Clin Pharma Ther. cpt* 3152. doi:10.1002/cpt.3152

Nebert, D. W. (1999). Pharmacogenetics and pharmacogenomics: why is this relevant to the clinical geneticist? pharmacogenetics and pharmacogenomics. *Clin. Genet.* 56, 247–258. doi:10.1034/j.1399-0004.1999.560401.x

Nicolae, D. L., Gamazon, E., Zhang, W., Duan, S., Dolan, M. E., and Cox, N. J. (2010). Trait-associated SNPs are more likely to Be eQTLs: annotation to enhance discovery from GWAS. *PLoS Genet.* 6, e1000888. doi:10.1371/journal.pgen.1000888

Nindra, U., Pal, A., Bray, V., Yip, P. Y., Tognela, A., Roberts, T. L., et al. (2023). Utility of multigene panel next-generation sequencing in routine clinical practice for identifying genomic alterations in newly diagnosed metastatic nonsmall cell lung cancer. *Intern. Med. J. imj* 2023, 16224. doi:10.1111/imj.16224

Niraula, D., Jamaluddin, J., Matuszak, M. M., Haken, R. K. T., and Naqa, I. E. (2021). Quantum deep reinforcement learning for clinical decision support in oncology: application to adaptive radiotherapy. *Sci. Rep.* 11, 23545. doi:10.1038/s41598-021-02910-y

Noor, F., Asif, M., Ashfaq, U. A., Qasim, M., and Tahir Ul Qamar, M. (2023). Machine learning for synergistic network pharmacology: a comprehensive overview. *Briefings Bioinforma.* 24, bbad120. doi:10.1093/bib/bbad120

Nozawa, T., Minami, H., Sugiura, S., Tsuji, A., and Tamai, I. (2005). Role of organic anion transporter Oatp1b1 (oatp-C) in hepatic uptake of irinotecan and its active metabolite, 7-ethyl-10-hydroxycamptothecin: *in vitro* evidence and effect of single nucleotide polymorphisms. *Drug Metab. Dispos.* 33, 434–439. doi:10.1124/dmd.104.001909

On, J., Park, H.-A., and Yoo, S. (2022). Development of a prediction models for chemotherapy-induced adverse drug reactions: a retrospective observational study using electronic health records. *Eur. J. Oncol. Nurs.* 56, 102066. doi:10.1016/j.ejon.2021.102066

Organ isation mondiale de la santé, Centre international de recherche sur le cancer (2020). "Soft tissue and bone tumours," in *World health organization classification of tumours*. 5th ed (Geneva: OMS).

Orozco-Arias, S., Piña, J. S., Tabares-Soto, R., Castillo-Ossa, L. F., Guyot, R., and Isaza, G. (2020). Measuring performance metrics of machine learning algorithms for detecting and classifying transposable elements. *Transposable Elem. Process.* 8, 638. doi:10.3390/pr8060638

Pacurari, A. C., Bhattarai, S., Muhammad, A., Avram, C., Mederle, A. O., Rosca, O., et al. (2023). Diagnostic accuracy of machine learning ai architectures in detection and classification of lung cancer: a systematic review. *Diagnostics* 13, 2145. doi:10.3390/diagnostics13132145

Park, A., Lee, Y., and Nam, S. (2023). A performance evaluation of drug response prediction models for individual drugs. *Sci. Rep.* 13, 11911. doi:10.1038/s41598-023-39179-2

Parsons, D. W., Janeway, K. A., Patton, D. R., Winter, C. L., Coffey, B., Williams, P. M., et al. (2022). Actionable tumor alterations and treatment protocol enrollment of pediatric and young adult patients with refractory cancers in the national cancer institute–children's oncology group pediatric MATCH trial. *JCO* 40, 2224–2234. doi:10.1200/JCO.21.02838

Patellongi, I., Amiruddin, A., Massi, M. N., Islam, A. A., Pratama, M. Y., Sutandyo, N., et al. (2023). Circulating miR-221/222 expression as microRNA biomarker predicting tamoxifen treatment outcome: a case–control study. *Ann. Med. Surg.* 85, 3806–3815. doi:10.1097/MS9.0000000000001061

Patti, G. J., Yanes, O., and Siuzdak, G. (2012). Innovation: metabolomics: the apogee of the omics trilogy. *Nat. Rev. Mol. Cell Biol.* 13, 263–269. doi:10.1038/nrm3314

Peeters, S. L., Deenen, M. J., Thijs, A. M., Hulshof, E. C., Mathijssen, R. H., Gelderblom, H., et al. (2023). *UGT1A1* genotype-guided dosing of irinotecan: time to prioritize patient safety. *Pharmacogenomics* 24, 435–439. doi:10.2217/pgs-2023-0096

Peng, D., Kryczek, I., Nagarsheth, N., Zhao, L., Wei, S., Wang, W., et al. (2015). Epigenetic silencing of TH1-type chemokines shapes tumour immunity and immunotherapy. *Nature* 527, 249–253. doi:10.1038/nature15520

Pixberg, C., Zapatka, M., Hlevnjak, M., Benedetto, S., Suppelna, J. P., Heil, J., et al. (2022). COGNITION: a prospective precision oncology trial for patients with early breast cancer at high risk following neoadjuvant chemotherapy. *ESMO Open* 7, 100637. doi:10.1016/j.esmoop.2022.100637

Podgorelec, V., Kokol, P., Stiglic, B., and Rozman, I. (2002). Decision trees: an overview and their use in medicine. *J. Med. Syst.* 26, 445–463. doi:10.1023/A:1016409317640

Polano, M., Bedon, L., Bo, M. D., Sorio, R., Bartoletti, M., De Mattia, E., et al. (2023). Machine learning application identifies germline markers of hypertension in ovarian cancer patients treated with carboplatin, taxane and bevacizumab. *Clin. Pharmacol. Ther.* 2023, 2960. doi:10.1002/cpt.2960

Pushpakom, S., Iorio, F., Eyers, P. A., Escott, K. J., Hopper, S., Wells, A., et al. (2019). Drug repurposing: progress, challenges and recommendations. *Nat. Rev. Drug Discov.* 18, 41–58. doi:10.1038/nrd.2018.168

Quintanilha, J. C. F., Geyer, S., Etheridge, A. S., Racioppi, A., Hammond, K., Crona, D. J., et al. (2022a). KDR genetic predictor of toxicities induced by sorafenib and regorafenib. *Pharmacogenomics J.* 22, 251–257. doi:10.1038/s41397-022-00279-3

Quintanilha, J. C. F., Wang, J., Sibley, A. B., Xu, W., Espin-Garcia, O., Jiang, C., et al. (2022b). Genome-wide association studies of survival in 1520 cancer patients treated with bevacizumab-containing regimens. *Intl J. Cancer* 150, 279–289. doi:10.1002/ijc.33810

Ramesh, P., Karuppasamy, R., and Veerappapillai, S. (2022). Machine learning driven drug repurposing strategy for identification of potential RET inhibitors against non-small cell lung cancer. *Med. Oncol.* 40, 56. doi:10.1007/s12032-022-01924-4

Relling, M. V., Schwab, M., Whirl-Carrillo, M., Suarez-Kurtz, G., Pui, C., Stein, C. M., et al. (2019). Clinical pharmacogenetics implementation Consortium guideline for thiopurine dosing based on *TPMT* and *NUDT 15* genotypes: 2018 update. *Clin Pharma Ther.* 105, 1095–1105. doi:10.1002/cpt.1304

Robles, J., Pintado-Berninches, L., Boukich, I., Escudero, B., De Los Rios, V., Bartolomé, R. A., et al. (2022). A prognostic six-gene expression risk-score derived from proteomic profiling of the metastatic colorectal cancer secretome. *J. Pathology CR* 8, 495–508. doi:10.1002/cjp2.294

Roden, D. M., McLeod, H. L., Relling, M. V., Williams, M. S., Mensah, G. A., Peterson, J. F., et al. (2019). Pharmacogenomics. *Lancet* 394, 521–532. doi:10.1016/S0140-6736(19)31276-0

Rojahn, S., Hambuch, T., Adrian, J., Gafni, E., Gileta, A., Hatchell, H., et al. (2022). Scalable detection of technically challenging variants through modified next-generation sequencing. *Molec Gen Gen Med* 10, e2072. doi:10.1002/mgg3.2072

Romero, A., Martín, M., Oliva, B., De La Torre, J., Furio, V., De La Hoya, M., et al. (2012). Glutathione S-transferase P1 c.313A > G polymorphism could be useful in the prediction of doxorubicin response in breast cancer patients. *Ann. Oncol.* 23, 1750–1756. doi:10.1093/annonc/mdr483

Romero, J. M., Titmuss, E., Wang, Y., Vafiadis, J., Pacis, A., Jang, G. H., et al. (2023). Chemokine expression predicts T cell-inflammation and improved survival with checkpoint inhibition across solid cancers. *npj Precis. Onc.* 7, 73. doi:10.1038/s41698-023-00428-2

Roy, B., Stepišnik, T., Vens, C., Džeroski, S., and Džeroski, S. (2022). Survival analysis with semi-supervised predictive clustering trees. *Comput. Biol. Med.* 141, 105001. doi:10.1016/j.compbiomed.2021.105001

Rudmann, D. G. (2013). On-target and off-target-based toxicologic effects. *Toxicol. Pathol.* 41, 310–314. doi:10.1177/0192623312464311

Ryan, D. K., Maclean, R. H., Balston, A., Scourfield, A., Shah, A. D., and Ross, J. (2023). Artificial intelligence and machine learning for clinical pharmacology. *Brit J. Clin. Pharma bcp* 2023, 15930. doi:10.1111/bcp.15930

Sajda, P. (2006). Machine learning for detection and diagnosis of disease. *Annu. Rev. Biomed. Eng.* 8, 537–565. doi:10.1146/annurev.bioeng.8.061505.095802

Sbaraglia, M., Bellan, E., and Dei Tos, A. P. (2020). The 2020 WHO classification of soft tissue tumours: news and perspectives. *Pathologica* 113, 70–84. doi:10.32074/1591-951X-213

Schoot, V. V. D., Viellevoije, S. J., Tammer, F., Brunner, H. G., Arens, Y., Yntema, H. G., et al. (2021). The impact of unsolicited findings in clinical exome sequencing, a qualitative interview study. *Eur. J. Hum. Genet.* 29, 930–939. doi:10.1038/s41431-021-00834-9

Schroth, W., Antoniadou, L., Fritz, P., Schwab, M., Muerdter, T., Zanger, U. M., et al. (2007). Breast cancer treatment outcome with adjuvant tamoxifen relative to patient CYP2D6 and CYP2C19 genotypes. *JCO* 25, 5187–5193. doi:10.1200/JCO.2007.12.2705

Sengupta, D., Zeng, L., Li, Y., Hausmann, S., Ghosh, D., Yuan, G., et al. (2021). NSD2 dimethylation at H3K36 promotes lung adenocarcinoma pathogenesis. *Mol. Cell* 81, 4481–4492.e9. doi:10.1016/j.molcel.2021.08.034

Sepulveda, A. R., Hamilton, S. R., Allegra, C. J., Grody, W., Cushman-Vokoun, A. M., Funkhouser, W. K., et al. (2017). Molecular biomarkers for the evaluation of colorectal cancer: guideline from the American society for clinical pathology, college of American pathologists, association for molecular pathology, and American society of clinical oncology. *J. Mol. Diagnostics* 19, 187–225. doi:10.1016/j.jmoldx.2016.11.001

Shahin, M. H., Barth, A., Podichetty, J. T., Liu, Q., Goyal, N., Jin, J. Y., et al. (2023). Artificial intelligence: from buzzword to useful tool in clinical pharmacology. *Clin Pharma Ther. cpt* 2023, 3083. doi:10.1002/cpt.3083

Sharma, M., Krüger, R., and Gasser, T. (2014). From genome-wide association studies to next-generation sequencing: lessons from the past and planning for the future. *JAMA Neurol.* 71, 5–6. doi:10.1001/jamaneurol.2013.3682

Shen, Y., Kim, I., and Tang, Y. (2023). Uncovering the heterogeneity of cardiac lin −KIT + cells: a scRNA-seq study on the identification of subpopulations. *Stem Cells* 41, 958–970. doi:10.1093/stmcls/sxad057

Shi, M., Sheng, Z., and Tang, H. (2021). Prognostic outcome prediction by semi-supervised least squares classification. *Briefings Bioinforma.* 22, bbaa249. doi:10.1093/bib/bbaa249

Shrestha, R., Llaurado Fernandez, M., Dawson, A., Hoenisch, J., Volik, S., Lin, Y.-Y., et al. (2021). Multiomics characterization of low-grade serous ovarian carcinoma identifies potential biomarkers of MEK inhibitor sensitivity and therapeutic vulnerability. *Cancer Res.* 81, 1681–1694. doi:10.1158/0008-5472.CAN-20-2222

Sims, D., Sudbery, I., Ilott, N. E., Heger, A., and Ponting, C. P. (2014). Sequencing depth and coverage: key considerations in genomic analyses. *Nat. Rev. Genet.* 15, 121–132. doi:10.1038/nrg3642

Sra, S., Nowozin, S., and Wright, S. J. (2012). *Optimization for machine learning, Neural information processing series*. Cambridge: MIT press.

Steinberg, A. N., Bowman, C. L., and White, F. E. (1999). "Revisions to the JDL data fusion model," in *Presented at the AeroSense '99*. Editor B. V. Dasarathy (Orlando, FL: SPIE Digital Library), 430. doi:10.1117/12.341367

Stevanovski, I., Chintalaphani, S. R., Gamaarachchi, H., Ferguson, J. M., Pineda, S. S., Scriba, C. K., et al. (2022). Comprehensive genetic diagnosis of tandem repeat expansion disorders with programmable targeted nanopore sequencing. *Sci. Adv.* 8, eabm5386. doi:10.1126/sciadv.abm5386

Stockley, T. L., Lo, B., Box, A., Corredor, A. G., DeCoteau, J., Desmeules, P., et al. (2023). CANTRK: a Canadian ring study to optimize detection of NTRK gene fusions by next-generation RNA sequencing. *J. Mol. Diagnostics* 25, 168–174. doi:10.1016/j.jmoldx.2022.12.004

Sweeney, C., Ambrosone, C. B., Joseph, L., Stone, A., Hutchins, L. F., Kadlubar, F. F., et al. (2003). Association between a glutathioneS-transferase A1 promoter polymorphism and survival after breast cancer treatment. *Int. J. Cancer* 103, 810–814. doi:10.1002/ijc.10896

Swen, J. J., Van Der Wouden, C. H., Manson, L. E., Abdullah-Koolmees, H., Blagec, K., Blagus, T., et al. (2023). A 12-gene pharmacogenetic panel to prevent adverse drug reactions: an open-label, multicentre, controlled, cluster-randomised crossover implementation study. *Lancet* 401, 347–356. doi:10.1016/S0140-6736(22)01841-4

Tabl, A. A., Alkhateeb, A., ElMaraghy, W., Rueda, L., and Ngom, A. (2019). A machine learning approach for identifying gene biomarkers guiding the treatment of breast cancer. *Front. Genet.* 10, 256. doi:10.3389/fgene.2019.00256

Tan, D., Mohd Nasir, N. F., Abdul Manan, H., and Yahya, N. (2023). Prediction of toxicity outcomes following radiotherapy using deep learning-based models: a systematic review. *Cancer/Radiothérapie* 27, 398–406. doi:10.1016/j.canrad.2023.05.001

Tan, H. T., Lee, Y. H., and Chung, M. C. M. (2012). Cancer proteomics: CANCER PROTEOMICS. *Mass Spectrom. Rev.* 31, 583–605. doi:10.1002/mas.20356

Tao, L. R., Ye, Y., and Zhao, H. (2023). Early breast cancer risk detection: a novel framework leveraging polygenic risk scores and machine learning. *J. Med. Genet. jmedgenet-* 60, 960–964. doi:10.1136/jmg-2022-108582

Tate, A. R., Underwood, J., Acosta, D. M., Julià-Sapé, M., Majós, C., Moreno-Torres, À., et al. (2006). Development of a decision support system for diagnosis and grading of brain tumours using*in vivo* magnetic resonance single voxel spectra. *NMR Biomed.* 19, 411–434. doi:10.1002/nbm.1016

The Cancer Genome Atlas Research NetworkWeinstein, J. N., Collisson, E. A., Mills, G. B., Shaw, K. R. M., Ozenberger, B. A., et al. (2013). The cancer genome Atlas pan-cancer analysis project. *Nat. Genet.* 45, 1113–1120. doi:10.1038/ng.2764

Toth, M., Boros, I. M., and Balint, E. (2012). Elevated level of lysine 9-acetylated histone H3 at the MDR1 promoter in multidrug-resistant cells. *Cancer Sci.* 103, 659–669. doi:10.1111/j.1349-7006.2012.02215.x

Treangen, T. J., and Salzberg, S. L. (2012). Repetitive DNA and next-generation sequencing: computational challenges and solutions. *Nat. Rev. Genet.* 13, 36–46. doi:10.1038/nrg3117

Ubels, J., Schaefers, T., Punt, C., Guchelaar, H.-J., and De Ridder, J. (2020). RAINFOREST: a random forest approach to predict treatment benefit in data from (failed) clinical drug trials. *Bioinformatics* 36, i601–i609. doi:10.1093/bioinformatics/btaa799

Uffelmann, E., Huang, Q. Q., Munung, N. S., De Vries, J., Okada, Y., Martin, A. R., et al. (2021). Genome-wide association studies. *Nat. Rev. Methods Prim.* 1, 59. doi:10.1038/s43586-021-00056-9

Van Der Lee, M., and Swen, J. J. (2023). Artificial intelligence in pharmacology research and practice. *Clin. Transl. Sci.* 16, 31–36. doi:10.1111/cts.13431

Vogel, C., De Sousa Abreu, R., Ko, D., Le, S., Shapiro, B. A., Burns, S. C., et al. (2010). Sequence signatures and mRNA concentration can explain two-thirds of protein abundance variation in a human cell line. *Mol. Syst. Biol.* 6, 400. doi:10.1038/msb.2010.59

Wang, L., Pelleymounter, L., Weinshilboum, R., Johnson, J. A., Hebert, J. M., Altman, R. B., et al. (2010). Very important pharmacogene summary: thiopurine S-methyltransferase. *Pharmacogenetics Genomics* 20, 401–405. doi:10.1097/FPC.0b013e3283352860

Wang, M. H., Cordell, H. J., and Van Steen, K. (2019). Statistical methods for genome-wide association studies. *Seminars Cancer Biol.* 55, 53–60. doi:10.1016/j.semcancer.2018.04.008

Wang, W., Li, X., Qin, X., Miao, Y., Zhang, Y., Li, S., et al. (2023). Germline *Neurofibromin 1* mutation enhances the anti-tumour immune response and decreases juvenile myelomonocytic leukaemia tumourigenicity. *Br. J. Haematol.* 202, 328–343. doi:10.1111/bjh.18851

Wang, X., Tokheim, C., Gu, S. S., Wang, B., Tang, Q., Li, Y., et al. (2021). *In vivo* CRISPR screens identify the E3 ligase Cop1 as a modulator of macrophage infiltration and cancer immunotherapy target. *Cell* 184, 5357–5374. doi:10.1016/j.cell.2021.09.006

Wang, Y., Xiao, F., Zhao, Y., Mao, C.-X., Yu, L.-L., Wang, L.-Y., et al. (2022). A two-stage genome-wide association study to identify novel genetic loci associated with acute radiotherapy toxicity in nasopharyngeal carcinoma. *Mol. Cancer* 21, 169. doi:10.1186/s12943-022-01631-8

Wang, Y., Yang, Y., Chen, S., and Wang, J. (2021). DeepDRK: a deep learning framework for drug repurposing through kernel-based multi-omics integration. *Briefings Bioinforma.* 22, bbab048. doi:10.1093/bib/bbab048

Weiss, L., Dorman, K., Boukovala, M., Schwinghammer, F., Jordan, P., Fey, T., et al. (2023). Early clinical trial unit tumor board: a real-world experience in a national cancer network. *J. Cancer Res. Clin. Oncol.* 149, 13383–13390. doi:10.1007/s00432-023-05196-x

Werner, R., Connolly, A., Bennett, M., Hand, C. K., and Burke, L. (2022). Implementation of an ISO15189 accredited next-generation sequencing service with the fully automated Ion Torrent Genexus: the experience of a clinical diagnostic laboratory. *J. Clin. Pathol. jcp* 2022, 208625. doi:10.1136/jcp-2022-208625

Wong, C. H., Siah, K. W., and Lo, A. W. (2019). Corrigendum: estimation of clinical trial success rates and related parameters. *Biostatistics* 20, 366. doi:10.1093/biostatistics/kxy072

Woodman, R. J., and Mangoni, A. A. (2023). A comprehensive review of machine learning algorithms and their application in geriatric medicine: present and future. *Aging Clin. Exp. Res.* 35, 2363–2397. doi:10.1007/s40520-023-02552-2

Wu, F., Lu, M., Qu, L., Li, D.-Q., and Hu, C.-H. (2015). DNA methylation of hMLH1 correlates with the clinical response to cisplatin after a surgical resection in Non-small cell lung cancer. *Int. J. Clin. Exp. Pathol.* 8, 5457–5463.

Wu, L.-X., Wen, C.-J., Li, Y., Zhang, X., Shao, Y.-Y., Yang, Z., et al. (2015). Interindividual epigenetic variation in ABCB1 promoter and its relationship with ABCB1 expression and function in healthy Chinese subjects: interindividual epigenetic variation in ABCB1 in healthy Chinese subjects. *Br. J. Clin. Pharmacol.* 80, 1109–1121. doi:10.1111/bcp.12675

Xu, J., Zheng, M., Thng, D. K. H., Toh, T. B., Zhou, L., Bonney, G. K., et al. (2023). NanoBeacon.AI: AI-enhanced nanodiamond biosensor for automated sensitivity prediction to oxidative phosphorylation inhibitors. *ACS Sens.* 8, 1989–1999. doi:10.1021/acssensors.3c00126

Xu, W., Yang, H., Liu, Y., Yang, Y., Wang, P., Kim, S.-H., et al. (2011). Oncometabolite 2-hydroxyglutarate is a competitive inhibitor of α-ketoglutarate-dependent dioxygenases. *Cancer Cell* 19, 17–30. doi:10.1016/j.ccr.2010.12.014

Yu, Y., Werdyani, S., Carey, M., Parfrey, P., Yilmaz, Y. E., and Savas, S. (2021). A comprehensive analysis of SNPs and CNVs identifies novel markers associated with disease outcomes in colorectal cancer. *Mol. Oncol.* 15, 3329–3347. doi:10.1002/1878-0261.13067

Yu, Z., Ye, X., Liu, H., Li, H., Hao, X., Zhang, J., et al. (2022). Predicting lapatinib dose regimen using machine learning and deep learning techniques based on a real-world study. *Front. Oncol.* 12, 893966. doi:10.3389/fonc.2022.893966

Zeng, X., Zhu, S., Lu, W., Liu, Z., Huang, J., Zhou, Y., et al. (2020). Target identification among known drugs by deep learning from heterogeneous networks. *Chem. Sci.* 11, 1775–1797. doi:10.1039/C9SC04336E

Zhang, D., Dorman, K., Heinrich, K., Weiss, L., Boukovala, M., Haas, M., et al. (2023). A retrospective analysis of biliary tract cancer patients presented to the molecular tumor board at the comprehensive cancer center munich. *Targ. Oncol.* 18, 767–776. doi:10.1007/s11523-023-00985-3

Zhang, H., Huang, J., Chen, R., Cai, H., Chen, Y., He, S., et al. (2022). Ligand- and structure-based identification of novel CDK9 inhibitors for the potential treatment of leukemia. *Bioorg. Med. Chem.* 72, 116994. doi:10.1016/j.bmc.2022.116994

Zhang, J., Baran, J., Cros, A., Guberman, J. M., Haider, S., Hsu, J., et al. (2011). International cancer genome Consortium data portal--a one-stop shop for cancer genomics data. *Database* 2011, bar026. doi:10.1093/database/bar026

Zhang, X., Wu, J., Baeza, J., Gu, K., Zheng, Y., Chen, S., et al. (2023). DeepTAP: an RNN-based method of TAP-binding peptide prediction in the selection of tumor neoantigens. *Comput. Biol. Med.* 164, 107247. doi:10.1016/j.compbiomed.2023.107247

Zhou, H., Hua, Z., Gao, J., Lin, F., Chen, Y., Zhang, S., et al. (2023). Multitask deep learning-based whole-process system for automatic diagnosis of breast lesions and axillary lymph node metastasis discrimination from dynamic contrast-enhanced-mri: a multicenter study. *Magn. Reson. Imaging jmri* 2023, 28913. doi:10.1002/jmri.28913

Zhou, M., Yan, J., Chen, Q., Yang, Y., Li, Y., Ren, Y., et al. (2022). Association of H3K9me3 with breast cancer prognosis by estrogen receptor status. *Clin. Epigenet* 14, 135. doi:10.1186/s13148-022-01363-y

Zhu, E. Y., and Dupuy, A. J. (2022). Machine learning approach informs biology of cancer drug response. *BMC Bioinforma.* 23, 184. doi:10.1186/s12859-022-04720-z

frontiers | Frontiers in Pharmacology

TYPE Original Research
PUBLISHED 31 January 2024
DOI 10.3389/fphar.2023.1320028

OPEN ACCESS

EDITED BY
Shaoqiu Chen,
University of Hawaii at Mānoa,
United States

REVIEWED BY
Xuanmao Jiao,
Baruch S. Blumberg Institute,
United States
Shuai Wang,
New York University, United States

*CORRESPONDENCE
Gang Luo,
455130699@qq.com
Chongwen Xu,
henao22@xjtu.edu.cn

RECEIVED 11 October 2023
ACCEPTED 11 December 2023
PUBLISHED 31 January 2024

CITATION
Feng L, Wang R, Zhao Q, Wang J, Luo G and Xu C (2024), Racial disparities in metastatic colorectal cancer outcomes revealed by tumor microbiome and transcriptome analysis with bevacizumab treatment.
Front. Pharmacol. 14:1320028.
doi: 10.3389/fphar.2023.1320028

Racial disparities in metastatic colorectal cancer outcomes revealed by tumor microbiome and transcriptome analysis with bevacizumab treatment

Lei Feng[1,2], Rui Wang[3], Qian Zhao[1], Jun Wang[4], Gang Luo[1,2]* and Chongwen Xu[1]*

[1]Department of Otorhinolaryngology-Head and Neck Surgery, The First Affiliated Hospital of Xi'an Jiaotong University, Xi'an, Shaanxi, China, [2]Department of Surgical Oncology, Hanzhong People's Hospital, Hanzhong, Shaanxi, China, [3]Department of Thoracic Surgery, Cancer Centre, The First Affiliated Hospital of Xi'an Jiaotong University, Xi'an, Shaanxi, China, [4]Tongji Hospital Tongji Medical College of HUST, Wuhan, China

Background: Metastatic colorectal cancer (mCRC) is a heterogeneous disease, often associated with poor outcomes and resistance to therapies. The racial variations in the molecular and microbiological profiles of mCRC patients, however, remain under-explored.

Methods: Using RNA-SEQ data, we extracted and analyzed actively transcribing microbiota within the tumor milieu, ensuring that the identified bacteria were not merely transient inhabitants but engaged in the tumor ecosystem. Also, we independently acquired samples from 12 mCRC patients, specifically, 6 White individuals and 6 of Black or African American descent. These samples underwent 16S rRNA sequencing.

Results: Our study revealed notable racial disparities in the molecular signatures and microbiota profiles of mCRC patients. The intersection of these data showcased the potential modulating effects of specific bacteria on gene expression. Particularly, the bacteria *Helicobacter* cinaedi and Sphingobium herbicidovorans emerged as significant influencers, with strong correlations to the genes SELENBP1 and SNORA38, respectively.

Discussion: These findings underscore the intricate interplay between host genomics and actively transcribing tumor microbiota in mCRC's pathogenesis. The identified correlations between specific bacteria and genes highlight potential avenues for targeted therapies and a more personalized therapeutic approach.

KEYWORDS

mCRC, transcriptomics, intratumoral microbiome, multi-omics, racial variations, bevacizumab

Introduction

Colorectal cancer, a global health challenge, ranks among the top causes of cancer-related deaths (Xi and Xu, 2021). Specifically, metastatic colorectal cancer (mCRC) represents a particularly aggressive form, often associated with poor prognosis (Mazzoli et al., 2022). Recent data indicate that while treatment strategies for mCRC have evolved, the

median survival for advanced-stage patients remains suboptimal, hovering around 29 months (Lonardi et al., 2022). Amidst the therapeutic arsenal available for mCRC, Bevacizumab, an angiogenesis inhibitor targeting the vascular endothelial growth factor (VEGF), has emerged as a frontrunner (Chionh et al., 2022; de Rauglaudre et al., 2022). Clinical trials have demonstrated its efficacy in prolonging survival and improving response rates when combined with standard chemotherapy regimens (Fang et al., 2023; He et al., 2023).

As the era of personalized medicine takes center stage in oncology, it becomes increasingly clear that traditional, broad-spectrum approaches often fall short in addressing the unique genetic and molecular profiles of individual tumors (Pauli et al., 2017; LeSavage et al., 2022). The shift towards tailored therapies is rooted in the growing recognition of the complexity and diversity of the tumor microenvironment (Vitale et al., 2019). This intricate milieu, rich in cellular interactions and molecular crosstalk, is a testament to the dynamic nature of cancer (Lee and Schmitt, 2019). A conglomerate of stromal cells, immune cells, signaling molecules, and a diverse array of microorganisms, the tumor microenvironment stands at the crossroads of cancer progression, dictating not only the trajectory of tumor growth but also its susceptibility or resistance to treatments (Wu and Dai, 2017; Maacha et al., 2019). Pioneering investigations have cast a spotlight on the tumor microbiome, unraveling its deep-seated influence on cancer biology (Helmink et al., 2019; Wong-Rolle et al., 2021). These microbial communities, often specific to tumor types or even individual patients, have been linked to various aspects of cancer development, ranging from tumorigenesis to metastasis (Fu et al., 2022; Fu et al., 2023). More intriguingly, emerging evidence points to the microbiome's role in modulating therapeutic responses, potentially by influencing drug metabolism, modulating the host immune response, or even directly interacting with therapeutic agents (Michaudel and Sokol, 2020; Nejman et al., 2020). Simultaneously, advances in genomics have ushered in the age of transcriptomics, providing unprecedented insights into the genetic orchestra that underpins tumor behavior (Tian et al., 2023). The tumor transcriptome, a real-time snapshot of gene expression, serves as a rich repository of information (Hunter et al., 2021). It not only charts the active genetic pathways within the tumor but also holds clues to potential points of vulnerabilities (Li et al., 2020). As such, transcriptomic analyses can unmask patterns of gene expressions that herald treatment resistances, or conversely, pinpoint genetic signatures predictive of therapeutic responsiveness (Casamassimi et al., 2017).

Nevertheless, while the intersections of the tumor microbiome and transcriptome with mCRC treatments have been explored, a significant blind spot remains: the influence of racial disparities (Carethers and Doubeni, 2020). It's well-documented that racial and ethnic differences can drastically affect disease outcomes (de Klerk et al., 2018). For instance, African Americans with colorectal cancer have a 20% higher incidence rate and a 40% higher mortality rate compared to their Caucasian counterparts (Cobb et al., 2022). Such disparities could arise from a confluence of genetic variations, environmental exposures, and even socio-economic factors (Zaki et al., 2023). However, the specific molecular and microbial underpinnings, especially in the context of mCRC and Bevacizumab treatment, remain largely uncharted.

In this comprehensive study, we endeavor to bridge this knowledge gap. We aim to dissect the interplay of racial disparities with the tumor microbiome and transcriptome in mCRC patients undergoing Bevacizumab treatment. By unraveling the microbial and genetic nuances specific to different racial groups, we aspire to pave the way for more tailored therapeutic strategies, ensuring that the promise of personalized medicine is extended across all racial and ethnic divides.

Materials and methods

Tumor microbiome profiling through RNA sequencing

To delve deeper into the tumor microbiome, we embarked on an analytical journey using high-throughput RNA sequencing (RNA-seq) data, which was obtained from the renowned public repository, GEO, under the accession number GSE196576 (Innocenti et al., 2022). The initial step in our analytical pipeline emphasized the significance of data quality. Thus, we applied FastQC, a widely recognized quality control tool for high throughput sequence data, ensuring that our RNA-seq reads were of optimal quality for subsequent analyses. Recognizing the potential interference of host-associated reads in our microbial profiling, it was imperative to segregate them. This was adeptly accomplished using Samtools, a suite that's pivotal for intricate interactions with high-throughput sequencing data. With the host reads meticulously filtered out, our focus transitioned to the crux of our analysis—taxonomic classification. For this intricate task, we employed Kraken2. Renowned for its unparalleled precision and efficiency in metagenomic classification, Kraken2 provided the granularity we sought in our taxonomic assignments.

Transcriptome data processing using the nf-core/rnaseq pipeline

In our quest to unravel the intricacies of the tumor transcriptome, we leveraged the prowess of the "nf-core/rnaseq" pipeline, a cutting-edge framework meticulously curated by the nextflow community. This pipeline is not just a mere tool but an embodiment of state-of-the-art practices in RNA-seq data processing, harmonizing multiple essential processes into a cohesive workflow. The "nf-core/rnaseq" pipeline commences with quality control checks on raw sequencing data using FastQC, ensuring the data's integrity. It then proceeds to read trimming, leveraging the capabilities of Trimmomatic to remove any adapters or low-quality sequences, ensuring only high-fidelity reads are retained for downstream processes. The trimmed reads are subsequently aligned to the reference genome using the STAR aligner, a tool celebrated for its speed and accuracy in RNA-seq read mapping. Post alignment, featureCounts tallies the number of reads associated with each gene, enabling a quantitative overview of gene expression. Moreover, the pipeline integrates various quality control metrics post-alignment using tools like RSeQC, ensuring that the resultant data remains of the highest caliber for downstream analyses.

Clinical sample collection

Clinical tissue samples were meticulously collected from patients diagnosed with metastatic colorectal cancer (mCRC). A total of 18 mCRC patients were enrolled in this study, with six individuals identifying as White and six as Black or African American and six Asian. Informed consent was obtained from all participants prior to sample collection, following the ethical guidelines set by the Institutional Review Board (IRB). Tissue samples were procured during surgical resection of primary tumors. The collected tissues were immediately snap-frozen in liquid nitrogen and stored at −80°C until further analysis to preserve the RNA and microbial integrity. Patient data, including age, sex, race, and clinical outcomes, were anonymized and recorded. Through this standardized and ethically compliant process, we ensured the reliability and validity of the clinical samples used in our study.

16S rRNA sequencing

To meticulously decipher the microbiota landscape within mCRC tissues, we employed 16S rRNA gene sequencing, a gold-standard technique for studying microbial communities present within biological samples. Tissue samples were diligently collected from 12 patients diagnosed with mCRC, with six identifying as White and the remaining six as Black or African American. Each sample was immediately snap-frozen to preserve the integrity of the microbial DNA. Subsequently, microbial DNA was extracted using a PureLink™ Microbiome DNA Purification Kit (Thermo Fisher, United States), adhering strictly to the manufacturer's protocol to ensure consistency and reliability in the extracted genetic material. The V3-V4 hypervariable regions of the 16S rRNA gene were amplified using universal primers; V3-V4 PRIMER-F 5′-CCTACGGRRBGCASCAGKVRVGAAT-3′and PRIMER -R 5′-GGACTACNVGGGTWTCTAATCC-3′. The PCR reaction was meticulously optimized to produce reliable and reproducible results. Upon completion of the PCR process, the amplified products were verified through agarose gel electrophoresis. Thereafter, the PCR products were purified, quantified, and pooled equimolarly for sequencing. The pooled samples were then sequenced on an Illumina MiSeq platform, utilizing a 2 × 300 bp paired-end configuration, thereby generating comprehensive and high-resolution data of the microbial communities present within each sample.

RT-PCR

Total RNA was extracted from the CRC tissue samples using the RNeasy Mini Kit (Qiagen, Hilden, Germany), following the manufacturer's protocol. The quality and concentration of the isolated RNA were meticulously assessed using the NanoDrop ND-1000 spectrophotometer (NanoDrop Technologies, Wilmington, DE, United States). Quantitative PCR was performed using the Power SYBR Green PCR Master Mix (Applied Biosystems, Foster City, CA, United States) on a 7,500 Fast Real-Time PCR System (Applied Biosystems). Primers for the target genes, SELENBP1 and SNORA38, and the housekeeping gene GAPDH were designed using the Primer Express Software (Applied Biosystems). The specific primer sequences of SELENBP1 forward: 5′-ACCCAGGGAAGAGATCGTCTA-3′, reverse: 5′-ACTTGG GGTCAACATCCACAG-3′; SNORA38 forward: 5′-CGTGTC TGTGGTTCCCTGTC-3′, reverse: 5′- AGCAAGCTGGCCTCA AAGTT-3′; GAPDH forward: 5′-CATGTACGTTGCTATCCA GGC-3′, reverse: 5′-CTCCTTAATGTCACGCACGAT-3′. Each reaction was conducted in triplicate, with the mean value used for further analysis. The thermal cycling conditions were as follows: initial denaturation at 95°C for 10 min, followed by 40 cycles of denaturation at 95°C for 15 s, and annealing and extension at 60°C for 1 min.

Revisiting the clinical trial

In the vast tapestry of the CALGB/SWOG 80405 trial, our present endeavor narrows its gaze on two specific regimens: bevacizumab and the synergistic cetuximab/bevacizumab combination. This refined focus stems from the quest to unravel the intricacies of these treatments in a more granular context. To discern the interplay of race and its potential influence on clinical outcomes, bridging the gap between genetics and therapeutic efficacy. Our investigation seeks to disentangle the nuanced relationship between diverse racial backgrounds and their respective clinical trajectories. By delving deep into the databank of the trial, we meticulously sift through patient demographics, juxtaposing them against an array of clinical parameters (Table 1). This rigorous exploration is not just an academic exercise but an attempt to unmask the subtle, often overlooked racial disparities that might modulate treatment responses. While the original CALGB/SWOG 80405 trial offered a broad panorama, our analysis is akin to a magnifying glass, emphasizing the details, drawing correlations, and aiming to enhance the personalized medicine paradigm. With the guiding light of trial identifier NCT00265850, we embark on this journey to understand better the racial tapestry in the context of bevacizumab and cetuximab/bevacizumab treatments.

Statistical analysis and data interpretation

Navigating the complex interplay between transcriptomics, the tumor microbiome, and racial disparities in metastatic colorectal cancer necessitated a robust and comprehensive statistical framework. Our analytical journey commenced with data acquisition from the public repository GSE196576, part of the GEO database. For differential expression analysis, we leveraged Python's "scipy.stats" library to perform the Student's *t*-test, ensuring a rigorous identification of genes with notable expression differences. The threshold of significance was set based on an adjusted *p*-value, incorporating the Benjamini–Hochberg correction, and was set at less than 0.05. All analyses were conducted using Python version 3.10. The microbial dimension of our study called for both alpha and beta diversity analyses. While alpha diversity provided a lens into the richness and evenness of microbial entities within individual samples, beta diversity was instrumental in highlighting the compositional variations between samples, thus elucidating

10.3389/fphar.2023.1320028

TABLE 1 Comprehensive clinical demographics and characteristics by ethnicity.

Characteristic/Attribute	Black or African American	White	Asian	Not reported
Total patients	33	314	7	5
Age (years)				
Median	54	61.5	57	57
Range	(32–79)	(24–82)	(25–74)	(50–70)
Gender				
Female	11	125	3	1
Male	22	189	4	4
Progression free survival time (months)				
Median	8.9	8.7	11.1	11.9
Follow up time (months)				
Median	22.7	22.2	16.9	26.3
ECOG performance status				
Median	1	1	1	0
Number of metastatic sites				
Liver (Median)	1	1	1	1
Adjuvant. Chemotherapy				
YES	10	121	3	2
NO	23	193	4	3
Pelvic. Radiation				
YES	2	32	0	0
NO	31	282	7	5
KRAS				
wt	10	116	—	1
mut	7	33	—	
Unknown	16	165	7	4
NRAS				
wt	17	144	—	1
mut	—	5	—	—
Unknown	16	165	7	4
MSI status				
MSS	13	128	—	1
MSI-H	2	12	—	—
MSI-L	2	6	—	—
Unknown	16	168	7	4
Side				
Right	8	80	—	1
Left	8	55	—	—

(Continued on following page)

TABLE 1 (*Continued*) **Comprehensive clinical demographics and characteristics by ethnicity.**

Characteristic/Attribute	Black or African American	White	Asian	Not reported
Transverse	—	7	—	—
Unknown	17	172	7	4

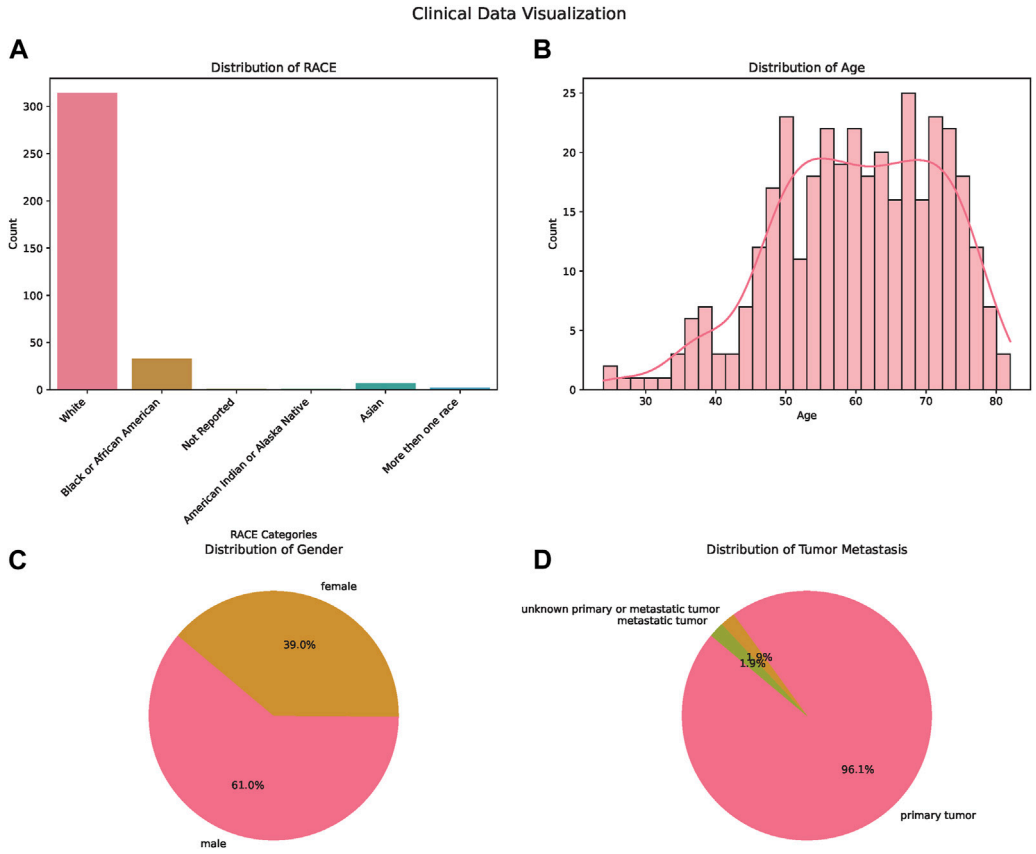

FIGURE 1
Demographic and Clinical Characteristics of the Study Population. **(A)** Bar chart illustrating the distribution of patients across different ethnicities: White, Asian, Black or African American, and American Indian or Alaska Native. **(B)** Bar chart displaying age distribution of the patients, providing insights into the age range and median age of the participants. **(C)** Pie chart showcasing the gender distribution of the study participants, highlighting the proportions of male and female patients. **(D)** Pie chart depicting the tumor metastasis status among the patients, signifying the proportion of patients with and without tumor metastasis.

intergroup differences. For correlation assessments, the Pearson correlation coefficients, derived using Python's "scipy" and "pandas" libraries, served as a beacon, revealing linear associations between specific microbiota and gene expression levels. Notably, only correlations with an absolute value of ($|r| > 0.5$) and a p-value below 0.05 were deemed significant. Survival patterns, central to understanding treatment efficacy, were dissected using Kaplan-Meier survival plots generated via the "lifelines" Python package. Distinctions between survival curves underwent rigorous statistical scrutiny via the log-rank test, while multivariate Cox regression analyses fine-tuned our understanding, bringing potential confounders into the analytical fold and pinpointing independent predictors of outcomes. The art of data visualization was paramount. With Python's "matplotlib" and "seaborn" libraries at our disposal, we crafted insightful visual representations, spanning from heatmaps to boxplots. Given the dimensionality of our transcriptomic data and the plethora of tests, the Benjamini–Hochberg procedure was indispensable in controlling the false discovery rate, cementing the statistical reliability of our findings.

Results

Ethnicity-centric clinical and genetic analysis of patients

In our comprehensive analysis of patient demographics and clinical characteristics stratified by ethnicity, we observed distinct patterns (Table 1). Most of the participants were of White descent

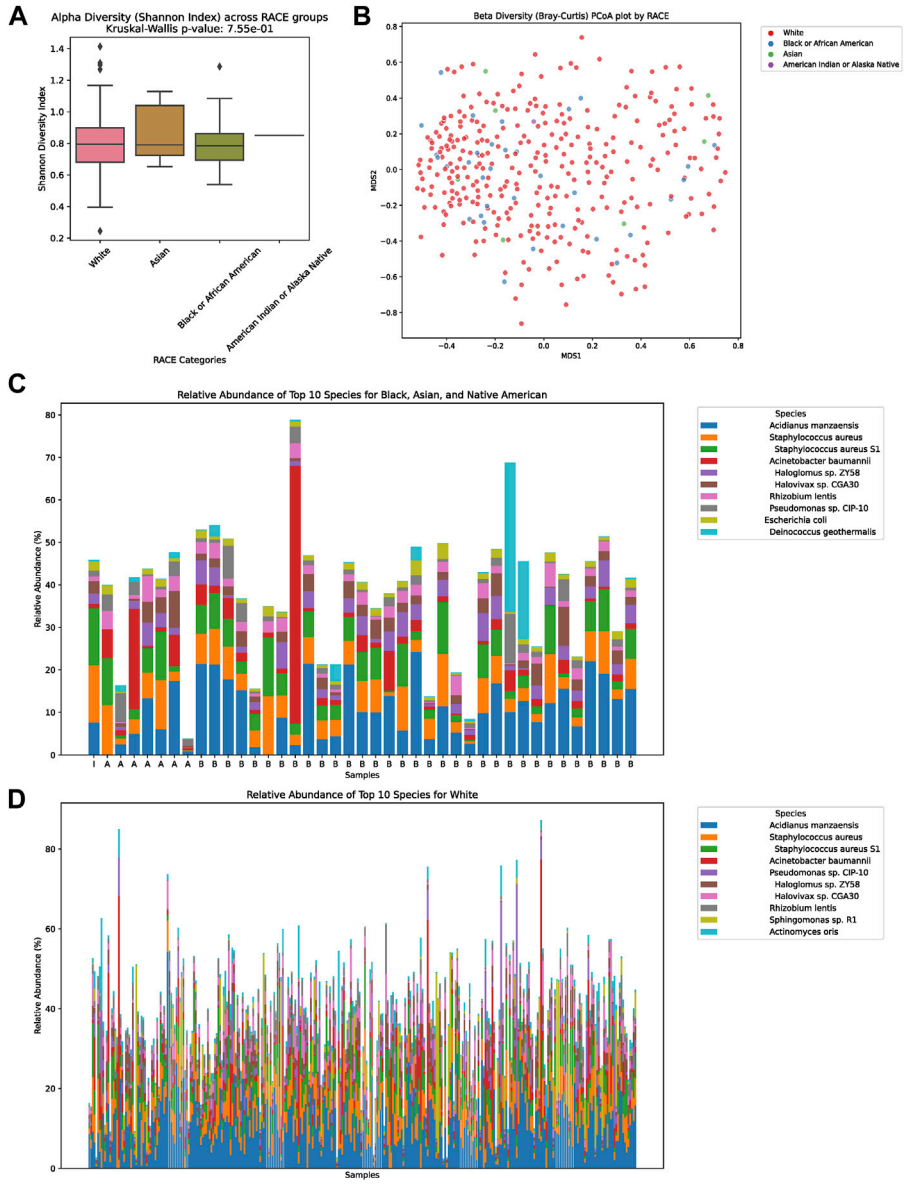

FIGURE 2
Diversity and Composition of the Tumor Microbiome Across Ethnic Groups. **(A)** Alpha diversity representation across the four ethnic groups: White, Asian, Black or African American, and American Indian or Alaska Native. No significant differences were observed among the groups (p = 0.755). **(B)** Beta diversity illustrated via a PCoA plot, showing microbial community differences between samples among the ethnicities. **(C)** Relative abundance of the top ten microbial species for the combined group of Asian, Black or African American, and American Indian or Alaska Native. The dominant species in this group were Acidianus manzaensis, *Staphylococcus aureus*, *Staphylococcus aureus* S1, *Acinetobacter* baumannii, Haloglomus sp. ZY58, Halovivax sp. CGA30, Rhizobium lentis, *Pseudomonas* sp. CIP-10, *Escherichia coli*, and Deinococcus geothermalis. **(D)** Relative abundance of the top ten microbial species for the White ethnic group. The predominant species for this group were Acidianus manzaensis, *Staphylococcus aureus*, *Staphylococcus aureus* S1, *Acinetobacter* baumannii, *Pseudomonas* sp. CIP-10, Haloglomus sp. ZY58, Halovivax sp. CGA30, Rhizobium lentis, Sphingomonas sp. R1, and *Actinomyces* oris.

(314), followed by Black or African American (33), Asian (7), with 5 individuals not reporting their ethnicity (Figure 1A). For age, White participants presented the highest median age at 61.5 years, while Black or African American and Not Reported groups both shared a median age of 57 years. The age ranges across the ethnicities varied, with the White group demonstrating the broadest span from 24 to 82 years (Figure 1B). Regarding gender distribution, males predominated in all ethnic groups except for the Asian cohort, where the ratio was almost equal. Specifically, the White group consisted of 189 males and 125 females (Figure 1C). When analyzing the Progression-Free Survival Time, Asian participants exhibited the longest median duration of 11.1 months. In contrast, the White group had a median of 8.7 months, slightly less than the Black or African American group's 8.9 months. Follow-up durations were relatively consistent across groups, with the Not Reported group having the longest median follow-up time at 26.3 months. The ECOG Performance Status was generally consistent across the groups, with a median score of 1, except for the Not Reported

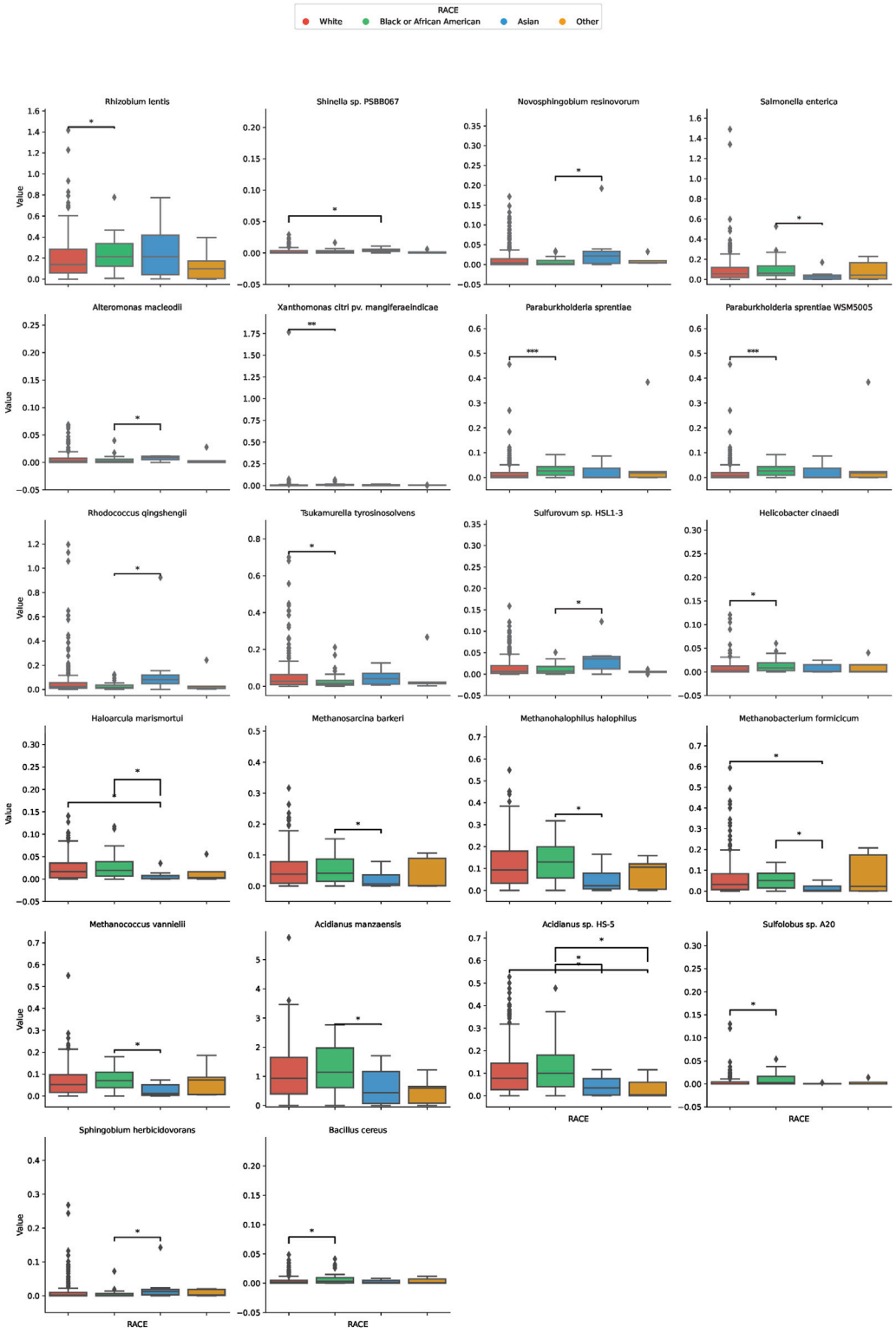

FIGURE 3
Differential Microbial Abundance Across Ethnicities. The boxplots in this figure depict the variation in microbial abundance for specific species across diverse ethnic groups. Each color represents a distinct ethnicity: red for White, green for Black or African American, blue for Asian, and yellow for Others. *, $p < 0.05$; **, $p < 0.01$.

group, which had a median score of 0. Genetic analyses revealed that a notable proportion of the White group exhibited wild-type KRAS (116) and NRAS (144). MSI status predominantly showed MSS phenotype in most groups where data was available. Tumor location displayed varied distributions across ethnicities, with the right side being the most common location in the Black or African American and White cohorts (Figure 1D).

Diversity of tumor microbiome across ethnic groups

In our detailed investigation into the tumor microbiome diversity across various ethnicities, we uncovered consistent patterns. The alpha diversity, which represents the variety of species in individual samples, displayed no significant variations among the White, Asian, Black or African American, and American Indian or Alaska Native groups ($p = 0.755$, Figure 2A). Similarly, the beta diversity, which underscores the microbial community differences between samples, also showed no pronounced distinction among the ethnicities, as illustrated in the PCoA plot (Figure 2B). Taking a closer look at the relative abundances of microbial species, for the combined group of Asian, Black or African American, and American Indian or Alaska Native, the top ten species were Acidianus manzaensis, *Staphylococcus aureus*, *S. aureus* S1, *Acinetobacter* baumannii, Haloglomus sp. ZY58, Halovivax sp. CGA30, Rhizobium lentis, *Pseudomonas* sp. CIP-10, *Escherichia coli*, and Deinococcus geothermalis (Figure 2C). On the other hand, for White individuals, the ten predominant species were Acidianus manzaensis, *S. aureus*, *S. aureus* S1, *Acinetobacter* baumannii, *Pseudomonas* sp. CIP-10, Haloglomus sp. ZY58, Halovivax sp. CGA30, Rhizobium lentis, Sphingomonas sp. R1, and *Actinomyces* oris (Figure 2D).

Differential microbial abundance across ethnicities

In our comprehensive assessment of microbial diversity across different ethnic groups, significant variations were identified in the abundance of specific species (Figure 3). These disparities were especially pronounced when comparing the White and Black groups, as well as between the White and Asian cohorts, and the Black and Asian cohorts. Among the White and Black cohorts, species such as *Tsukamurella* tyrosinosolvens and *Helicobacter* cinaediwere found to be more abundant in the White group, with fold changes of 1.79 and 0.40, respectively. On the contrary, Sulfolobus sp. A20 showed a substantial decrease in abundance in the White group with a fold change of 0.081. For the White and Asian cohorts, Haloarcula marismortui and Methanobacterium formicicum were notably more abundant in the White population, with fold changes of 23.16 and 8.98, respectively. However, Shinella sp. PSBB067 demonstrated a decreased presence in the White group, registering a fold change of 0.166. Comparing the Black and Asian groups, there was an overwhelming abundance of Haloarcula marismortui and Methanobacterium formicicum in the Black cohort, with fold changes of 26.88 and 14.34, respectively. In contrast, Sphingobium herbicidovorans recorded a diminished presence in the Black group with a fold change of 0.074. The comprehensive list of microbial species and their fold changes across ethnic groups can be found in Supplementary Table S1.

Prognostic implications of differential microbial abundance

Our analysis extended to understanding the potential prognostic implications of the microbial abundance in tumor samples (Figure 4). Of particular interest, two microbial species demonstrated a significant association with progression-free survival (PFS). Elevated expression of *Helicobacter* cinaedi was associated with a poorer survival outcome, as evidenced by a *p*-value of 0.0337. Similarly, higher levels of Sphingobium herbicidovorans also indicated a worse prognosis with a *p*-value of 0.0146. These findings underscore the potential prognostic value of specific microbial species within tumor samples and warrant further exploration into their role in patient outcomes.

Dissecting racial disparities: differentially expressed genes and their interplay with tumoral microbiota

In our comprehensive exploration of the racial differences in gene expression and their potential interaction with the tumor microbiome, we observed striking contrasts. Figure 5A presents a Venn diagram detailing the overlap of differentially expressed genes between the three racial groups. Remarkably, 39 genes were commonly differentially expressed across all pairwise comparisons. However, exclusive gene expression patterns also emerged: 886 genes were uniquely altered between White and Black populations, 640 genes between Black and Asian, and 475 genes between White and Asian. The heatmaps in Figure 5B, delve deeper, visualizing these differentially expressed genes for the Black vs. Asian, White vs. Asian, and White vs. Black comparisons, respectively. For in-depth gene details and annotations, we refer readers to Supplementary Tables S2–S4. Transitioning from the genomic landscape to its interplay with the microbiome, we analyzed the association between these racially differentiated genes and the two microbial species previously identified to be prognostically significant. Figure 6A showcases the top 10 genes correlated with *Helicobacter* cinaedi. Among these, SELENBP1 emerged as the most significantly associated gene. Similarly, Figure 6B highlights the top 10 genes correlated with Sphingobium herbicidovorans, with SNORA38 standing out as the most notable. Upon meticulous examination of the independently collected PFS survival data from 12 patients, it is evident that lower expression levels of Sphingobium herbicidovorans correlate with improved survival rates, as substantiated by a *p*-value less than 0.05 (Figure 6C). Conversely, while no significant disparity in survival rates is observed between low and high expression levels of *Helicobacter* cinaedi ($p = 0.07$), a conspicuous divergence trend between the two expression levels is noticeable (Figure 6D; Supplementary Figure S1D). Additionally, an in-depth analysis revealed a significant upregulation of both Sphingobium

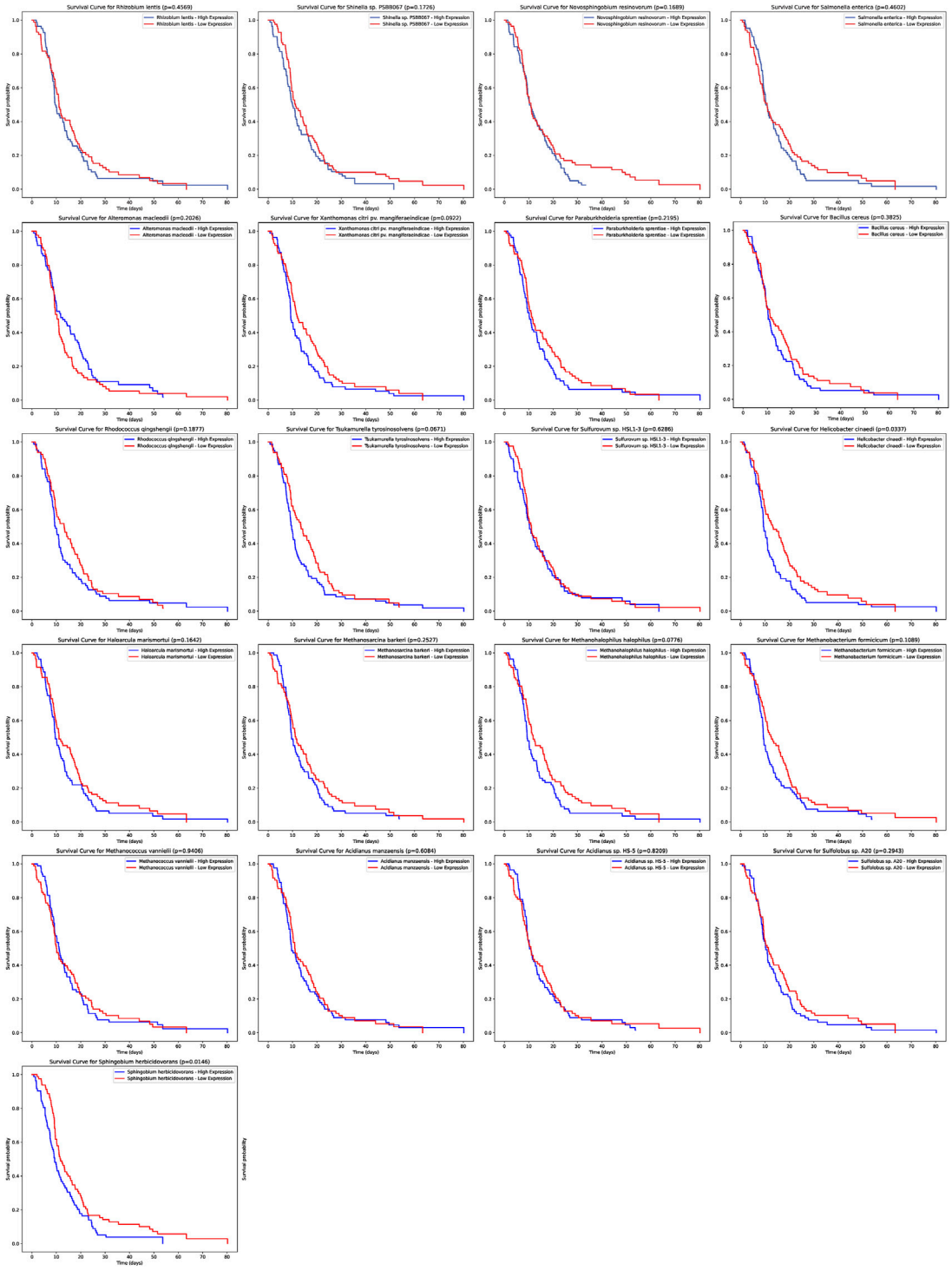

FIGURE 4
Prognostic Significance of Microbial Abundance in Tumor Samples. The survival curves depict the progression-free survival (PFS) based on the expression of two microbial species. Elevated levels of *Helicobacter* cinaedi and Sphingobium herbicidovorans were associated with poorer survival outcomes, with *p*-values of 0.0337 and 0.0146 respectively.

herbicidovorans and *Helicobacter* cinaedi in the Black or African American patient group (Figure 6E; Supplementary Figure S1E). In synchrony with these findings, the expressions of SELENBP1 and SNORA38—which are correlated with the respective bacterial strains—were also validated. Remarkably, the expression of SELENBP1 is significantly reduced in the Black or African American group, as depicted in Figure 6F. On the other hand, no significant difference was observed in the expression levels of SNORA38 between the groups. According to the comprehensive TCGA (COAD) dataset analysis, it was observed that

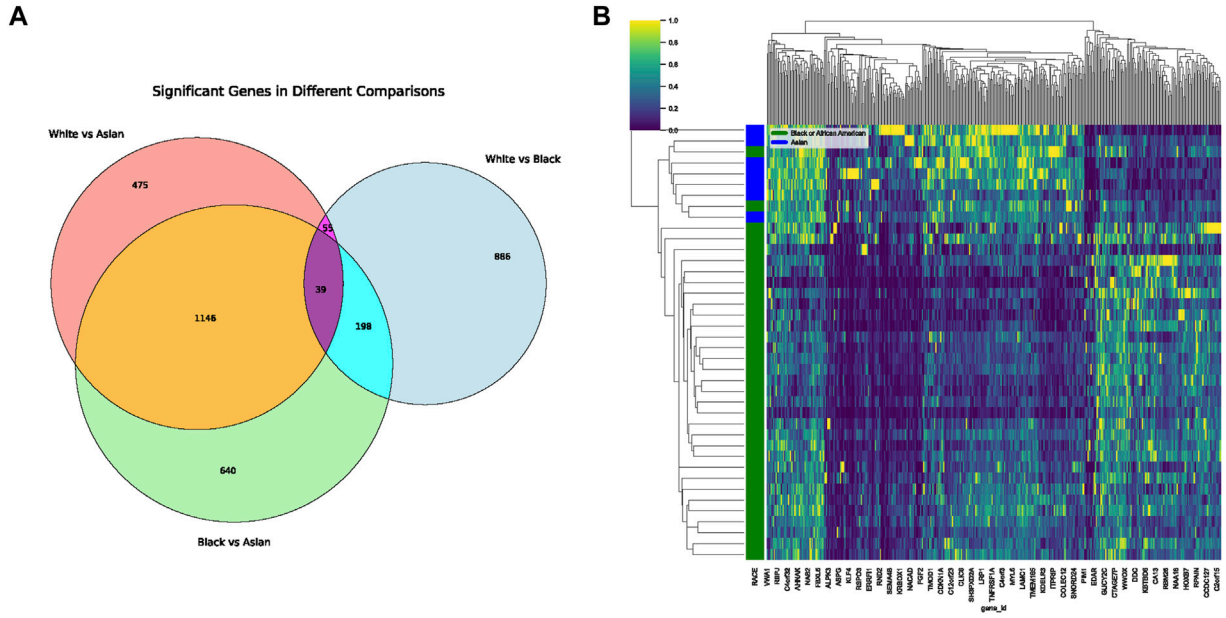

FIGURE 5
Differential Gene Expression Across Racial Groups. **(A)** Venn diagram displaying the overlap of differentially expressed genes among White, Black, and Asian populations. The shared and unique gene expressions are represented in their respective intersections. **(B)** Heatmap representing differentially expressed genes unique to the Black vs. Asian comparison. Gene details can be found in Supplementary Table S2.

SELEBP1 expression levels were the lowest in White individuals and highest in Black or African American individuals, denoting a significant disparity (Figure 6G). Intriguingly, the expression levels in Asian individuals were intermediate, showing no significant differences when compared to either group, in a study encompassing 317 subjects (Asians = 11, Black or African American = 65, and White = 241).

Discussion

Metastatic colorectal cancer (mCRC) remains a significant clinical challenge, with its heterogeneity and adaptability often leading to therapy resistance and dismal outcomes (Xi and Xu, 2021; Mazzoli et al., 2022). Bevacizumab, an angiogenesis inhibitor, has emerged as a promising therapeutic agent in the treatment of mCRC (Garcia et al., 2020). By targeting vascular endothelial growth factor (VEGF), Bevacizumab reduces tumor blood supply, making it a cornerstone in the current mCRC treatment paradigm (Chionh et al., 2022; de Rauglaudre et al., 2022). A distinguishing feature of our study lies in the methodological approach of extracting microbiota data from RNA-SEQ. Unlike previous endeavors that sourced microbial abundance data from genomic sequences, our approach ensured that the microbial data we analyzed represented bacteria actively transcribing within the tumor milieu. The utilization of RNA-seq derived data for the training set and DNA-based 16S rRNA sequencing for validation indeed introduces methodological nuances. While RNA-seq offers insights into the active microbial community by capturing expressed genes, 16S rRNA sequencing identifies the broader microbial composition. The potential discrepancy between these methodologies underscores the importance of interpreting results within the context of the chosen method. Though each approach has its strengths, their combined use in our study seeks to provide a comprehensive view of the microbial landscape, with RNA-seq highlighting functional dynamics and 16S rRNA offering a snapshot of overall microbial diversity. Essentially, this means that the bacteria identified are not mere transient inhabitants but are actively participating in the tumor ecosystem, potentially influencing tumor behavior and treatment outcomes.

In our study, as delineated in Figure 2, we discerned a notable distinction in alpha diversity, while beta diversity remained relatively consistent. Alpha diversity primarily gauges the richness and evenness of species within a single sample. The marked difference suggests a variation in the number or distribution of microbial species within individual communities across different ethnic groups. On the other hand, beta diversity evaluates the dissimilarity between microbial communities from different samples. The lack of significant difference in beta diversity implies that while the individual communities might harbor varied species or their distributions, the overall microbial community structures across racial groups remain somewhat analogous.

This observation is of paramount importance. The pronounced difference in alpha diversity could be indicative of unique microbial species or strains that are predominant in one racial group but less prevalent or absent in others. Such microbial distinctions can potentially influence host metabolic activities, immune responses, and even drug metabolism, thereby impacting the efficacy and outcome of metastatic colorectal cancer treatments across different racial groups.

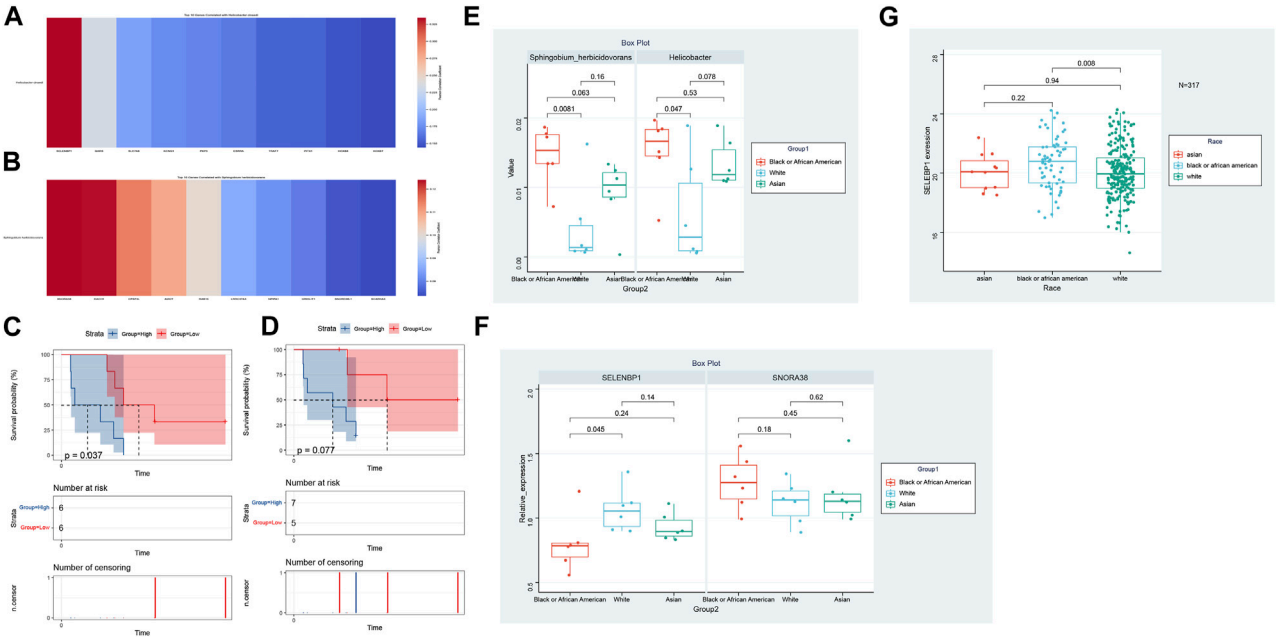

FIGURE 6
Genomic-Microbiota Associations in Tumors. **(A)** Top 10 genes exhibiting significant correlation with *Helicobacter* cinaedi. The most notably associated gene in this set is SELENBP1. **(B)** Top 10 genes displaying pronounced correlation with Sphingobium herbicidovorans Among these, SNORA38 emerges as the gene with the highest significance. **(C)** Kaplan-Meier Survival Analysis of Patients with Varied Sphingobium herbicidovorans Expression Levels. The figure illustrates the survival curves of mCRC patients with low (red line) versus high (blue line) expression levels of Sphingobium herbicidovorans. A statistically significant improvement in patient survival is observed with lower expression levels of this bacterial strain, as evidenced by a *p*-value of <0.05. **(D)** Survival Analysis of Patients Based on *Helicobacter* cinaedi Expression Levels. The Kaplan-Meier survival curves for patients with low (red line) and high (blue line) expression levels of *Helicobacter* cinaedi are depicted. While there isn't a statistically significant difference in survival between the two groups ($p = 0.07$), a noticeable trend of separation between the curves suggests potential implications of *Helicobacter* cinaedi expression levels on patient survival. **(E)** Differential Expression of Sphingobium herbicidovorans and *Helicobacter* cinaedi in Racial Groups. This figure demonstrates the upregulation of Sphingobium herbicidovorans and *Helicobacter* cinaedi in Black or African American mCRC patients compared to their Caucasian counterparts. The Asian group shows no significant difference in the expression levels of these bacterial strains compared to both Black or African American and Caucasian groups. Each bar represents the average expression level of the respective bacterial strain in each racial group, with error bars indicating the standard deviation. **(F)** Expression Analysis of SELENBP1 and SNORA38 in Different Racial Groups. The bar graph illustrates the expression levels of SELENBP1 and SNORA38 in Caucasian and Black or African American mCRC patients, with significant differences noted in SELENBP1 expression between these two groups. The addition of the Asian group shows that there are no significant differences in the expression of SELENBP1 and SNORA38 when compared to both the Caucasian and Black or African American groups. Error bars represent standard deviation. **(G)** Expression Analysis of SELENBP1 in Different Racial Groups of TCGA (COAD).

Our comprehensive investigation, driven by the objective of exploring racial variations in mCRC's molecular and microbiological profiles, has unearthed pivotal insights. Notably, the intersection of microbiota and host genomics revealed the potential modulating effects of specific bacteria on gene expression. Of particular interest were the bacteria *Helicobacter* cinaedi and Sphingobium herbicidovorans and their correlated genes SELENBP1 and SNORA38, respectively. SELENBP1, or Selenium Binding Protein 1, has been increasingly recognized in oncology circles for its nuanced role in cancer biology (Pol et al., 2018). Several studies have postulated its role as a tumor suppressor. Reduced SELENBP1 expression has been linked to poor prognosis in several cancers, including lung and ovarian cancers (Huang et al., 2006; Wang et al., 2021). Its function is believed to be intricately linked with selenium; an essential trace element known to have anti-carcinogenic properties. SNORA38, on the other hand, is a part of the small nucleolar RNAs (snoRNAs) family, which primarily functions in the modification and processing of ribosomal RNA (rRNA) (Song et al., 2022). Emerging evidence suggests that dysregulation of snoRNAs can profoundly impact cellular homeostasis and potentially drive oncogenesis (Schulten et al., 2017). Particularly, SNORA38 has been identified as an oncogene in certain cancer types, playing a role in cellular proliferation and survival (Song et al., 2022). *Helicobacter* cinaedi, a bacterium traditionally associated with gastrointestinal infections, has recently been implicated in colorectal carcinogenesis (Liu et al., 2019). Its pro-inflammatory attributes potentially drive the inflammatory cascade, a recognized precursor to oncogenesis (Overacre-Delgoffe et al., 2021). Sphingobium herbicidovorans, though less studied, has its ties with xenobiotic degradation, which might have implications in carcinogen detoxification within the gut (Qiu et al., 2014). The final section of our study, focusing on the TCGA (COAD) data, reveals a remarkable pattern in the expression levels of SELEBP1 across different racial groups. This analysis underscores the nuanced interplay between genetics and race, particularly in the context of colorectal adenocarcinoma. The data unequivocally shows that SELEBP1 expression is lowest in White individuals and highest in Black or African American individuals, a finding that could have significant implications for personalized medicine and understanding racial disparities in cancer outcomes. However, it's crucial to

acknowledge the limitations of this study, primarily due to the disproportionate representation of racial groups in the sample. The notably lower number of Asian participants (N = 11) compared to Black or African American (N = 65) and White (N = 241) individuals may skew the interpretability and applicability of these findings to broader populations. This underrepresentation underscores a recurring challenge in genetic research: the need for more inclusive and diverse population samples to ensure that conclusions drawn are reflective of the global population.

In conclusion, our study underscores the intricate interplay between host genomics, actively transcribing tumor microbiota, and their collective role in mCRC pathogenesis. These findings can pave the way for a more personalized and racially tailored therapeutic approach, optimizing outcomes in the diverse mCRC patient population.

Data availability statement

The datasets presented in this study can be found in online repositories. The names of the repository/repositories and accession number(s) can be found in the article/Supplementary Material.

Ethics statement

The studies involving humans were approved by the First Affiliated Hospital of Xi'an Jiaotong University. The studies were conducted in accordance with the local legislation and institutional requirements. The participants provided their written informed consent to participate in this study.

Author contributions

LF: Data curation, Methodology, Resources, Writing–original draft, Writing–review and editing. RW: Formal Analysis, Supervision, Writing–original draft, Writing–review and editing. QZ: Writing– original draft, Writing–review and editing, Data curation, Formal analysis, Visualization. JW: Writing– original draft, Writing–review and editing, Methodology, Resources. GL: Investigation, Project administration, Software, Writing–original draft, Writing–review and editing. CX: Conceptualization, Data curation, Methodology, Writing–original draft, Writing–review and editing.

Funding

The author(s) declare financial support was received for the research, authorship, and/or publication of this article. The research leading to these results mainly received funding from the Basic Natural Science Research Program of Shaanxi Province 2021JQ-386, 2021JQ-405, and 2022JM-610 (Referred to CX), funding from the Clinical Research Award of the First Affiliated Hospital of Xi'an Jiaotong University, XJTU1AF-CRF-2020-020 (Referred to CX). This study also received funding from Key Research and Development Program of Shaanxi Province, 2022SF-159 (Referred to CX), National Natural Science Foundation of China, No. 82103568 (Referred to CX).

Conflict of interest

The authors declare that the research was conducted in the absence of any commercial or financial relationships that could be construed as a potential conflict of interest.

Publisher's note

All claims expressed in this article are solely those of the authors and do not necessarily represent those of their affiliated organizations, or those of the publisher, the editors and the reviewers. Any product that may be evaluated in this article, or claim that may be made by its manufacturer, is not guaranteed or endorsed by the publisher.

Supplementary material

The Supplementary Material for this article can be found online at: https://www.frontiersin.org/articles/10.3389/fphar.2023.1320028/full#supplementary-material

SUPPLEMENTARY FIGURE S1
(A) Heatmap illustrating differentially expressed genes unique to the White vs. Asian comparison. Further information on these genes is provided in Supplementary Table S3. **(B)** Heatmap depicting differentially expressed genes unique to the White vs. Black comparison. Detailed annotations are available in Supplementary Table S4. **(C)** Western blot analysis of SELENBP1 protein expression in colorectal cancer samples. Two distinct groups are represented: B (Black or African American) and W (White). The bands indicate the relative abundance of SELENBP1 protein in each group. Notably, the W group exhibits a significantly higher expression of SELENBP1 compared to the B group.

References

Carethers, J. M., and Doubeni, C. A. (2020). Causes of socioeconomic disparities in colorectal cancer and intervention framework and strategies. *Gastroenterology* 158, 354–367. doi:10.1053/j.gastro.2019.10.029

Casamassimi, A., Federico, A., Rienzo, M., Esposito, S., and Ciccodicola, A. (2017). Transcriptome profiling in human diseases: New advances and perspectives. *Int. J. Mol. Sci.* 18, 1652. doi:10.3390/ijms18081652

Chionh, F., Gebski, V., Al-Obaidi, S. J., Mooi, J. K., Bruhn, M. A., Lee, C. K., et al. (2022). VEGF-A, VEGFR1 and VEGFR2 single nucleotide polymorphisms and outcomes from the AGITG MAX trial of capecitabine, bevacizumab and mitomycin C in metastatic colorectal cancer. *Sci. Rep.* 12, 1238. doi:10.1038/s41598-021-03952-y

Cobb, S., Ekwegh, T., Adinkrah, E., Ameli, H., Dillard, A., Kibe, L. W., et al. (2022). Examining colorectal cancer screening uptake and health provider recommendations among underserved middle aged and older African Americans. *Health Promot. Perspect.* 12, 399–409. doi:10.34172/hpp.2022.52

de Klerk, C. M., Gupta, S., Dekker, E., Essink-Bot, M. L., and Expert Working Group 'Coalition to reduce inequities in colorectal cancer screening' of the World Endoscopy Organization (2018). Socioeconomic and ethnic inequities within organised colorectal cancer screening programmes worldwide. *Gut* 67, 679–687. doi:10.1136/gutjnl-2016-313311

de Rauglaudre, B., Sibertin-Blanc, C., Fabre, A., Le Malicot, K., Bennouna, J., Ghiringhelli, F., et al. (2022). Predictive value of vascular endothelial growth factor polymorphisms for maintenance bevacizumab efficacy in metastatic colorectal cancer:

an ancillary study of the PRODIGE 9 phase III trial. *Ther. Adv. Med. Oncol.* 14, 17588359221141307. doi:10.1177/17588359221141307

Fang, X., Zhong, C., Weng, S., Hu, H., Wang, J., Xiao, Q., et al. (2023). Sintilimab plus bevacizumab and CapeOx (BBCAPX) on first-line treatment in patients with RAS mutant, microsatellite stable, metastatic colorectal cancer: study protocol of a randomized, open-label, multicentric study. *BMC cancer* 23, 676. doi:10.1186/s12885-023-11139-z

Fu, A., Yao, B., Dong, T., and Cai, S. (2023). Emerging roles of intratumor microbiota in cancer metastasis. *Trends Cell Biol.* 33, 583–593. doi:10.1016/j.tcb.2022.11.007

Fu, A., Yao, B., Dong, T., Chen, Y., Yao, J., Liu, Y., et al. (2022). Tumor-resident intracellular microbiota promotes metastatic colonization in breast cancer. *Cell* 185, 1356–1372.e26. doi:10.1016/j.cell.2022.02.027

Garcia, J., Hurwitz, H. I., Sandler, A. B., Miles, D., Coleman, R. L., Deurloo, R., et al. (2020). Bevacizumab (Avastin®) in cancer treatment: a review of 15 years of clinical experience and future outlook. *Cancer Treat. Rev.* 86, 102017. doi:10.1016/j.ctrv.2020.102017

He, J., Liu, Y., Liu, C., Hu, H., Sun, L., Xu, D., et al. (2023). A randomized phase III study of anlotinib versus bevacizumab in combination with capeox as first-line therapy for RAS/BRAF wild-type metastatic colorectal cancer: a clinical trial protocol. *Technol. cancer Res. Treat.* 22, 15330338231152350. doi:10.1177/15330338231152350

Helmink, B. A., Khan, M. A. W., Hermann, A., Gopalakrishnan, V., and Wargo, J. A. (2019). The microbiome, cancer, and cancer therapy. *Nat. Med.* 25, 377–388. doi:10.1038/s41591-019-0377-7

Huang, K. C., Park, D. C., Ng, S. K., Lee, J. Y., Ni, X., Ng, W. C., et al. (2006). Selenium binding protein 1 in ovarian cancer. *Int. J. cancer* 118, 2433–2440. doi:10.1002/ijc.21671

Hunter, M. V., Moncada, R., Weiss, J. M., Yanai, I., and White, R. M. (2021). Spatially resolved transcriptomics reveals the architecture of the tumor-microenvironment interface. *Nat. Commun.* 12, 6278. doi:10.1038/s41467-021-26614-z

Innocenti, F., Yazdani, A., Rashid, N., Qu, X., Ou, F.-S., Van Buren, S., et al. (2022). Tumor immunogenomic features determine outcomes in patients with metastatic colorectal Cancer treated with standard-of-care combinations of Bevacizumab and Cetuximab. *Clin. Cancer Res.* 28, 1690–1700. doi:10.1158/1078-0432.CCR-21-3202

Lee, S., and Schmitt, C. A. (2019). The dynamic nature of senescence in cancer. *Nat. Cell Biol.* 21, 94–101. doi:10.1038/s41556-018-0249-2

LeSavage, B. L., Suhar, R. A., Broguiere, N., Lutolf, M. P., and Heilshorn, S. C. (2022). Next-generation cancer organoids. *Nat. Mater.* 21, 143–159. doi:10.1038/s41563-021-01057-5

Li, F., Wu, T., Xu, Y., Dong, Q., Xiao, J., Xu, Y., et al. (2020). A comprehensive overview of oncogenic pathways in human cancer. *Briefings Bioinforma.* 21, 957–969. doi:10.1093/bib/bbz046

Liu, I. L., Tsai, C. H., Hsu, C. H., Hu, J. M., Chen, Y. C., Tian, Y. F., et al. (2019). *Helicobacter pylori* infection and the risk of colorectal cancer: a nationwide population-based cohort study. *QJM Mon. J. Assoc. Physicians* 112, 787–792. doi:10.1093/qjmed/hcz157

Lonardi, S., Nimeiri, H., Xu, C., Zollinger, D. R., Madison, R. W., Fine, A. D., et al. (2022). Comprehensive genomic profiling (CGP)-Informed personalized molecular residual disease (MRD) detection: an exploratory analysis from the PREDATOR study of metastatic colorectal cancer (mCRC) patients undergoing surgical resection. *Int. J. Mol. Sci.* 23, 11529. doi:10.3390/ijms231911529

Maacha, S., Bhat, A. A., Jimenez, L., Raza, A., Haris, M., Uddin, S., et al. (2019). Extracellular vesicles-mediated intercellular communication: roles in the tumor microenvironment and anti-cancer drug resistance. *Mol. cancer* 18, 55. doi:10.1186/s12943-019-0965-7

Mazzoli, G., Cohen, R., Lonardi, S., Corti, F., Elez, E., Fakih, M., et al. (2022). Prognostic impact of performance status on the outcomes of immune checkpoint inhibition strategies in patients with dMMR/MSI-H metastatic colorectal cancer. *Eur. J. cancer (Oxford, Engl. 1990)* 172, 171–181. doi:10.1016/j.ejca.2022.05.044

Michaudel, C., and Sokol, H. (2020). The gut microbiota at the service of immunometabolism. *Cell metab.* 32, 514–523. doi:10.1016/j.cmet.2020.09.004

Nejman, D., Livyatan, I., Fuks, G., Gavert, N., Zwang, Y., Geller, L. T., et al. (2020). The human tumor microbiome is composed of tumor type-specific intracellular bacteria. *Sci. (New York, N.Y.)* 368, 973–980. doi:10.1126/science.aay9189

Overacre-Delgoffe, A. E., Bumgarner, H. J., Cillo, A. R., Burr, A. H. P., Tometich, J. T., Bhattacharjee, A., et al. (2021). Microbiota-specific T follicular helper cells drive tertiary lymphoid structures and anti-tumor immunity against colorectal cancer. *Immunity* 54, 2812–2824.e4. doi:10.1016/j.immuni.2021.11.003

Pauli, C., Hopkins, B. D., Prandi, D., Shaw, R., Fedrizzi, T., Sboner, A., et al. (2017). Personalized *in vitro* and *in vivo* cancer models to guide precision medicine. *Cancer Discov.* 7, 462–477. doi:10.1158/2159-8290.CD-16-1154

Pol, A., Renkema, G. H., Tangerman, A., Winkel, E. G., Engelke, U. F., de Brouwer, A. P. M., et al. (2018). Mutations in SELENBP1, encoding a novel human methanethiol oxidase, cause extraoral halitosis. *Nat. Genet.* 50, 120–129. doi:10.1038/s41588-017-0006-7

Qiu, S., Gözdereliler, E., Weyrauch, P., Lopez, E. C., Kohler, H. P., Sørensen, S. R., et al. (2014). Small (13)C/(12)C fractionation contrasts with large enantiomer fractionation in aerobic biodegradation of phenoxy acids. *Environ. Sci. Technol.* 48, 5501–5511. doi:10.1021/es405103g

Schulten, H. J., Bangash, M., Karim, S., Dallol, A., Hussein, D., Merdad, A., et al. (2017). Comprehensive molecular biomarker identification in breast cancer brain metastases. *J. Transl. Med.* 15, 269. doi:10.1186/s12967-017-1370-x

Song, J., Zheng, A., Li, S., Zhang, W., Zhang, M., Li, X., et al. (2022). Clinical significance and prognostic value of small nucleolar RNA SNORA38 in breast cancer. *Front. Oncol.* 12, 930024. doi:10.3389/fonc.2022.930024

Tian, L., Chen, F., and Macosko, E. Z. (2023). The expanding vistas of spatial transcriptomics. *Nat. Biotechnol.* 41, 773–782. doi:10.1038/s41587-022-01448-2

Vitale, I., Manic, G., Coussens, L. M., Kroemer, G., and Galluzzi, L. (2019). Macrophages and metabolism in the tumor microenvironment. *Cell metab.* 30, 36–50. doi:10.1016/j.cmet.2019.06.001

Wang, H., Wang, X., Xu, L., Cao, H., and Zhang, J. (2021). Nonnegative matrix factorization-based bioinformatics analysis reveals that TPX2 and SELENBP1 are two predictors of the inner sub-consensuses of lung adenocarcinoma. *Cancer Med.* 10, 9058–9077. doi:10.1002/cam4.4386

Wong-Rolle, A., Wei, H. K., Zhao, C., and Jin, C. (2021). Unexpected guests in the tumor microenvironment: microbiome in cancer. *Protein & Cell* 12, 426–435. doi:10.1007/s13238-020-00813-8

Wu, T., and Dai, Y. (2017). Tumor microenvironment and therapeutic response. *Cancer Lett.* 387, 61–68. doi:10.1016/j.canlet.2016.01.043

Xi, Y., and Xu, P. (2021). Global colorectal cancer burden in 2020 and projections to 2040. *Transl. Oncol.* 14, 101174. doi:10.1016/j.tranon.2021.101174

Zaki, T. A., Liang, P. S., May, F. P., and Murphy, C. C. (2023). Racial and ethnic disparities in early-onset colorectal cancer survival. *Clin. Gastroenterology Hepatology* 21, 497–506.e3. doi:10.1016/j.cgh.2022.05.035

frontiers | Frontiers in Pharmacology

TYPE Original Research
PUBLISHED 17 April 2024
DOI 10.3389/fphar.2024.1364160

OPEN ACCESS

EDITED BY
Jian Gao,
Shanghai Children's Medical Center, China

REVIEWED BY
Chu Xianming,
The Affiliated Hospital of Qingdao University, China
Zhipeng Liu,
Purdue University, United States

*CORRESPONDENCE
Zhibiao Chen,
chzbiao@126.com

†These authors have contributed equally to this work

RECEIVED 01 January 2024
ACCEPTED 05 April 2024
PUBLISHED 17 April 2024

CITATION
Qin X, Ding R, Lu H, Zhang W, Wei S, Ji B, Geng R, Wu L and Chen Z (2024), Identification of pivotal genes and regulatory networks associated with atherosclerotic carotid artery stenosis based on comprehensive bioinformatics analysis and machine learning. *Front. Pharmacol.* 15:1364160. doi: 10.3389/fphar.2024.1364160

Identification of pivotal genes and regulatory networks associated with atherosclerotic carotid artery stenosis based on comprehensive bioinformatics analysis and machine learning

Xiaohong Qin[1,2†], Rui Ding[1†], Haoran Lu[1,2], Wenfei Zhang[1], Shanshan Wei[3], Baowei Ji[1], Rongxin Geng[1], Liquan Wu[1] and Zhibiao Chen[1*]

[1]Department of Neurosurgery, Renmin Hospital of Wuhan University, Wuhan, Hubei, China, [2]Central Laboratory, Renmin Hospital of Wuhan University, Wuhan, Hubei, China, [3]Department of Oncology, Wuchang Hospital Affiliated to Wuhan University of Science and Technology, Wuhan, China

Objective: Bioinformatics methods were applied to investigate the pivotal genes and regulatory networks associated with atherosclerotic carotid artery stenosis (ACAS) and provide new insights for the treatment of this disease.

Methods: The study utilized five ACAS datasets (GSE100927, GSE11782, GESE28829, GSE41571, and GSE43292) downloaded from the NCBI GEO database. The first four datasets were combined as the training set (n = 99), while GSE43292 (n = 64) was used as the validation set. Difference analysis and functional enrichment analysis were then performed on the training set. The pathogenic targets of ACAS were screened by protein-protein interaction networks and MCODE analyses, combined with three machine learning algorithms. The results were next verified by analysis of inter-group differences and ROC curve analysis. Next, immune-related function and immune cell correlation analyses were performed, and plaques of human ACAS were applied to verify the results via immunohistochemistry (IH) and immunofluorescence (IF). Finally, the competing endogenous RNAs (ceRNA) and transcription factors (TFs) regulatory networks of the characterized genes were constructed.

Results: A total of 177 differentially expressed genes were identified, including 67 genes downregulated and 110 genes upregulated. Gene set enrichment analysis revealed that five pathways were active in the experimental group, including xenograft rejection, autoimmune thyroid disease, graft-versus-host disease, leishmaniasis infection, and lysosomes. Four key genes were identified, with C3AR1 being upregulated and FBLN5, PPP1R12A, and TPM1 being

Abbreviations: ACAS, atherosclerotic carotid artery stenosis; AUC, area under the curve; CAS, carotid artery stenosis; ceRNA, competing endogenous RNAs; DEGs, differentially expressed genes; GO, Gene Ontology; GSEA, gene set enrichment analysis; KEGG, Kyoto Encyclopedia of Genes and Genomes; LASSO, least absolute shrinkage and selection operator; MCODE, molecular complex detection; ML, machine learning; MCP7, mast cell protease 7; MPO, myeloperoxidase; NETs, neutrophil extracellular traps; PCA, principal component analysis; PPI, Protein-protein interaction networks; RF, random forest; SVM-RFE, support vector machine-recursive feature elimination; TF, transcription factor; TIA, transient ischemic attack.

downregulated. The analysis of inter-group differences demonstrated that the four characterized genes were differentially expressed in both the control and experimental groups. The ROC analysis showed that they had high AUC values in both the training and validation sets. Therefore, a predictive ACAS patient nomogram model based on the screened genes was established. Correlation analysis revealed a positive correlation between C3AR1 expression and neutrophils, which was further validated in IH and IF. One or multiple lncRNAs may compete with the characterized genes for binding miRNAs. Additionally, each characterized gene interacts with multiple TFs.

Conclusion: Four pivotal genes were screened, and relevant ceRNA and TFs were predicted. These molecules may exert a crucial role in ACAS and serve as potential biomarkers and therapeutic targets.

KEYWORDS

carotid artery stenosis, atherosclerosis, machine learning, pathogenic markers, therapeutic targets

1 Introduction

As of 2019, stroke remains the second leading cause of death worldwide and the third leading cause of death and disability (Feigin et al., 2021). Ischemic stroke accounts for 87% of these cases (Saini et al., 2021). The primary cause of ischemic stroke is ischemia and even necrosis of brain tissue due to carotid artery stenosis (CAS), occlusion, or detachment of carotid plaque (Feske, 2021). ACAS is a narrowing of the carotid artery diameter due to the formation of carotid atherosclerotic plaques, which is very common, affecting one in five patients with stroke or transient ischemic attack (TIA), and occurs mostly in the bifurcation of the common carotid artery and the beginning of the internal carotid artery (Cheng et al., 2019; Heck and Jost, 2021). Some stenotic lesions may even progress to complete occlusion, resulting in severe neurological deficits, such as coma, limb paralysis, speech disorders, sensory deficits, hemianopsia, intellectual disability, and infarctions in certain areas, such as the brainstem, may even result in sudden death (Kappelle, 2002; Campbell et al., 2019). Treatment options depend on the degree of CAS and the patient's symptoms, and include medical, surgical, or interventional therapy. Conservative medical treatment aims to reduce the symptoms of cerebral ischemia and lower the risk of stroke; controlling existing diseases such as hypertension, diabetes mellitus, hyperlipidemia and coronary heart disease is the main strategy (Bonati et al., 2022). The aim of surgical treatment is to prevent the onset of stroke, followed by prevention and slowing of the onset of TIA. The standard surgical procedure is carotid endarterectomy (CEA), but CEA also carries potential risks of stroke, heart attack, and hyperperfusion syndrome (Bonati et al., 2022). Carotid angioplasty and stenting is an alternative to CEA, especially in cases where the neck anatomy is not conducive to surgery (White et al., 2022). It is a minimally invasive procedure in which a stent is placed into the carotid arteries to increase blood flow, but there are still problems with intraprocedural endothelial tearing, postprocedural elastic regression of the vessel, and restenosis (Bonati et al., 2022; White et al., 2022). In conclusion, each of the three treatments has its own set of advantages, disadvantages, and indications. With the advancements in vascular imaging technology, the prevalence of ACAS is gradually increasing, how to block or reverse the process of carotid atherosclerotic plaque formation at an early stage and improve the ACAS is the hot spot of current research. Therefore, an in-depth and comprehensive investigation of the causes of carotid atherosclerotic plaque formation and related pathogenic factors is urgently required.

In recent years, machine learning (ML) has been continuously applied to clinical diseases for disease diagnosis, target screening, patient prognosis prediction, and therapeutic programmes due to its powerful computational power, lower error rate and better predictive performance (Swanson et al., 2023; Theodosiou and Read, 2023). In this study, protein-protein interaction networks (PPI) and molecular complex detection (MCODE) analyses were combined with three ML algorithms, namely least absolute shrinkage and selection operator (LASSO), support vector machine-recursive feature elimination (SVM-RFE) and random forest (RF), to screen out critical targets of ACAS, which can offer a new theoretical reference for precise therapy of the illness.

2 Materials and methods

2.1 Retrieval and merging of datasets

We obtained five datasets from the NCBI GEO database (https://www.ncbi.nlm.nih.gov/geo/): GSE100927 (12 controls + 29 carotid atherosclerosis), GSE11782 (9 controls + 9 carotid atherosclerosis), GESE28829 (13 controls + 16 carotid atherosclerosis), GSE41571 (6 controls + 5 carotid atherosclerosis), and GSE43292 (32 controls + 32 carotid atherosclerosis). The first four datasets were combined as the training set ($n = 99$), while GSE43292 ($n = 64$) was used as the validation set. We then applied the sva package for batch calibration and visualized the pre- and post-correction results using principal component analysis (PCA).

2.2 Patients and samples with ACAS

Twenty patients diagnosed with ACAS and admitted to Renmin Hospital of Wuhan University between 2021 and 2023 were included in the study. The control group consisted of 10 ACAS patients who underwent CEA, and the experimental group consisted of 10 ACAS patients who also underwent CEA. The study collected

neighboring intima around atherosclerotic plaques in the control group and atherosclerotic plaques in the experimental group, resulting in a total of 20 cases. The atherosclerotic plaques and adjacent intima were collected within 10 min of CEA and stored at −80°C for future use. The study protocol was approved by the Clinical Research Ethics Committee of Renmin Hospital of Wuhan University (Ethics Approval No. WDRY2023-K123), and all methods used complied with relevant guidelines and regulations. Informed consent forms were signed by all participants.

2.3 Identification of differentially expressed genes (DEGs)

To find the DEGs between the control and experimental groups, the gene expression patterns of each group were normalized and analyzed using the "limma" package. The filtering criteria for the DEGs were set to a corrected p-value of < 0.05, $|\log FC| \geq 1$. A heatmap was visualized using the "pheatmap" package.

2.4 Functional enrichment analysis

"ClusterProfiler," "enrichplot," and "org.Hs.eg.db" packages were used to analyze important functions and pathways of DEGs, including Gene Ontology (GO) and Kyoto Encyclopedia of Genes and Genomes (KEGG) (Qin et al., 2023). The reference genome file "c2.cp.kegg.Hs.symbols.gmt" was used for gene set enrichment analysis (GSEA) to understand the differences in pathways between control and experimental groups (Qin et al., 2023). All results were visualized by the "ggplot2" software package.

2.5 PPI and MCODE analysis

The DEGs were uploaded to the online website STRING (http://string-db.org), and the PPI was constructed with a medium confidence level of 0.400. The PPI was then beautified by applying the software Cytoscape_3.8.0. MCODE analysis is to find out the key sub-networks and genes based on the relationship of edges and nodes in a huge PPI network, which facilitates downstream analysis to screen out the key genes (Bader and Hogue, 2003). Thus, MCODE in Cytoscape was chosen to calculate the information of each node in the PPI to produce the final functional module. The parameters were set as follows: Degree Cutoff: 2, Node Score Cutoff: 0.2, K-Core: 2, Max. Depth from Seed: 100.

2.6 Three ML algorithms for screening feature genes

We use the LASSO, SVM-RFE and RF algorithms (Qin et al., 2023) to screen key genes in the above functional modules. The feature genes were first screened using the LASSO algorithm to obtain a "LASSO coefficient path" and a "LASSO regularization path" (also known as Lasso regression analysis cross-validation curve). The former shows the variation of feature coefficients for different values of the regularization parameter (λ) in the LASSO algorithm. The latter shows the model fitting effect for different values of λ in the LASSO algorithm. The results of this figure allow us to find an optimal value of λ that gives the best Lasso fit and minimizes the cross-validation error. The number of genes corresponding to the point with the smallest cross-validation error is the number of disease signature genes. Then SVM-RFE algorithm can obtain a graph of cross-validation accuracy and a graph of cross-validation error. The horizontal coordinates of the two graphs represent the number of feature genes, and the vertical coordinates, "10 X CV Accuracy" and "10 X CV Error," represent the accuracy and error rate of the curve changes after 10-fold cross-validation, respectively. In the next RF algorithm, random forest trees were first constructed by setting the number of trees $n_{tree} = 500$, obtaining a random forest tree graph. Find the number of trees corresponding to the point with the smallest cross-validation error in the graph as the best tree value. And score the importance of the genes based on the best tree value so as to rank the genes and select the genes with gene importance greater than 1 for subsequent analysis. Finally, the intersection of the three algorithm screening results was taken and the Venn diagram was plotted using the "VennDiagram" R package. The R package "pROC" and "InpROC" were also applied to plot the ROC curves and calculate the area under the curve (AUC), respectively, to determine the predictive value of these characterized genes in the training set and validation set.

2.7 Creation of ACAS nomogram

The R package "rms" "rmda" was applied to construct nomogram of the identified signature genes and a calibration curve was plotted to assess the accuracy of the nomogram. Then the clinical impact curves of the model were plotted and evaluated. Finally, the decision curve analysis was used to evaluate the clinical utility of the nomogram.

2.8 Immune-related functions and immune cell correlation analysis

The 59 ACAS samples in the training group were categorized into high and low groups according to the expression of target genes. The cited R packages "GSVA," "GSEABase," "ggpubr," "reshape2," and "ggExtra" show the differences of different immune-related functions between the high and low expression groups of the characterized genes, as well as explore the correlation analysis of the characterized genes with immune cells.

2.9 Immunohistochemistry and immunofluorescence double-labeling

Twenty specimens were first paraffin-embedded and then sliced into 5 μm thin slices using a paraffin slicer (Leica RM2235). Immunohistochemistry steps: Briefly, the sections were first dewaxed to water. Then antigen repair was performed under the condition (citric acid solution, microwave medium heat for 8 min, cease-fire for 8 min, turn to medium-low heat for 7 min). Endogenous peroxidase was next blocked with a 3% hydrogen peroxide solution. The tissue was covered evenly with drops of 3% BSA in the histochemistry circle and closed at room temperature

for 30 min. Primary antibodies (C3AR1, GTX114293, 1:200, GeneTex; MPO, GB12224, 1:1500, Servicebio; MCP7, GB12110, 1; 500, Servicebio) were added and incubated overnight at 4°C. After cleaning, the slices were incubated with homologous secondary antibodies for another 1 h. Freshly prepared DAB solution was added to develop the color and then restained with hematoxylin for about 3 min. Then, the sections were dehydrated and sealed with xylene. Photographs were taken utilizing a microscope (Olympus BX53) and quantified using ImageJ (v1.8.0) analysis software.

Steps of homologous immunofluorescence double-labeling staining: the preparation process of the paraffin section, including antigen repair, was consistent with that of immunohistochemistry. The slices were added with the first primary antibody (C3AR1, GTX114293, 1:200, GeneTex) and incubated overnight at 4°C. After washing, incubate with the secondary antibody for 1 h. Then TSA dye was added and incubated for 10 min at room temperature away from light. After washing, antigen repair was again performed. The second primary antibody (MPO, GB12224, 1:4000, Servicebio) was supplemented and incubated overnight at 4°C and then incubated with the secondary antibody for another 1 h. Next, the nuclei were restained with DAPI and incubated at room temperature away from light for 10 min. Finally, images were captured using a fluorescence microscope (Olympus BX53) and quantified utilizing ImageJ (v1.8.0).

2.10 Construction of ceRNA and TF regulatory networks

The software miRanda, miRDB and TargetScan were applied to jointly predict miRNAs bound by characterized genes. miRNAs identified by all three software were saved for subsequent analysis. The spongeScan (Furió-Tarí et al., 2016) network was applied to predict miRNA-bound lncRNAs. The results were then imported into Cytoscape software to map the ceRNA regulatory network. Meanwhile, NetworkAnalyst (Zhou et al., 2019) (http://www.networkanalyst.ca) was utilized to construct the characteristic gene TFs regulatory network.

2.11 Statistical analysis

Statistical analysis was done using R version 4.2.3. The *t*-test was used for normally distributed variables and the Wilcoxon test was used for non-normally distributed variables. Linear relationships were analyzed using Pearson analysis, while monotonic relationships were analyzed using Spearman analysis. All statistical *p*-values were two-sided and $p < 0.05$ was considered statistically significant.

3 Results

3.1 177 DEGs were obtained

Before performing the analysis of variance, we performed a batch correction. The PCA analysis showed that in the pre-correction graphs, the samples from different experiments were separated, meaning that there was a batch effect between these samples (Figure 1A). After batch correction, these samples were randomly distributed, eliminating the effect of batch effects (Figure 1B). All gene volcanoes were then mapped (Figure 1C). The final differential analysis yielded 177 DEGs, which contained 67 downregulated and 110 upregulated genes (Figure 1D).

3.2 Function and pathway exploration of 177 DEGs

Next, functional enrichment analysis was performed on these DEGs. The GO and KEGG results indicated that these genes were primarily involved in leukocyte-mediated immunity, leukocyte migration, collagen-containing extracellular matrix, and actin binding functions (Figure 2A), as well as tuberculosis, *staphylococcus aureus* infection, lysosome, and phagosome pathways (Figure 2B). To understand the differences in pathways between the control and experimental groups, GSEA analysis was performed. The data demonstrated that these five pathways were active in the control: arrhythmogenic right ventricular cardiomyopathy, dilated cardiomyopathy, hypertrophic cardiomyopathy, ribosome, and vascular smooth muscle contraction (Figure 2C). In contrast, the experimental group showed activity in five different pathways: allograft rejection, autoimmune thyroid disease, graft versus host disease, leishmania infection, and lysosome (Figure 2D).

3.3 MCODE analysis yielded 7 important functional modules containing 63 genes

Next, the PPI map of the 177 DEGs was constructed (Figure 3A). To further investigate the underlying mechanisms of ACAS, a modular network was created applying the MCODE algorithm to reveal the core therapeutic targets. The algorithm identified highly relevant network targets from the PPI network, and a total of 7 significant modules were generated (Figures 3B–H), containing 63 genes. Table 1 provides specific information for each module.

3.4 Three ML algorithms screened for four feature genes

Next, the study began with a LASSO analysis of 63 genes, resulting in the identification of 9 genes: C3AR1, CTSB, CTSD, FBLN5, FERMT2, MMP9, PPP1R12A, RHOB, and TPM1 (Figures 4A, B). Subsequently, the SVM-RFE algorithm was employed to screen seven genes, namely PPP1R12A, FBLN5, C3AR1, MYL9, HMOX1, MFAP4, and TPM1 (Figures 4C, D). Meanwhile, the RF algorithm identified 15 feature genes with relative importance greater than 1, including FERMT2, VCL, FBLN5, PPP1R12A, PPP1CB, FCGR2A, CD68, TPM1, IRF8, LY86, HCK, TAGLN, FCER1G, LMOD1, and C3AR1 (Figures 4E, F). Finally, we took the intersection of the genes screened by the three algorithms resulted in the identification of four characterized genes: C3AR1, FBLN5, PPP1R12A, and TPM1 (Figure 4G).

10.3389/fphar.2024.1364160

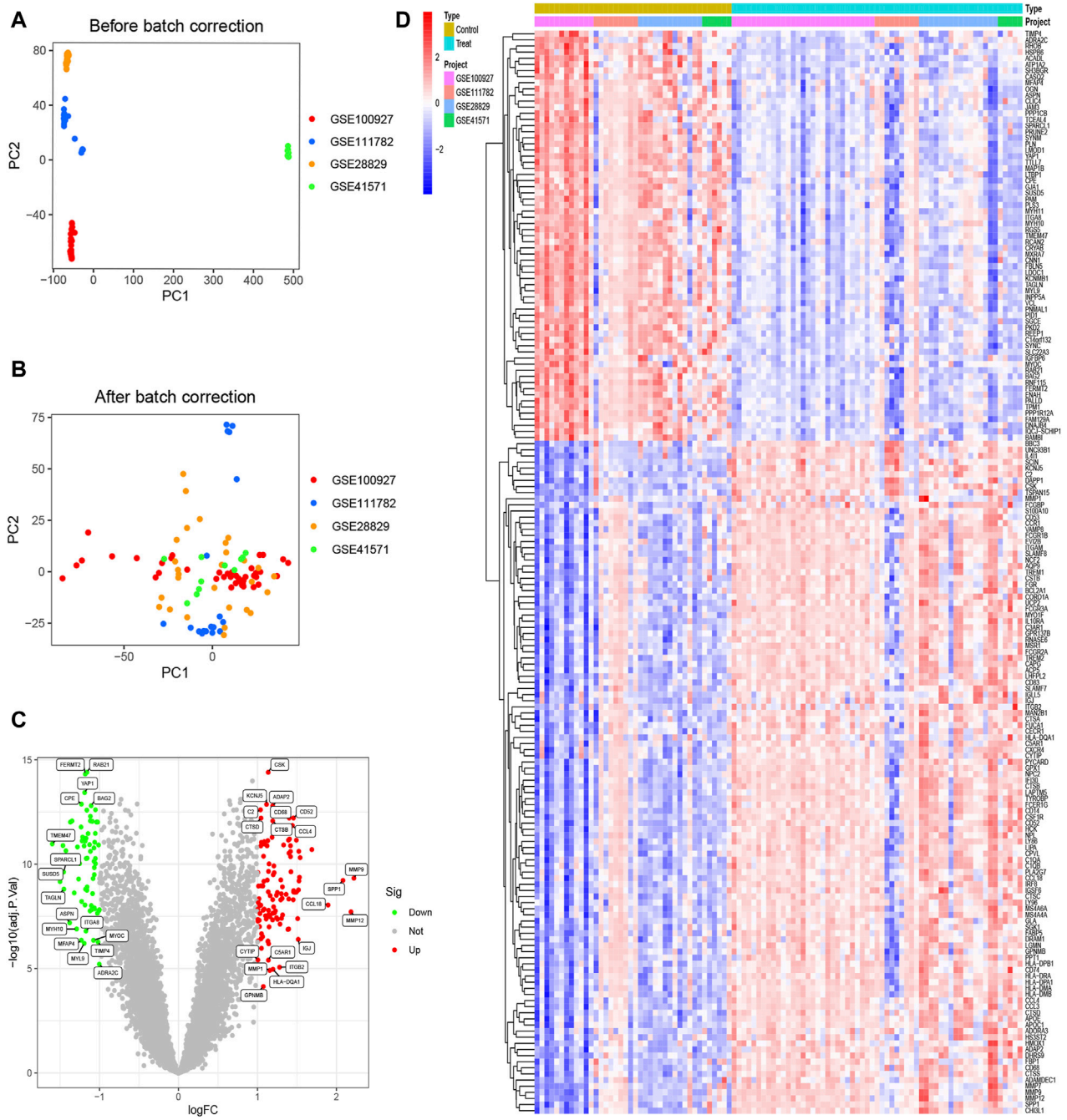

FIGURE 1
Identification of DEGs. **(A)** Samples from four datasets were shown to exist with batch effects; **(B)** Samples from four datasets eliminated the effects of batch effects; **(C)** Volcano plots of all genes; **(D)** Heatmaps of 67 downregulated genes and 110 upregulated genes.

3.5 The four characterized genes had group differences in the control and experimental group

Adjacently, to probe into whether the expression of the four characterized genes differed between the control and experimental groups, violin plots and line plots were plotted. The results from both the training and validation sets indicate that the four characterized genes were differentially expressed in both the control and experimental groups ($p < 0.01$, Figures 5A, B). Additionally, C3AR1 was highly expressed in the experimental group, while FBLN5, PPP1R12A, and TPM1 were expressed at low levels in the experimental group (Figure 5C).

3.6 ROC analysis of the four characterized genes

ROC analysis was performed to verify the accuracy of the screened feature genes. In the training set, C3AR1, FBLN5, PPP1R12A and TPM1 had AUC values of 0.896, 0.908, 0.906,

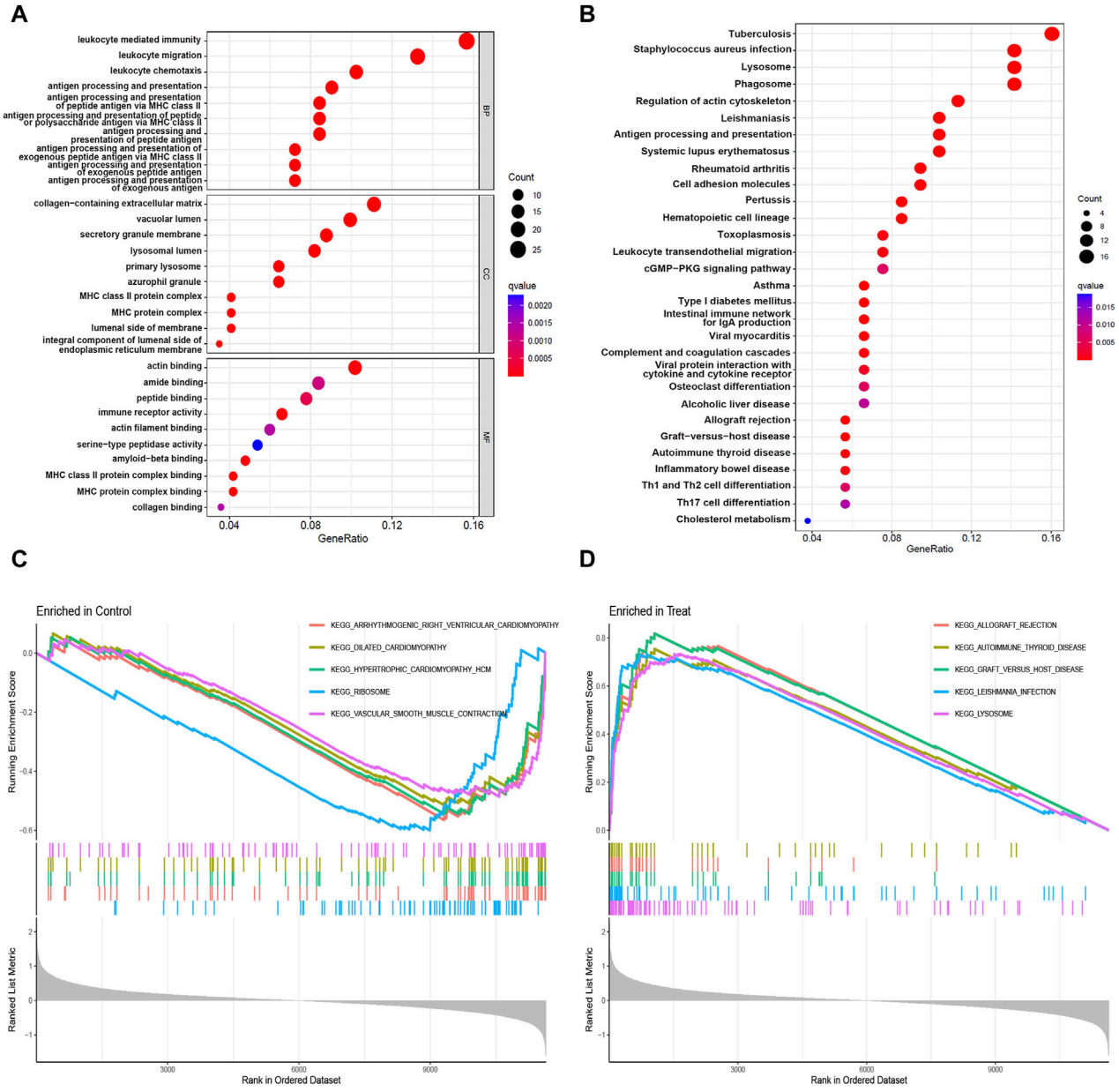

FIGURE 2
Functional enrichment analysis of 177 DEGs. **(A)** GO analysis results; **(B)** KEGG analysis results; **(C)** Five active pathways in the control group; **(D)** Five active pathways in the experimental group.

and 0.918, respectively (Figure 6A). In the validation set, the AUC values for C3AR1, FBLN5, PPP1R12A and TPM1 were 0.801, 0.837, 0.824, and 0.756, respectively (Figure 6B).

3.7 Construction of nomogram for predicting patients with ACAS based on four characterized genes

Next, a nomogram was constructed as a diagnostic tool for ACAS by combining the four characterized genes (Figure 7A). The scores corresponding to each of the characterized genes were summed to obtain a total score, which corresponded to the risk of prevalence of ACAS. The calibration curve discovered that the accuracy of the nomogram in predicting prevalence was high (Figure 7B). The clinical impact curve also showed significant predictive power of the nomogram model (Figure 7C). Decision curve analysis hinted that patients with ACAS could benefit from the nomogram (Figure 7D).

3.8 Immune-related function and immune cell correlation analysis of the four characterized genes

Next, the immune-related function analysis displayed that diverse immune-related functions differed to varying degrees

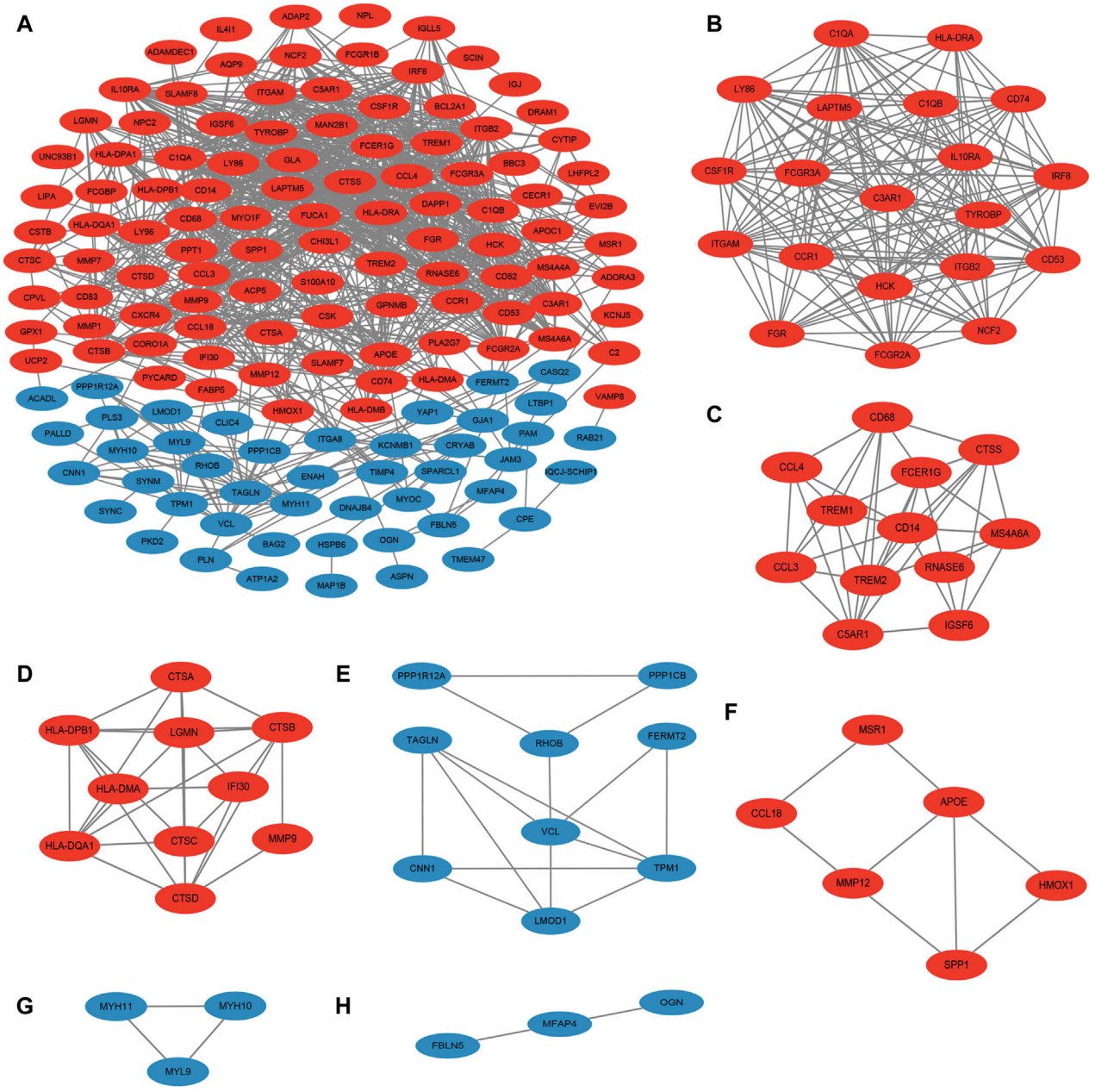

FIGURE 3
PPI and MCODE analysis. **(A)** PPI of DEGs; **(B–H)** seven important functional modules obtained from MCODE analysis. Red represents upregulated genes and blue represents downregulated genes.

between high and low expression groups of the four characterized genes (Figures 8A–D). We then explored the correlation analysis between genes and immune cells. The results showed that C3AR1 expression was positively correlated with neutrophils and mast cells activated, and negatively correlated with B cells memory, mast cells resting, and plasma cells (Figure 8E). FBLN5 showed an inverse correlation with T cells follicular helper (Figure 8F), whereas TPM1 was positively correlated with T cells CD4 memory activated (Figure 8H). The statistical significance of PPP1R12A's result was inconclusive (Figure 8G).

3.9 Immunohistochemical and fluorescent dual-labeling validation of C3AR1 expression in patients with ACAS

Based on the results presented in Figure 8E, there appears to be a positive correlation between C3AR1 expression and neutrophils and mast cells activated in carotid atherosclerotic plaques. To verify this relationship, we examined the expression levels of C3AR1, myeloperoxidase (MPO), a neutrophil marker (Schmekel et al., 1990), and mast cell protease 7 (MCP7), a mast cell marker (Matsumoto et al., 1995), in the carotid intima and

TABLE 1 The results of the MCODE analysis.

Cluster	Score	Nodes	Edges	Node IDs
1	17.895	20	170	LAPTM5, LY86, ITGB2, CD74, CD53, FCGR2A, IRF8, TYROBP, CSF1R, ITGAM, HLA-DRA, CCR1, C1QA, IL10RA, HCK, FCGR3A, FGR, NCF2, C1QB, C3AR1
2	7.091	12	39	CCL4, IGSF6, CD14, TREM1, CD68, CCL3, FCER1G, MS4A6A, RNASE6, CTSS, C5AR1, TREM2
3	6.444	10	29	IFI30, CTSA, CTSD, CTSC, HLA-DPB1, HLA-DQA1, HLA-DMA, MMP9, LGMN, CTSB
4	3.75	9	15	RHOB, LMOD1, PPP1CB, PPP1R12A, TPM1, TAGLN, CNN1, FERMT2, VCL
5	3.2	6	8	APOE, MMP12, CCL18, MSR1, HMOX1, SPP1
6	3	3	3	MYH11, MYH10, MYL9
7	3	3	3	FBLN5, OGN, MFAP4

plaque tissues of various patients with ACAS who underwent CEA, using immunohistochemistry. Furthermore, through quantitative analysis, correlation analysis and immunofluorescence double labeling method, a close connection between C3AR1 and MPO as well as MCP7 was found in carotid atherosclerotic plaque tissues. More notably, IH staining revealed significantly higher expression of C3AR1, MPO, and MCP7 in plaques from patients with ACAS compared to the intima ($p < 0.001$, Figures 9A, C–E). IF double-labeling of plaques also revealed a significant co-localization relationship between C3AR1 and MPO-positive neutrophils (Figure 9B). Correlation analysis demonstrated a positive correlation between C3AR1 and both MPO expression level (Figure 9F) and MCP7 expression level (Supplementary Figure S1).

3.10 Construction of ceRNA and TFs regulatory networks for four characterized genes

Finally, to further explore the molecular mechanism of ACAS, the present study constructed the regulatory networks of ceRNA and TFs of four target genes. The ceRNA hypothesis reveals a new mechanism for RNA interactions. The ceRNA is a newly discovered mechanism to regulate gene expression, which includes mRNA encoding proteins, lncRNA, miRNA and circRNA (Salmena et al., 2011). We predicted the miRNAs bound to each characterized gene and also predicted the miRNA-bound lncRNAs. The results showed that seven lncRNAs competed with C3AR1 to bind hsa-miR-361-3p (Figure 10A). Thirty-nine lncRNAs competed with FBLN5 for binding to eight miRNAs (hsa-miR-27a-3p, hsa-miR-518a-5p, hsa-miR-939-5p, hsa-let-7a-3p, hsa-miR-888-5p, hsa-miR-615-5p, hsa-miR-892a, and hsa-miR-214-3p) (Figure 10B). Eighteen lncRNAs competed with TPM1 to bind four miRNAs (hsa-miR-542-3p, hsa-let-7a-3p, hsa-miR-558 and hsa-miR-297) (Figure 10C). While up to ninety-one lncRNAs competed with PPP1R12A for binding to nineteen miRNAs (hsa-miR-20a-3p, hsa-miR-450b-5p, hsa-miR-323a-5p, hsa-miR-767-3p, hsa-miR-148a-3p, hsa-miR-1207-5p hsa-miR-377-3p, hsa-miR-129-5p, hsa-miR-1227-3p, hsa-miR-561-3p, hsa-miR-182-5p, hsa-miR-141-3p, hsa-miR-181a-2-3p, hsa-miR-186-5p, hsa-miR-140-5p,hsa-miR-570-3p, hsa-miR-877-3p, hsa-miR-194-3p, and hsa-miR-449c-5p), respectively (Figure 10D). Thus, one or more lncRNAs would compete with the characterized genes to bind miRNAs. In addition, this study also predicted the TFs bound to each characterized gene. Among them, twelve transcription factors could bind to C3AR1 (Figure 11A). Nineteen transcription factors could bind to FBLN5 (Figure 11B). Forty-one transcription factors were able to bind to PPP1R12A (Figure 11C). And forty transcription factors were able to bind to TPM1 (Figure 11D). Thus, each characterized gene possesses multiple TFs.

4 Discussion

In recent years, due to hypertension, dyslipidaemia, diabetes, tobacco, obesity and other factors, cerebrovascular disease in young adults, especially ischemic stroke, has shown an increasing trend (Goldstein, 2020). Its extremely high mortality rate, disability rate, recurrence rate, and further complications bring a huge economic burden to people. Here, we investigated its main etiology, ACAS, and probed into the pivotal genes and regulatory networks associated with carotid atherosclerotic plaques employing bioinformatics methods.

Our study screened out four genes characterized by ACAS: C3AR1, FBLN5, PPP1R12A, and TPM1. Of these, C3AR1 was upregulated and FBLN5, PPP1R12A, and TPM1 were downregulated. The results of the analysis of variance in both the training and validation sets highlighted that the four characterized genes were differentially expressed in both the control and experimental groups. And the ROC analysis for the four genes revealed that they had high AUC values in both the training and validation sets, indicating the accuracy of our screening results. In addition, immunohistochemistry and fluorescence double labeling further confirmed that C3AR1 was highly expressed in atherosclerotic plaques of patients with ACAS. Therefore, we venture to hypothesize that these key diagnostic genes are tightly intertwined with the pathogenesis of ACAS and deserve to be explored in depth.

The C3AR1 gene encodes the C3a allergenic toxin chemotactic receptor, which belongs to the G protein-coupled receptor 1 family and stimulates chemotaxis, granzyme release

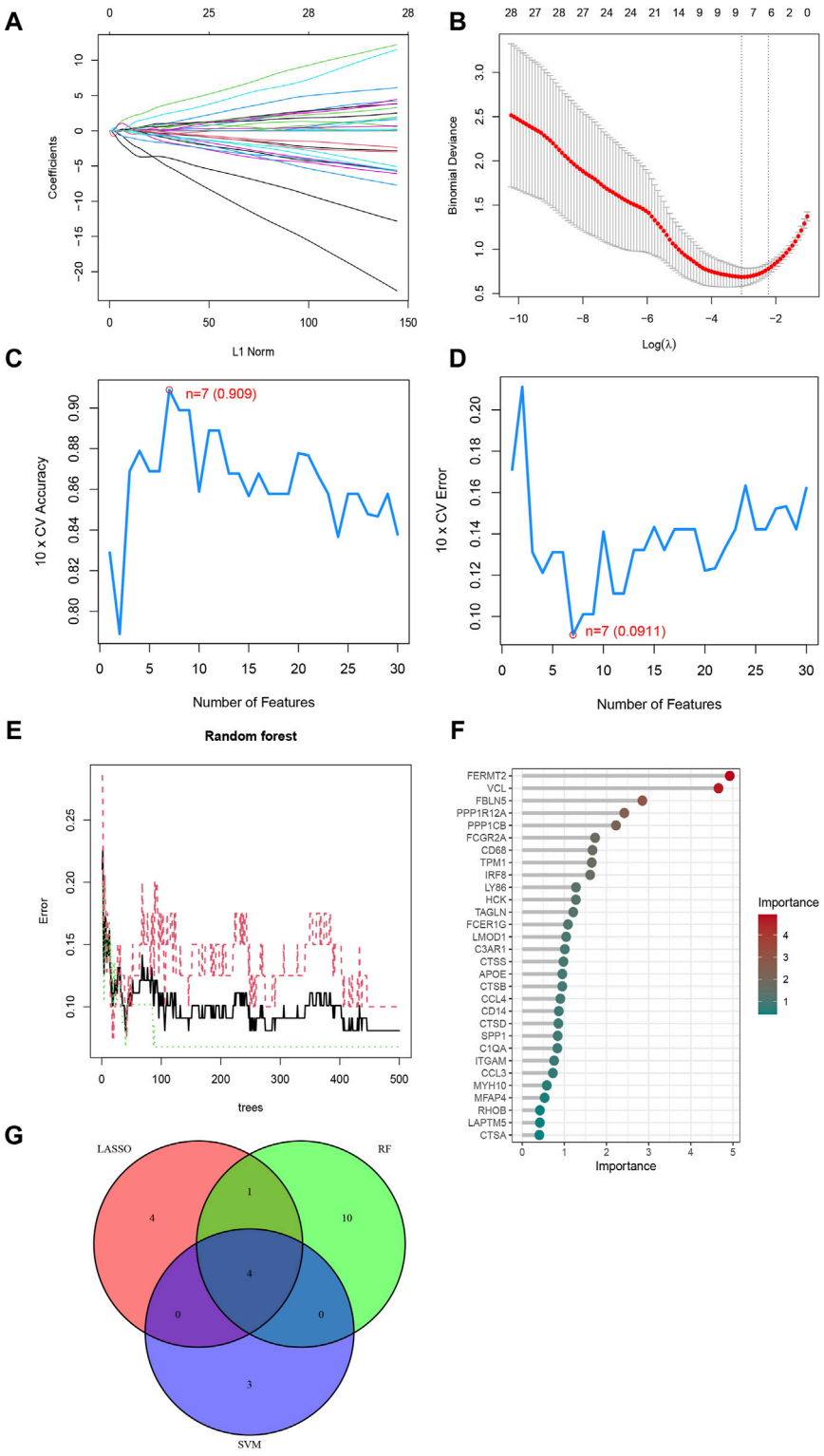

FIGURE 4
Three ML algorithms to screen feature genes. **(A)** LASSO coefficient path diagram, each curve represents one gene; **(B)** Lasso regression analysis cross-validation curve. When nine genes are used in the analysis, Lasso fits best and cross-validation error is minimized. **(C)** SVM-RFE algorithm determined the highest accuracy (0.909) when there were 7 genes; **(D)** SVM-RFE algorithm determined the lowest error rate (0.0911) when there were 7 genes; **(E)** The relationship between the number of Random Forest Trees and the error rate; **(F)** Genes are arranged in descending order of importance; **(G)** Venn diagrams of the genes obtained by the three algorithms.

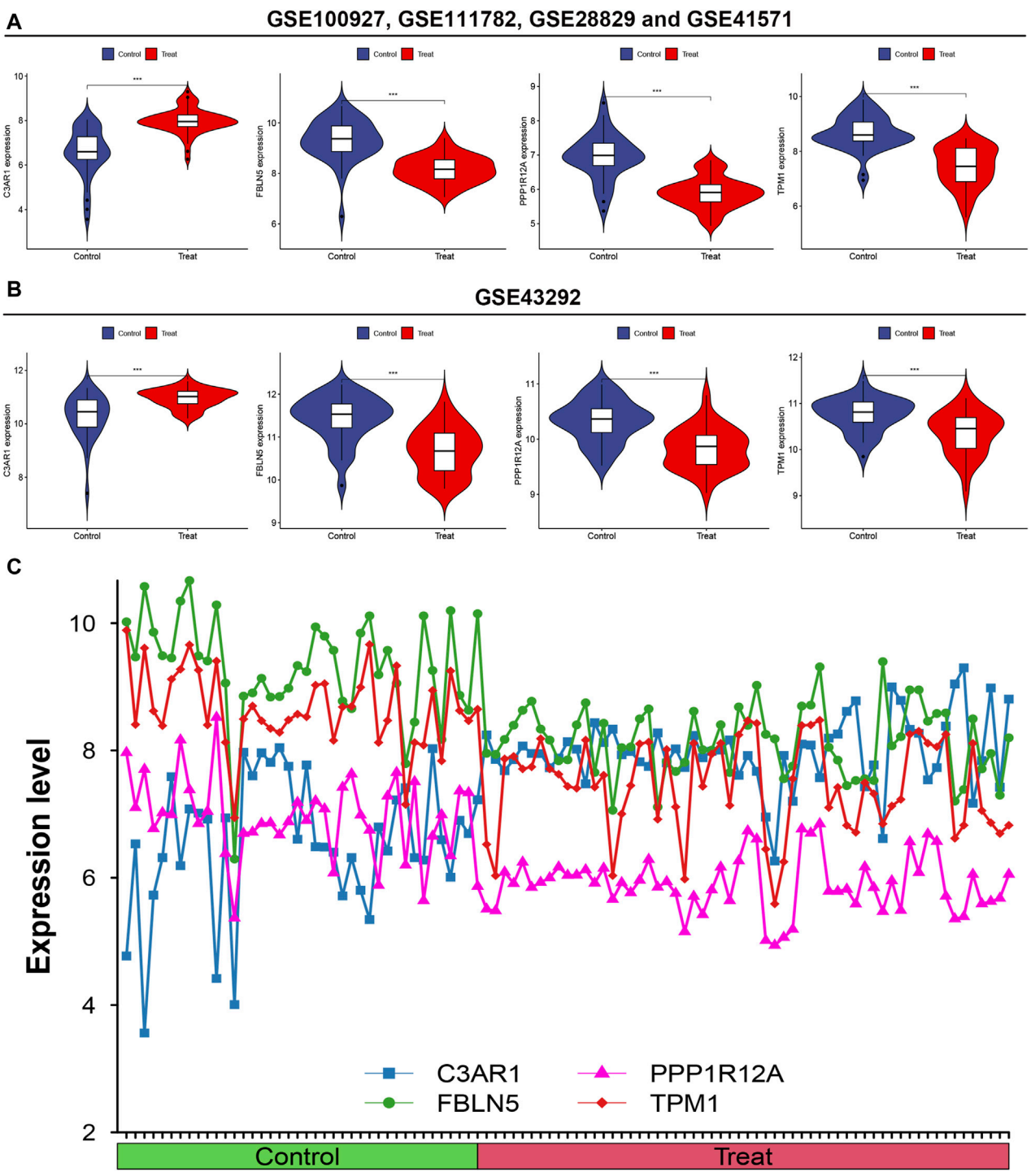

FIGURE 5
Intergroup difference analysis of the four characterized genes. **(A)** Differential analysis of the expression of the four feature genes in the training set illustrated by Violin plots; **(B)** Differential analysis of the expression of the four feature genes in the validation set shown by Violin plots; **(C)** Line plots of the expression levels of the four feature genes.

and superoxide anion production. This gene is not only a key gene in carotid atherosclerosis (Meng et al., 2021), but also its signaling pathway C3a/C3aR1/VCAM1 mediates neuroinflammation in aging and neurodegenerative diseases (Propson et al., 2021). In our study, this gene also showed a positive correlation with the level of infiltrating neutrophils and mast cells activated. Previous studies have discovered that C3aR1 controls neutrophil mobilization after spinal cord injury through physiological antagonism of CXCR2 (Brennan et al., 2019). Besides, neutrophils can trigger atherosclerosis and

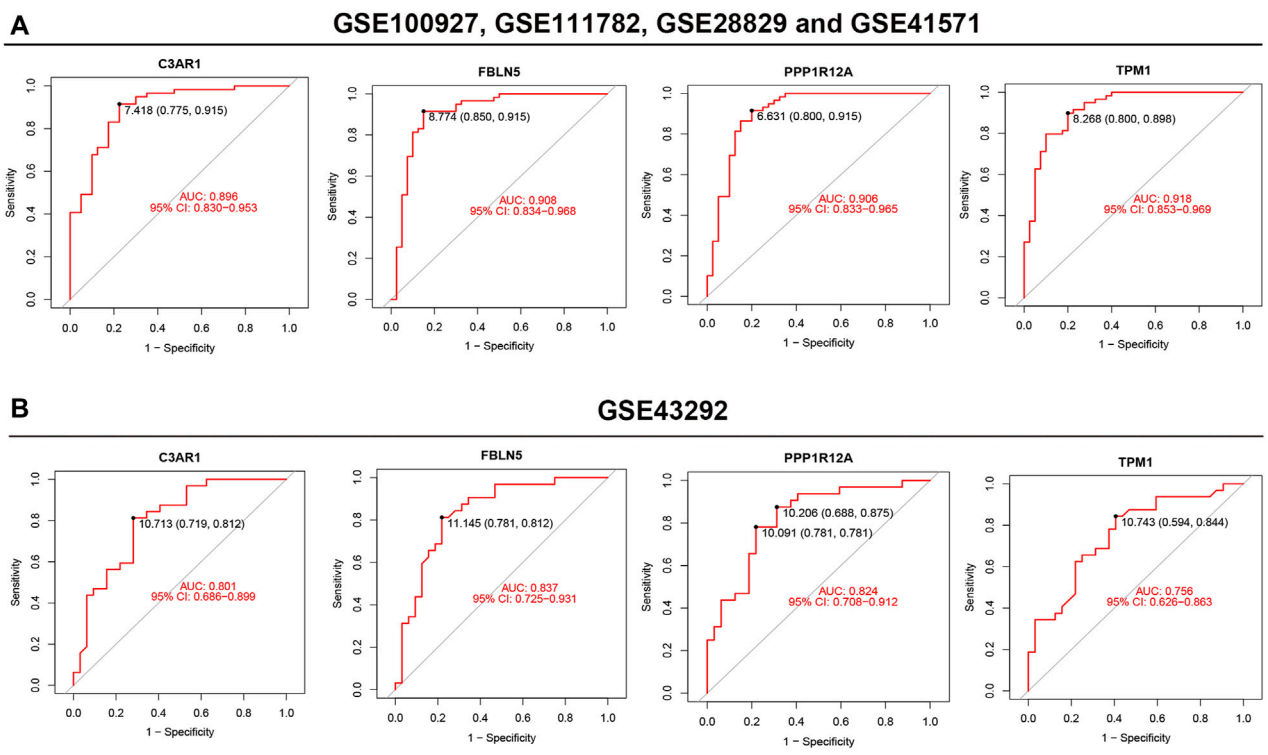

FIGURE 6
ROC analysis of the four feature genes. **(A,B)** ROC analysis results of the four feature genes in the training set **(A)** and validation set **(B)**, respectively.

promote atherosclerotic plaque destabilization and endothelial detachment (Silvestre-Roig et al., 2020). Notably, the formation of neutrophil extracellular traps (NETs) in neutrophils is one of the mechanisms of early atherosclerosis (Herrero-Cervera et al., 2022). Furthermore, activated diseased SMCs attract neutrophils to form NETs, which cause the histone H4 they contain to bind to and cleave SMCs, leading to plaque instability (Silvestre-Roig et al., 2019). Therefore, in our future studies, it is necessary to investigate how C3AR1 mediates the role of neutrophils in atherosclerosis and the potential specific mechanisms, so as to design neutrophil-targeted therapeutic strategies to stabilize atherosclerotic plaques, reverse ACAS, and reduce the incidence of stroke. In contrast, the interaction between C3AR1 and mast cells in atherosclerotic plaques has been less studied and needs to be explored in depth.

FBLN5 is a member of the fibronectin family and is essential for elastic fiber formation. It was discovered that FBLN5 may play an important role in carotid atherosclerosis via has-mir-128 and has-mir-532-3p (Zheng et al., 2022). PPP1R12A, also known as MYPT1, is a key regulator of protein phosphatase 1C. Evidence suggests that ROS-mediated downregulation of MYPT1 in smooth muscle cells is a potential mechanism for abnormal myocyte contractility in atherosclerosis (Cheng et al., 2013). TPM1, the pro-myosin α-1 chain, binds to actin filaments in muscle and non-muscle cells. It has been shown to be downregulated in unstable carotid atherosclerotic plaques (Guo et al., 2022). In short, these previous studies further support the reliability of our screening results. Hence, we established a predictive ACAS patient nomogram model based on the four characterized genes of our screening. This model can lead to the joint diagnosis or prediction of the pathogenic risk of patients with ACAS by the four characteristic gene indicators and provide an accurate digitalized risk probability for each patient, thus assisting clinicians in decision-making and individualized medical treatment.

Importantly, GSEA analysis revealed that five pathways were activated in the experimental group, encompassing xenograft rejection, autoimmune thyroid disease, graft-versus-host disease, leishmaniasis infection and lysosomes. It has been shown that allograft vasculopathy is a special case of immune-mediated atherosclerosis (Libby, 2012). Moreover, lysosomes are key nodes connecting lipid degradation, autophagy, apoptosis, inflammatory vesicles, lysosomal biogenesis and macrophage polarization, and may play a predominant role in the initiation, development and progression of atherosclerotic plaques (Zhang et al., 2021). However, the remaining pathways such as autoimmune thyroid disease, graft-versus-host disease and leishmaniasis infection have not been reported to be associated with atherosclerosis. Therefore, future exploration of the role of these pathways in ACAS may offer more effective and precise avenues for drug development and therapy.

More intriguingly, with the completion of the human genome sequencing project and the continuous optimization of sequencing technologies, the richness of the RNA world and the diversity of TFs have been continuously recognized, opening

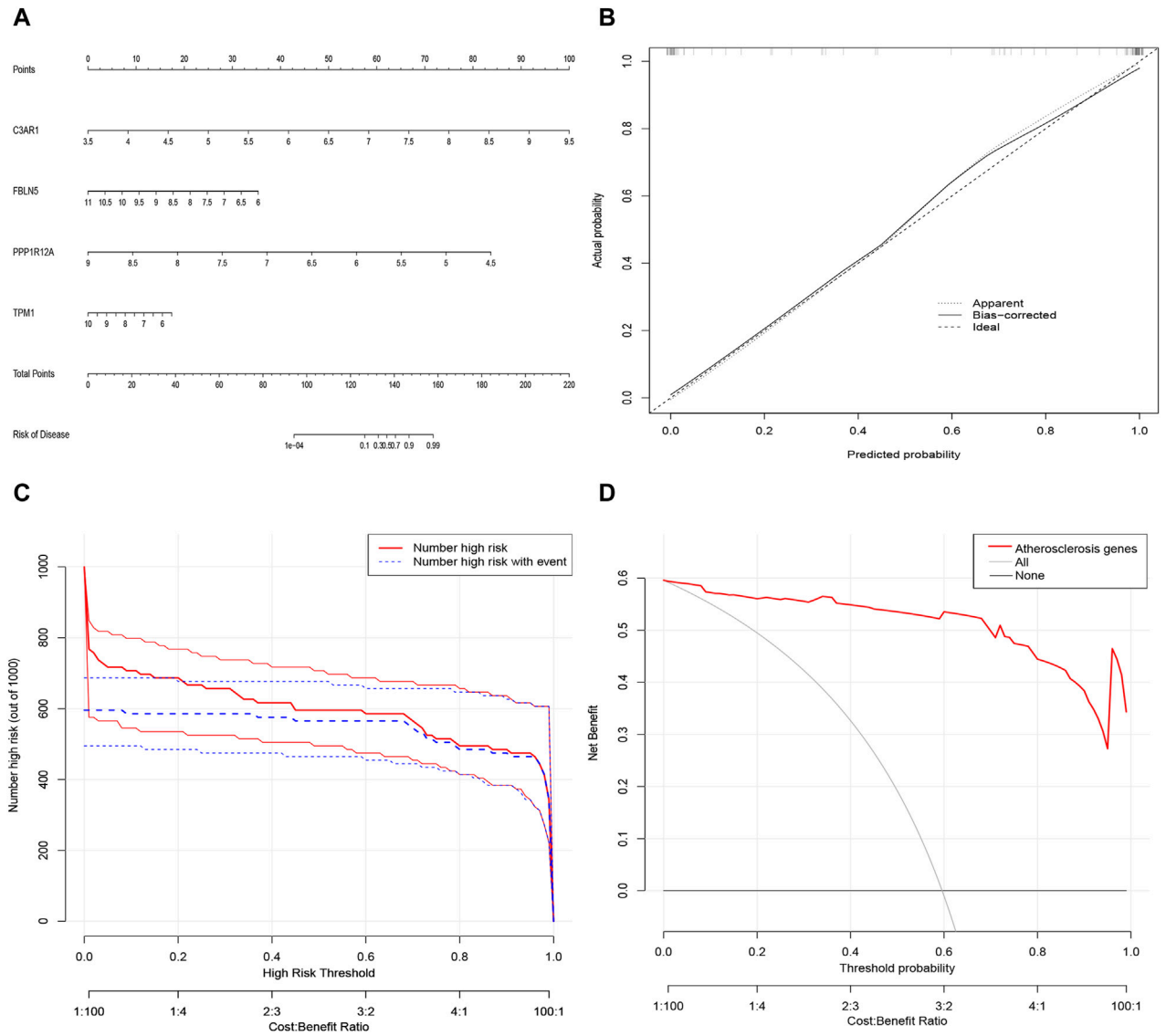

FIGURE 7
Alignment diagram model for predicting the risk of ACAS. **(A)** Alignment diagram for predicting ACAS. **(B)** Calibration curve to assess the predictive accuracy of the model. **(C)** Clinical impact curve to assess the model. **(D)** Decision curve analysis showing benefit in patients with ACAS.

up new frontiers for the treatment of diseases. Therefore, to further enrich future therapeutic strategies for ACAS, we constructed the ceRNA and transcription factor regulatory networks of four target genes.

The ceRNA include mRNA, miRNA, lncRNA and so on (Salmena et al., 2011). Studies have shown that many miRNAs are involved not only in atherosclerosis-related physiological and pathological processes, but also in lipid processing, inflammation and cellular behaviors (such as proliferation, migration and phenotypic transformation) (Navarro et al., 2020). For example, extracellular vesicles-derived hsa-miR-27a-3p promotes M2 macrophage polarization, thereby promoting cell proliferation and migration (Zhao et al., 2022). Inhibition of hsa-miR-140-5p expression can induce upregulation of C-reactive protein, which is involved in atherogenesis (Teng and Meng, 2019). In addition, one or more lncRNAs compete with signature genes to bind miRNAs. lncRNAs coordinate and integrate a variety of signaling pathways and play important roles in development, differentiation and disease (Navarro et al., 2020). lncRNAs affect the expression levels of genes closely related to endothelial dysfunction, smooth muscle cell proliferation, macrophage dysfunction, abnormal lipid metabolism and cellular autophagy in atherosclerotic plaques, and thus are involved in regulating the onset and progression of atherogenesis (Ma et al., 2023). For example, the long non-coding RNA HOXC-AS1 inhibits oxidized low-density lipoprotein (ox-LDL)-induced cholesterol accumulation by promoting the expression of HOXC6 in THP-1 macrophages (Huang et al., 2016). LINC01123 is highly expressed in patients with CAS and promotes cell proliferation and migration by regulating the ox-LDL-induced miR-1277-5p/KLF5 axis in vascular smooth muscle cells

10.3389/fphar.2024.1364160

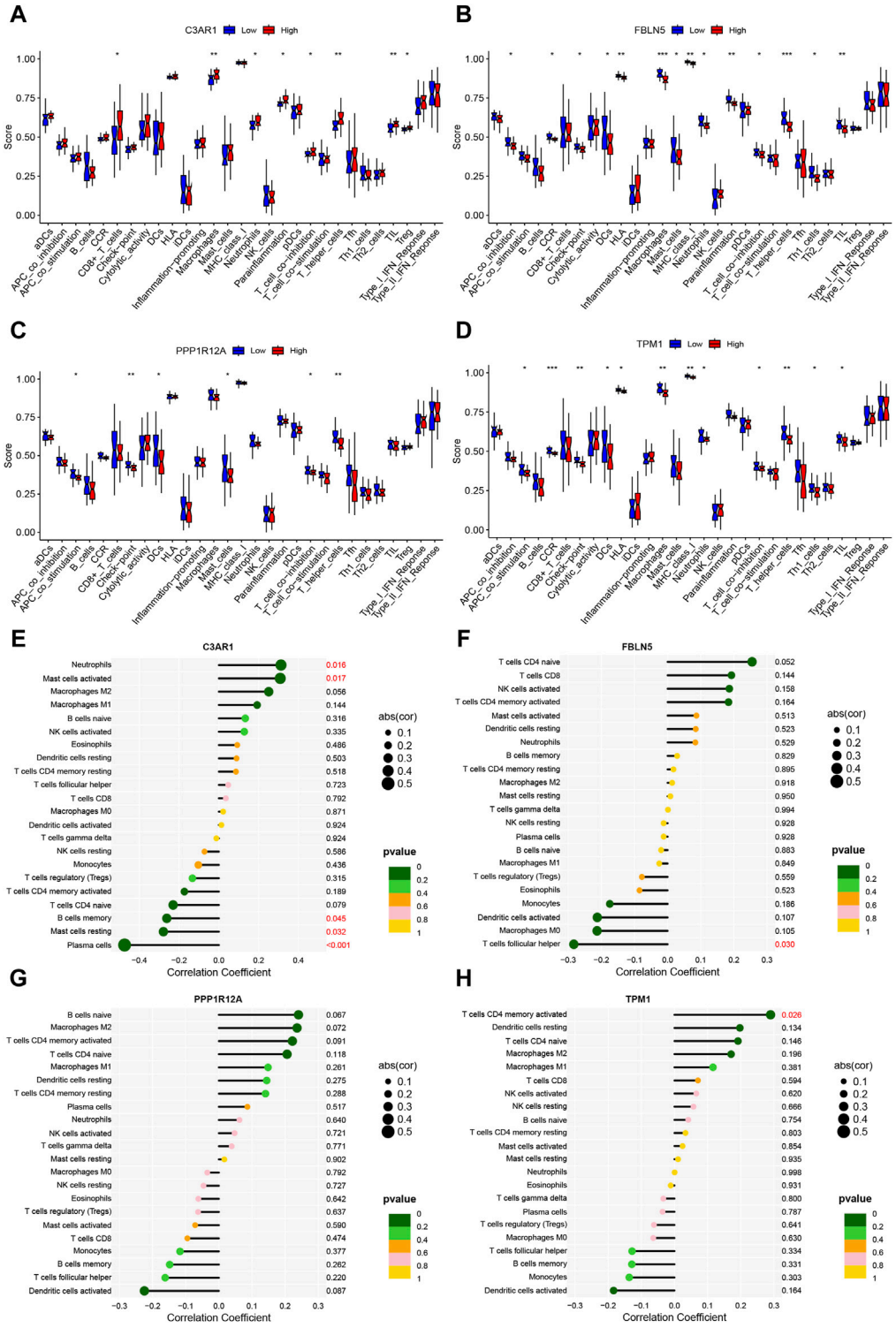

FIGURE 8
Immune-related functions and immune cell correlation analysis of characterized genes. **(A–D)** Box line plots of the differences between high and low expression groups for immune-related functions in C3AR1 **(A)**, FBLN5 **(B)**, PPP1R12A **(C)**, and TPM1 **(D)**, respectively; **(E–H)** Lollipop charts of the correlation of C3AR1 **(E)**, FBLN5 **(F)**, PPP1R12A **(G)** and TPM1 **(H)**, respectively, with 22 immune cell types.

(Weng et al., 2021). In addition, TFs can regulate macrophages in atherosclerosis through mechanisms involved in cytokine signaling, lipid signaling, and foam cell formation (Kuznetsova et al., 2020). For instance, decreasing RUNX1 expression in macrophages inhibits ox-LDL-induced lipid accumulation and inflammation (Liu et al., 2022). Endothelial Foxp1 inhibits atherosclerosis by regulating Nlrp3 inflammasome activation (Zhuang et al., 2019). In conclusion, these findings further support the accuracy of the

10.3389/fphar.2024.1364160

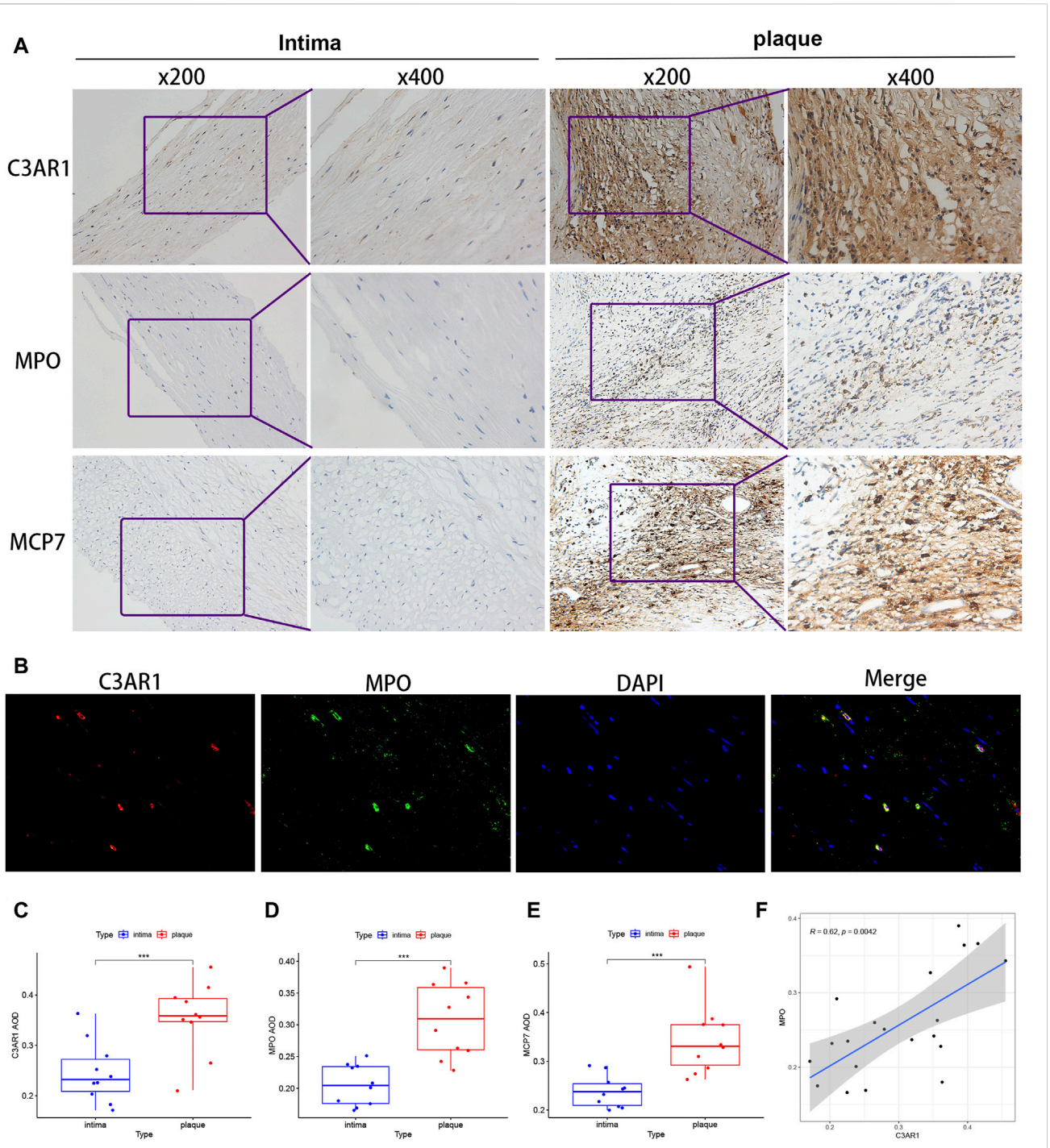

FIGURE 9
C3AR protein level in intima and plaques of patients with ACAS. **(A)** IH staining of C3AR1, MPO and MCP7 in the intima (left) and plaques (right) of patients with ACAS. **(B)** IF staining for C3AR1 (red) and MPO (green) in plaques from patients with ACAS (magnification, ×400). **(C–E)** Significant difference analysis of IH results for C3AR1, MPO and MCP7 present by box plots. ***, indicate $p < 0.001$. **(F)** Correlation plot of C3AR1 and MPO protein expression. MPO: myeloperoxidase (neutrophil marker); MCP7: mast cell protease 7 (mast cell marker).

ceRNA and TFs regulatory networks of the characterized genes constructed in this study. Therefore, an in-depth understanding of the mechanisms and functions of these ceRNA and TFs will help us to better ravel out the mysteries of the regulation of these characterized genes and provide new ideas for the future treatment of ACAS.

Undeniably, there are some limitations to this study. First, although this study identified four signature genes for ACAS based on ML algorithms and validated their diagnostic efficacy in an external dataset, prospective cohorts are needed to further investigate the biological significance of these signature genes in predicting ACAS. Second, we validated the high expression of

10.3389/fphar.2024.1364160

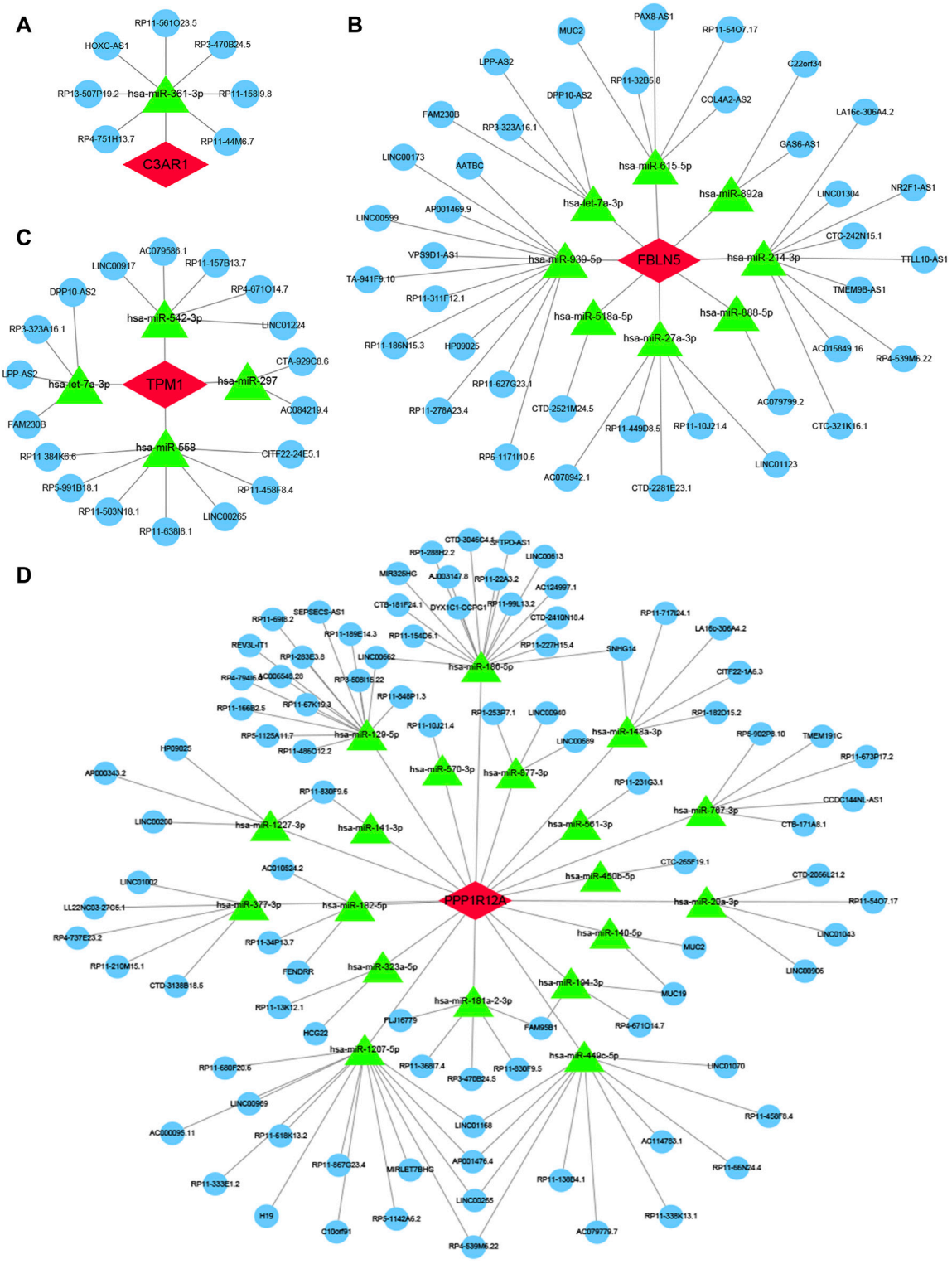

FIGURE 10
ceRNA of characterized genes. **(A–D)** The ceRNA regulatory networks of C3AR1 **(A)**, FBLN5 **(B)**, PPP1R12A **(C)**, and TPM1 **(D)**, separately. Red represents characterized genes, green represents miRNAs, and blue represents lncRNAs.

C3AR1 in patients with ACAS only in human plaque tissue, whereas the levels of FBLN5, PPP1R12A and TPM1 in plaques need to be further clarified. In conclusion, further *in vivo* and *in vitro* studies are needed to elucidate the potential mechanisms of action of C3AR1, FBLN5, PPP1R12A and TPM1 in ACAS.

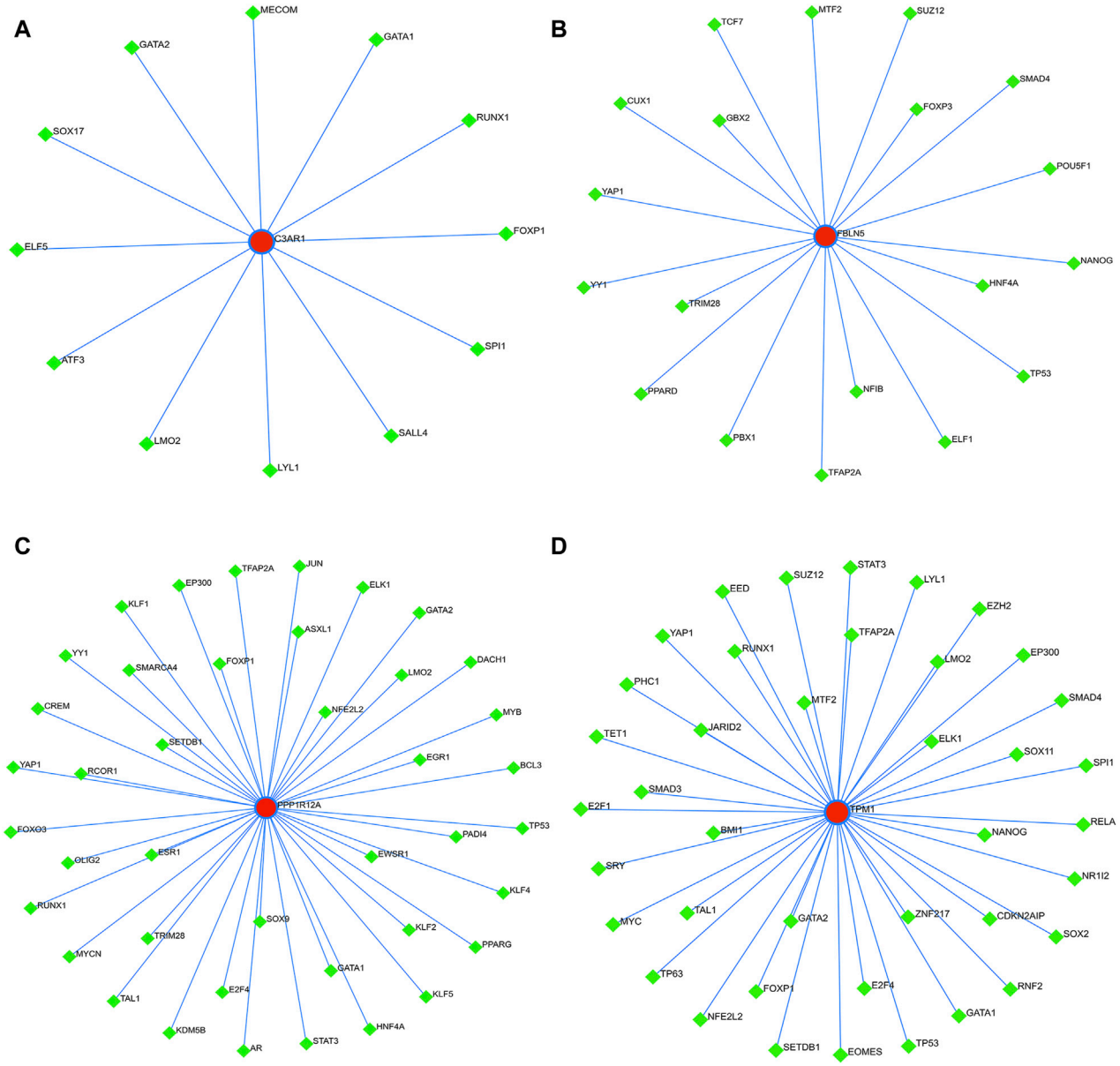

FIGURE 11
TFs regulatory networks of characterized genes. **(A–D)** TFs regulatory networks of C3AR1 **(A)**, FBLN5 **(B)**, PPP1R12A **(C)**, and TPM1 **(D)**, respectively.

5 Conclusion

Four pivotal genes were screened, and relevant ceRNA and TFs were predicted. These molecules may play a crucial role in ACAS and serve as potential biomarkers and therapeutic targets.

Data availability statement

The original contributions presented in the study are included in the article/Supplementary Material, further inquiries can be directed to the corresponding author.

Ethics statement

The studies involving humans were approved by the study protocol was authorized by the Clinical Research Ethics Committee of Renmin Hospital of Wuhan University (Ethics Approval No. WDRY2023-K123). The studies were conducted in accordance with the local legislation and institutional requirements. The human samples used in this study were acquired from primarily isolated as part of your previous study for which ethical approval was obtained. Written informed consent for participation was not required from the participants or the participants' legal guardians/next of kin in accordance with the national legislation and institutional requirements.

Author contributions

XQ: Conceptualization, Data curation, Methodology, Resources, Software, Validation, Visualization, Writing–original draft, Writing–review and editing. RD: Conceptualization, Data curation, Funding acquisition, Investigation, Project administration, Supervision, Validation, Writing–review and editing. HL: Formal Analysis, Methodology, Resources, Software, Validation, Visualization, Writing–review and editing. WZ: Data curation, Investigation, Project administration, Resources, Supervision, Validation, Writing–review and editing. SW: Methodology, Resources, Software, Validation, Visualization, Writing–review and editing. BJ: Data curation, Investigation, Project administration, Resources, Supervision, Writing–review and editing. RG: Data curation, Methodology, Project administration, Software, Supervision, Writing–review and editing. LW: Data curation, Funding acquisition, Methodology, Project administration, Supervision, Writing–review and editing. ZC: Conceptualization, Data curation, Funding acquisition, Investigation, Project administration, Supervision, Writing–review and editing.

Funding

The author(s) declare financial support was received for the research, authorship, and/or publication of this article. This work was supported by the Fundamental Research Funds for the Central Universities (Grant number: 2042023kf0007) and the Youth Foundation of the National Natural Science Foundation of China (Grant number: 82301536).

Conflict of interest

The authors declare that the research was conducted in the absence of any commercial or financial relationships that could be construed as a potential conflict of interest.

Publisher's note

Supplementary material

The Supplementary Material for this article can be found online at: https://www.frontiersin.org/articles/10.3389/fphar.2024.1364160/full#supplementary-material

References

Bader, G. D., and Hogue, C. W. (2003). An automated method for finding molecular complexes in large protein interaction networks. *Bmc Bioinforma.* 4, 2. doi:10.1186/1471-2105-4-2

Bonati, L. H., Jansen, O., de Borst, G. J., and Brown, M. M. (2022). Management of atherosclerotic extracranial carotid artery stenosis. *Lancet Neurol.* 21 (3), 273–283. doi:10.1016/s1474-4422(21)00359-8

Brennan, F. H., Jogia, T., Gillespie, E. R., Blomster, L. V., Li, X. X., Nowlan, B., et al. (2019). Complement receptor C3aR1 controls neutrophil mobilization following spinal cord injury through physiological antagonism of CXCR2. *Jci Insight* 4 (9), e98254. doi:10.1172/jci.insight.98254

Campbell, B. C. V., De Silva, D. A., Macleod, M. R., Coutts, S. B., Schwamm, L. H., Davis, S. M., et al. (2019). Ischaemic stroke. *Nat. Rev. Dis. Prim.* 5, 70. doi:10.1038/s41572-019-0118-8

Cheng, J. C., Cheng, H. P., Tsai, I. C., and Jiang, M. J. (2013). ROS-mediated downregulation of MYPT1 in smooth muscle cells: a potential mechanism for the aberrant contractility in atherosclerosis. *Lab. Investig.* 93 (4), 422–433. doi:10.1038/labinvest.2013.40

Cheng, S. F., Brown, M. M., Simister, R. J., and Richards, T. (2019). Contemporary prevalence of carotid stenosis in patients presenting with ischaemic stroke. *Br. J. Surg.* 106 (7), 872–878. doi:10.1002/bjs.11136

Feigin, V. L., Stark, B. A., Johnson, C. O., Roth, G. A., Bisignano, C., Abady, G. G., et al. (2021). Global, regional, and national burden of stroke and its risk factors, 1990-2019: a systematic analysis for the Global Burden of Disease Study 2019. *Lancet Neurol.* 20 (10), 795–820. doi:10.1016/s1474-4422(21)00252-0

Feske, S. K. (2021). Ischemic stroke. *Am. J. Med.* 134 (12), 1457–1464. doi:10.1016/j.amjmed.2021.07.027

Furió-Tarí, P., Tarazona, S., Gabaldón, T., Enright, A. J., and Conesa, A. (2016). spongeScan: a web for detecting microRNA binding elements in lncRNA sequences. *Nucleic Acids Res.* 44 (W1), W176–W180. doi:10.1093/nar/gkw443

Goldstein, L. B. (2020). Introduction for focused updates in cerebrovascular disease. *Stroke* 51 (3), 708–710. doi:10.1161/strokeaha.119.024159

Guo, J. L., Ning, Y. C., Su, Z. X., Guo, L. R., and Gu, Y. Q. (2022). Identification of hub genes and regulatory networks in histologically unstable carotid atherosclerotic plaque by bioinformatics analysis. *Bmc Med. Genomics* 15 (1), 145. doi:10.1186/s12920-022-01257-1

Heck, D., and Jost, A. (2021). Carotid stenosis, stroke, and carotid artery revascularization. *Prog. Cardiovasc. Dis.* 65, 49–54. doi:10.1016/j.pcad.2021.03.005

Herrero-Cervera, A., Soehnlein, O., and Kenne, E. (2022). Neutrophils in chronic inflammatory diseases. *Cell. Mol. Immunol.* 19 (2), 177–191. doi:10.1038/s41423-021-00832-3

Huang, C., Hu, Y. W., Zhao, J. J., Ma, X., Zhang, Y., Guo, F. X., et al. (2016). Long noncoding RNA HOXC-AS1 suppresses ox-LDL-induced cholesterol accumulation through promoting HOXC6 expression in THP-1 macrophages. *DNA Cell Biol.* 35 (11), 722–729. doi:10.1089/dna.2016.3422

Kappelle, L. J. (2002). Symptomatic carotid artery stenosis. *J. Neurology* 249 (3), 254–259. doi:10.1007/s004150200001

Kuznetsova, T., Prange, K. H. M., Glass, C. K., and de Winther, M. P. J. (2020). Transcriptional and epigenetic regulation of macrophages in atherosclerosis. *Nat. Rev. Cardiol.* 17 (4), 216–228. doi:10.1038/s41569-019-0265-3

Libby, P. (2012). Inflammation in atherosclerosis. *Arteriosclerosis Thrombosis Vasc. Biol.* 32 (9), 2045–2051. doi:10.1161/atvbaha.108.179705

Liu, M. X., Tao, G. Z., Cao, Y. M., Hu, Y., and Zhang, Z. (2022). Silencing of IGF2BP1 restrains ox-LDL-induced lipid accumulation and inflammation by reducing RUNX1 expression and promoting autophagy in macrophages. *J. Biochem. Mol. Toxicol.* 36 (4), e22994. doi:10.1002/jbt.22994

Ma, Y., He, S. Q., Xie, Q., Tang, Z. H., and Jiang, Z. S. (2023). LncRNA: an important regulator of atherosclerosis. *Curr. Med. Chem.* 30 (38), 4340–4354. doi:10.2174/0929867330666230111125141

Matsumoto, R., Sali, A., Ghildyal, N., Karplus, M., and Stevens, R. L. (1995). Packaging of proteases and proteoglycans in the granules of mast-cells and other hematopoietic-cells - a cluster of histidines on mouse mast-cell protease-7 regulates its binding to heparin serglycin proteoglycans. *J. Biol. Chem.* 270 (33), 19524–19531. doi:10.1074/jbc.270.33.19524

Meng, Y. S., Zhang, C. L., Liang, L. C., Wei, L., Wang, H., Zhou, F. K., et al. (2021). Identification of potential key genes involved in the carotid atherosclerosis. *Clin. Interventions Aging* 16, 1071–1084. doi:10.2147/cia.S312941

Navarro, E., Mallén, A., Cruzado, J. M., Torras, J., and Hueso, M. (2020). Unveiling ncRNA regulatory axes in atherosclerosis progression. *Clin. Transl. Med.* 9 (1), 5. doi:10.1186/s40169-020-0256-3

Propson, N. E., Roy, E. R., Litvinchuk, A., Köhl, J., and Zheng, H. (2021). Endothelial C3a receptor mediates vascular inflammation and blood-brain barrier permeability during aging. *J. Clin. Investigation* 131 (1), e140966. doi:10.1172/jci140966

Qin, X. H., Yi, S. F., Rong, J. T., Lu, H. R., Ji, B. W., Zhang, W. F., et al. (2023). Identification of anoikis-related genes classification patterns and immune infiltration characterization in ischemic stroke based on machine learning. *Front. Aging Neurosci.* 15, 1142163. doi:10.3389/fnagi.2023.1142163

Saini, V., Guada, L., and Yavagal, D. R. (2021). Global epidemiology of stroke and access to acute ischemic stroke interventions. *Neurology* 97 (20S), S6–S16. doi:10.1212/wnl.0000000000012781

Salmena, L., Poliseno, L., Tay, Y., Kats, L., and Pandolfi, P. P. (2011). A ceRNA hypothesis: the rosetta stone of a hidden RNA language? *Cell* 146 (3), 353–358. doi:10.1016/j.cell.2011.07.014

Schmekel, B., Karlsson, S. E., Linden, M., Sundstrom, C., Tegner, H., and Venge, P. (1990). Myeloperoxidase in human lung lavage. I. A marker of local neutrophil activity. *Inflammation* 14 (4), 447–454. doi:10.1007/bf00914095

Silvestre-Roig, C., Braster, Q., Ortega-Gomez, A., and Soehnlein, O. (2020). Neutrophils as regulators of cardiovascular inflammation. *Nat. Rev. Cardiol.* 17 (6), 327–340. doi:10.1038/s41569-019-0326-7

Silvestre-Roig, C., Braster, Q., Wichapong, K., Lee, E. Y., Teulon, J. M., Berrebeh, N., et al. (2019). Externalized histone H4 orchestrates chronic inflammation by inducing lytic cell death. *Nature* 569 (7755), 236–240. doi:10.1038/s41586-019-1167-6

Swanson, K., Wu, E., Zhang, A., Alizadeh, A. A., and Zou, J. M. (2023). From patterns to patients: advances in clinical machine learning for cancer diagnosis, prognosis, and treatment. *Cell* 186 (8), 1772–1791. doi:10.1016/j.cell.2023.01.035

Teng, L. L., and Meng, R. F. (2019). Long non-coding RNA MALAT1 promotes acute cerebral infarction through miRNAs-mediated hs-CRP regulation. *J. Mol. Neurosci.* 69 (3), 494–504. doi:10.1007/s12031-019-01384-y

Theodosiou, A. A., and Read, R. C. (2023). Artificial intelligence, machine learning and deep learning: potential resources for the infection clinician. *J. Infect.* 87 (4), 287–294. doi:10.1016/j.jinf.2023.07.006

Weng, G. H., Gu, M. H., Zhang, Y. F., Zhao, G. F., and Gu, Y. (2021). LINC01123 promotes cell proliferation and migration via regulating miR-1277-5p/KLF5 axis in ox-LDL-induced vascular smooth muscle cells. *J. Mol. Histology* 52 (5), 943–953. doi:10.1007/s10735-021-10010-4

White, C. J., Brott, T. G., Gray, W. A., Heck, D., Jovin, T., Lyden, S. P., et al. (2022). Carotid artery stenting: JACC state-of-the-art review. *J. Am. Coll. Cardiol.* 80 (2), 155–170. doi:10.1016/j.jacc.2022.05.007

Zhang, Z. Q., Yue, P. F., Lu, T. Q., Wang, Y., Wei, Y. Q., and Wei, X. W. (2021). Role of lysosomes in physiological activities, diseases, and therapy. *J. Hematol. Oncol.* 14 (1), 79. doi:10.1186/s13045-021-01087-1

Zhao, G. F., Yu, H. Q., Ding, L. J., Wang, W. Y., Wang, H., Hu, Y., et al. (2022). microRNA-27a-3p delivered by extracellular vesicles from glioblastoma cells induces M2 macrophage polarization via the EZH1/KDM3A/CTGF axis. *Cell Death Discov.* 8 (1), 260. doi:10.1038/s41420-022-01035-z

Zheng, L., Yue, X. Y., Li, M. H., Hu, J., Zhang, B. J., Zhang, R. J., et al. (2022). Contribution of FBLN5 to unstable plaques in carotid atherosclerosis via mir128 and mir532-3p based on bioinformatics prediction and validation. *Front. Genet.* 13, 821650. doi:10.3389/fgene.2022.821650

Zhou, G. Y., Soufan, O., Ewald, J., Hancock, R. E. W., Basu, N., and Xia, J. G. (2019). NetworkAnalyst 3.0: a visual analytics platform for comprehensive gene expression profiling and meta-analysis. *Nucleic Acids Res.* 47 (W1), W234–W41. doi:10.1093/nar/gkz240

Zhuang, T., Liu, J., Chen, X. L., Zhang, L., Pi, J. J., Sun, H. M., et al. (2019). Endothelial Foxp1 suppresses atherosclerosis via modulation of Nlrp3 inflammasome activation. *Circulation Res.* 125 (6), 590–605. doi:10.1161/circresaha.118.314402

Frontiers in Genetics

Highlights genetic and genomic inquiry relating to all domains of life

The most cited genetics and heredity journal, which advances our understanding of genes from humans to plants and other model organisms. It highlights developments in the function and variability of the genome, and the use of genomic tools.

Discover the latest Research Topics

See more →

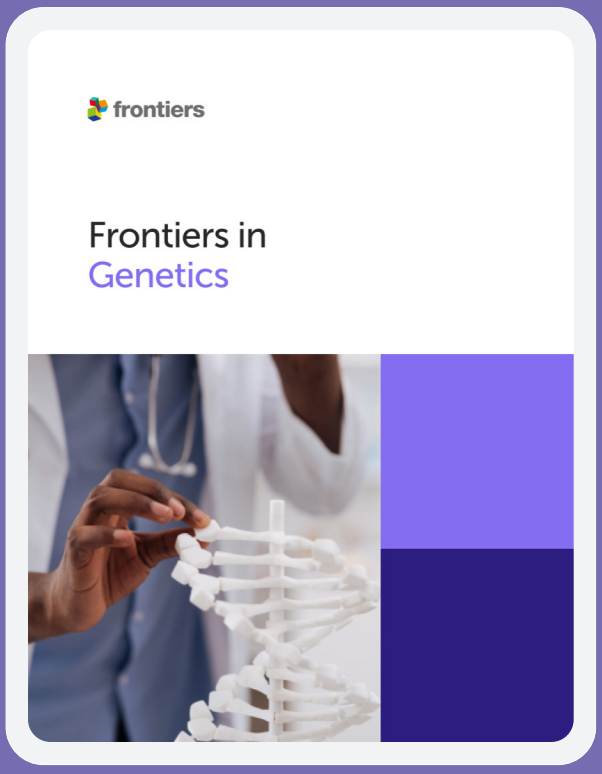

Frontiers

Avenue du Tribunal-Fédéral 34
1005 Lausanne, Switzerland
frontiersin.org

Contact us

+41 (0)21 510 17 00
frontiersin.org/about/contact